EXPERIMENTAL INVESTIGATION OF EFFECTS OF COOLANT CONCENTRATION ON SUBCOOLED BOILING AND CRUD DEPOSITION ON REACTOR CLADDING AT HIGH PRESSURES AND HIGH TEMPERATURES

by

VIJAYA RAGHAVA PARAVASTU PATTARABHIRAN

B.TECH, Jawaharlal Nehru Technological University, INDIA, 2003

A THESIS

**Submitted in partial fulfillment of the
Requirements for the degree**

MASTER OF SCIENCE

**Department of Mechanical and Nuclear Engineering
College of Engineering**

**KANSAS STATE UNIVERSITY
Manhattan, Kansas**
2008

Approved by:

**Major Professor
Dr. Donald L. Fenton**

ABSTRACT

Increase in demand for energy necessitates nuclear power units to increase their peak power limits. This increase implies significant changes in the design of the nuclear power unit core in order to provide better economy and safety in operations. A major hindrance to the increase of nuclear reactor performance especially in Pressurized Water Reactors (PWR) is the so called 'Axial Offset Anomaly (AOA)'. An Axial Offset Anomaly (AOA) is the unexpected change in the core axial power distribution during the operation of a PWR from the predicted distribution. This problem is thought to be occurring because of precipitation and deposition of lithiated compounds such as lithium metaborate ($LiBO_2$) on the fuel rod. Due to its intrinsic property, the deposited boron absorbs neutrons thereby affecting the total power distribution in the reactor. AOA is thought to occur when there is sufficient build up of crud deposits on the cladding during subcooled nucleate boiling.

Predicting AOA is difficult because there is little information regarding the heat and mass transfer during subcooled nucleate boiling. This thesis describes the experimental investigation that was conducted to study the heat transfer characteristics during subcooled nucleate boiling at prototypical PWR conditions. Pool boiling tests were conducted with varying concentrations of $LiBO_2$ and boric acid (H_2BO_3) solutions along with deionized water. The experimental data collected includes the effect of coolant concentration, degree of subcooling, system pressure and heat flux on pool boiling heat transfer coefficients. An analysis of deposits formed on the fuel rod during subcooled nucleate boiling is also included in the thesis.

The experimental results reveal that the pool boiling heat transfer coefficient is degraded by the presence of boric acid and lithium metaborate in water. At concentration of 5000 ppm in water, the boric acid solution reduced the heat transfer coefficient by 23% and lithium metaborate solution reduced the heat transfer coefficient by 26%.

ACKNOWLEDGEMENTS

I would like to express my gratitude to Dr. Donald L. Fenton for giving me the opportunity to work with him for this project. Taking this opportunity, I would like to express my heartfelt thanks to him for making my stay at Kansas State University a memorable time in my life. His constant guidance, encouragement and patience were invaluable to me in finishing this project.

I would like to thank Dr. Ken Shultis and Dr. Terry Beck for serving on my thesis committee. I thank them for their patient review of this document and for their suggestions.

I would also thank the faculty and staff of the Department of Mechanical and Nuclear Engineering at Kansas State University. I express my gratitude to the Department of Energy (DOE), for providing the funding for this project.

I would like to thank Dr. Larry Glasgow, Chemical Engineering for allowing me to use his high magnification camera for the project. I would also like to thank Mr. Jason Selland, MNE workshop for his assistance in setting up the experimental equipment.

I would like to thank my parents and my brother for their constant encouragement, but for them many things would not have been possible. Lastly but not the least I would like to thank all my friends who have always been helpful to me and supported me all the time. Support from my parents and friends has always been great to me and I take this opportunity to thank everyone who has directly or indirectly helped me during my stay at Kansas State University.

TABLE OF CONTENTS

LIST OF FIGURES

LIST OF TABLES

LIST OF SYMBOLS

R = resistance of tube in ohms.

ρ = electrical resistivity of material (inconel) in Ωm

D_o = outer diameter of the tube in meters.

D_i = inner diameter of the tube in meters.

h_l = pressure difference between source and outlet of water in meters of hg.

P_1 = Supply pressure of water at inlet to the heat exchanger in N/m^2.

P_2 = Outlet Pressure of water in heat exchanger in N/m^2.

f = friction factor.

Re = Reynolds number

ρ= Density of the fluid in kg/m^3

μ = Dynamic viscosity of the fluid in N/m^2.

Nu = Nusselt Number

Pr = Prandtl Number

K = Thermal conductivity of the fluid in W/mk.

V = velocity of the water flowing through the tube in m/sec.

Q = flow rate in m^3/sec.

K_{water} = Thermal Conductivity of water at 300K =0.613 W/mk.

E_{max} = Maximum heat generated in Inconel tubes in Watts.

T_i = Inlet Temperature of water entering the heat exchanger in ^oC.

T_o = Outlet Temperature of water leaving the heat exchanger in ^oC.

A_{surf} = Surface area of the heat exchanger in m^2.

ΔP = Pressure drop in the heat exchanger in N/m^2.

R_I = diameter of heater element (filament) = 0.0031111m

R_{CI} = copper sleeve radius = 0.004178m

R_O = outside diameter of heater rod (cladding) = 0.00475m

Z_{LB} = boiling region length = 0.0254 m

$Z_{LNC} = Z_{LB}$ = natural convection length =0.0254 m

Z_{EER} = copper sleeve length = 0.0508 m

A_{CU} = cross – sectional area of copper sleeve in m^2.

V = voltage drop across heater in volts

I= electrical current flowing though the heater in amperes

R = resistance of the test heater = 0.07Ω

T_{CAVE}= average temperature of heater surface which is determined from four thermocouple temperatures T_{C1}, T_{C2}, T_{C3}, T_{C4} in ^oC.

$T_{KAVE} = T_{CAVE}$ +273.15 K

T_{BAVE} = bulk fluid temperature (^oC)

R_C = thermal contact resistance between copper sleeve and zr-4 clad (m^2 .K/W)

$\boldsymbol{\Delta T_L}$ = temperature difference between T_{CAVE} and bulk temperature (^oC)

R_{TOT} = total thermal resistance (m^2.K/W)

Q = total input power to the test heater. (W)

q" = heat transfer flux (W/m^2)

Q_{LOSS} = heat loss in cladding due to conduction in copper sleeve (W)

K_{CONDCU} = thermal conductivity for copper = 391.0 W/ (m. K)

K_{CONDZR} = thermal conductivity of zircalloy (W/m.K)

ΔT_{DEL} = Temperature difference between heater wall temperature and bulk temperature

$K_{CONDZR} = 7.51 + 0.0209T_{KAVE} - (1.45*10^{-5})\ T^2_{KAVE} + (7.67*10^{-9})\ T^3_{KAVE}$ (W/m.k)

h = coefficient of convective heat transfer in W/m^2K

ppm = Parts per million

1 INTRODUCTION

1.1 Overview

To meet the increasing demand for energy, it is essential that the electrical power be generated at greater economy and safer conditions. Many of the existing nuclear pressurized water reactors (PWR) are planning to increase their licensed peak power limits to meet the higher demand for energy. Consequently, to provide better economy and improve the safety of operating nuclear reactors, core designs require higher peaking factors.

The higher power increases the possibility of a portion of core being subjected to subcooled nucleate boiling due to higher temperatures in the core. However, these new demands on reactors contribute to a phenomenon known as the "Axial Offset Anomaly" (AOA), which is the unexpected deviation in axial power distribution in the core from the predicted distribution. AOA is thought to occur when the crud deposits build up on the fuel rod cladding undergoing subcooled nucleate boiling [Frattini et all; 2001]. During subcooled nucleate boiling, several compounds become supersaturated near boiling sites leading to precipitation on the surface of the heater. This effect of subcooled nucleate boiling has a major consequence, especially in the case of lithiated compounds of boron such as lithium metaborate ($LiBO_2$) and boric acid (H_3BO_3), because of its high neutron capture cross section. The high neutron capture cross section of boron in lithiated compounds has a major effect on the local power distribution in a reactor by absorbing

the neutrons in the core. The change in the neutron density in the core affects the axial power distribution in the reactor thereby causing the "Axial Offset Anomaly".

To resolve the problem of AOA, it is very important to understand the process affecting AOA. As AOA occurs during subcooled nucleate boiling upon the build up of crud deposits, it is essential to understand the phenomenon of subcooled boiling very well. The crud that builds on the Zircaloy-4 (Zr-4) clad fuel rod surface consists of corrosion products released in the reactor coolant system. The crud deposits are porous and hence affect the nucleation sites on the clad surface which in turn affect the rate of boron precipitation on the surface of fuel rod. The deposition rates are affected by several factors, which include the surface temperature, coolant concentration, and degree of subcooling of the bulk fluid. However, the information available about interactions between subcooled boiling and lithium and boron deposits is very scarce. Hence, an experimental study was conducted to understand the interaction of subcooled boiling and boron and lithium deposition on the surface of zircaloy clad rods.

The experimental study was conducted using specially designed high pressure boiling experimental equipment to measure the subcooled boiling heat transfer coefficient under varying operating conditions. The boiling tests were performed at prototypical PWR conditions with an electrical test heater simulating a fuel rod in the core of a reactor. The boiling tests were conducted with varying concentrations of boric acid and lithium metaborate solutions in deionized water to measure the effect of coolant concentration on the boiling heat transfer coefficient.

1.2 Working of a PWR

A Pressurized water reactor or PWR is a nuclear reactor, where the water is used as a primary coolant as well as a secondary coolant. A schematic of a working model of the pressurized water reactor is shown in Figure 1-1. The reactor vessel encloses the core, which consist of bundles of fuel rods. The purpose of the primary coolant is to remove the heat generated at the core, which is caused when the energy released in nuclear reactions is transformed by collisions into random molecular motion (heat) [Nero, 1979]. Highly pressurized deionized water is passed through the core in the reactor vessel; the deionized water is then passed through a steam generator where a secondary coolant

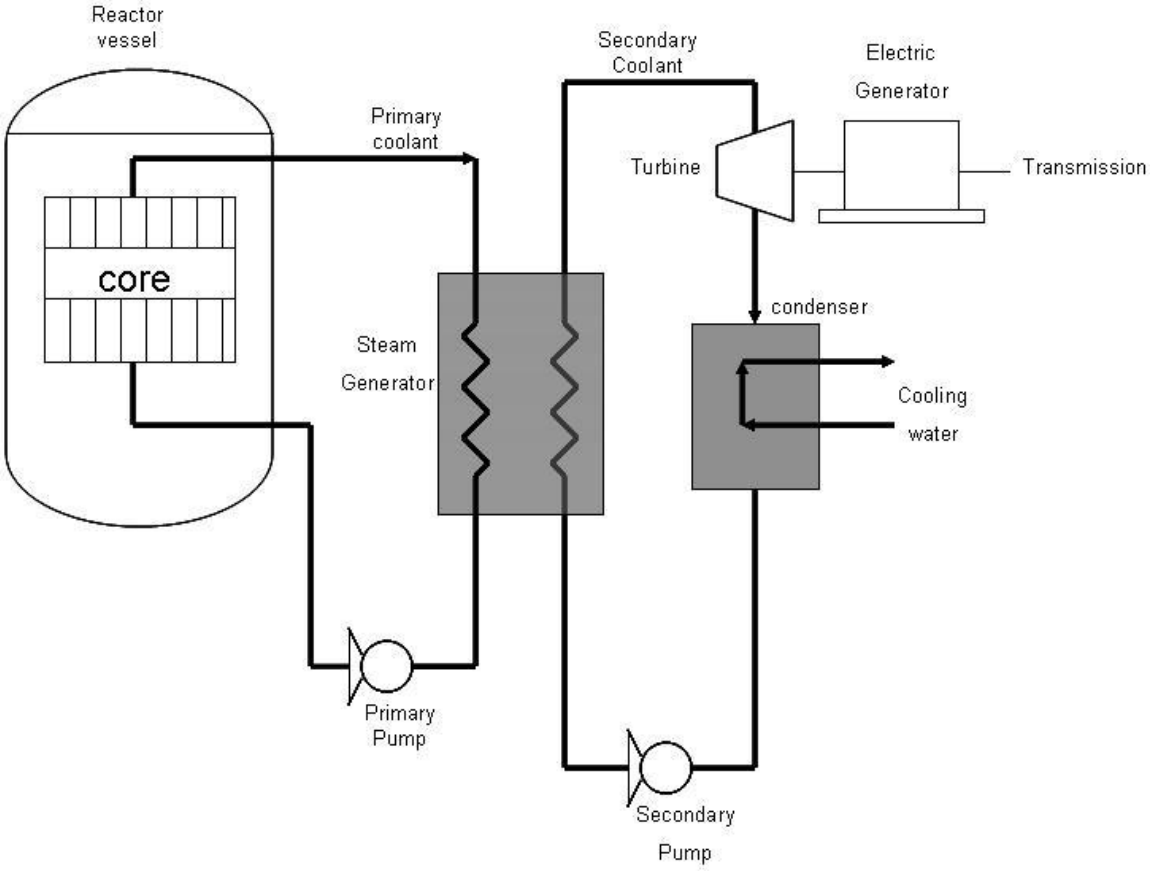

Figure 1-1 Schematic of working model of a pressurized water reactor (PWR)

(water) is allowed to boil, producing steam to run the turbine. Using a secondary coolant helps in making the nuclear reactor safe by preventing any nuclear waste from mixing with steam supplying the turbines. The primary coolant also serves the purpose of neutron moderator by slowing down the neutrons in the reactor vessel. Boric acid is added to the primary coolant to control the power generated in the PWR, as boron is a good absorber of neutrons. The heat transfer from the fuel rods to the primary coolant (deionized water) in the reactor vessel occurs by subcooled boiling. AOA is believed to occur when there is sufficient build up of deposits on the fuel rod under subcooled boiling conditions.

1.3 Organization of Thesis

This thesis has been primarily divided into 6 chapters. The first chapter introduces the project. The literature concerning previous research related to AOA is discussed in Chapter 2. The experimental equipment used for obtaining the pool boiling results are explained in detail in Chapter 3, and Chapter 4 gives the procedures employed in carrying out the experimental work. Chapter 5 presents the results obtained for pool boiling tests conducted at pressures of 100 psia, 200 psia, 500 psia and 1000 psia. The results of particulate boron and lithium deposits onto the Zr-4 clad are also presented in Chapter 5. Analysis of results obtained from the pool boiling experiments are developed and presented in Chapter 6. The effect of each parameter that affects the boiling heat transfer coefficient is discussed in Chapter 6. Chapter 7 gives the conclusions generated by this investigation.

2 LITERATURE SURVEY

2.1 Overview

This chapter discusses the previous relevant research work done regarding subcooled pool boiling and effect of particulate deposits on heat transfer.

2.2 Pool Boiling Heat Transfer

"Pool boiling is defined as boiling from heated surface submerged in a large volume of stagnant liquid" [Collier and Thome 1994]. If this liquid is at the boiling point, it is called 'saturated pool boiling', or if the temperature of the bulk liquid is below its boiling point, then it is called 'subcooled pool boiling'. As the surface temperature of the heater exceeds the saturation temperature of the liquid, nucleation begins on the heater surface.

The boiling process depends upon the nature of the surface, thermo physical properties of the fluid and vapor bubble dynamics [Sachdeva 2001].The results obtained from the boiling experiments are usually represented in the form of a "boiling curve" which is a plot of surface heat flux against the heater wall surface temperature (T_w). Boiling curves are sometimes presented with wall superheat instead of wall temperature. Wall superheat is defined as the temperature difference between the wall temperature and bulk fluid temperature (T_b). For boiling tests with coolant at saturation temperature, wall superheat (T_w-T_b) is equivalent to T_w-T_s, where T_s is the saturation temperature. Figure 2-1 shows the pool boiling curve for deionized water at atmospheric pressure. The region

AB is the natural convection heat transfer region, where the temperature gradients are set up in a pool.

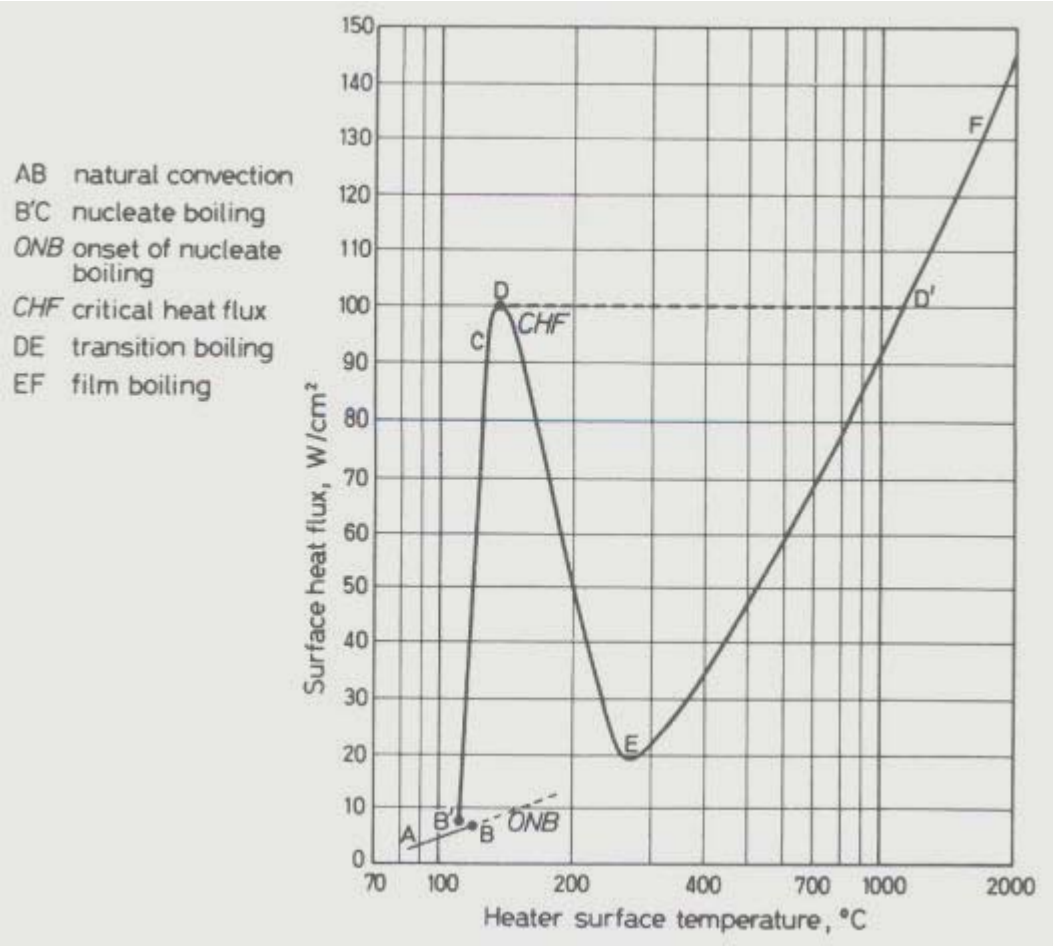

Figure 2-1 Pool boiling curve for water at atmospheric pressure [Source: Collier and Thome, 1999]

The onset of nucleate boiling (ONB) is the condition where the wall superheat temperature becomes sufficiently large to cause vapor nucleation at the heater surface. Nucleate boiling condition usually occurs close to the meeting point of AB and B'C as shown in Figure 2-1. The B'C in Figure 2-1 indicates the nucleate boiling region where vapour nucleation occurs at the heater surface. The nucleation begins with a few individual bubbles at low heat flux and with increasing heat flux, the vapour structure

changes because of bubble coalescence. With further increasing heat flux, vapour patches and columns are formed close to the surface. The critical heat flux (CHF or point D) indicates the upper limit of nucleate boiling where the interaction between the liquid and vapour streams restrict the liquid supply to the heating surface.

The transition boiling region (DE) is marked by the formation of an unstable vapour blanket over the heating surface that releases large patches of vapour at more or less regular intervals. At this point, the nucleation rate becomes so high that the flow of fresh liquid to the heater surface becomes restricted by the vapour film formed, causing a decline in the heat transfer coefficients. Wetting of the heating surface is only intermittent in this region. The film boiling region (EF) is characterized by formation of a stable vapor film which covers the entire heating surface and vapor is released from the film as regularly spaced bubbles. The heat transfer occurs by conduction and convection through the vapour. Heat transfer occurring through radiation becomes significant as the surface temperature of the heater increases to a very high value.

2.3 Boiling for Mixtures

Kamoshida and Isshiki have investigated the nucleate pool boiling of multi component lithium halide salt solutions at saturation under atmospheric pressure (Kamoshida and Isshiki, 1994). Kamoshida and Isshiki have performed pool boiling tests with binary system solutions of H_2O/LiCl and H_20/LiBr and ternary system solutions of H_2O/LiCl+LiBr. It was found that the boiling curves of salt solutions, in the higher heat flux regions, have a higher degree of superheat than deionized water. Their results also indicated that the mixed salt solutions have higher superheat in the transition region and

therefore have lower heat transfer coefficients than a normal solution. The reduction in heat transfer for mixed solutions was attributed to lower coalescence of bubbles than with the other solutions.

The work done on pool boiling indicates that the heat transfer coefficients for mixtures vary significantly from their pure components. For the deionized water-ethylene glycol mixture, system reductions in heat transfer coefficients on the order of 65% were observed on both smooth and the Turbo BIII tubes at a mole fraction of 0.5 (Schnelle, 2002). These experiments were conducted at saturation temperatures near atmospheric pressures. Schnelle noted that the variation in the heat transfer coefficient depends on many factors such as concentration of the solution, level of subcooling, and surface roughness (schnelle, 2002).

2.4 Influence of Particulate Deposits

Two studies have been found indicating that deposits and scaling generated during boiling considerably affect the heat transfer coefficient. Consequently, nucleate boiling heat transfer may be reduced by scale formation even when the bulk foulant concentration is below its saturation level (Steinhagen and Jamialahmadi 1990). Steinhagen and Jamialahmadi have studied the interaction between scale formation and bubble formation and its effect on heat transfer using calcium sulphate ($CaSO_4$) solution. It was found that the variation of heat transfer coefficient as a function of time was characterized by a sharp decrease to a minimum, followed next by an increase to a maximum and then a decrease to an asymptotic minimum. Pool boiling tests were performed using a saturated $CaS0_4$ solution over a period of 130 hours. The heat transfer

coefficient decreased by nearly 30% for a constant heat flux of 38.5 kW/m^2. This change in heat transfer coefficient is attributed to the dissolved and deposited $CaSO_4$. Particulate deposition occurs due to evaporation at the base of the growing bubbles. Even though nucleation behavior has been studied for pool boiling, there is no generally accepted model to explain bubble growth behavior due to the complexity of boiling heat transfer. With the addition of ethylenediaminetetraacetic acid (EDTA) to the $CaS0_4$ solution, the boiling heat transfer coefficients was found higher than pool boiling heat transfer coefficient for saturated $CaS0_4$ solution under similar test conditions (Steinhagen and Jamialahmadi, 1991). The increase in pool boiling heat transfer coefficient under the influence of EDTA was explained by the decreased calcium deposits on the heater surface, indicating that the deposits of the precipitate have an influence on the heat transfer coefficients.

Zhao and Tsuruta (2002) studied bubble growth behavior and developed the micro layer theory. The cycle of a bubble consists of two parts, one being the lifetime and other is the waiting time of nucleus activity. "The lifetime of the individual bubble consist of three durations: initial growth duration, final growth duration and the condensation duration before the individual bubble collapses" [Zhao and Tsuruta 2002].

2.5 Axial Offset Anomaly

An AOA is the unexpected change in the core axial power distribution during operation of PWR from the predicted distribution. The problem of AOA is widely reported in many of the operating PWR's. Axial offset indicates the difference between the power generated in the upper and lower halves of the core. A report on the

performance cycles of the Callaway nuclear power plant indicated a maximum axial offset of about 10% decrease and an axial offset of 6% increase in the power generated in the upper half of the core relative to the lower half (Konya, et all 1993). This study indicates the deviation from predicted power in cycles 4 and 5 of the Callaway power plant owned by Union Electric (St Louis, Missouri). One trend which was common in cycles 4 and 5 was that the negative deviation in the core axial offset was more significant that the positive deviation from the predicted power generation. Defloor (1993) has explained another significant AOA problem that has occurred in the DOEL Plant in Belgium (Konya, et all, 1993). During the plant's 11^{th} cycle of operation it was observed that there was a negative deviation from the predicted power and the maximum offset was found to be only about 4%. Further examination of AOA at the DOEL plant has revealed a thick layer of crud deposits on the surface of fuel. Investigations by Union Electric and Westinghouse into the AOA problem at Callaway plant indicated a 25 ppm increase in boron concentration after a power trip during the period when axial offset was observed. The increase in the boron concentration implies that there is a relation between axial offset observed in PWR and boron concentration on the fuel rod. Even though the performance reports of nuclear power plants indicate a strong relationship between the boron concentration and AOA, there has been little research done detailing the how boron concentration affects the axial offset. In order to understand the interaction between coolant concentration and the total power shifts, it is very important to study how the coolant concentration affects the heat transfer coefficients between fuel rods and the coolant.

The main reason for the AOA problem is believed to be the effect of particulate deposits on subcooled nucleate boiling (Frattini, et.all 2001). Earlier studies indicated that subcooled nucleate boiling causes corrosion deposition in the upper spans of the fuel assemblies. Although the main causes of AOA are known in general, the mechanism is still not well understood. Corrosion deposits tend to occur at the boiling regions. To understand the mechanism of deposition, it is essential to understand the relation between rate of heat transfer and deposition. Even though there have been extensive studies on the effect of some additives like $CaSo_4$ on heat transfer coefficient, there has been no significant work done on the effect of boron and lithium metaborate precipitation on heat transfer coefficient. Hence, an experimental study was proposed to study the effect of coolant solution concentration on heat transfer characteristics at test conditions simulating the fuel rod of a PWR.

2.6 Objectives

The primary objective of this project was to obtain experimental data for subcooled pool boiling heat transfer coefficients on Zircaloy clad rods for coolants with varying concentrations of boron and lithium. The experimental data obtained will include influence of coolant concentration, bulk fluid subcooling, bulk fluid system pressure and heat flux on heat transfer coefficient. In reference to the pool boiling curve in Figure 2-1, the heat flux in all the boiling tests performed varies between points A and C in Figure 2-1. The aim was to obtain the boiling test results lies in between points A and C in the reference boiling curve Figure 2-1. The project also aims at obtaining characteristic information about the deposits of boron and lithium on Zr-4 rods including a visual

record of nucleation for subcooled boiling on Zr-4 clad rods with longer duration of boiling tests. The aim was to obtain an average of the deposition of boric acid and lithium metaborate for the duration of tests lasting more than 100 hours.

3 EXPERIMENTAL EQUIPMENT

3.1 Overview

This chapter presents a description of the experimental Equipment used for pool boiling tests. The experimental test facility was designed in such a way that it would simulate the conditions of a fuel rod in the core of a Pressurized Water Reactor (PWR). This was done using a test chamber which could withstand very high pressures typical of a PWR vessel. An electrical test heater was used to simulate the fuel rod of a PWR. A specially built 'DC electrical power supply unit' was used to power the test heater. A nitrogen cylinder and a compressed gas accumulator were used in combination to increase the coolant pressure to very high values. Pool boiling conditions were assumed for all the experimental tests conducted, because simulating the flow conditions of the primary coolant in a PWR is a very complex task requiring expensive equipment. The details of all the equipment used to perform subcooled boiling tests are discussed in this chapter. However, some subcooled boiling tests were conducted at a pressure of 100 psia, using a preliminary somewhat different experimental set-up, somewhat different from that of the existing experimental set-up. To differentiate between the test set-up used for lower pressure (100 psia) and higher pressures, the existing pool boiling test equipment is hereafter referred to as "new pool boiling equipment" (higher pressures). This chapter primarily is divided into two parts. The first part describes the preliminary pool boiling test facility and the second part provides a detailed description of the new pool boiling test facility. As some of the equipment used in both preliminary and new pool boiling test setup is the same, it is explained in greater detail under the new experimental set up.

3.2 Preliminary Pool Boiling Test Equipment

The pool-boiling test facility consisted of a high-pressure test chamber, bulk heater, test heater, nitrogen cylinder and a hydro-pneumatic accumulator. A schematic diagram of the pool boiling test facility is shown in Figure 3-1. The experimental investigation necessitates use of a test chamber, which can operate under high pressures. Typically the pressures of the coolant in a PWR range from 6.8MPa (1000psia) to 15.5MPa (2200psia) (Loftness, 1964). A unique high pressure vessel with view ports on either side of the pressure vessel was used for the pool boiling test setup.

The pressure vessel was designed and constructed by Van Vleet (1985) to investigate subcooled and saturated nucleate boiling on thin wires under transient conditions under high pressure conditions. The pressure vessel, made of 316 stainless steel, was used for conducting the experimental investigation. The test chamber (pressure vessel) was 40.64 cm in length with outer diameter of 12.065cm and inner diameter of 9.8425cm (Vleet, 1985). The test chamber had two optical ports located on either side of the chamber, facilitating the observation of the bubble formation on the test heater. The clear fused quartz windows were seated in tapered Teflon cushioning. The windows were held tight by clamping bushings with the help of eight socket head screws.

The bulk heater was inserted axially at the center of a flange at one end of the test chamber. The specially built test heater was placed axially at the center of the other flange. The large diameter base and inside mounting of the bulk and test heaters accommodate high pressures by means of a compression fitting in the holder base. Copper O-rings [Duniway, 2006] prevent leakage from the test chamber on the bulk

heater end. The bulk heater's function is to raise the temperature of the coolant in the test chamber. A 500 W immersion type cartridge heater manufactured by Watlow Inc [Watlow, 2006] was used for bulk heating of the water for pressures 100 and 200 psia.

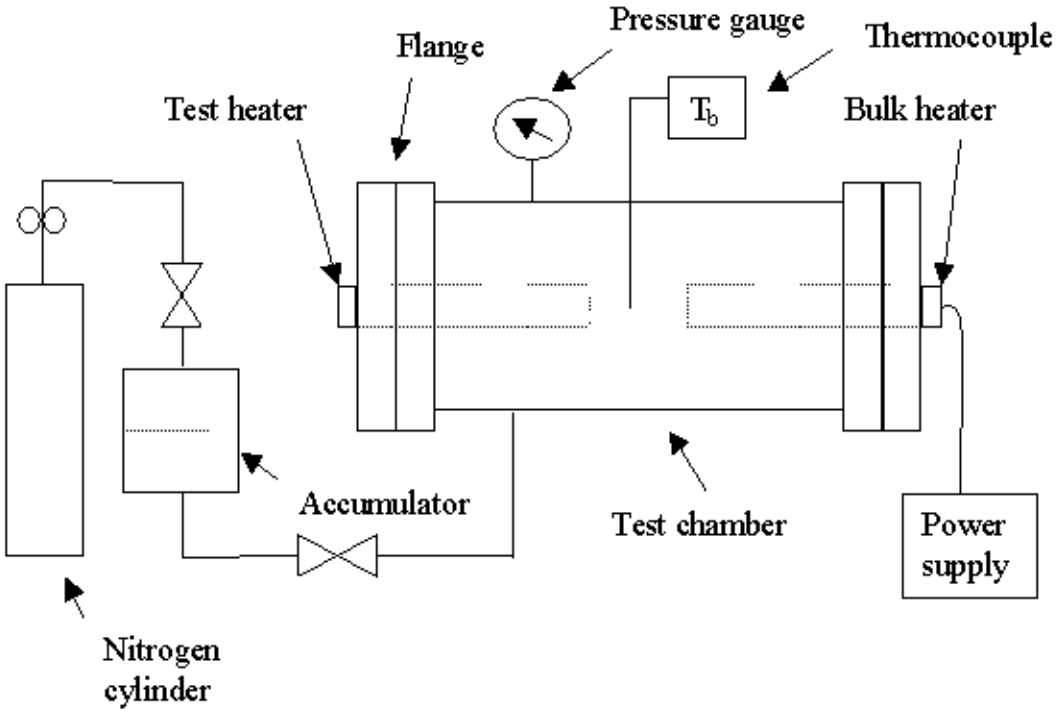

Figure 3-1 Schematic diagram of pool boiling test equipment

The test heater had Zr-4 cladding and was obtained from a commercial reactor fuel supplier. Care was taken to prevent any damage to the outer surface of cladding. The heating element of the test heater was made of inconel 718. The test heater had an outer diameter of 9.5 mm (0.374 inch) and a heating element length of 2.5 cm (1 inch). The test heater simulated the conditions of a fuel rod inside a pressurized deionized water nuclear reactor. PTFE O-rings were used for effective sealing between the test heater flange and the pressure vessel. Power supplied to the test and bulk heater was manually controlled with potentiometers to regulate the amount of heat transfer to the fluid inside the test

chamber. The test heater and bulk heater were operated on a 115 V AC 60 hz power supply.

A combination of a nitrogen cylinder and an accumulator was used to regulate the pressure of the fluid in the test chamber. As the water is incompressible, nitrogen gas is used to indirectly build pressure inside the testing chamber. The gas compressed hydraulic accumulator contained a bladder to prevent the nitrogen from mixing with the deionized water. A pressure regulator connected to nitrogen cylinder controlled the pressure inside the test chamber. A pressure transducer connected to the test chamber indicated the pressure inside the testing chamber. A relief valve was used to bleed the excessive pressure. A T-type thermocouple was used to monitor the bulk temperature of the coolant. The voltage across the test heater was measured by a voltmeter connected in parallel. As measuring current requires placing an ammeter in series to the electrical circuit, a one ohm resistor was connected in series to the test heater. The current through the test heater was measured indirectly by monitoring the voltage drop across the resistor. The use of potentiometers helped to better control the electrical power supplied to the test heater by preventing voltage fluctuations.

3.3 New Pool Boiling Test Facility

A new electrical test heater was acquired to operate at the higher pressures and higher temperatures. A 100-ampere DC power supply already existing in the lab was used for supplying the power to the heater. Changes were made to the existing pool boiling test setup for operation of the new test heater. A schematic of the new pool boiling test

facility is shown in Figure 3-2. Details of each component for the new pool boiling setup are explained later in this chapter.

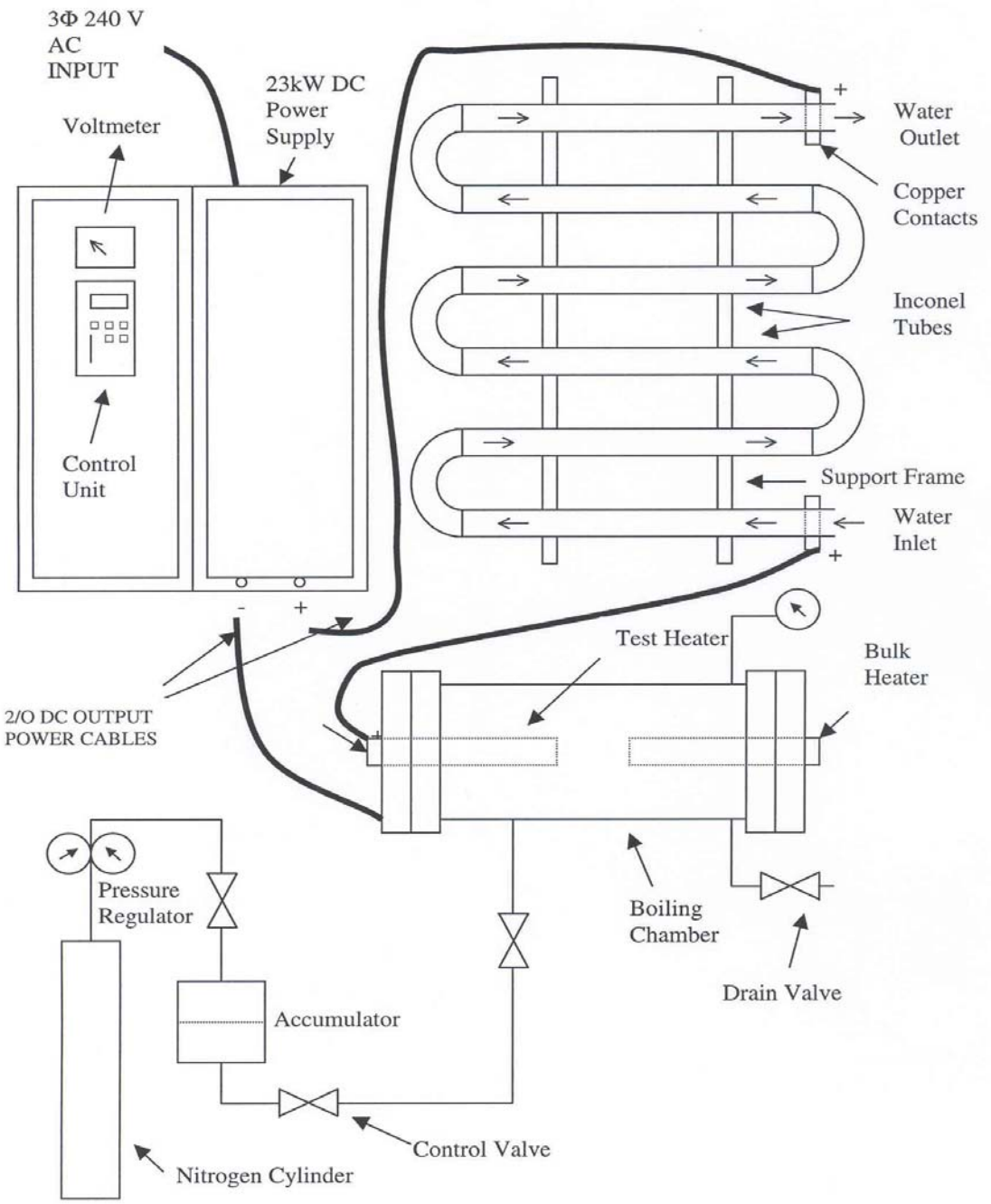

Figure 3-2 Schematic of new pool boiling test facility

3.3.1 Test Heater

The new test heater clad with zircaloy drew power from the 23 kW DC power supply unit. Stern Laboratories Inc. (Hamilton, Ontario, Canada) manufactured the heater. A picture of the test heater with four thermocouples can be seen in Figure 3-3. A specially designed inner sleeve with holes drilled axially for four K-type thermocouples and INCONEL 718 filament was press fitted into the Zr-4-tube as seen in Figure 3-4. The fiberglass sleeve acts as a thermal insulator for copper lead conductor. The physical parameters of the heater were not changed from that of the previous heater to maintain the same heating configuration.

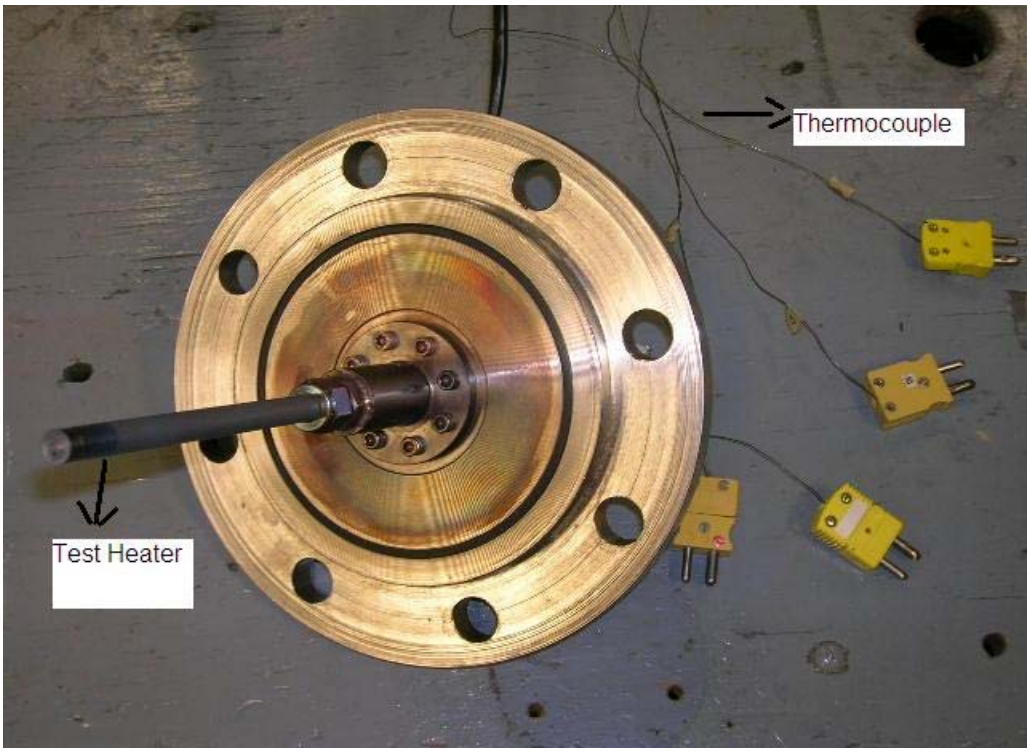

Figure 3-3 Photograph of test heater and connecting flange

The physical parameters of the heaters are as follows.

Zr-4 Sheath O. D =0.374inches.

Sheath Overall Length =6.75 inches.

Maximum Heat Flux = 3 MW/m^2.

Heated Length (boiling region) = 1.0 inch.

The schematics of front and side view cross sections of the test heater are shown in Figure 3-4. The front cross section shows the location of the heating element along with dimensions from both ends of the test heater. The side cross sectional view shows the orientation of thermocouples which are placed axially at 90° angle to each other.

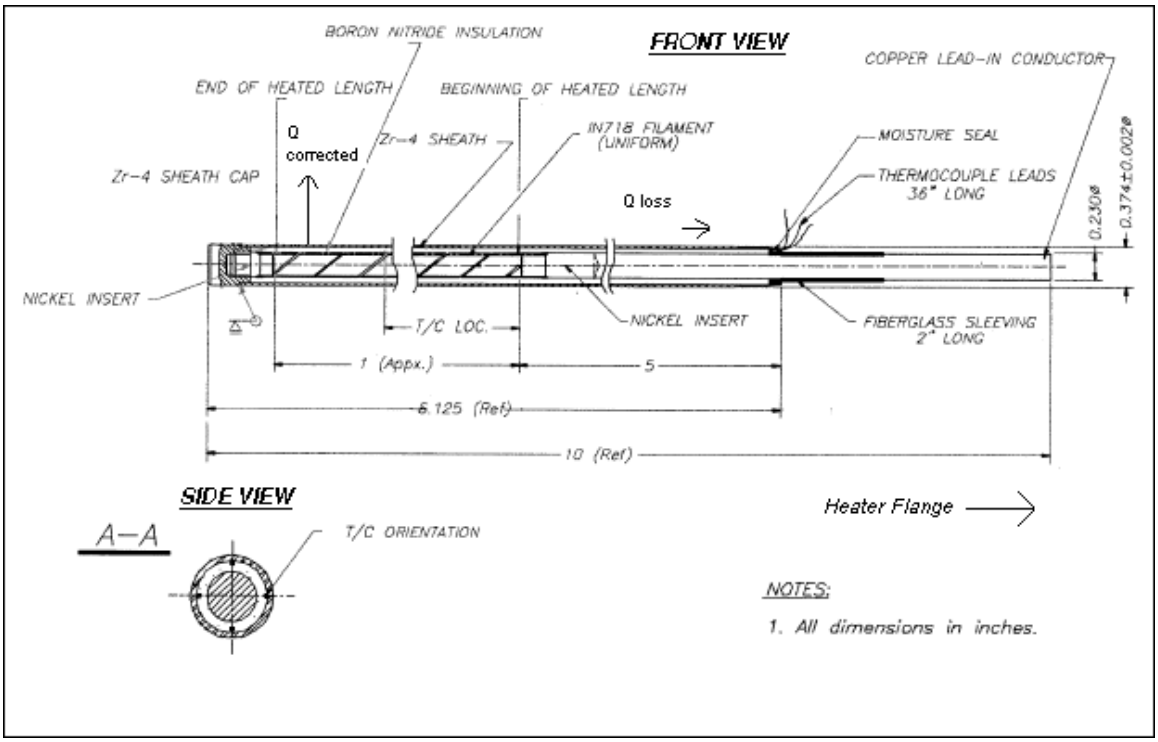

Figure 3-4 Schematic of cross section of test heater

3.3.2 Electrical DC Power Supply Unit

The electrical DC power supply had a combination of three 25 kVA single phase dry type distribution transformers and six silicon controlled rectifier (SCR) units to supply the required DC output from 3 phase AC input. The power supply system converted 208 Volts AC, 3 phase, 3 wire, and 60 Hz delta connected power supply into a controlled output. "The output ranged from '0 to 120' VDC output at up to 180 amperes" [Hamilton, R C, 2000]. The power supply had operational limits due to the possible damage of the silicon controlled rectifiers (SCR's) at their lower thermal limit. This unit cannot be operated beyond 130 VDC. The operating range of the power supply unit is represented in Figure 3-4 where the voltage and the current output should be within the envelope given. The load powered by the "electrical DC power supply" was required to have a minimum electrical resistance of 0.42Ω to prevent damage to the SCR's.

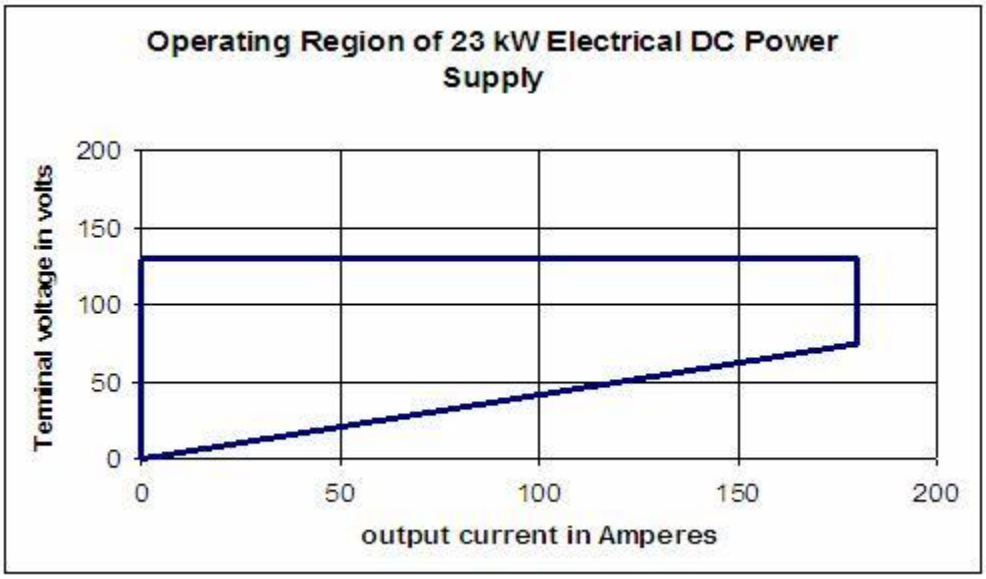

Figure 3-5 Operating limits of 23kW DC power supply unit

The maximum operating current to the load from the “electrical DC power supply” was 180 A. The total heat generation due to electrical losses depended upon the ‘current’ through the resistor and the electrical resistance of the resistor. The electrical resistance of the test heater (0.07Ω) does not meet the minimum requirement condition for the operation of the “DC electrical power supply”. Hence, an additional load was added in series to the electrical test heater. The resistor (load) prevented damage to SCR. The power supplied by the “Electrical DC Power Supply” was controlled manually using the keys on ‘Fisher Rosemount DPR950 Controller display’.

3.4 Heat Exchanger

The use of the ‘electrical DC power supply unit’ was restricted by the electrical resistance of the total load. An additional resistor was added in series to the test heater to ensure that the total electrical resistance of the load is in the operation range of the ‘electrical DC power supply unit’. Due to the high current in the resistor, the heat generated in the resistor (conduction losses) was very high. At a maximum current of 180 A, the heat generated is 18 kW for a resistor with an electrical resistance of 0.55Ω. Hence, a resistor with good heat dissipation characteristics was fabricated. As heat transfer by natural convection is not sufficient, the heat generated in the resistor must be removed by cold water. “Inconel 600” tubes served the dual purpose of acting as a resistor in the electric circuit and providing an effective means of heat dissipation. Hence, the name “heat exchanger” is used instead of the conventional “resistor”.

Laboratory tap water was used to cool the inconel tubes. The unique property of inconel is that its electrical resistivity remains fairly constant over a broad range of temperatures. The photograph of the heat exchanger is provided in Figure 3-6.

Figure 3-6 Photograph of Inconel heat exchanger

3.4.1.1 Heat Exchanger Design Calculations

The length of the inconel tubes was calculated from the electrical resistance required. The resistivity of inconel is known to be 1.03 μΩm at 20° C. Even at 100°C, its resistivity is 1.04 μΩm. The electrical resistance of a tube is given by the equation (3.1)

$$R = \frac{\rho l}{A} \tag{3.1}$$

where:

R = resistance of tube in ohms

A = cross-section of the tube in sq m.

ρ = electrical resistivity of material (inconel) in Ωm.

L = length of the tube in meters.

The heat generated had to be removed constantly to avoid the over heating of the inconel tubes. The minimum and maximum allowable electrical resistance of the heat exchanger (resistor) was 0.41Ω and 0.71Ω, respectively. Considering an electrical resistance of 0.55Ω (average) for the heat exchanger, the maximum heat generated was 18 kW. Cold tap water was circulated through the inconel tubes to remove the generated heat.

The design characteristics of the heat exchanger tubes were as follows:

- The total electrical resistance of the tubes should lie within the thermal limit of the 'electrical DC power supply'. Consequently, the electrical resistance of the heater has to be greater than 0.41Ω and less than 0.71Ω.
- The rate of heat dissipation in the inconel tubes (heat exchanger) is dependent on the flow rate of the water through the inconel tubes.

Turbulent flow was maintained in the inconel tubes to ensure the maximum heat transfer between the tubes and water. Hence, the velocity of the water inside the tubes was high enough such that the Reynolds number was at least 2300 (transition for conduits). A hose of length 15 meters supplied tap water to inconel tubes. As a result, a

maximum pressure drop of 40 psi was assumed over total length of hose and tubes. The flow velocity was computed from the Darcy Weisbach formula using Moody's chart for the friction factor.

The following variables were used in the calculations:

D_o = outer diameter of the tube in meters.

D_i = inner diameter of the tube in meters.

h_l = pressure difference between source and outlet of water in meters of hg.

P_1 = Supply pressure of water at inlet to the heat exchanger in N/m^2.

P_2 = Outlet Pressure of water in heat exchanger in N/m^2.

f = friction factor.

L = Total length of the Inconel tubing in meters.

Re = Reynolds number

ρ= Density of the fluid in kg/m^3

μ = Dynamic viscosity of the fluid in N/m^2.

Nu = Nusselt Number

Pr = Prandtl Number

K = Thermal conductivity of the fluid in W/mk.

Q = flow rate in m^3/sec.

A = hollow cross section of the Inconel tubes in m^2.

V = velocity of the water flowing through the tube in m/sec.

Q = Water flow rate in heat exchanger in m^3/sec

K_{water} = Thermal Conductivity of water at 300K =0.613 W/mk.

E_{max} = Maximum heat generated in Inconel tubes in Watts.

T_i = Inlet Temperature of water entering the heat exchanger in ^oC.

T_o = Outlet Temperature of water leaving the heat exchanger in ^oC.

A_{surf} = Surface area of the heat exchanger in m^2.

The flow calculations were performed with an initial assumption of D_o =.25" and L=1m. The final dimensions of the inconel tubes were obtained by iterating the initial

guess values. The iterations were done with tube diameter varying from 0.25 inch to 1 inch.

$$\Delta P = P_1 - P_2 \tag{3.2}$$

The pressure of the tap water supply in the laboratory was 40 psig. The outlet pressure was atmospheric pressure and the pressure head was calculated from equation (3.2). The pressure head difference in meters is h_l. The friction factor f was initially guessed and corrected with iterations. The velocity of the water inside the tube was calculated using Darcy's formula using equation (3.3)

$$V = \sqrt{\frac{2gD_i h_l}{fL}} \tag{3.3}$$

The Reynolds number was computed from equation (3.4) once the flow velocity and physical properties of the fluid were known.

$$\mathrm{Re} = \left(\frac{VD_i \rho}{\mu} \right) \tag{3.4}$$

If the Reynolds number was greater than 2300 (critical Reynolds number for internal flow) it was considered to be turbulent flow. Moody's chart gives a graphical relation between the Reynolds number, roughness factor, and friction factor. The relative roughness value for tubes was assumed as 0.004 based on the surface finish of the tubes. Hence, the friction factor was estimated from Moody's chart.

The Dittus-Boelter equation (3.5) was used to determine the Nusselt number for turbulent flow in tubes.

$$Nu = 0.023\, Re^{\left(\frac{4}{5}\right)}\, Pr^{n} \tag{3.5}$$

where n is 0.4 for heating (surface temperature Ts > Tb bulk temperature) and Pr for water is 5.8466. The water flow rate can be calculated from the velocity by equation (3.6)

$$Q = A * V \tag{3.6}$$

The coefficient of convective heat transfer h can be determined from the Nusselt number using the equation (3.7) as follows:

$$h = \left(\frac{NuK_{water}}{D_i} \right) \tag{3.7}$$

The maximum heat generated is 18 kW. For the cooling to be efficient, the outlet temperature of water through the inconel tubes should be less than its boiling temperature. The heat lost by the inconel tubes is gained by the flowing tap water. From an energy balance , the outlet temperature of water from the inconel heat exchanger was calculated using

$$T_o = T_i + \frac{E_{\max}}{hA_{surf}} \tag{3.8}$$

Iterations of standard values of inconel tube diameter were carried out using equations (3.1) to (3.8) until the electrical resistance of heat exchanger was higher than 0.41Ω. A sample calculation is included in the appendix. It was found that an inconel tube diameter of half inch and length of thirty feet would satisfy the requirements. A tap water flow rate of 2.9gpm was found to be sufficient to cool the inconel tubing.

To fabricate the heat exchanger, the 30 ft long inconel tube was cut into 6 pieces of 5 feet each. The inconel tubes were laid parallel, ends joined by copper tube bends as seen in Figure 3.5. Wooden frames supported the tubes and two garden hoses transported the tap water flow to and from the heat exchanger.

3.5 Bulk Heater

A bulk heater was used to control the bulk temperature of the fluid. As the boiling tests were conducted at higher pressures, the saturation temperatures were also high; hence more power was needed to raise the temperature of fluid. So the preliminary bulk heater of 500W capacity was replaced with a specially built 2 kW "Fire" rod immersion type heater (Watlow, Inc.) suitable for operation at pressures up to 2000 psia. The input power to the heater was controlled using a conventional rheostat. A photograph of the bulk heater is given in Figure 3-7.

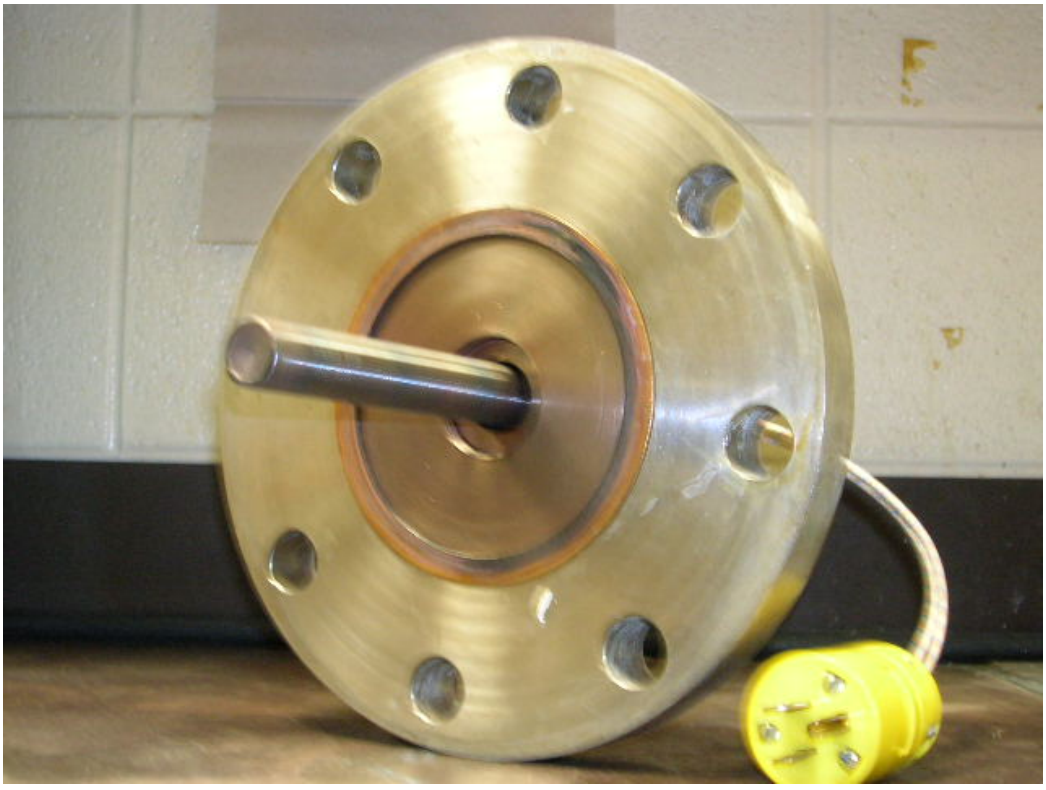

Figure 3-7 Bulk heater with flange and copper gasket for the preliminary test equipment

3.5.1 Electric Circuit

The DC power supply supplied electrical current to the test heater and heat exchanger which were connected in series. The resistance of the test heater was very low at about 0.07Ω. The total resistance of the load was within the operational limits of the DC power supply unit. A special control unit on the DC power supply was used in metering the power input to the heater. A voltmeter in conjunction with the readout of the control unit indicated voltage across the load and total power supplied to the load. The test heater was a sheath return type heater. It is designed in such a way that only the positive terminal of power supply was connected directly to the heater. The negative terminal was connected to the test chamber. The test chamber was electrically grounded. Sheath return type heaters are more commonly used for high current applications.

3.5.2 High Speed Camera

To understand the phases of the bubble growth at the nucleation sites, a high-speed camera was used. Because the bubbles rise and collapse very quickly, it is a tough task to identify the exact growth process of bubbles rising from the heater surface. A high-speed camera can capture images at a relatively fast rate compared to a conventional movie camera. Some high speed cameras can capture images at speeds of 12,000 pictures per second (PPS) where conventional movie cameras capture images at a speed of 30 PPS.

The high-speed camera used here was a 'HYCAM model # 41-0005' manufactured by Redlake Corp and was used for observing the bubble growth behaviour.

A photograph of the Hycam is provided in Figure 3-7. It was a high speed 16mm motion picture camera with a rotating prism. The maximum speed of the camera was 11,000 half frames per second. The film transport had a maximum film capacity of 400 feet of standard thickness film where spools of 100', 200' and 400' films can be loaded in the camera. The PPS dial in the high-speed camera was used to set the frame rates as per the requirement. The capture speed of the camera was adjusted by rotating the dial in conjunction with the multiplier switch. The minimum speed was 20 frames per second. The shutter exposure ratio used is 0.4. Exposure time is given by shutter exposure ratio divided by the frame rate.

Figure 3-8 photograph of high speed camera Hycam model '41-0005'

Deciding the optimum speeds for running the film was an important task. With increase in speed, higher images can be captured but capturing images at higher speeds require very good lighting conditions. The maximum speed of the film is limited by the lighting conditions. The high-speed camera is placed in front of optical ports of the test chamber to observe the bubbles. As the object of focus is inside the high-pressure chamber, penetration of light is restricted by size of optical port. Two electric bulbs were used to provide enough illumination through the optical ports. A spool of Kodak Hawkeye Surveillance film 16mm x 450', type 2485 film was used to capture the boiling images. The Kodak Hawkeye Surveillance film was designed for conditions with less light and is commonly used for surveillance of traffic at night time.

3.5.3 Pressure Transducer

A pressure transducer was used to monitor the bulk fluid pressure inside the test chamber. The pressure transducer used for the preliminary pool boiling set up was replaced with a pressure transducer measuring gauge pressure, Model PX35K1-3KGV (Omega Engineering, Inc.). The pressure transducer was calibrated for a range from 0 to 3000 psig and had an operating temperature range from 15 to 70^{o}C. A stainless steel tube connects the pressure transducer and test chamber separating the transducer from the heat generation in the test chamber. A pressure transducer was preferred over a pressure gauge for better accuracy. The calibration data for the transducer is provided in Table 3-1. The excitation for the transducer was 10 V DC. The accuracy of the transducer is 0.25% which includes linearity, hysteresis and repeatability. The characteristics of the pressure transducer are given in Table 3-2.

The transducer was connected to a strain gauge panel meter to read the pressure. The DP25-S strain gauge panel meter (Omega Engineering, Inc.) used the calibrated output voltage from the transducer to display the pressure in psi. The DP25-S panel meter had a digital display, and its broad scaling capability allowed for the display of most engineering units (Omega Engineering 2002). The strain gauge panel meter also had a facility for biasing the output value for measuring the change in pressures.

Serial No	Pressure (Psig)	Transducer Output Data (mV DC)
1	0.0	0.000
2	1500.0	15.031
3	3000.0	30.004
4	1500.0	15.055
5	0.0	0.015

Table 3-1 Calibration data for Pressure transducer (Omega Engineering Inc.)

Serial No	Parameters	Value
1	Balance	0.310 mVdc
2	Sensitivity	30.004 mVdc
3	Input Resistance	350.3 ohms
4	Output Resistance	351.0 ohms

Table 3-2 Pressure transducer characteristics (Omega Engineering, Inc.)

4 EXPERIMENTAL PROCEDURE

4.1 Solution Preparation

Boiling tests were performed with pure deionized water, boric acid solution and lithium metaborate solution with various concentrations.

PPM or parts per million can be defined as the number of solute particles per million parts of Solution. It can be represented by equation (4.1)

$$PPM = \left(\frac{Mass\ of\ solute}{Mass\ of\ solution} \right) \times 1000000 \tag{4.1}$$

One ppm is equivalent to 1 milligram of solute per liter of deionized water (mg/l). The weight of the solute can be calculated from equation (4.1) when the parts per million and weight of the solution are known.

Boiling Experiments were conducted at 500 PPM, 1000 PPM, 2000 PPM and 5000 PPM concentration levels. Measurement of the weight of the solute (boric acid and lithium metaborate) was done with help of a weighing scale. The weighing scale could measure a maximum weight of 2.61 kg. The least count of weighing scale is 0.1g. The boric acid solution was prepared by mixing the measured quantity of boric acid powder into a measured quantity of distilled deionized water. Typically, for every pool boiling test conducted, the coolant required was about a gallon. The weight of solute corresponding to a solvent volume of one gallon is presented in Table 4-1. The values shown in the Table 4-1 are applicable for both boric acid and lithium metaborate solutions. The uncertainty in the measurement of the weight of the solute is 0.1g.

Serial No	Coolant Concentration (PPM)	Weight of the solute (g/gallon)
1	500	1.9 ± 0.1
2	1000	3.8 ± 0.1
3	2000	7.6 ± 0.1
4	5000	19 ± 0.1

Table 4-1 Coolant concentration and weight of the solute

4.2 Boric Acid

Boric acid is a white powder soluble in water. The chemical properties of boric acid are presented below obtained from material safety data sheet [msds-fisher, 2005].

Physical State: Solid (powdered)

pH value**:** 3.6-4.0 (4% aqueous solution)

Solubility: 4.9g/100g in water @ 20^{o}C

Specific Density: 1.44 (water=1.0)

Molecular Formula: H_3BO_3

Molecular Weight: 61.83

A boric acid solution in deionized water was used as coolant to determine the pool boiling heat transfer coefficient. The boiling tests were performed with varying concentration of 500 ppm, 1000 ppm, 2000 ppm and 5000 ppm, respectively.

4.3 Lithium Metaborate

The Physical and Chemical Properties of lithium Metaborate are as presented below obtained from the material safety data sheet [msds-fisher, 2005]

Physical State: Crystalline Powder

Density: 1.397 g/cm^3 at 20^o C

Molecular Formula: $LiBO_2$

Melting Point: 845^{o}C

The boiling tests were performed with the same concentration for boric acid and lithium metaborate solution. The pool boiling tests were performed with concentrations of 500 ppm, 1000 ppm, 2000 ppm and 5000 ppm lithium metaborate solution in deionized water.

4.4 Experimental Procedure

The experimental procedure used to obtain the boiling test data with the new setup was as follows:

1. The pressure vessel, test heater and bulk heater were cleaned with acetone to remove any deposits, settled due to earlier experiments. The cleaning of the surface ensures that all the boiling tests are performed at similar conditions.

2. The flanges of the pressure vessel were firmly fastened with eight bolts. Copper o-ring provides the necessary sealing arrangement. Care was taken to avoid leakage as improper fittings may lead to mechanical failure at high pressures. The

3. The solution for the boiling test was prepared. A weight balance was used to measure the quantity of the solute in solution. The test chamber is filled with prepared solution through the filling port.

4. A T- type thermocouple (model HTQIN 316G-12) made of copper and constantan [omega, 2005] was used to measure the temperature of the bulk fluid. "HTQIN 316G-12" is a "quick disconnect" type thermocouple.

5. The four k-type thermocouples, which measure the surface temperature of the electrical test heater, were connected to the thermocouple reader [DP-24 T, 2001] mounted on the measurement panel.

6. The pressure of the coolant was measured from the transducer connected to the test chamber through 3/16" stainless tubing. The output from the transducer was fed into the DP-25 strain gage panel meter.

7. The pressure of the coolant in the test chamber was then increased to the required level. The required pressure was obtained by pressurizing the gas side of accumulator from a nitrogen cylinder. The pressure was controlled by a regulatory valve on nitrogen cylinder. This resulted in an increase in the pressure of the solution inside the test chamber.

8. After the solution was pressurized to the required pressure, the electrical bulk fluid heater was turned on to heat the solution. The amount of heat supplied to the

solution was controlled by regulating the power supplied to bulk fluid heater. A rheostat was used to regulate the power supplied to the bulk heater. The temperature of the bulk fluid (coolant) was maintained at a constant temperature equal to the test subcooled condition. For 20^{o}C subcooled condition at 1000 psi pressure, the coolant is maintained at temperature of 264.8^{o}C, 20^{o}C below saturation temperature of 284.8 ^{o}C.

9. Power was supplied to the "electrical DC power supply" by turning on the 3ϕ, 240 volts, 100 Amps AC input. The power input to the test heater was slowly increased with the help of a control unit on the DC power supply unit panel. As the input power to the test heater was increased, the power supply to the bulk heater was decreased to keep the bulk temperature constant.

10. Cold water was circulated through the heat exchanger to remove the heat generated due to its electrical resistance.

11. The voltage drop across the electrical test heater was measured using a multimeter. The voltmeter on the 'electrical DC power supply unit' panel measured the voltage drop across the total load.

12. The current flowing through the electrical test heater was measured using a clamp- on type ammeter to avoid breakage of the circuit [fluke, 2005].

13. The power supplied to the test heater was increased in steps, and the measurements mentioned in steps 3, 4, 5, 11 and 12 were taken at each step after the test heater temperatures reached a steady state.

14. The test chamber was brought back to ambient conditions after the test was conducted by gradually decreasing the power supplied to the test heater and bulk heater respectively.

15. The pressure of the coolant was decreased by bleeding off nitrogen gas in the accumulator.

4.5 Equipment Maintenance

This section discusses the details about equipment failures that occurred during the subcooled pool boiling tests and precautions that needed to be taken for proper functioning of the pool boiling experimental equipment.

The test heater hook up wire was burnt, causing sparks and disrupting the power circuit of the boiling set up. It was found that improper thermal insulation caused the two power supply wires to get in contact shorting the circuit. Since the temperature of the pressure vessel rises to about 250^{o}C at 1000-psia pressure, the power cables should have excellent electrical and thermal insulation. Fiberglass sleeve and high temperature resistant thermal tape was used to safeguard the power supply wires.

The quartz window in the optical view port, which was subjected to high pressure and temperature, had a high thermal gradient across its thickness. The quartz window used in the pool boiling tests failed, even when the operating temperature was below the maximum working temperature of quartz window. The cracking of the quartz window has been observed thrice during the operation of tests. The reason for breakage is likely due to the additional stress on the quartz window due to the unequal expansion rates of

the stainless steel housing and quartz. It was thought that the failure could be due to improper cushioning and failure of the gasket. A new gasket (size 1.75" OD X 1.0" ID X 0.0625" thickness) made of 'Non Asbestos C4401' was used to replace the failed gasket [Ernest, 2005]. The 'Non Asbestos C4401' material is a high temperature resistant and high pressure resistant material. These gaskets are manufactured by combining non – asbestos fiber with rubber. The non–asbestos C4401 can operate at a maximum temperature of 399^{o}C. Replacing the gaskets has fixed the problem to a large extent. However, care should be taken to avoid sudden changes in temperatures of test chamber as it may lead to cracking of the optical windows.

4.6 Data Reduction

The measured parameters in the pool boiling test are the bulk fluid temperature in the test chamber, surface temperatures of the test heater, the current flowing through the heater, the pressure inside the test chamber and the total voltage drop across the test heater and the heat exchanger. These measurements are used in the determination of heat flux and temperature difference between the test heater surface and the bulk fluid. The details of calculations for determination of heat flux are presented below.

The variables and constants used in the calculations of heat flux are as follows:

R_I = diameter of heater element (filament) = 0.0031111m

R_{CI} = copper sleeve radius = 0.004178m

R_O = outside diameter of heater rod (cladding) = 0.00475m

Z_{LB} = boiling region length = 0.0254 m

$Z_{LNC} = Z_{LB}$ = natural convection length =0.0254 m

Z_{EER} = copper sleeve length = 0.0508 m

A_{CU} = cross – sectional area of copper sleeve in m^2.

V = voltage drop across heater in volts

I= electrical current flowing though the heater in amperes

R = resistance of the test heater = 0.07Ω

T_{CAVE}= average temperature of heater surface which is determined from four thermocouple temperatures T_{C1}, T_{C2}, T_{C3}, T_{C4} in ^oC.

$T_{KAVE} = T_{CAVE}$ +273.15 K

T_{BAVE} = bulk fluid temperature (^oC)

R_C = thermal contact resistance between copper sleeve and zr-4 clad (m^2 .K/W)

ΔT_L = temperature difference between T_{CAVE} and bulk temperature (^oC)

R_{TOT} = total thermal resistance (m^2.K/W)

Q = total input power to the test heater. (W)

q" = heat transfer flux (W/m^2)

K_{CONDZR} = thermal conductivity of zircalloy (W/m.K)

$K_{CONDZR} = 7.51 + 0.0209T_{KAVE} - (1.45*10^{-5})\ T^2_{KAVE} + (7.67*10^{-9})\ T^3_{KAVE}$ (W/m.k)

ΔT_{DEL} = Temperature difference between heater wall temperature and bulk temperature

Q_{LOSS} = heat loss in cladding due to conduction in copper sleeve (W)

K_{CONDCU} = thermal conductivity for copper = 391.0 W/ (m. K)

The electrical power input to the test heater is given by equation (4.2). The current was measured from a special ammeter, which was used to measure high currents by using the principle of magnetic field induction.

$$Q = I^2 R \tag{4.2}$$

The measurements from the four thermocouples located between the cladding and copper sleeve of the test heater was used for computing the average surface temperature of test heater. The four thermocouples were located at 90^o angle to each other from the center of heater. The average temperature of the test heater is given by equation (4.3) as follows :

$$T_{CAVE} = \left(\frac{T_{C1} + T_{C2} + T_{C3} + T_{C4}}{4} \right) \tag{4.3}$$

The actual wall temperature of the test heater was determined by applying a steady state heat conduction equation. The wall temperature of the heater will be slightly less than average thermocouple temperature because of the thermal resistance. The wall temperature was computed from equation (4.5) below.

$$Q = \left(\frac{T_{WALL} - T_{CAVE}}{R_{TOT}} \right) \tag{4.4}$$

$$T_{WALL} = T_{CAVE} - QR_{TOT} \tag{4.5}$$

The thermal resistance was due to cladding material between the thermocouples and outer wall of test heater. As heat transfer occurs in radial direction, the thermal resistance R_{TOT} can be calculated by using steady state heat equation for a hollow cylinder. The thermal resistance of a hollow cylinder is given by equation (4.6) (Sachdeva, 1988).

$$R_{thermal} = \frac{\ln\left(\frac{r_{outer}}{r_{inner}}\right)}{2\pi kL} \tag{4.6}$$

Rewriting equation (4.6) with test heater parameters, we have

$$R_{TOT} = \frac{\ln\left(\frac{R_O}{R_T}\right)}{2\pi k_{CONDZR} Z_{LB}} + R_C \tag{4.7}$$

R_C is thermal contact resistance, which is calculated from natural convection cooling tests. The contact resistance is given by equation (4.8)

$$R_C = \frac{0.0000692}{2\pi R_T Z_{LB}} \tag{4.8}$$

Substituting (4.7) equation into equation (4.5), the wall temperature of the test heater can be computed from equation (4.9)

$$T_{WALL} = T_{CAVE} - Q\left[\frac{\ln\left(\frac{R_0}{R_T}\right)}{2\pi k_{CONDZR} Z_{LB}} + R_C\right] \tag{4.9}$$

The heat transfer Q should be corrected for conduction loss through the copper conductor connected to test chamber. The corrected Q, or $Q_{CORRECTED}$, is the actual heat transfer occurring from test heater to bulk fluid, given by

$$Q_{CORRECTED} = Q - Q_{LOSS} \tag{4.10}$$

Q_{LOSS} Signifies the heat transfer from the test heater to the test chamber through the copper sleeve and does not have any effect on nucleation on test heater surface. This can be seen in Figure 3-4. The heat loss can be calculated by

$$Q_{LOSS} = \frac{k_{CONDCU} A_{CU} \Delta T_L}{Z_{EER}} \tag{4.11}$$

The temperature of the coolant is the bulk fluid temperature. The heat transfer is directly proportional to the temperature difference between wall temperature of test heater and bulk fluid temperature. This temperature difference is defined by ΔT_{DEL} given by

$$\Delta T_{DEL} = T_{WALL} - T_{BAVE} \tag{4.12}$$

The heat flux across the test heater can represented as follows :

$$q" = \frac{Q_{CORRECTED}}{2\pi R_O Z_L} \tag{4.13}$$

The coefficient of convective heat transfer is represented by the equation (4.14)

$$\boldsymbol{h = \frac{q"}{\Delta T_{DEL}}} \tag{4.14}$$

A FORTRAN program was used to compute the heat flux and coefficient of convective heat transfer incorporating the necessary equations. Dr. Steve Bajorek and Dr. Ken Shultis wrote a program for data reduction for pool boiling heat transfer analysis. Changes were made to the program to suit to the present test heater conditions. The program is presented in the appendix. (PROGRAM). The program gives two output files.

4.7 Uncertainty

The thermocouples used to measure the surface temperatures of the electrical test heater have an uncertainty of 0.1^{o}C. The thermocouple used for measuring the bulk temperature of the liquid had an uncertainty of 0.2^{o}C. The accuracy of the thermocouple measurements influences the accuracy of the superheat value. The tolerance of the test heater diameter was .002 mm. The readings from the pressure transducer had an uncertainty of ±0.25% full scale. The uncertainty in the measurements of current and voltage is ±3 % full scale and ±2%, full scale respectively. The maximum deviation in the heat flux due to uncertainty in the measurements was 4.5%. The maximum deviation in the superheat value was 2.5% and the uncertainty in the heat transfer coefficients due to the inaccuracies of the instrumentation was 7.2%.

5 RESULTS

5.1 Boiling Curves

Subcooled boiling tests were performed at pressures of 100 psia, 200 psia, 500 psia and 1000 psia. All the pressures indicated in the thesis are in absolute scale. The boiling tests were performed at subcoolings of 30^{o} C, 20^{o} C, 10^{o} C and saturation temperatures respectively. The boiling tests performed using deionized water serve as reference for comparison with tests of boric acid and lithium metaborate. The results for boiling tests performed at 100 psia, 200 psia, 500 psia and 1000 psia are presented in this chapter respectively. Results at each pressure include tests done with variation of degree of subcooling and variation of additive concentration.

5.2 Tests at Pressure of 100 psia.

Boiling tests were performed using the old experimental set up (with AC electrical power supply) at 100 psia (6.9 bara). The variation in the heat transfer characteristics can be observed from boiling curves. Each test was numbered for reference.

Boiling tests were conducted with pure deionized water and with varying concentrations of boric acid and lithium metaborate solution. The results for tests done with deionized water are shown in Figure 5-1. The variation of heat flux with superheat has been plotted in Figure 5-1. Boiling curves have been plotted for conditions with coolant at 30 ^{o}C subcooling, 20 ^{o}C subcooling, 10 ^{o}C subcooling and at saturation conditions respectively. The abscissa in Figure 5-1 represents the temperature difference

between test heater surface and coolant (deionized water) in degree centigrade. This is also called the superheat. The ordinate in Figure 5-1 represents heat flux across the electrical test heater in kW/m^2.

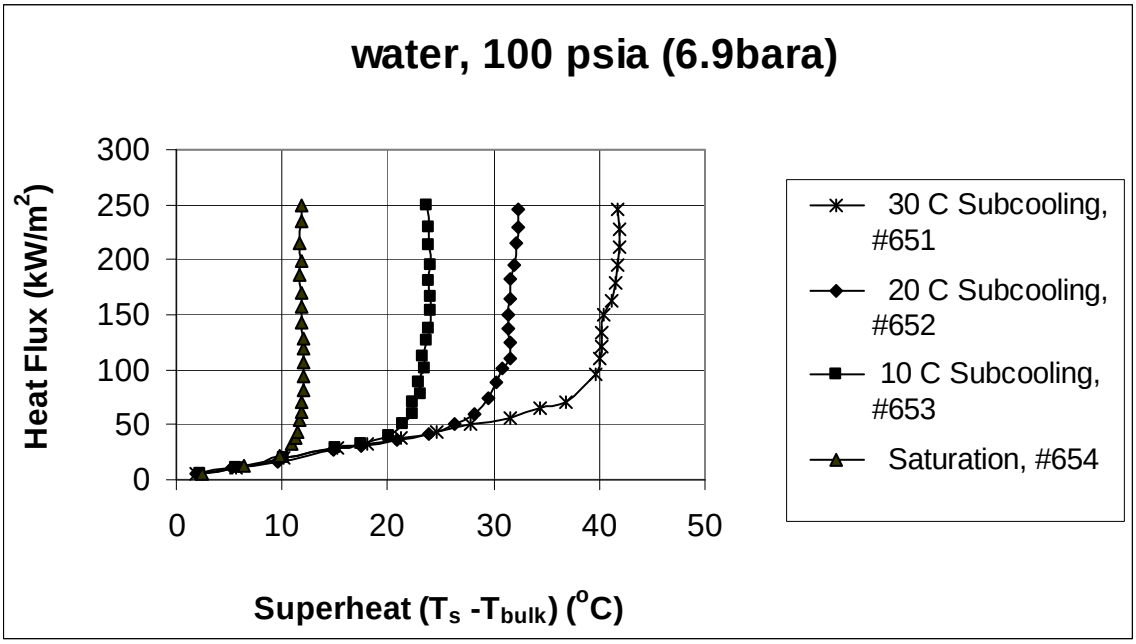

Figure 5-1 Boiling curves for deionized water at 100 psia pressure

The results of tests numbered 651 through 654 for deionized water can be seen in Figure 5-1. From Figure 5-1, it can be observed that boiling curves for all subcooling conditions match well for lower heat flux. The heat transfer occurs through free convection and the heat transfer coefficient remains fairly constant in this phase. The surface temperature of the test heater is insufficient to cause nucleate boiling in this phase. The heat flux varies only with superheat and can be estimated through equation (4.14). The slope of the boiling curves for lower heat flux is predictable as it remains constant with change in superheat. A steep change in slope of the boiling curve signifies the onset of nucleate boiling. A comparison of heat transfer coefficients can be done from

two boiling curves as the heat transfer coefficient is a ratio of heat flux to the super heat. For easy comparison of the boiling curves at different conditions, the symbols used for representing boiling curves are consistent with the degree of subcooling. The maximum heat flux is about 250 kW/m^2 for all the subcooling curves, which is below the critical heat flux for deionized water. For a constant heat flux, heat transfer coefficient is directly dependent only on super heat and is inversely proportional to degree of superheat. Consequently it can be observed from Figure 5-1 that for same heat flux, the degree of superheat is increases with increase in subcooling for different subcoolings indicating that the heat transfer coefficient decreases with increase of subcooling. The heat transfer coefficients corresponding to the boiling curves shown in Figure 5-1 are shown in Figure 5-2.

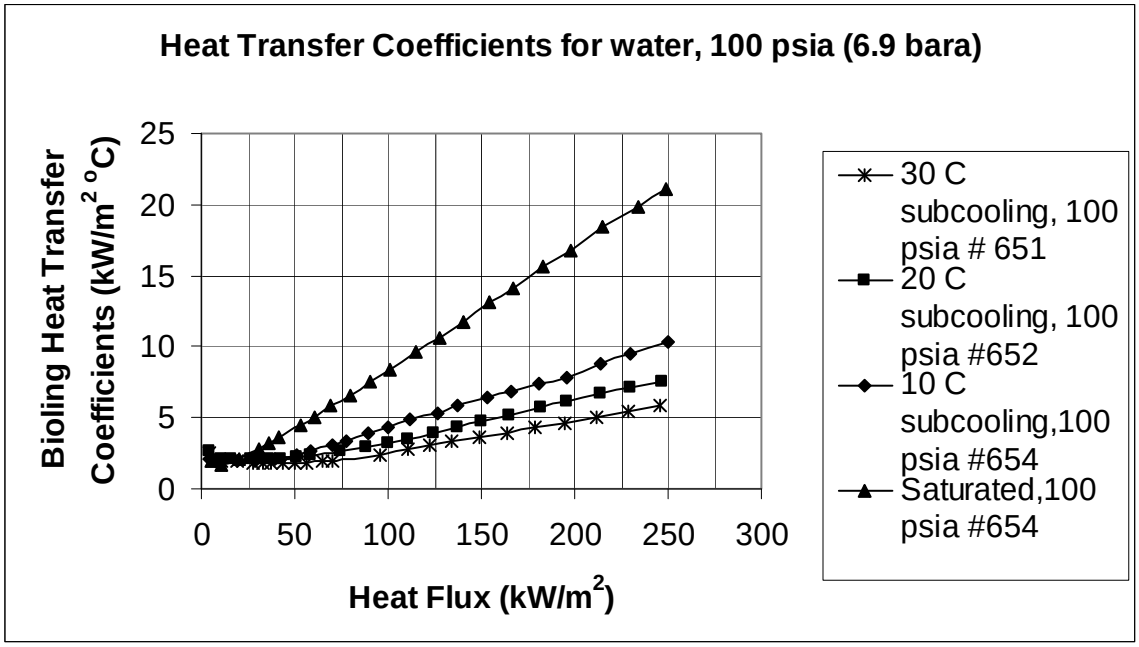

Figure 5-2 Heat transfer coefficients for deionized water at 100 psia pressure

In Figure 5-1, the boiling curve for test 651 increases almost linearly with increase in heat flux until 70 kW/m^2 and then rises steeply. This behavior can be explained by a change in phase of the water at the surface of heater. The heat transfer between the heater and the coolant occurs by natural convection until the onset of nucleate boiling in the liquid. Beyond the saturation temperature, the heat transfer between heater and coolant occurs through nucleate boiling. The beginning of bubble formation is termed as nucleation. Since the temperature of the coolant is below its saturation temperature, the process is called subcooled nucleate boiling. The increase in the slope of heat transfer coefficients is due to subcooled nucleate boiling. A Similar phenomenon is observed for boiling curves at different subcooling rates.

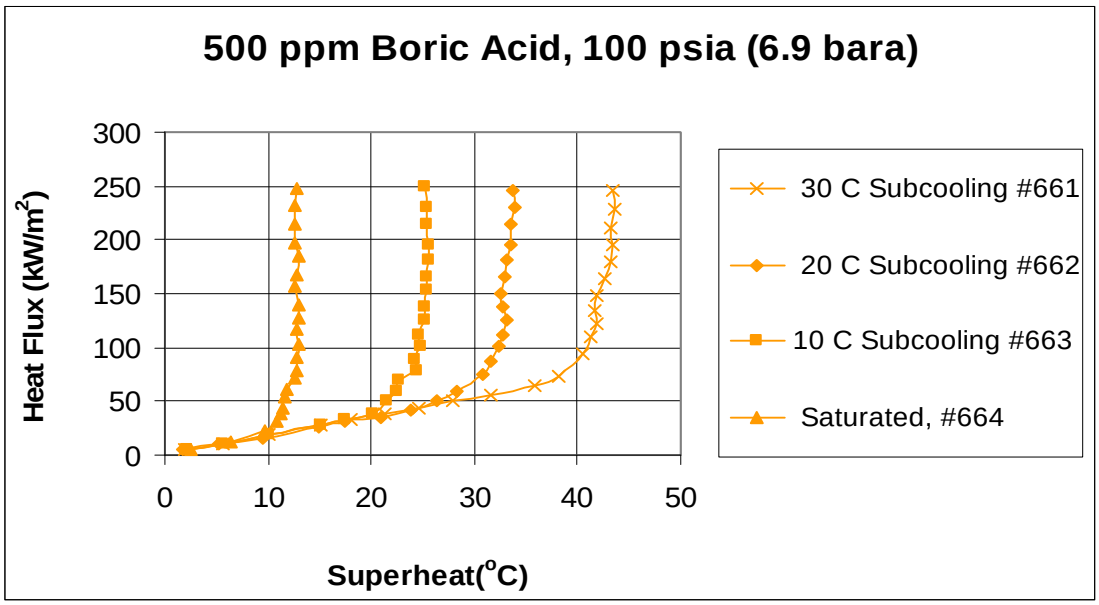

Figure 5-3 Boiling curves for 500 ppm boric acid solution at 100 psia pressure

Figure 5-3 shows results for tests done from #661 to 664 for 500 ppm concentrated boric acid solution. The results have a similar trend to that of Figure 5-1 but with an increase in superheat values. The boiling curves for 500 ppm boric acid and

deionized water are compared in Figure 5-4. The boiling curves for 500 ppm boric acid tests coincide very well with that of deionized water for lower heat flux values. This indicates that the addition of boron at 500ppm concentration does not have a significant effect on heat transfer coefficients in the natural convection region. Upon keen observation it can be found that the boiling curves for 500 ppm boric acid solution appear to have slightly higher degree of super heat for similar heat flux values than that obtained with deionized water. The difference in boiling curves for deionized water and 500 ppm boric acid is evident from Figure 5-4.

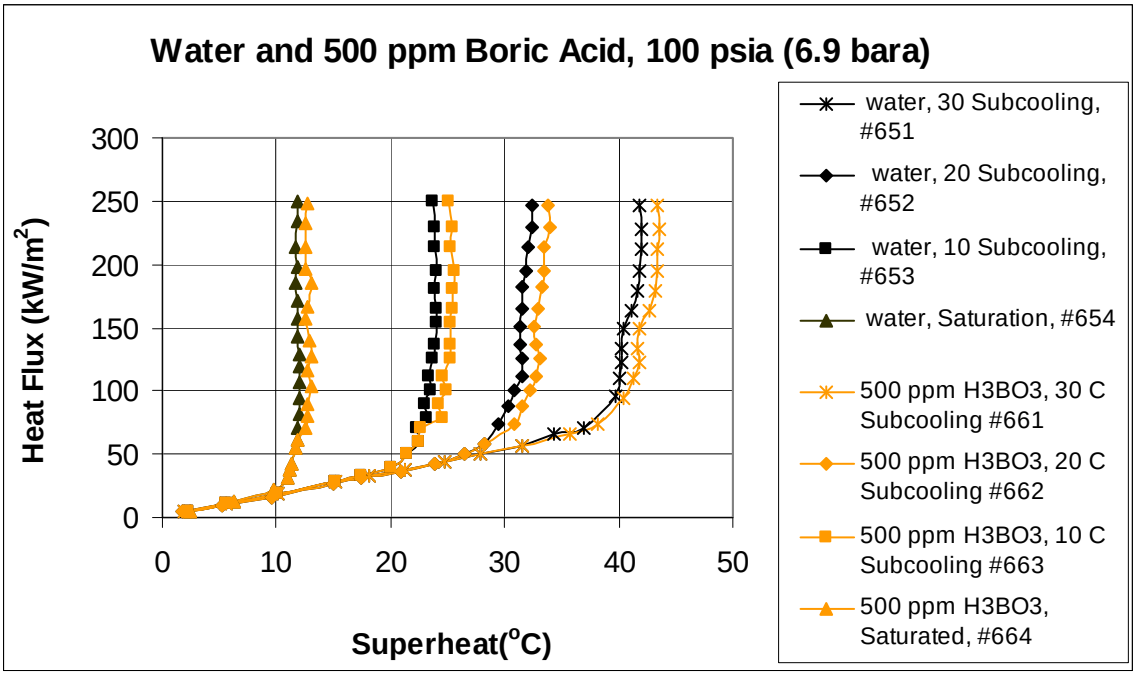

Figure 5-4 Comparison of boiling curves for deionized water and 500 ppm boric acid solution at 100 psia

It can also be noted that for constant heat flux, the difference in superheat values for 500 ppm boric acid tests is small when compared to the actual superheat values for deionized water. However the small increase in superheat values is due to change in fluid

physical properties, which causes less nucleation than deionized water. It can be concluded that boric acid has relatively small effect on the heat transfer coefficient at a concentration level of 500 ppm and at 100 psia pressure. For instance, the heat transfer coefficient decreased by only 3.0% due to 500 ppm boric acid solution at heat flux of about 250 kW/m^2 and 20°C subcooling.

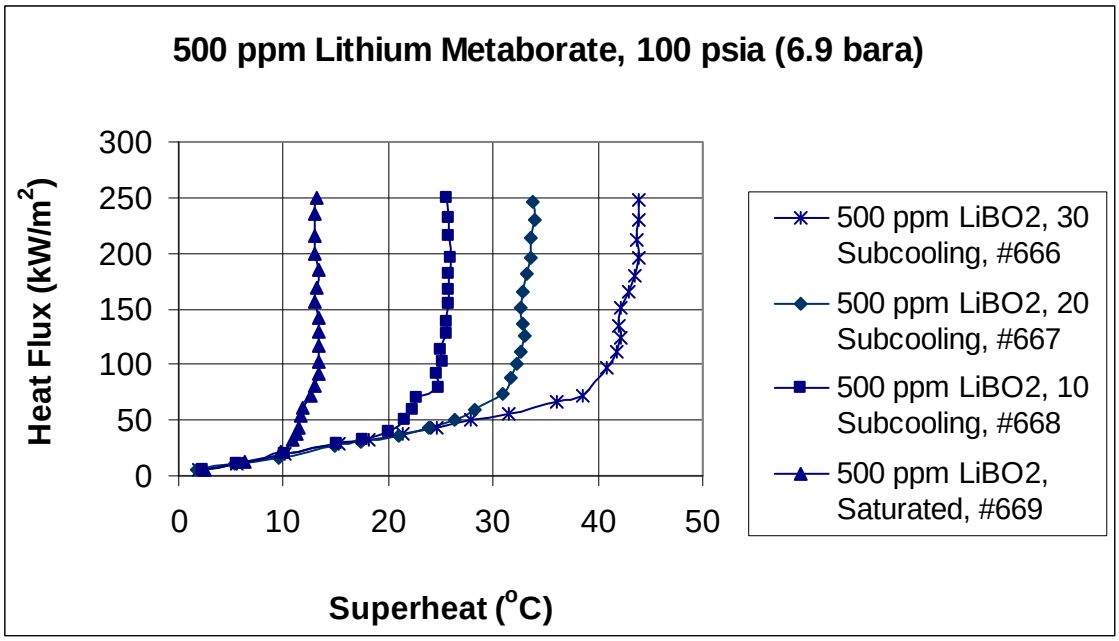

Figure 5-5 Boiling curves for 500 ppm lithium metaborate solution at 100 psia

The test results with 500 ppm lithium metaborate solution are presented in Figure 5-5. The heat transfer coefficients can be inferred from boiling curves as the ratio of heat flux to the degree of superheat. It can be observed that there is a change in the superheat values of 500 ppm lithium metaborate solution with respect to deionized water but it is not a very significant. However degradation of boiling heat transfer coefficients seems to be marginally more in case of lithium metaborate than boric acid for the same concentration 500ppm of coolant. This effect can be seen in Figure 5-6 indicating the

change in degree of super heat with constant heat flux and at 30°C subcooling. This signifies that the lithium metaborate at 500 ppm concentration results in a reduction of heat transfer coefficient by about 6 %, when compared to water at 100 psia pressure. The degradation in heat transfer due to the presence of boric acid at 500 ppm and lithium metaborate at 500 ppm concentration can be inferred from Figure 5-6.

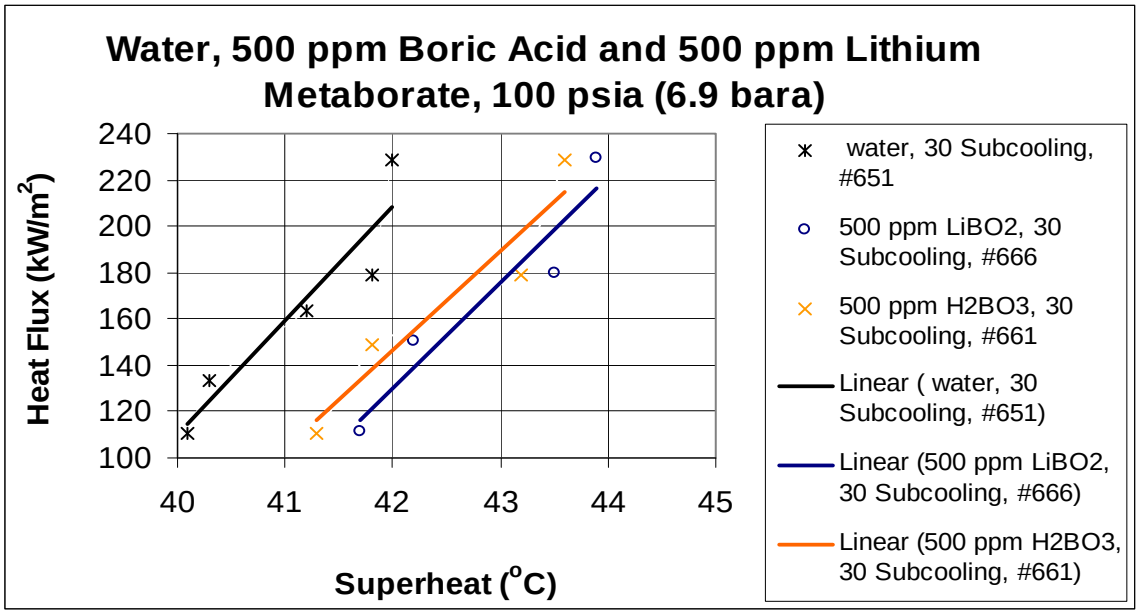

Figure 5-6 Comparison of deionized water, 500 ppm boric acid and 500 ppm lithium metaborate test results at 100 psia

However degradation of boiling heat transfer coefficients seems to be marginally more in case of lithium metaborate than boric acid for the same concentration of coolant additive. For instance, at a heat flux of 164 kW/m^2, the solution of 500 ppm boric acid (test #661) at 30 ^{o}C subcooling resulted in 4.5% decrease in heat transfer coefficients and a reduction of 4.8% in heat transfer coefficients for the case of 500 ppm lithium metaborate (test #666) at 30 ^{o}C subcooling. The reference for comparison of heat transfer coefficients is test #651 for deionized water, which has a boiling heat transfer coefficient

of 39.72 kW/m^{2o}C at a similar heat flux value as that of 500 ppm boric acid 500 ppm lithium metaborate solutions at 30 ^{o}C subcooling.

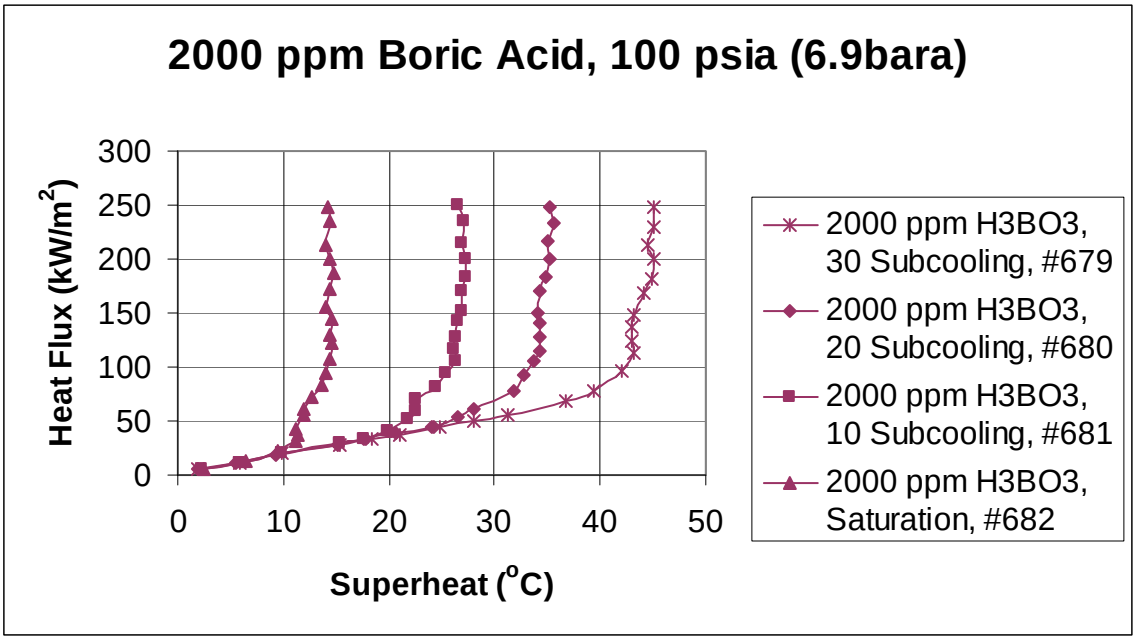

Figure 5-7 Boiling curves for 2000 ppm boric acid solution at 100 psia

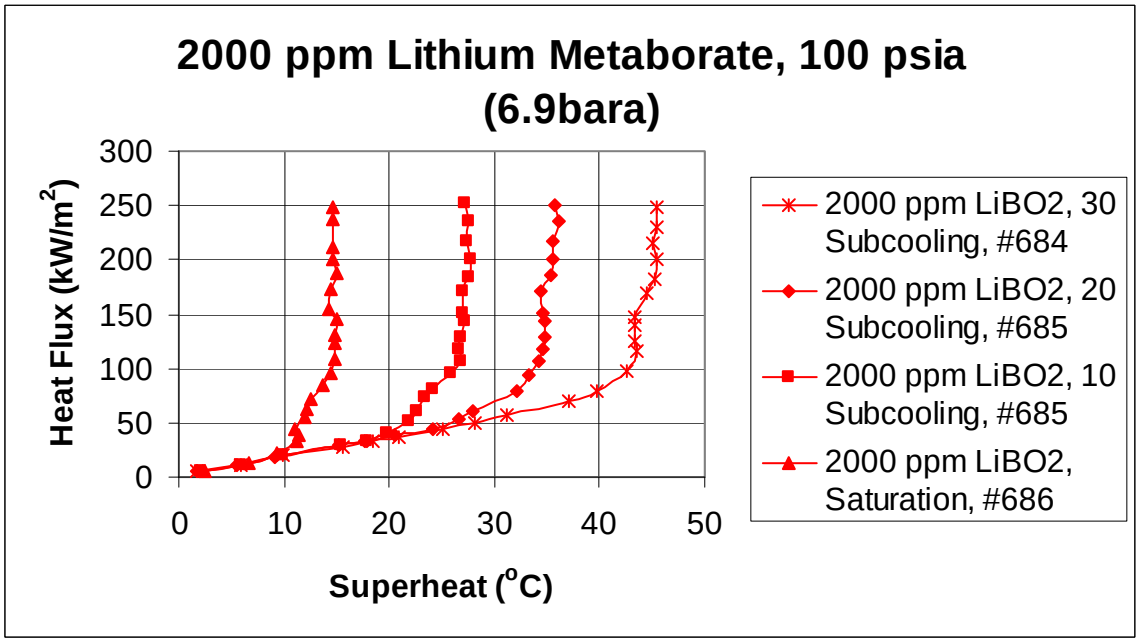

Figure 5-8 Boiling curves for 2000 ppm lithium Metaborate solution at 100 psia

Test results with 2000 ppm boric acid solution are presented in Figure 5-7 . It can be observed that there is considerable change in the pool boiling heat transfer coefficients with the 2000 ppm boric acid solution. Figure 5-8 shows the results of boiling tests with 2000-ppm lithium metaborate solution. Figure 5-9 shows the effect of lithium metaborate on boiling heat transfer coefficients at 2000 ppm concentration. For a heat flux of 250 kW/m2, the boiling heat transfer coefficient decreased by 20% when compared to deionized water at the saturation temperature.

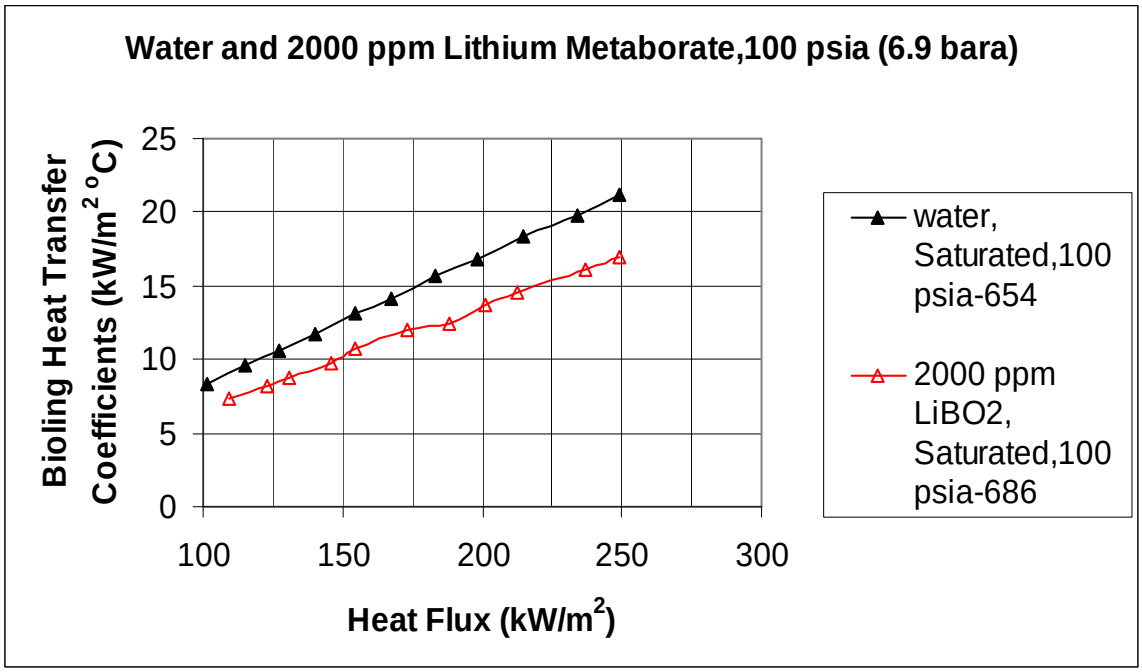

Figure 5-9 Degradation of boiling heat transfer coefficients with 2000 ppm lithium metaborate solution

Test results for 5000 ppm boric acid solution are presented in Figure 5-10. As in results of other boiling curves it can be seen that all four boiling curves coincide at lower heat flux indicating that concentration level of coolant has no effect on the natural convective heat transfer.

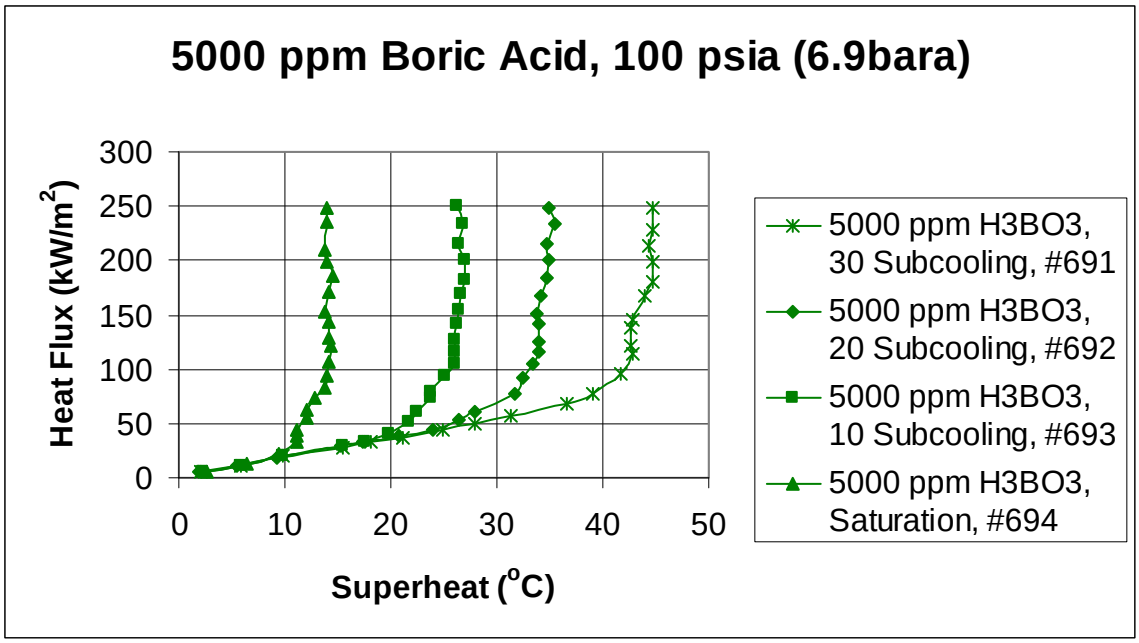

Figure 5-10 Boiling curve for 5000 ppm boric acid solution at 100 psia pressure

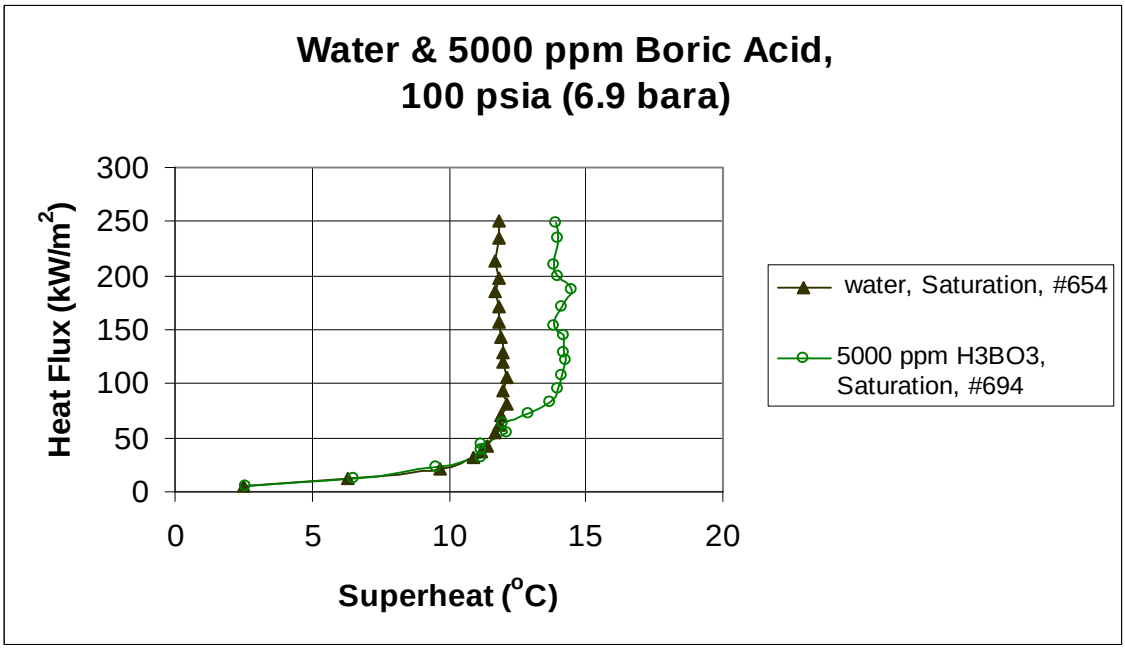

Figure 5-11 Comparison of boiling curves at saturated condition for deionized water and 5000 ppm concentrated solution at 100 psia

A comparison of test results for test 694 and 654 is shown in Figure 5-11 at the 10 ^{o}C subcooled condition. It can be clearly observed in Figure 5-11 that the temperature difference between heater wall and coolant solution is considerably higher in case of 5000 ppm boric acid solution compared to that of deionized water. The decrease in heat transfer coefficient is likely due to the non uniform nucleation that was observed during the boiling test. Figure 5-12 shows the boiling curves obtained for the boiling test with 5000 ppm concentrated lithium metaborate solution.

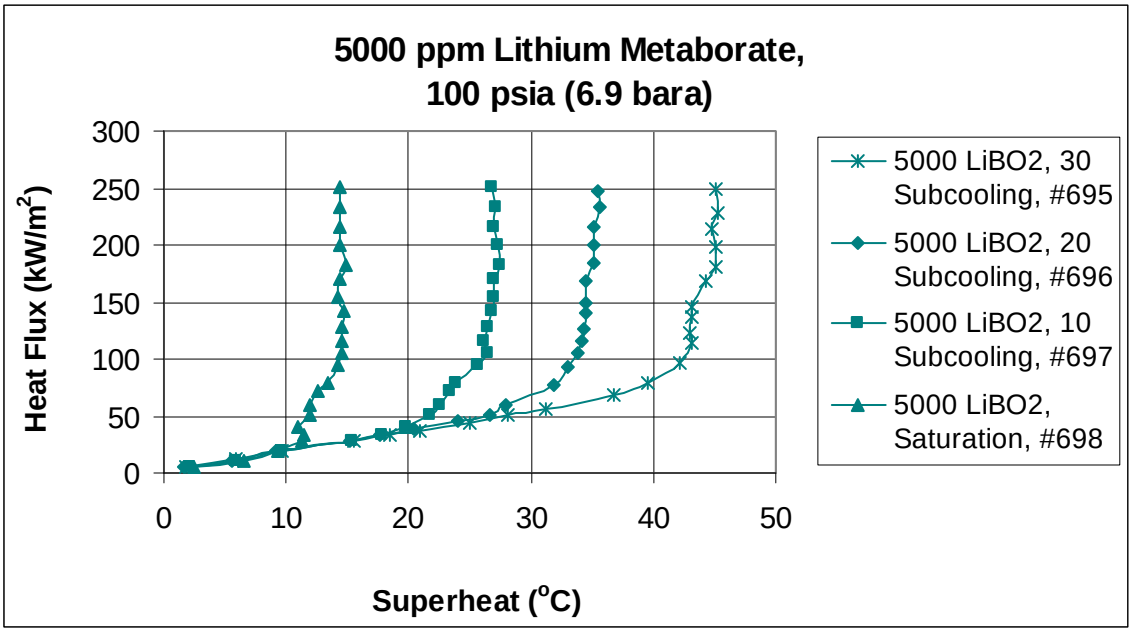

Figure 5-12 Boiling curves for 5000 ppm lithium Metaborate solution at 100 psia

Figure 5-13 shows a reduction in heat transfer coefficients by 24% in boiling test with 5000 ppm boric acid solution (for 153 kW/m^2) at saturated condition compared to the boiling heat transfer coefficient of deionized water, which was 13.08 kW/m^{2o}C (for 153 kW/m^2). Similarly, a reduction of 25.5% was observed in boiling heat transfer

coefficients with 5000 ppm lithium metaborate solution (for 154 kW/m^2) as shown in Figure 5-13 when compared with that obtained from deionized water at similar heat flux.

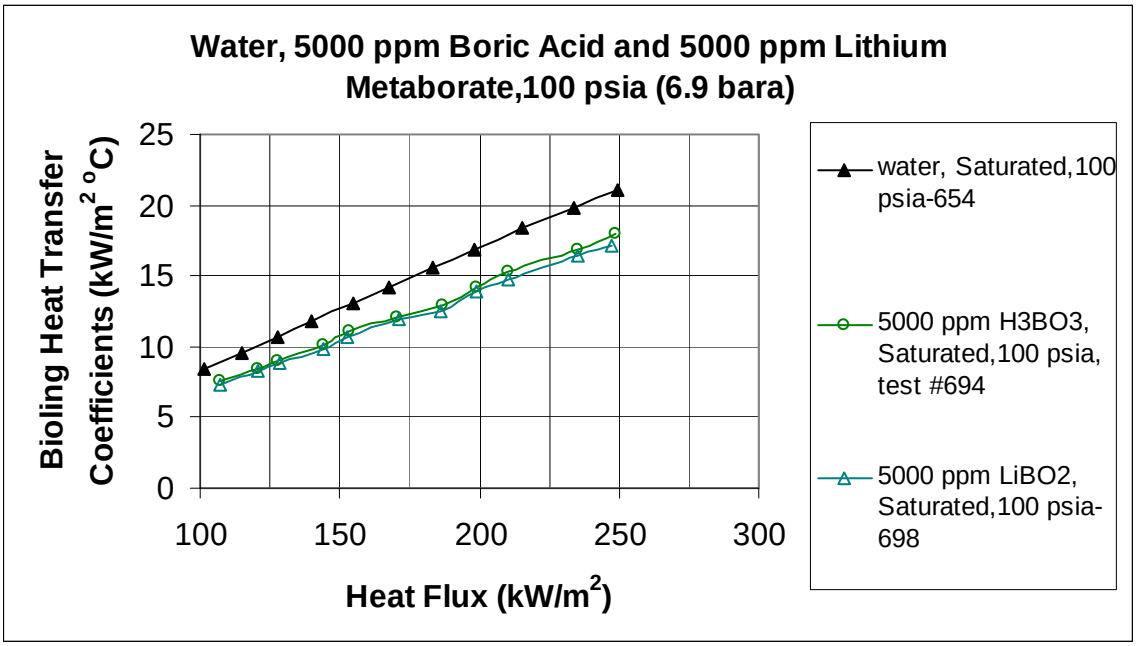

Figure 5-13 Degradation of boiling heat transfer coefficients with 5000 ppm boric acid and 5000 ppm lithium metaborate solution

5.3 Tests with New Experimental Equipment

Boling tests were performed at 100 psia with the new experimental set-up (DC electrical power supply) to compare the results of the old experimental set up. The new test heater had the same dimensional and material properties as the old heater. The test results for deionized water (tests through 721 to 725) are presented in Figure 5-14. The boiling test results from the experimental set up match very well with results from preliminary set-up. The average variation in heat transfer coefficient between preliminary boiling set-up and new boiling set-up was found to be about 1.2%. Figure 5-14 shows the results obtained from tests through 721 to 725 (new setup) and tests 651 through 655 (old

set up). The results obtained for water with new experimental setup verify that results obtained from new experimental set-up are consistent with those obtained from preliminary set up. A similar trend was obtained for tests done with 2000 ppm boric acid and 2000 ppm lithium metaborate.

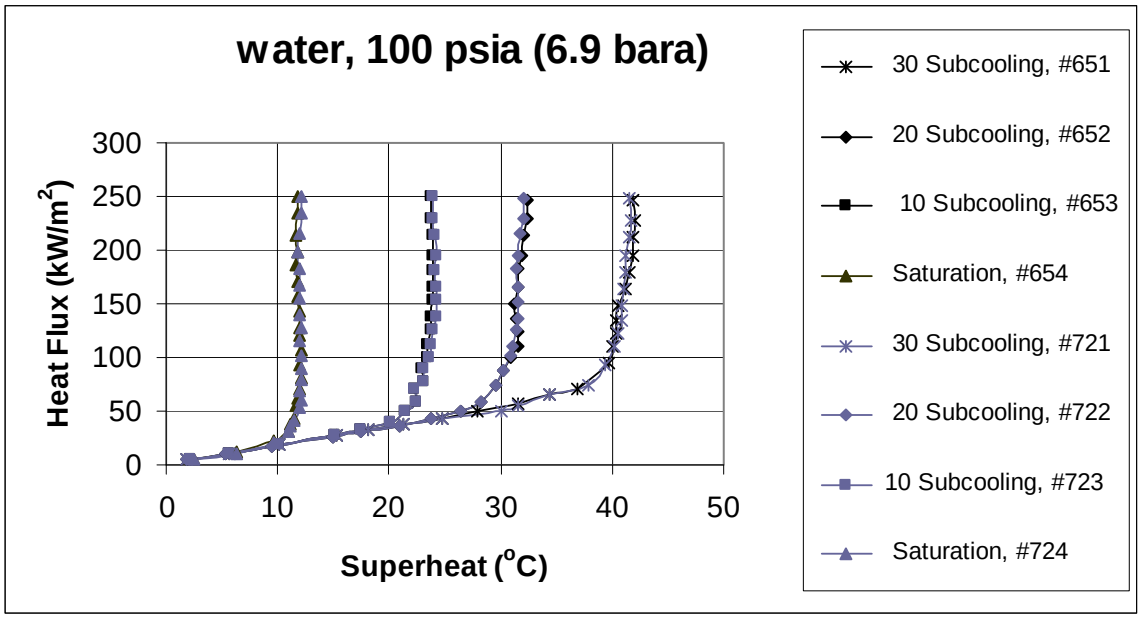

Figure 5-14 Comparison results from old and new experimental set up

5.4 Tests at Pressure of 200 psia

Boiling tests performed at a pressure of 200 psia (13.3bara) showed similar results to that of tests conducted at a lower pressure. The tests were conducted using the new experimental setup. Figure 5-15 shows results indicating boiling curves for varying degree of subcooling for deionized water. It can be clearly observed from the results that, at lower heat flux, the boiling curves coincide very well. This can be explained due to lack of nucleation and this region indicates heat transfer takes place through natural convection. The boiling curves begin to rise steeply after a point indicating the onset of

nucleate boiling. Because of nucleation, the rate of heat transfer increases rapidly. The boiling curves rise steadily with increase of heat flux.

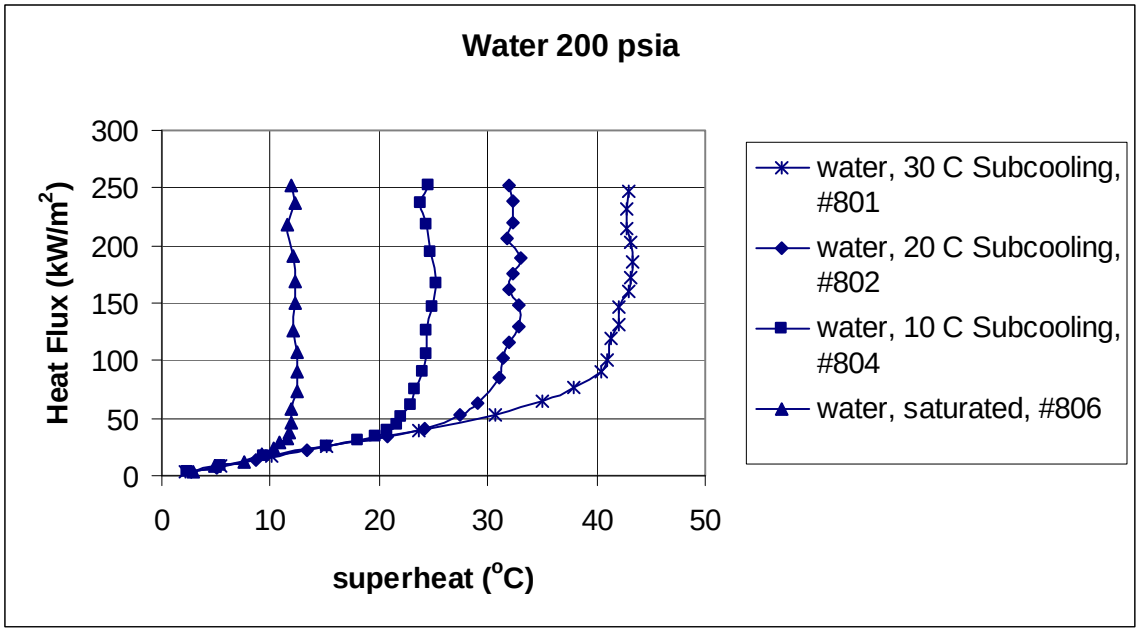

Figure 5-15 Boiling curves for deionized water at 200 psia (13.3bara)

The boiling curves indicate the increase in superheat values with increase of degree of subcooling as seen in Figure 5-15. As the heat transfer coefficient is a ratio of heat flux to superheat, it can inferred that the heat transfer coefficient decreases with increase of degree of subcooling. It has also been observed that the onset of nucleate boiling (ONB) is dependent on degree of subcooling. For instance, the onset of nucleate boiling seems to occur at a heat flux of 45 kW/m^2 for saturated conditions whereas ONB occurs at the heat flux of 101 kW/m^2 for 30^{o}C subcooled conditions. The maximum heat flux for all degrees of subcooling is well below the critical heat flux value of 1 MW/m^2 of deionized water (Incropera, 2001). The boiling curves with deionized water at 200 psia pressure had slightly higher superheat values (T_s- T_{bulk}) when compared with boiling

curves with deionized water at 100 psia pressure indicating a decline in heat transfer coefficient.

Boiling tests were performed with varying concentrations of boric acid in the coolant. Tests were performed with concentrations of 500 ppm, 1000 ppm, 2000 ppm and 5000 ppm similar to tests at 100 psia.

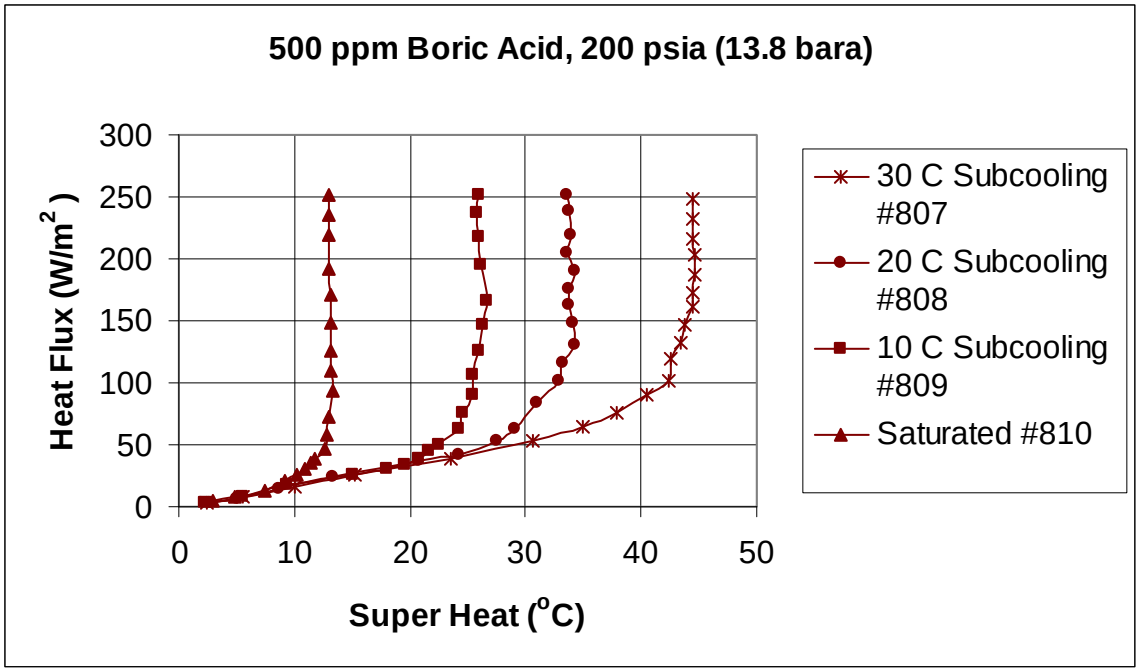

Figure 5-16 Boiling Curve for 500 ppm boric acid at 200 psia (13.8 bara)

Figure 5-16 shows the heat transfer coefficients for 500 ppm concentrated boric acid solution. Figure 5-22, Figure 5-27, and Figure 5-28 represent the results of pool boiling tests for 1000 ppm, 2000 ppm and 5000 ppm concentrations of boric acid, respectively. Figure 5-18, Figure 5-24, Figure 5-30, Figure 5-36 show the results of tests for 500 ppm, 1000 ppm, 2000 ppm and 5000 ppm concentration level of lithium metaborate, respectively.

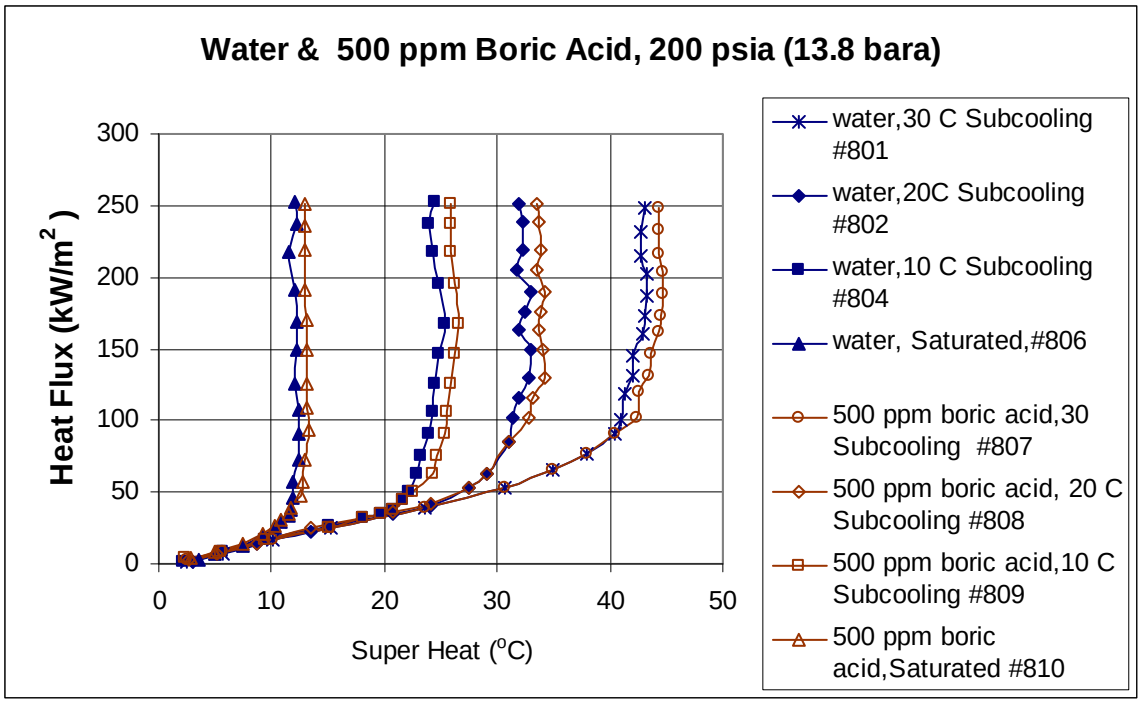

Figure 5-17 Boiling curves for deionized water and 500 ppm boric acid at 200 psia

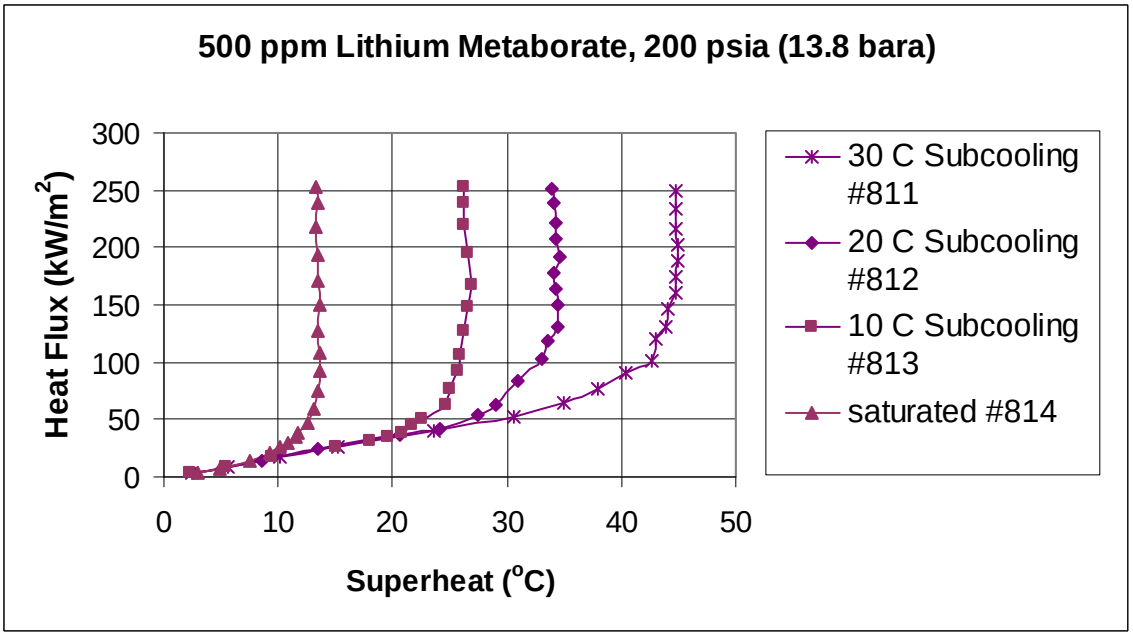

Figure 5-18 Boiling curves for 500 ppm $LiBO_2$ Solution, 200 psia

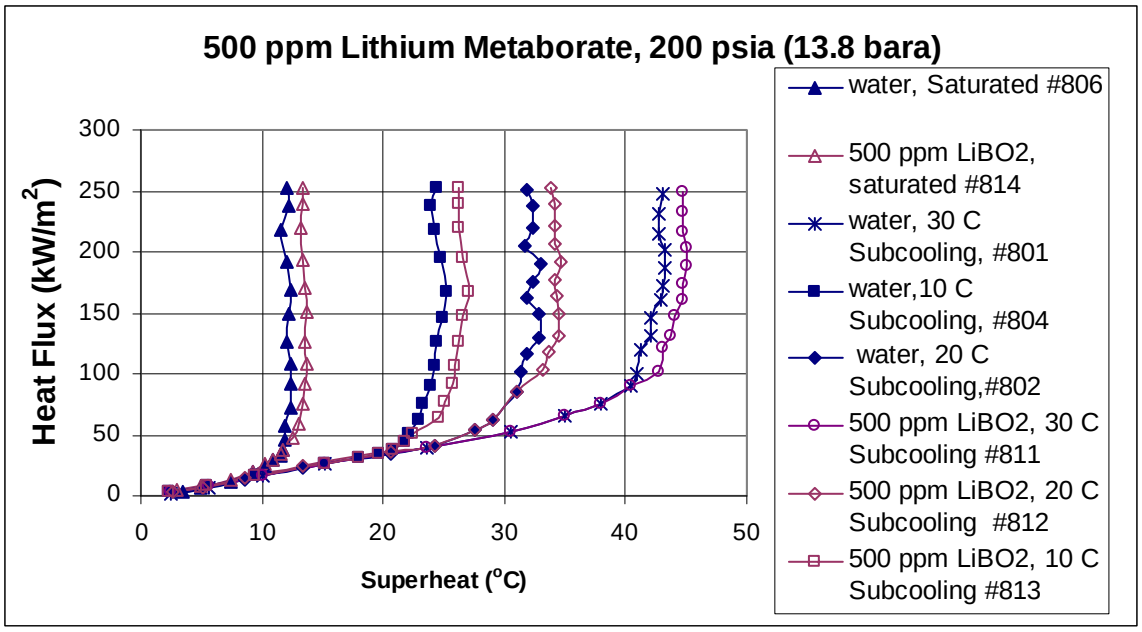

Figure 5-19 Boiling curves for deionized water and 500 ppm $LiBO_2$ solution, 200 psia (13.8 bara)

The effect of 500 ppm boric acid solution on boiling curves can be seen in Figure 5-17. A decrease in heat transfer coefficient by 5.8% was observed at 10°C subcooling for 500 ppm boric acid solution. Observations from the results of the boiling tests indicate that the pool boiling heat transfer coefficients for pressure of 200 psia are influenced by coolant concentration. Observations from Figure 5-19, Figure 5-21 indicates increased superheat for 500 ppm lithium metaborate over deionized water at same heat flux, indicating a decrease of heat transfer coefficient for 500 ppm lithium metaborate solution. A decrease in heat transfer coefficient by 6.5% was observed at 10°C subcooling for 500 ppm lithium metaborate solution in Figure 5-20 .

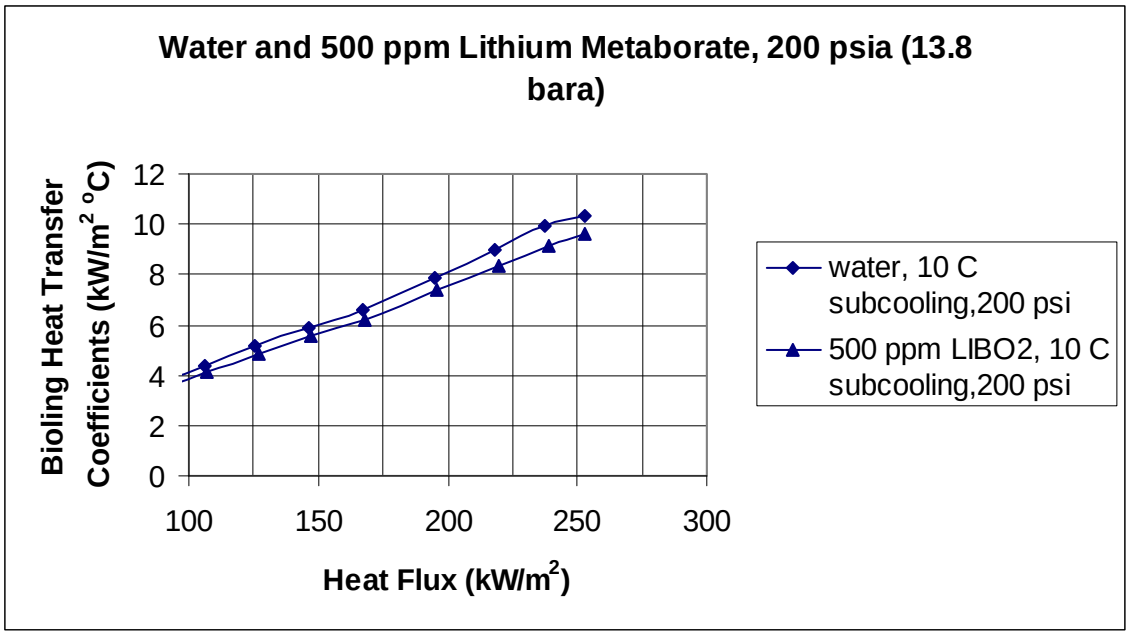

Figure 5-20 Comparison of heat transfer coefficients of water and 5000 ppm lithium metaborate at 200 psia pressure

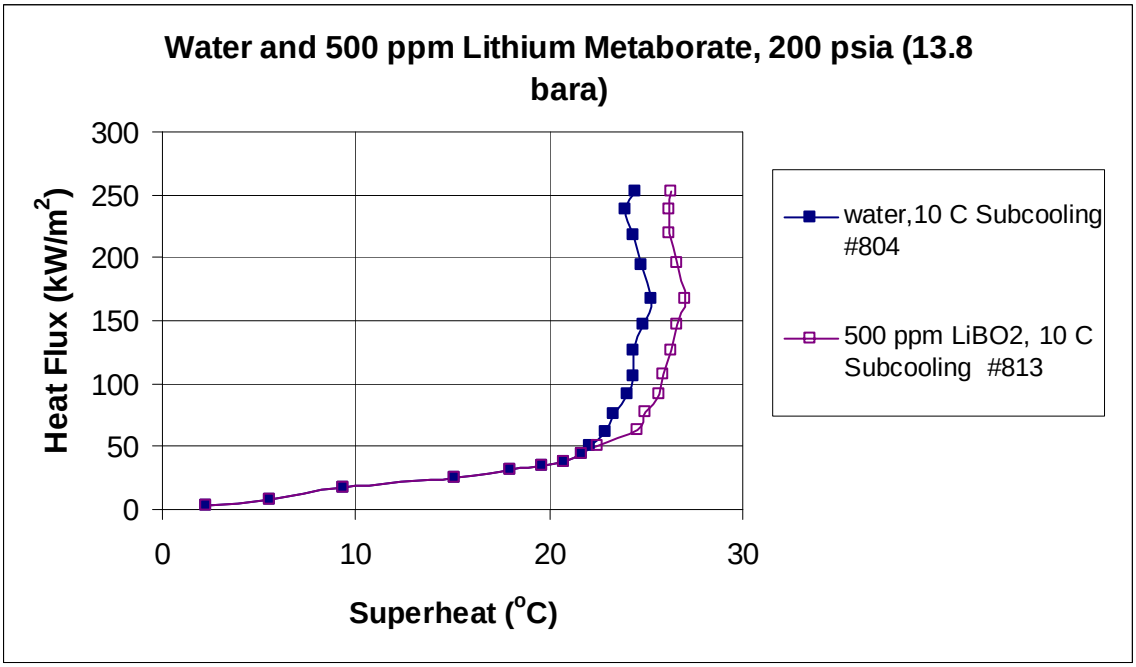

Figure 5-21 Boiling curves for deionized water and 500 ppm $LiBO_2$ solution, 10^o C Subcooling and 200 psia (13.8 bara)

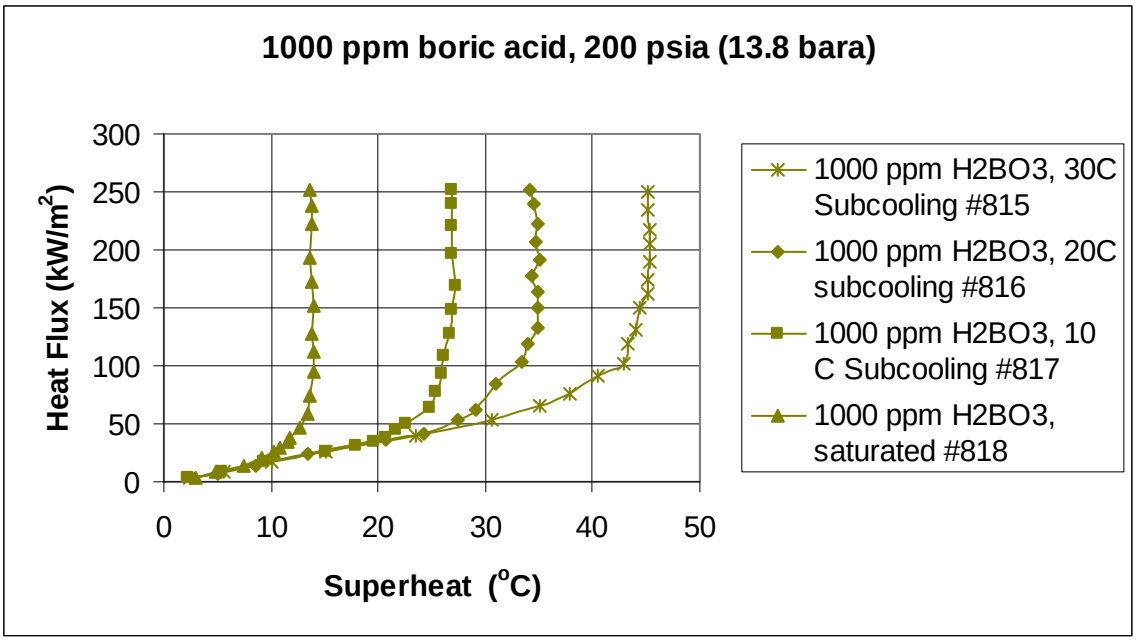

Figure 5-22 Boiling curves for 1000 ppm boric acid solution, 200 psia

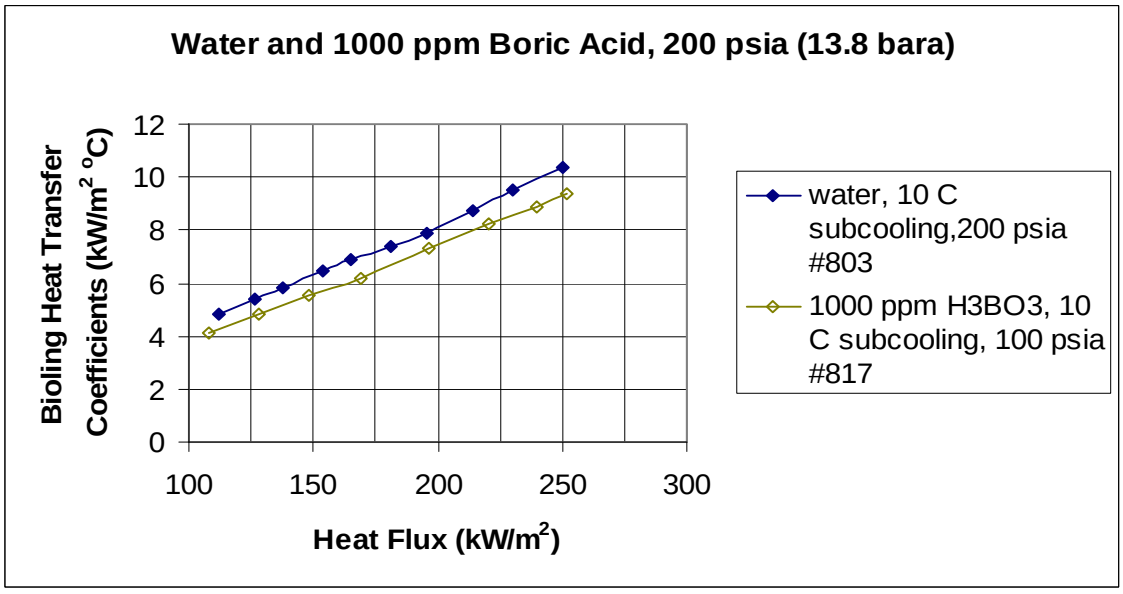

Figure 5-23 Degradation of boiling heat transfer coefficients due to1000 ppm boric acid concentration at 10^{o} C bulk fluid subcooling, 200 psia

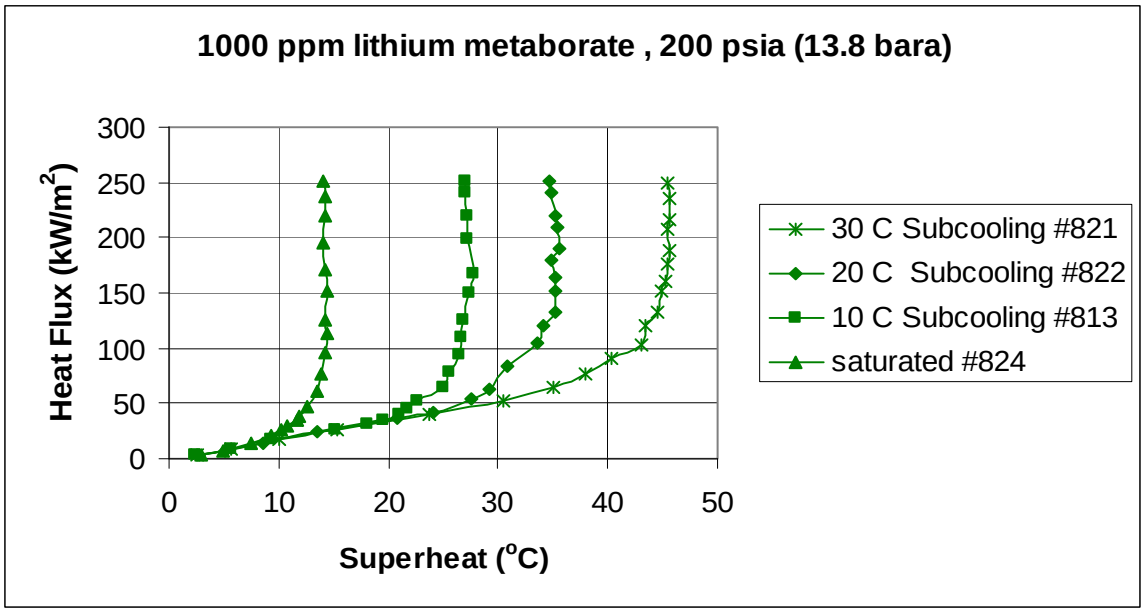

Figure 5-24 Boiling curves for deionized water and 1000 ppm $LiBO_2$ solution, 200 psia (13.8) bara

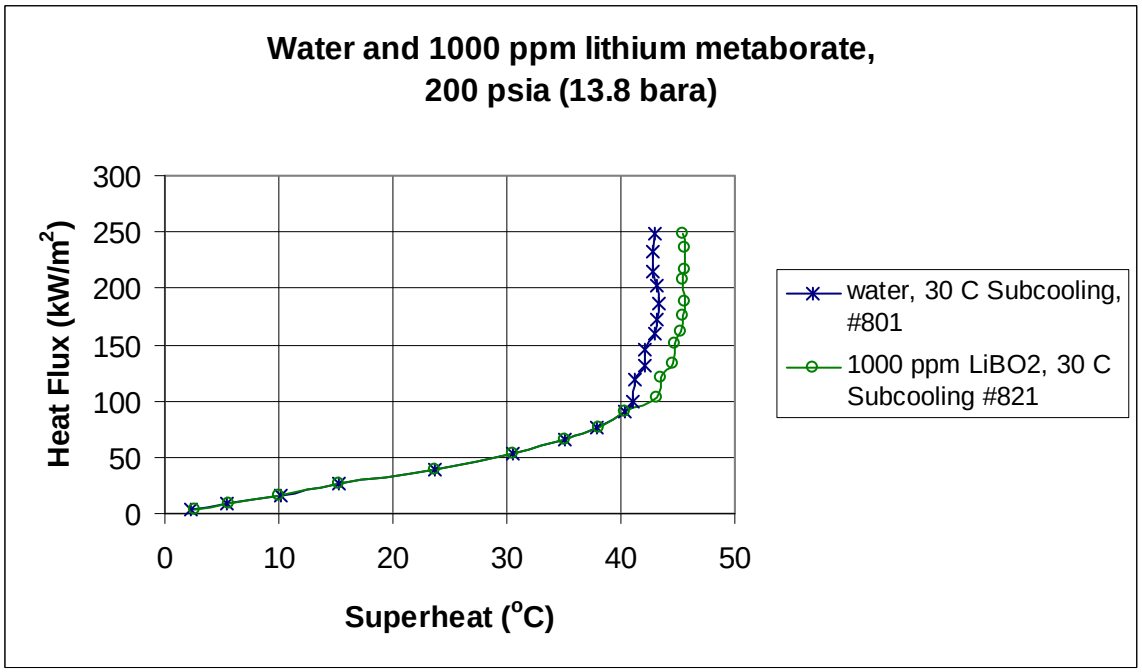

Figure 5-25 Effect of lithium metaborate concentration on heat transfer at 30 ^{o}C subcooling and 200 psia pressure

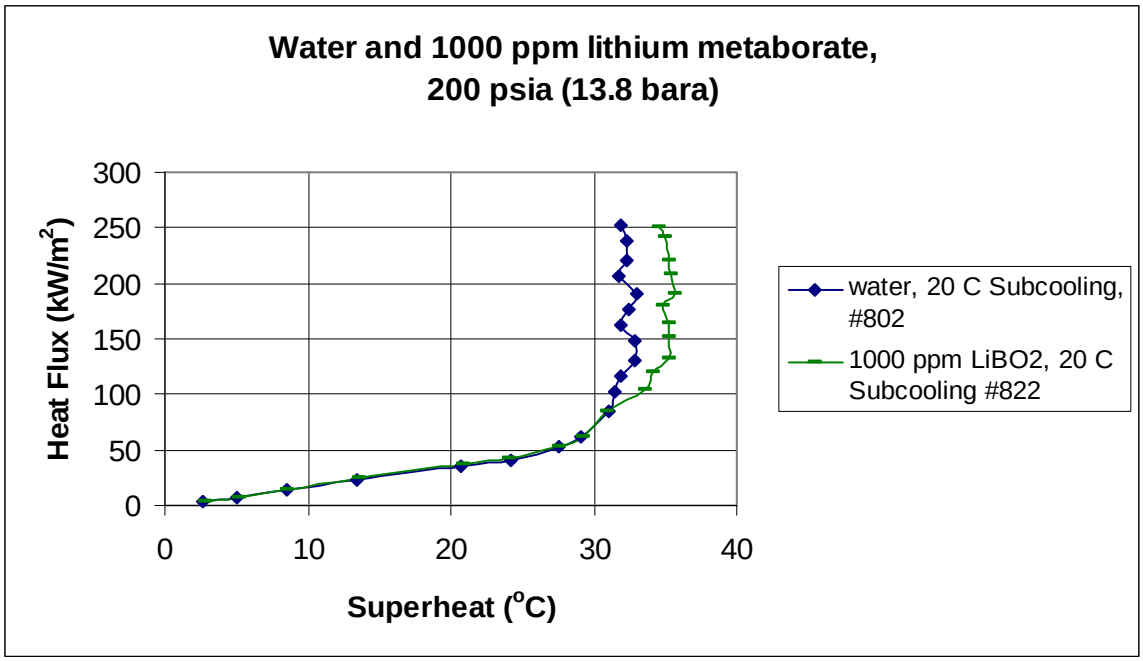

Figure 5-26 Effect of lithium metaborate concentration on heat transfer at 20 °C subcooling and 200 psia pressure

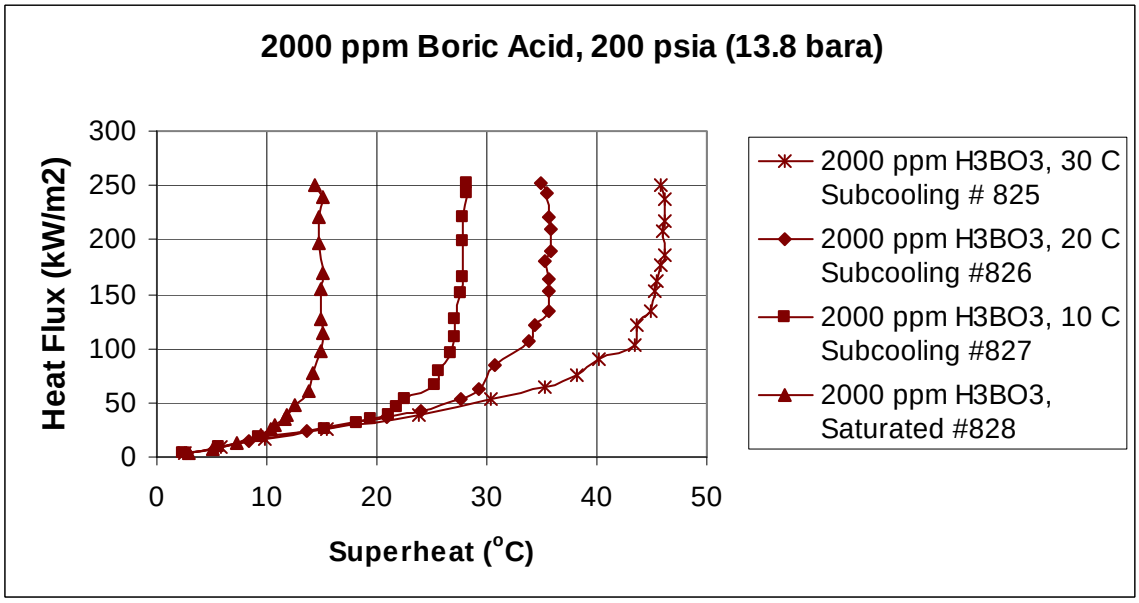

Figure 5-27 Boiling curves for tests with 2000 ppm concentration boric acid solution at 200 psia

Figure 5-23 indicates the decrease in boiling heat transfer coefficients due to the presence of boron at 1000 ppm concentration at 10°C subcooling. For a heat flux of 218

kW/m^2, the heat transfer coefficient for 1000 ppm boric acid solution was 8.2 kW/m^{2o}C compared to a value of 9.1 kW/m^{2o}C for deionized water indicating almost a 9% drop. It can be observed from Figure 5-28 and Figure 5-29 that the boric acid presence has significant effect on heat transfer coefficients. The heat transfer coefficients have decreased with increase in concentration level of boric acid from 500 ppm to 5000 ppm. The decrease in heat transfer coefficients can be explained by the change in nucleation. For deionized water, bubbles were found to rise uniformly along the heater surface. For tests 825 and 826, the bubbles departed the surface in irregular clumps. At higher heat flux, the bubbles departed the heating surface in a sporadic manner for tests numbered 825 and 826. The reduction in nucleation results in less heat removal thereby decreasing the heat transfer coefficient with an increase in boric acid concentration.

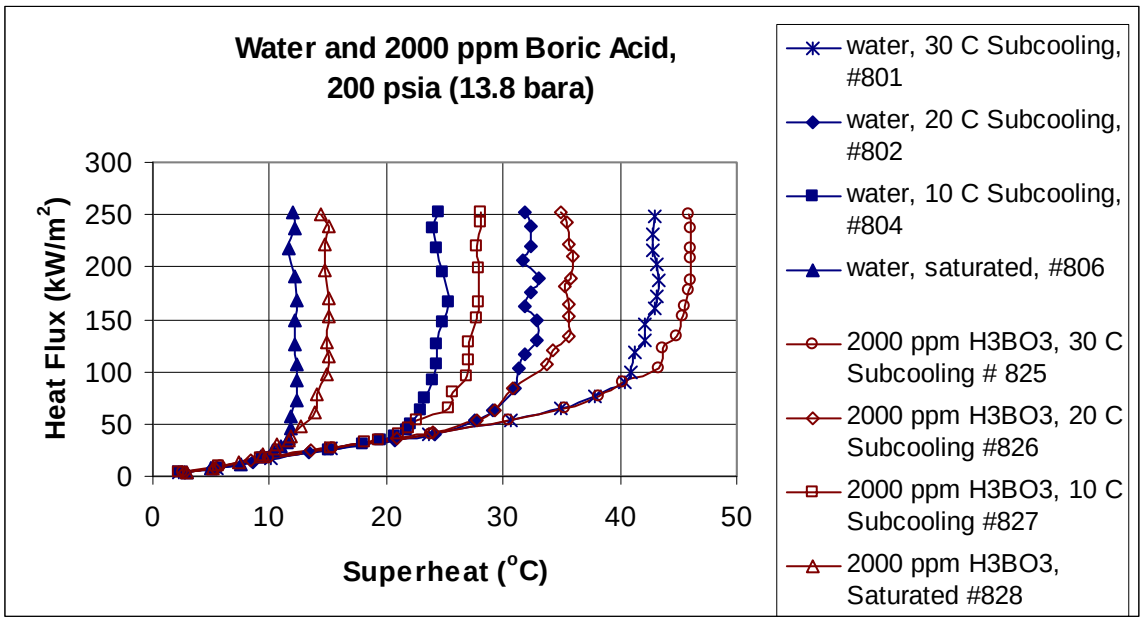

Figure 5-28 Boiling curves for deionized water and 2000 ppm concentration boric acid at 200 psia

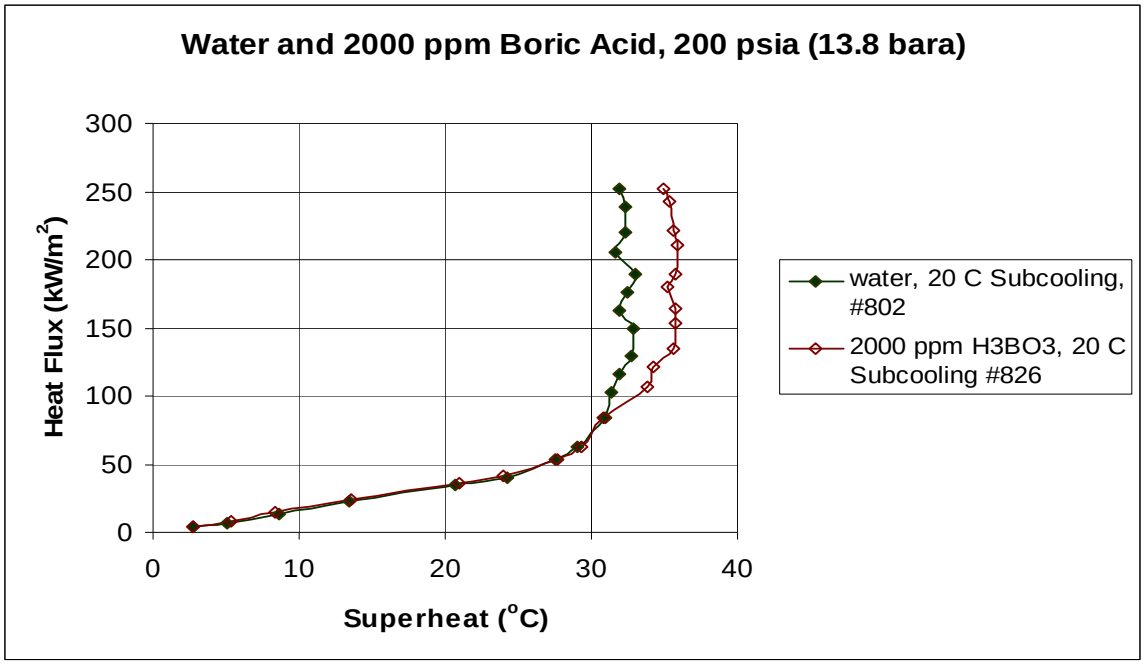

Figure 5-29 Effect of 2000 ppm boric acid concentration on heat transfer at 20° C subcooling and 200 psia

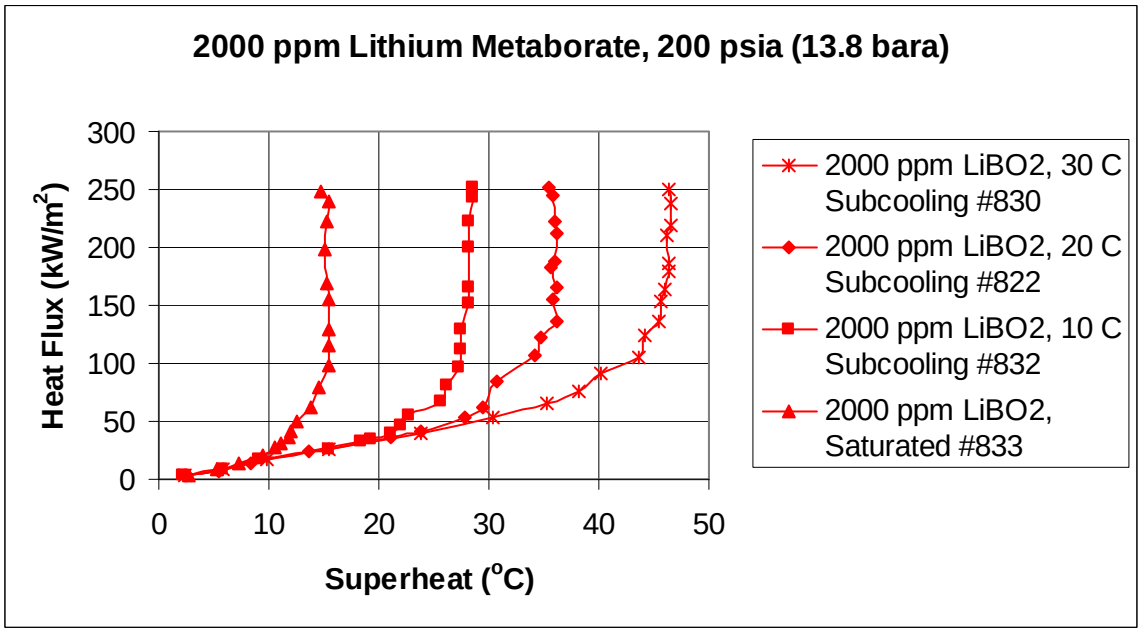

Figure 5-30 Boiling curves for 2000 ppm $LiBO_2$ solution, 200 psia

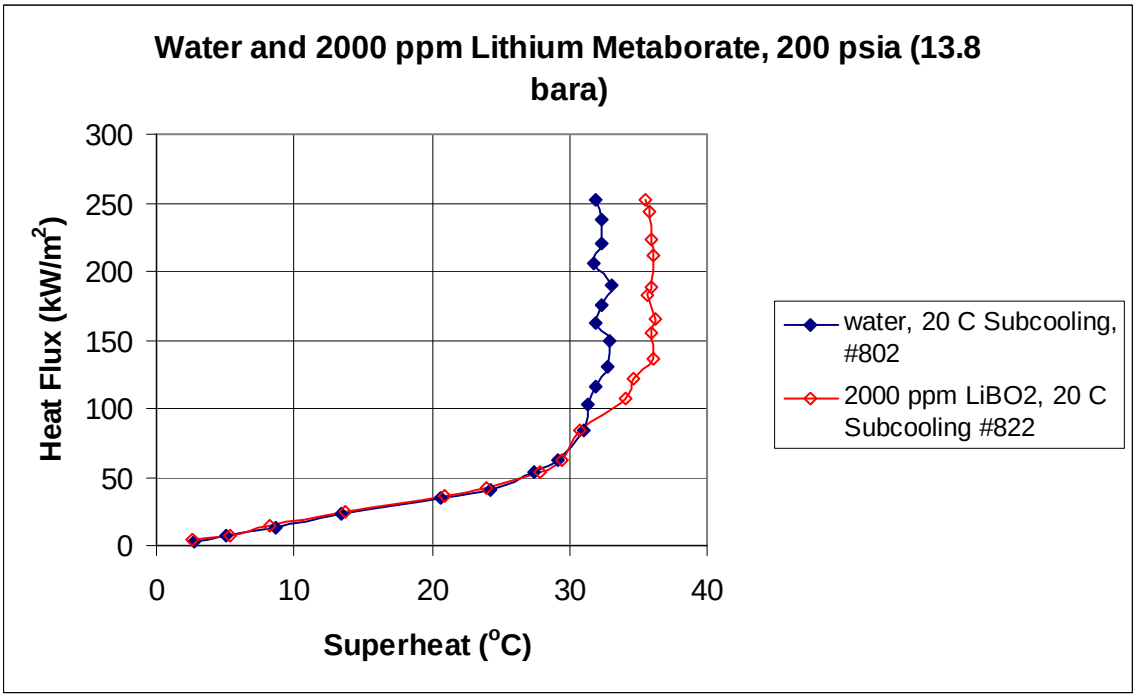

Figure 5-31 Effect of 2000 ppm lithium metaborate concentration on heat transfer at 20° C subcooling and 200 psia pressure

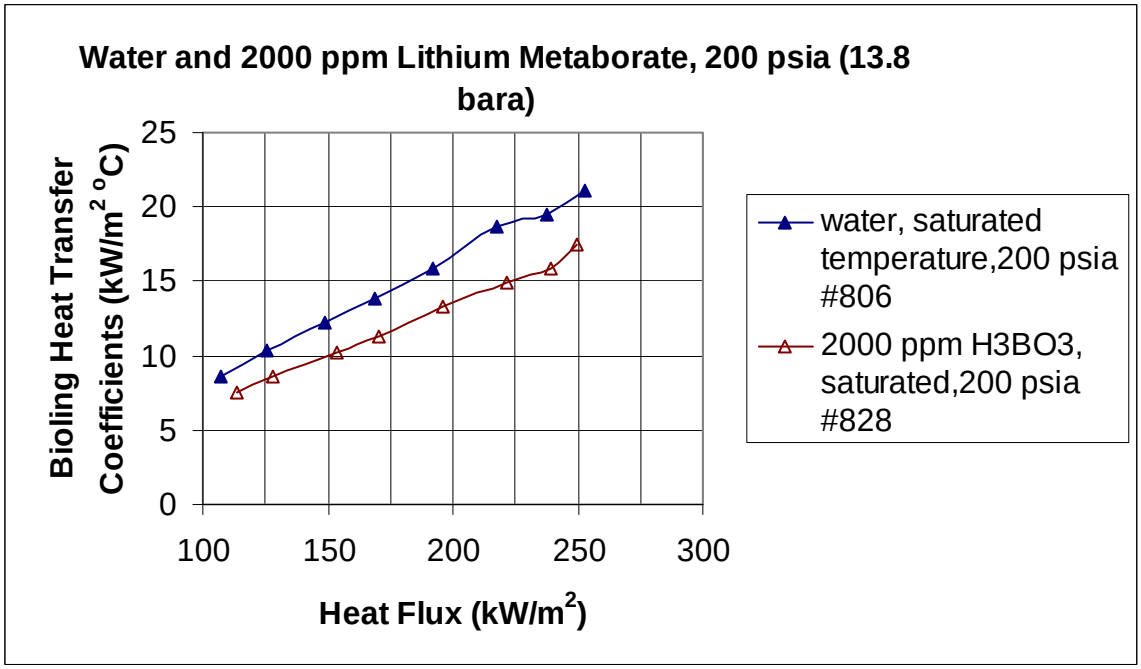

Figure 5-32 Comparison of heat transfer coefficients of water and 2000 ppm boric acid at 200 psia pressure

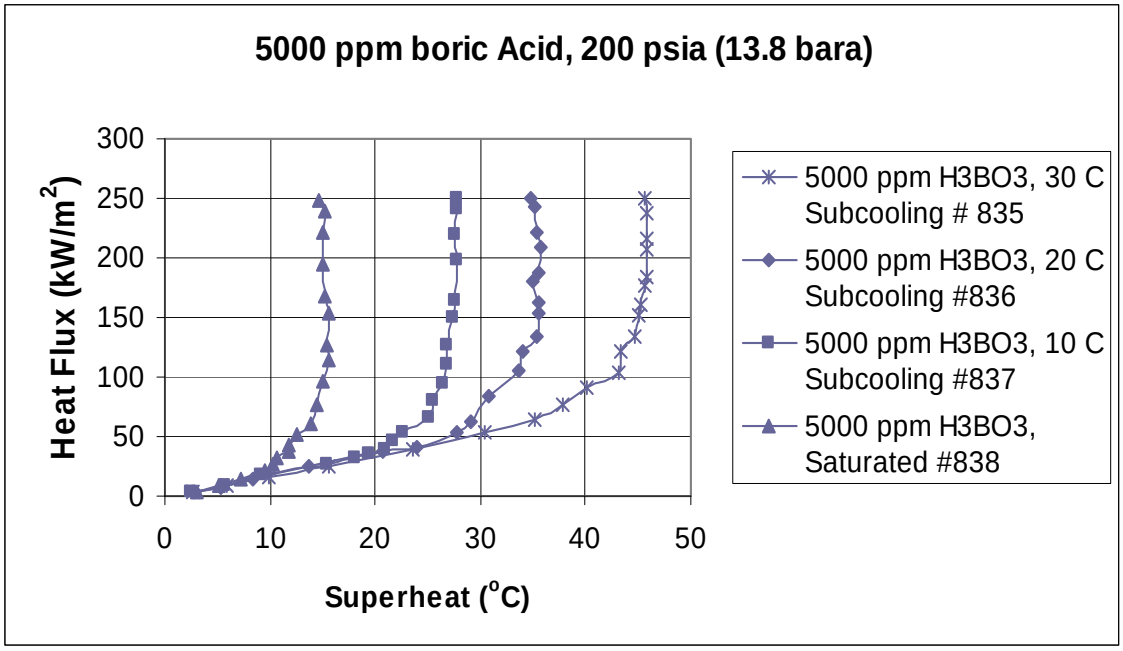

Figure 5-33 Boiling curves for tests with 5000 ppm concentration boric acid solution at 200 psia

For a 2000 ppm concentration of boron, a reduction of 21.5% was observed for heat transfer coefficient at the saturated condition (heat flux of 221W/m^2) as seen in Figure 5-32. Figure 5-35 shows the variation of heat transfer coefficient in presence of boron at 5000 ppm concentration at 10^{o}C conditions. Comparing Figure 5-34 and Figure 5-29, it can be observed that the variation in the superheat values for 5000 ppm concentrated boric acid solution compared to superheat values for 2000 ppm concentrated boric acid solution was less than one degree centigrade for same heat flux. This indicates that the change in heat transfer coefficients between 2000 ppm and 5000 ppm concentrated solutions is less significant compared to decrease in heat transfer coefficients between deionized water and 2000 ppm concentrated boric acid solution.

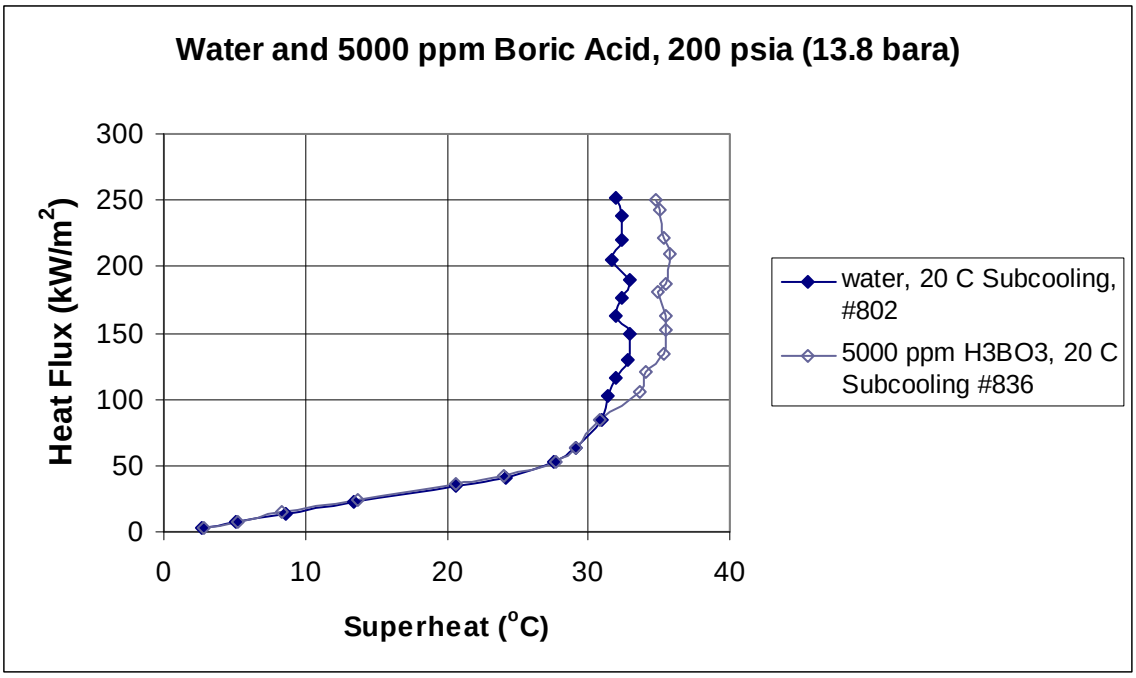

Figure 5-34 Effect of 5000 ppm boric acid concentration on heat transfer at 20° C subcooling and 200 psia pressure

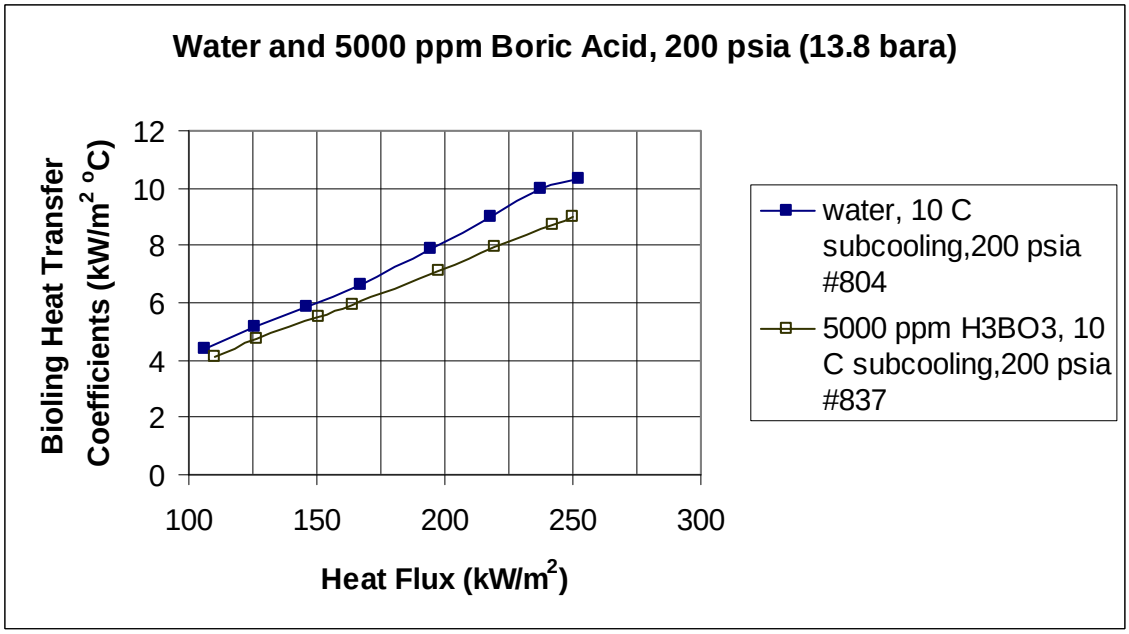

Figure 5-35 Effect of 5000 ppm boric acid concentration on heat transfer at 10° C subcooling and 200 psia pressure

Figure 5-19, Figure 5-26, Figure 5-31 , and Figure 5-37 show the influence of lithium metaborate solution relative to deionized water at 200 psia. Tests with lithium metaborate for pressure of 200 psia showed a similar trend of reduction in heat transfer coefficient with increased concentration, as that of tests done with the bulk liquid pressure of 100 psia. The boiling tests results indicated a reduction of heat transfer coefficient by 23% for a heat flux value of 221kW/m^2 for saturated temperature for 5000 ppm lithium metaborate solution.

Comparing the boiling curves from Figure 5-33 and Figure 5-36, indicate that lithium metaborate has more influence on heat transfer coefficients than boric acid.

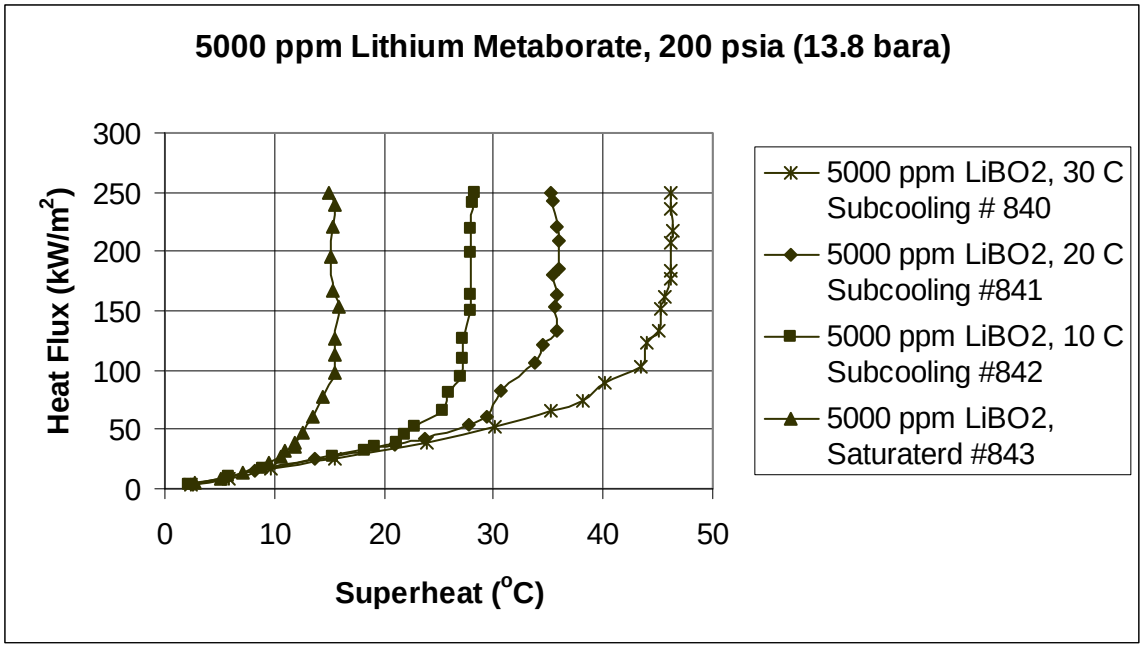

Figure 5-36 Boiling curves for 5000 ppm $LiBO_2$ solution, 200 psia

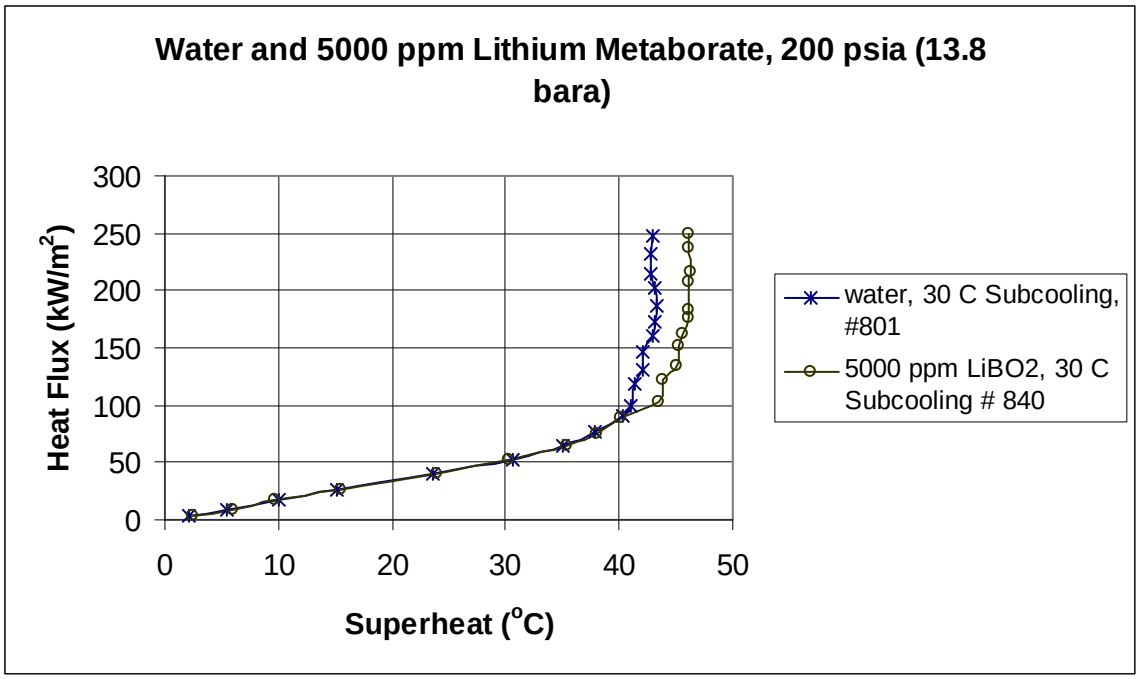

Figure 5-37 Effect of lithium metaborate concentration (5000 ppm) on heat transfer at 30^{o} C subcooling and 200 psia

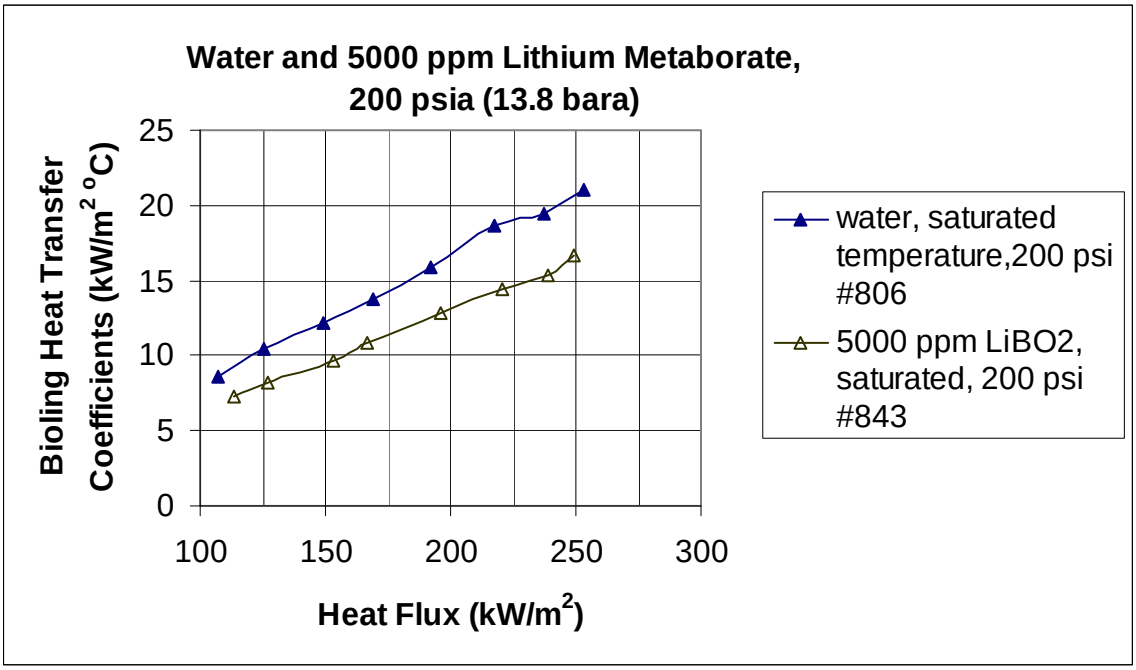

Figure 5-38 Degradation of heat transfer coefficients due to lithium metaborate (5000 ppm) at saturation and 200 psia

5.5 Tests at Pressure of 500 psia

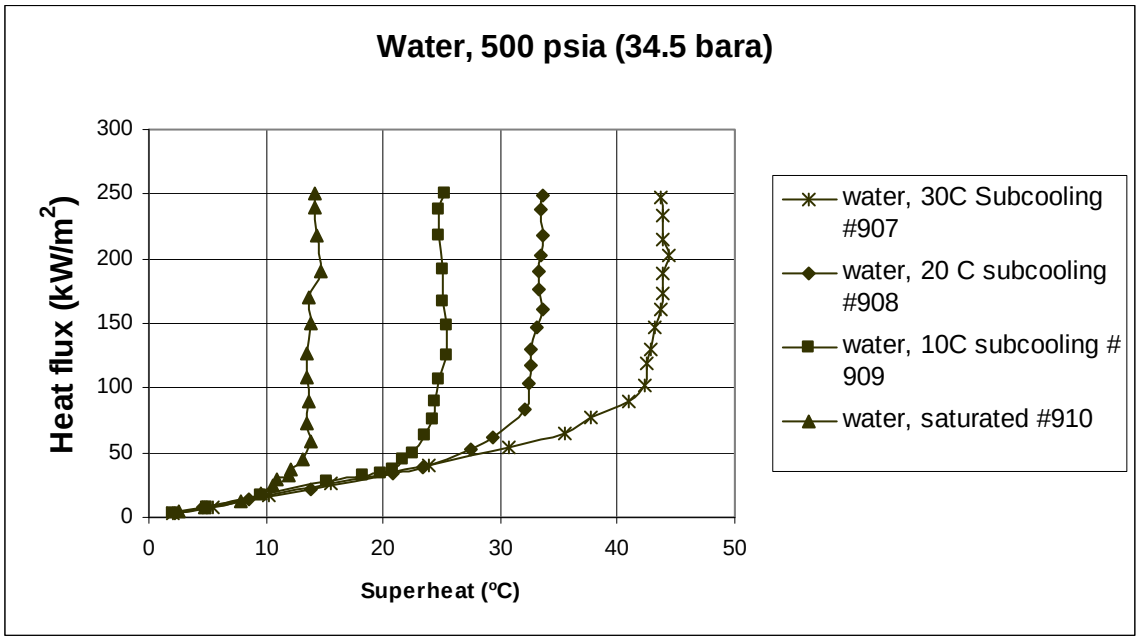

Figure 5-39 Boiling curves for deionized water at 500 psia

Boiling tests were conducted at a higher pressure of 500 psia. The boiling curves for pure deionized water at 500 psia are presented below in Figure 5-39. For lower heat flux, the boiling curves match well indicating the 'natural convection heat transfer' phase.

5.5.1 Tests with Boric Acid Solution

Figure 5-40 shows the results with 500 ppm boric acid. The variation in superheat values at constant heat flux can be observed in Figure 5-41. As with lower pressures, it was observed that 500 ppm boric acid solution at pressure of 500 psia has less influence on boiling heat transfer coefficients compared to solutions with higher concentrations of boric acid in it.

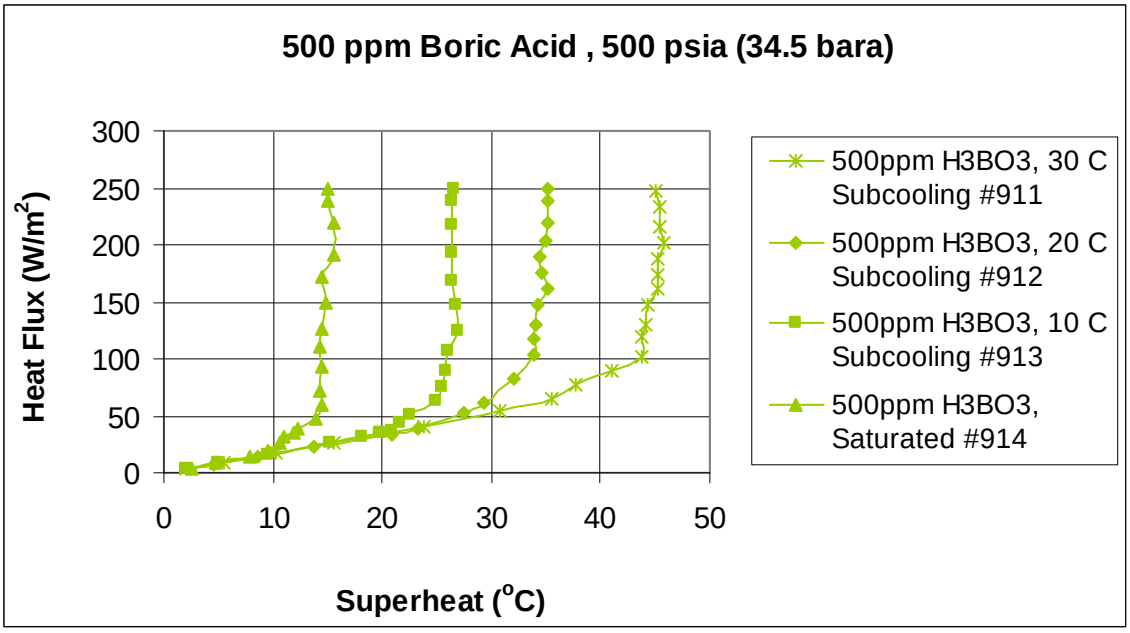

Figure 5-40 Boiling curves for tests with 500 ppm concentration boric acid solution at 500 psia

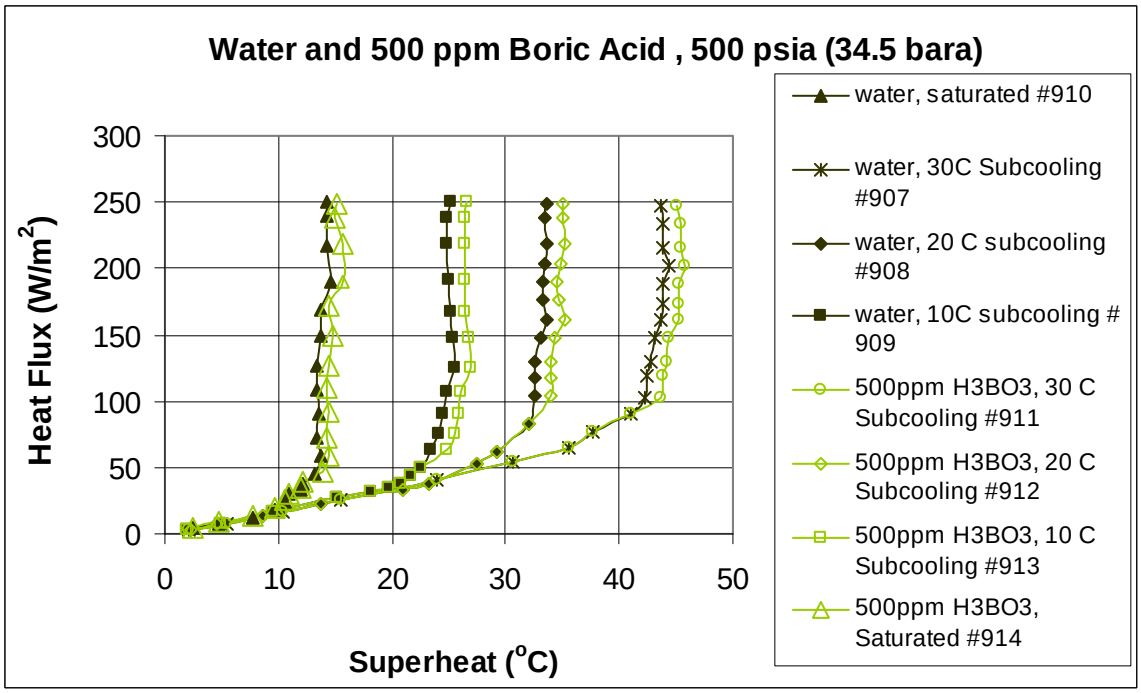

Figure 5-41 Boiling curves for deionized water and 500 ppm concentration boric acid solution at 500 psia

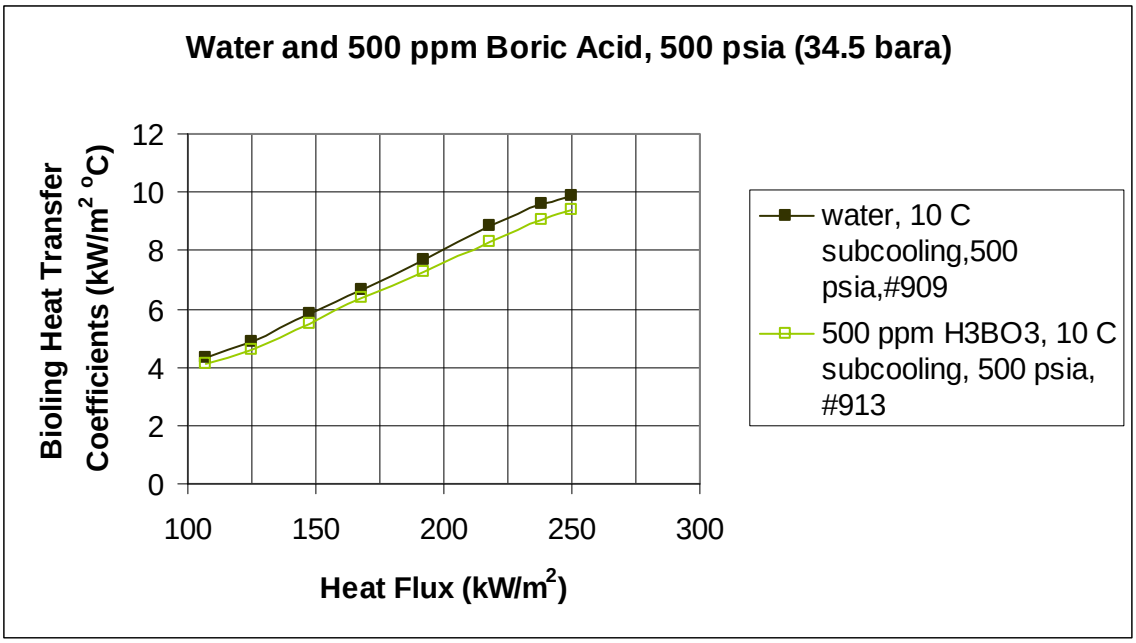

Figure 5-42 Comparison of heat transfer coefficients for water and 500 ppm boric acid solution at 10°C Subcooling and 500 psia

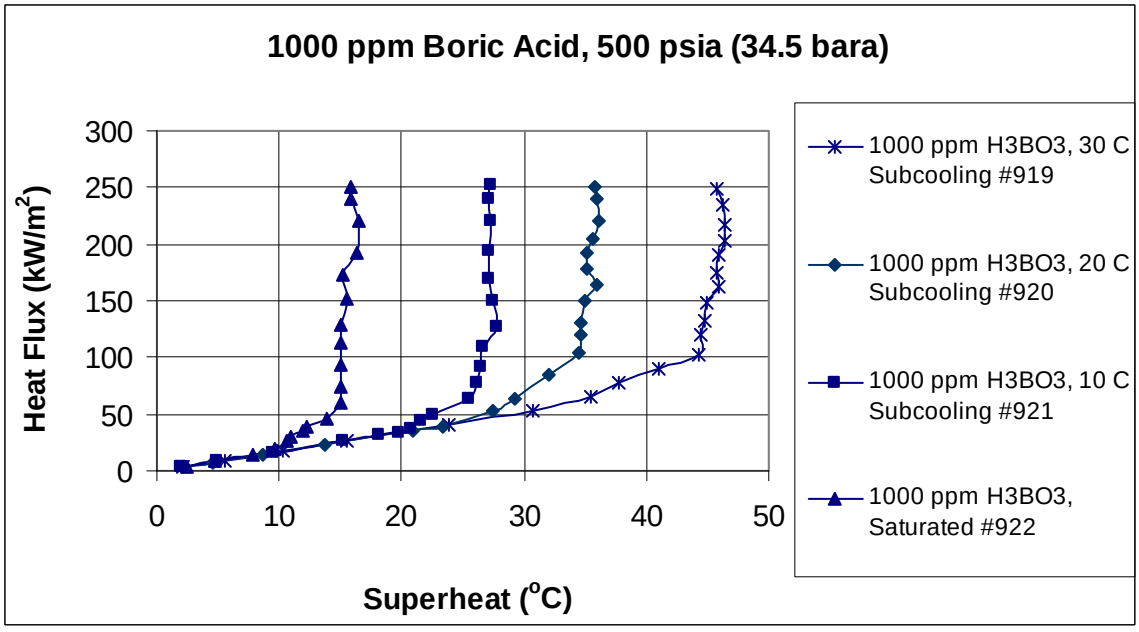

Figure 5-43 Boiling curves for tests with 1000 ppm concentration boric acid solution at 500 psia

Figure 5-42 indicates the change in boiling heat transfer coefficients in presence of 500 ppm boric acid compared to boiling heat transfer coefficients for deionized water.

The average decrease in heat transfer coefficient was found to be 5.5 % for 500 ppm boric acid, relative to water.

The boiling test results of 1000 ppm boric acid and 2000 ppm boric acid are shown in Figure 5-43 and Figure 5-45 respectively. Figure 5-46 indicates the decrease in heat transfer coefficient in presence of boric acid at 2000 ppm concentration with respect to deionized water. From Figure 5-46 the degradation in boiling heat transfer coefficient for 2000 ppm boric acid solution was found to be reduced by 21%, when compared with deionized water (#930 & #904) at 500 psia. Figure 5-44 shows the variation in boiling curves for 1000 ppm boric acid solution test and for deionized water at 10^{o}C subcooling of 231.4^{o}C.

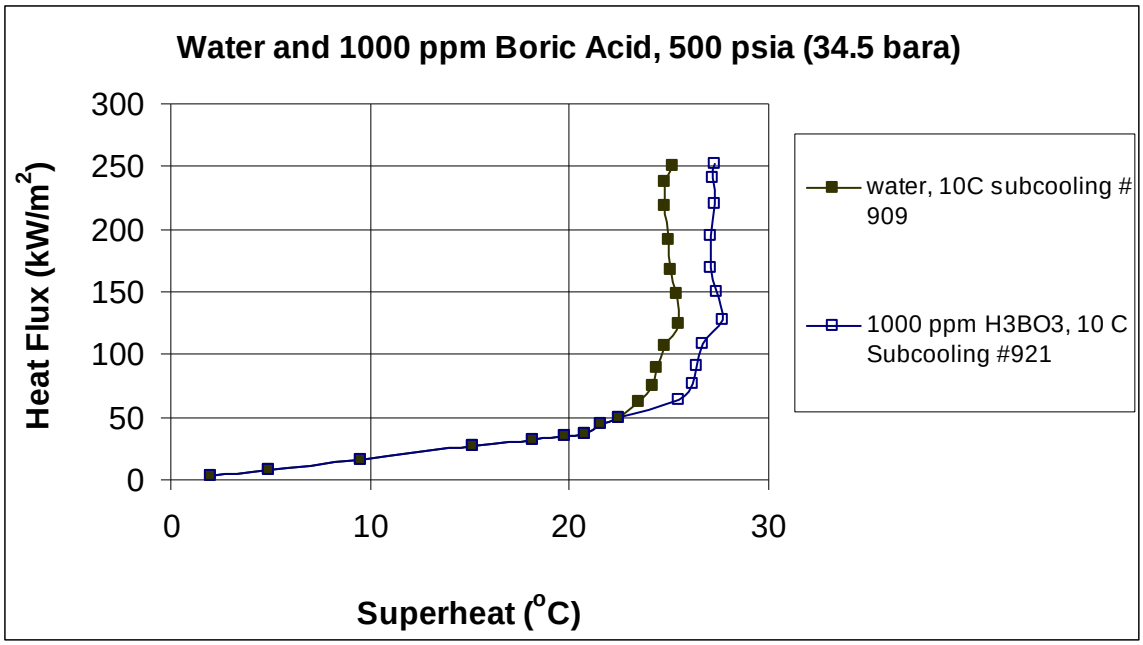

Figure 5-44 Effect of boric acid concentration on heat transfer at 10^{o} C subcooling and 500 psia pressure

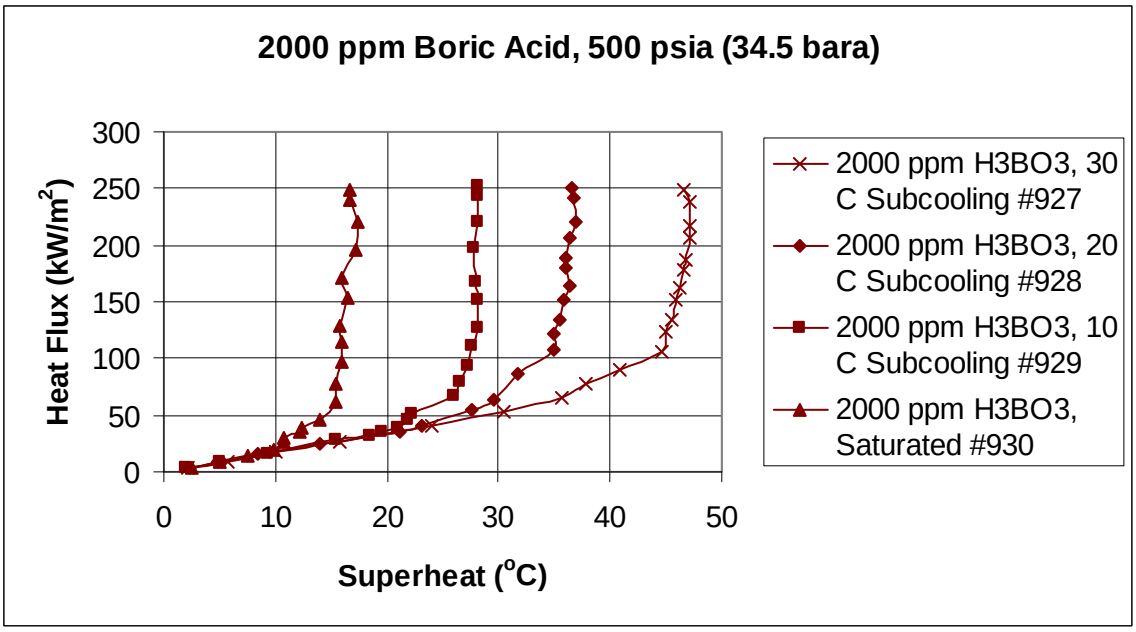

Figure 5-45 Boiling curves for tests with 2000 ppm concentration boric acid solution at 500 psia

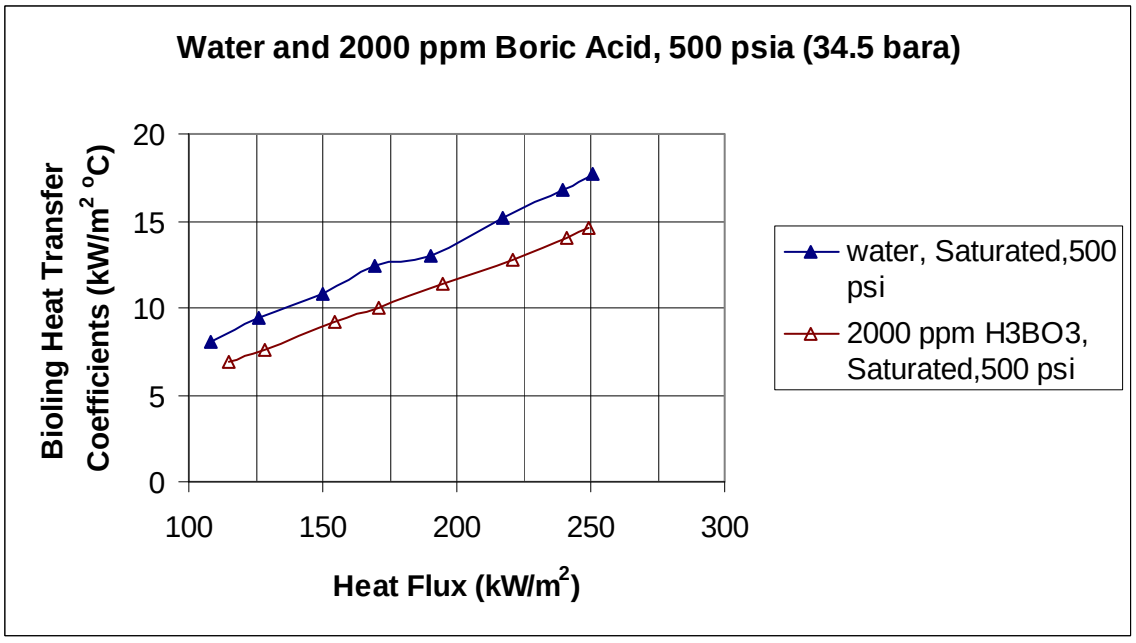

Figure 5-46 Degradation of boiling heat transfer coefficients due to 2000 ppm boric acid solution at 500 psia

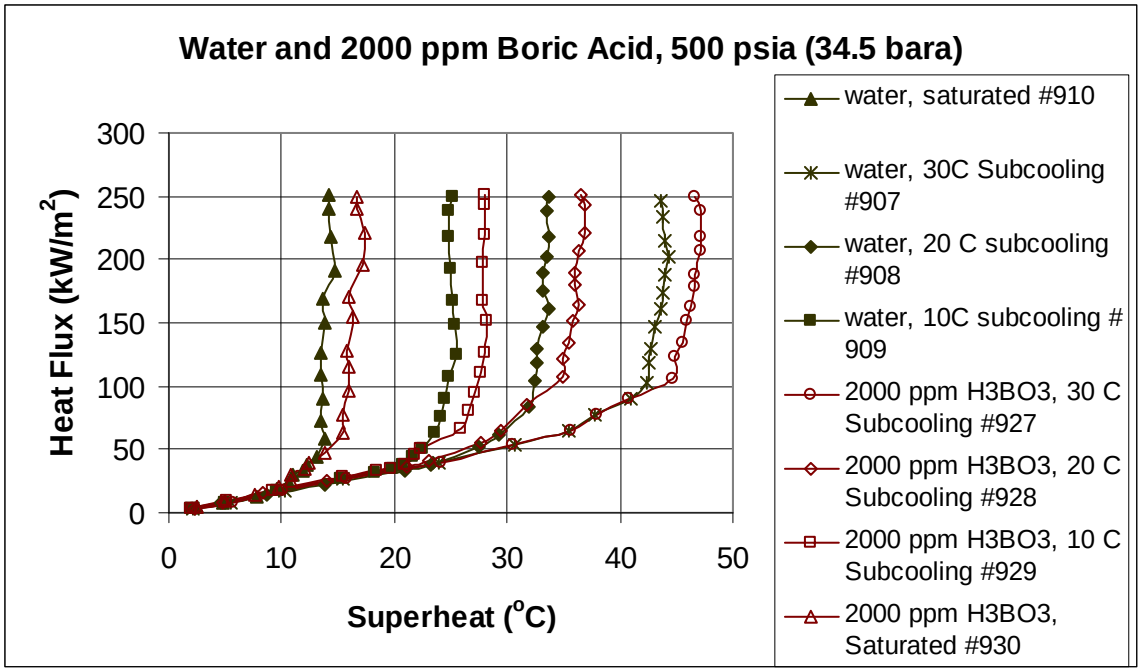

Figure 5-47 Boiling curves for deionized water and 2000 ppm concentration boric acid solution at 500 psia

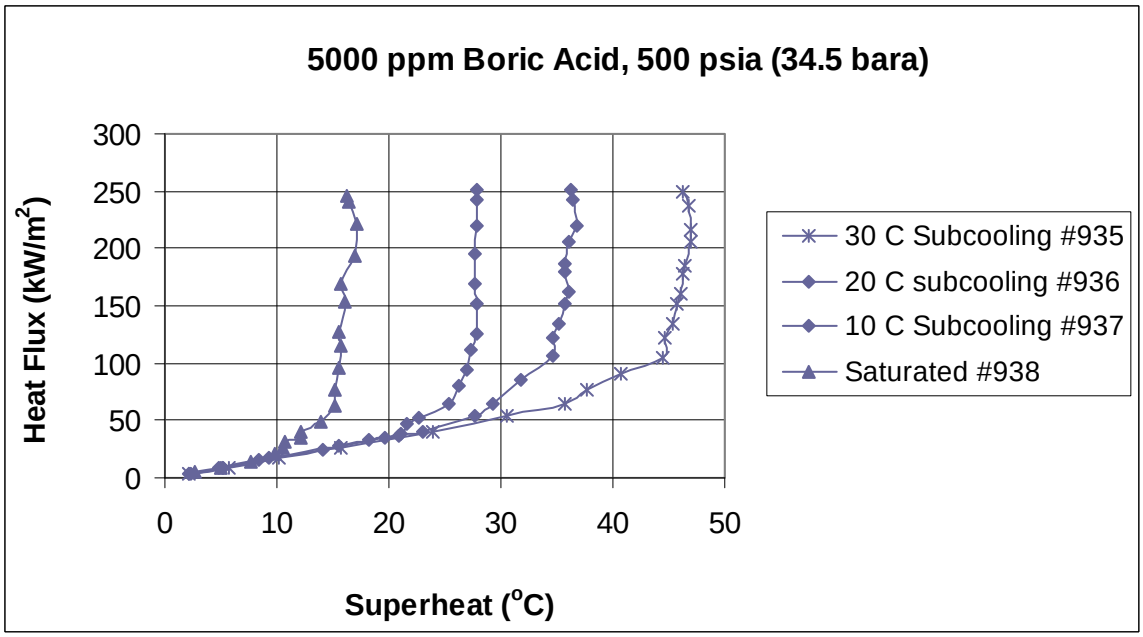

Figure 5-48 Boiling curves for tests with 5000 ppm concentration boric acid solution at 500 psia

Figure 5-48 shows tests through 935 and 939 where the degree of subcooling ranges from 30 ^{o}C to 0^{o}C for pool boiling test with 5000 ppm concentrated boric acid solution. Figure 5-41, Figure 5-47 and Figure 5-49 represent the change in the boiling curves for 500 ppm, 2000 ppm and 5000 ppm concentrated boric acid solution respectively, with reference to boiling curve deionized water at saturation and various subcooled conditions.

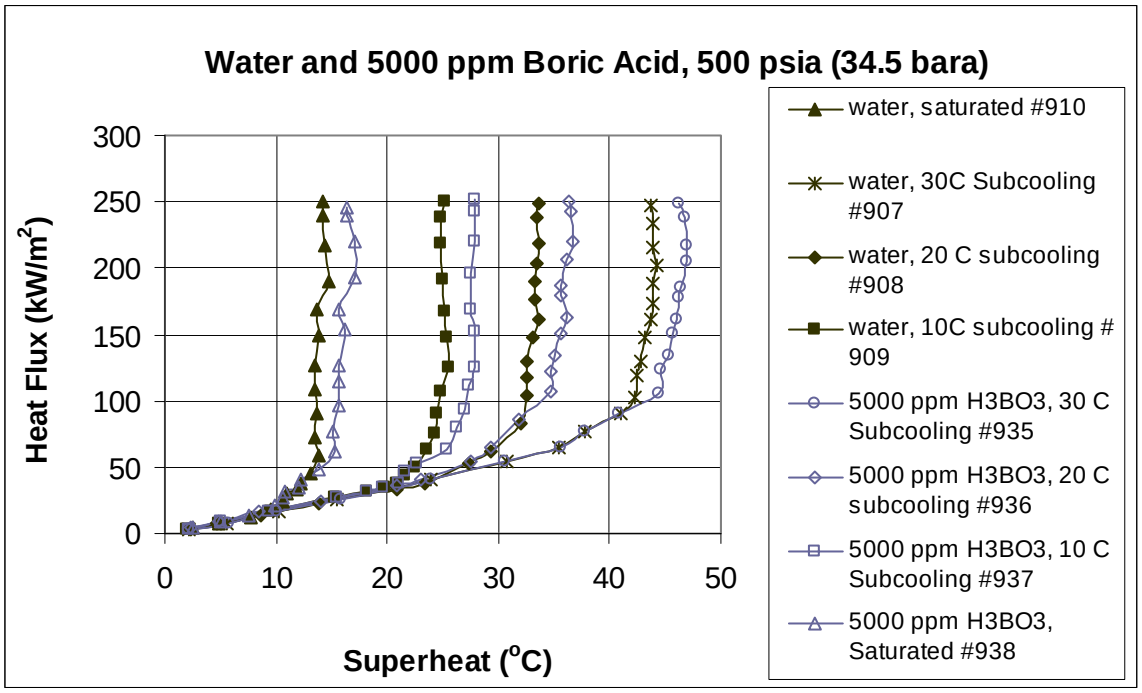

Figure 5-49 Boiling curves for deionized water and 5000 ppm concentration boric acid solution at 500 psia

From Figure 5-49, it can be observed that the superheat for 5000 ppm boric acid solution is considerably greater than that of deionized water at saturation temperature of 284.4^{o}C, at 10^{o}C Subcooling, at 20^{o}C Subcooling and 30^{o}C Subcooling. This indicates that the temperature difference between the heater surface and bulk fluid is increased due to resistance offered by the boric acid solution. The nucleation pattern for 5000 ppm

boric acid solution was not uniform unlike that of deionized water and this could explain the reason for decrease in heat transfer coefficients. The decrease in heat transfer coefficients can be explained by poor coalescence of bubbles in the presence of boric acid, leading to lesser nucleation and hence lower heat transfer coefficients than deionized water.

5.5.2 Tests with Lithium Metaborate

The Figure 5-50 shows the test results from 915 through 918 for 500 ppm lithium metaborate concentration. The Figure 5-51 shows the reduction in heat transfer coefficient for 500 ppm lithium metaborate in comparison with deionized water.

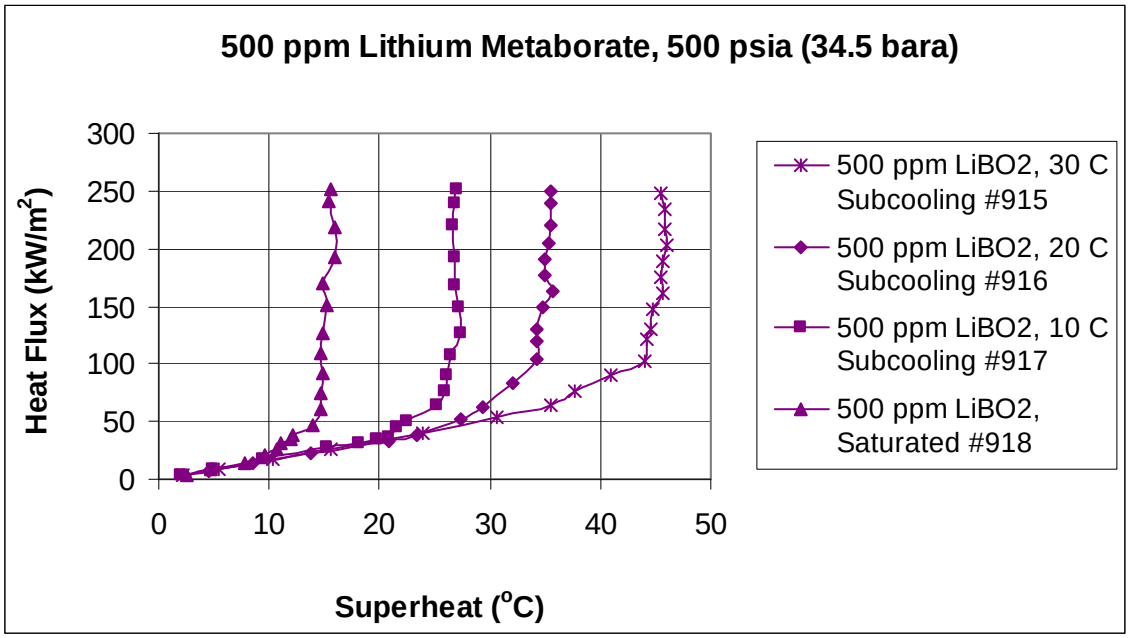

Figure 5-50 Boiling curves for tests with 500 ppm lithium metaborate solution at pressure of 500 psia

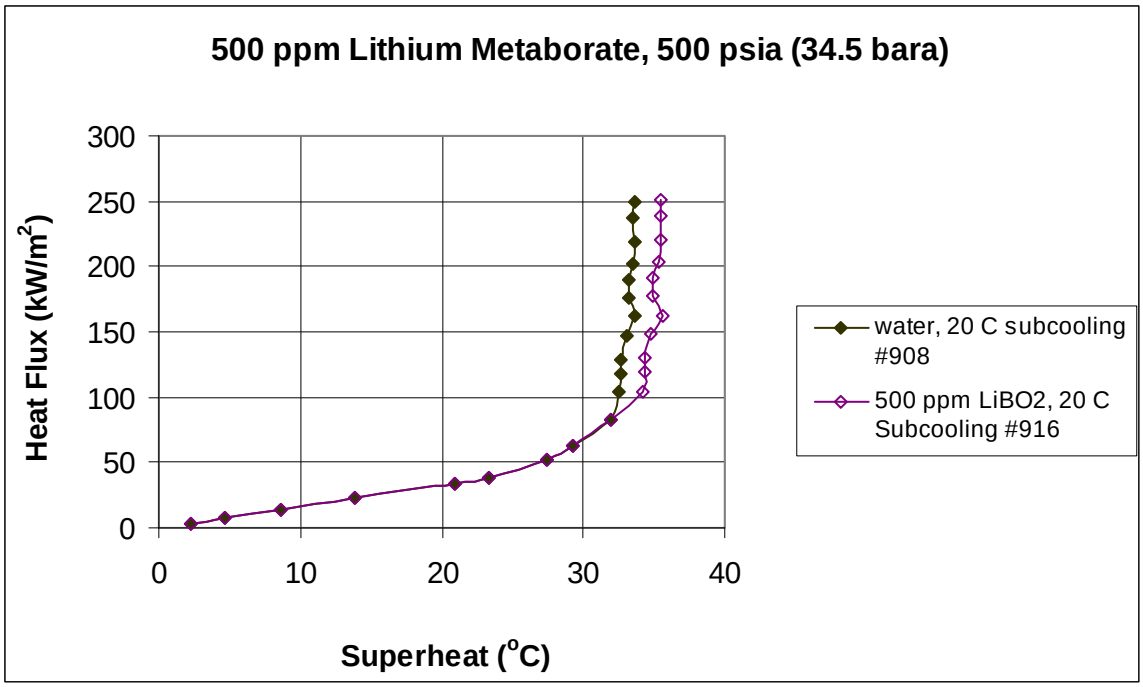

Figure 5-51 Effect of 500 ppm lithium metaborate concentration on heat transfer at 20^{o} C Subcooling condition and 500 psia pressure

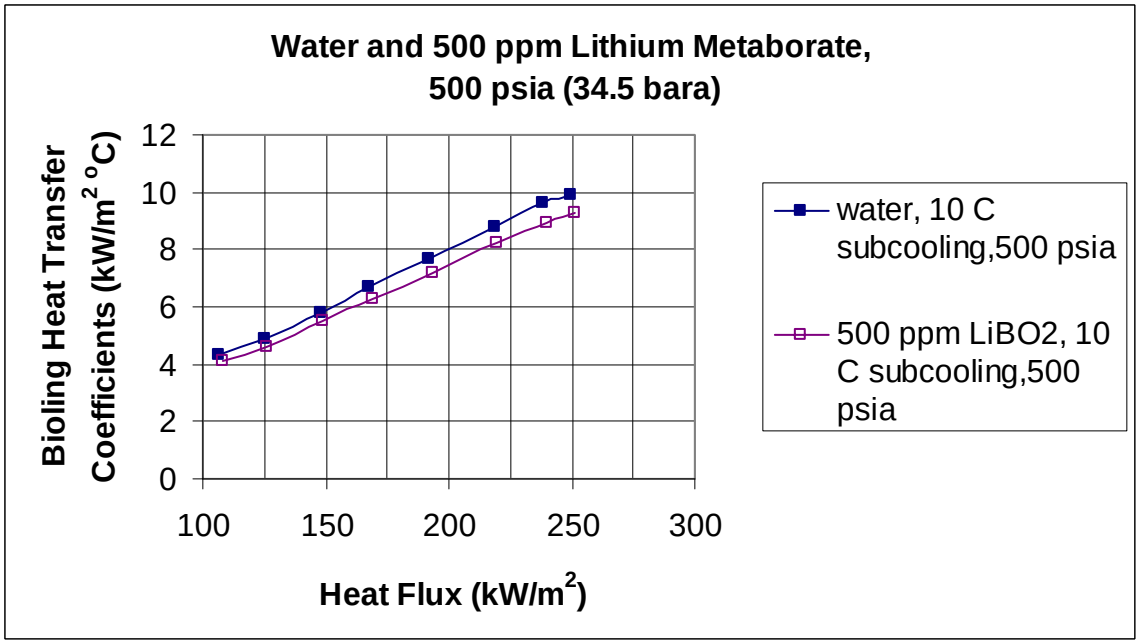

Figure 5-52 Comparison of the heat transfer coefficients of water and 500 ppm boric acid at 10^{o}C subcooling and 500 psia

The average reduction in heat transfer coefficient for 10°C subcooling was found to be 5.3% indicating that the heat transfer coefficient remains less affected for a concentration level of 500 ppm. The reduction in heat transfer coefficients for all the subcooling for 500 ppm lithium metaborate solution varied between 4.0%and 5.9% when compared to water at 500 psia pressure.

Figure 5-53, Figure 5-55 and Figure 5-58 show the results of tests with 1000 ppm, 2000 ppm and 5000 ppm concentration of lithium metaborate, respectively. These figures indicate that temperature difference between the test heater surface and coolant increases with increase in coolant concentration.

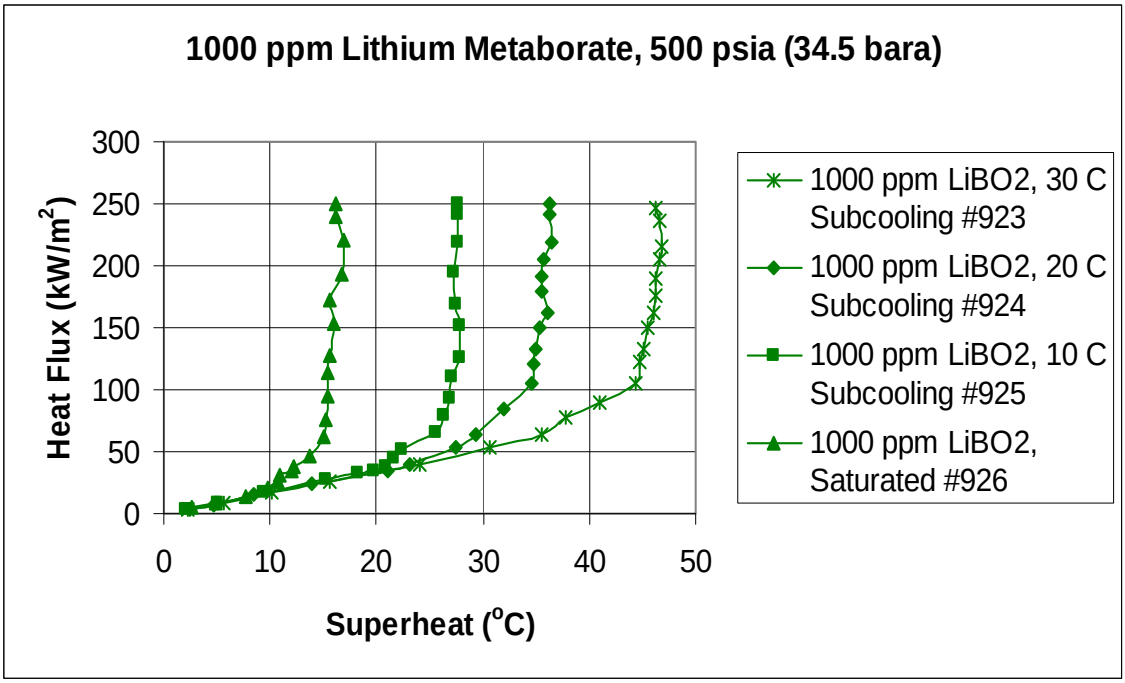

Figure 5-53 Boiling curves for tests with 1000 ppm lithium metaborate solution at pressure of 500 psia

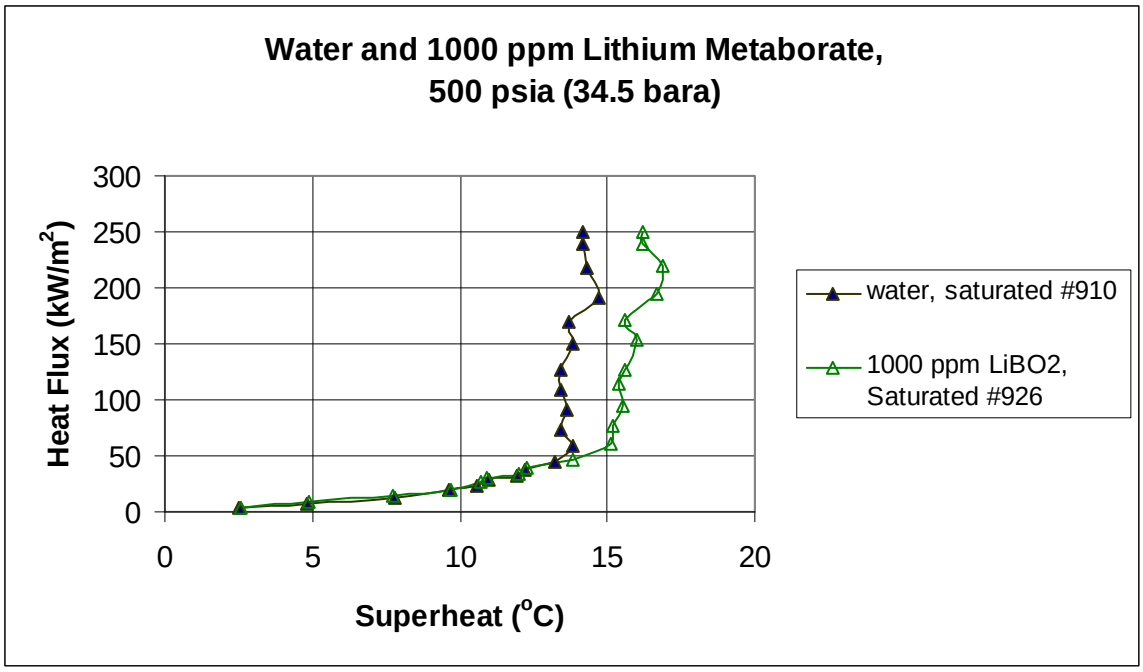

Figure 5-54 Effect of 1000 ppm lithium metaborate concentration on heat transfer at saturated condition and 500 psia pressure

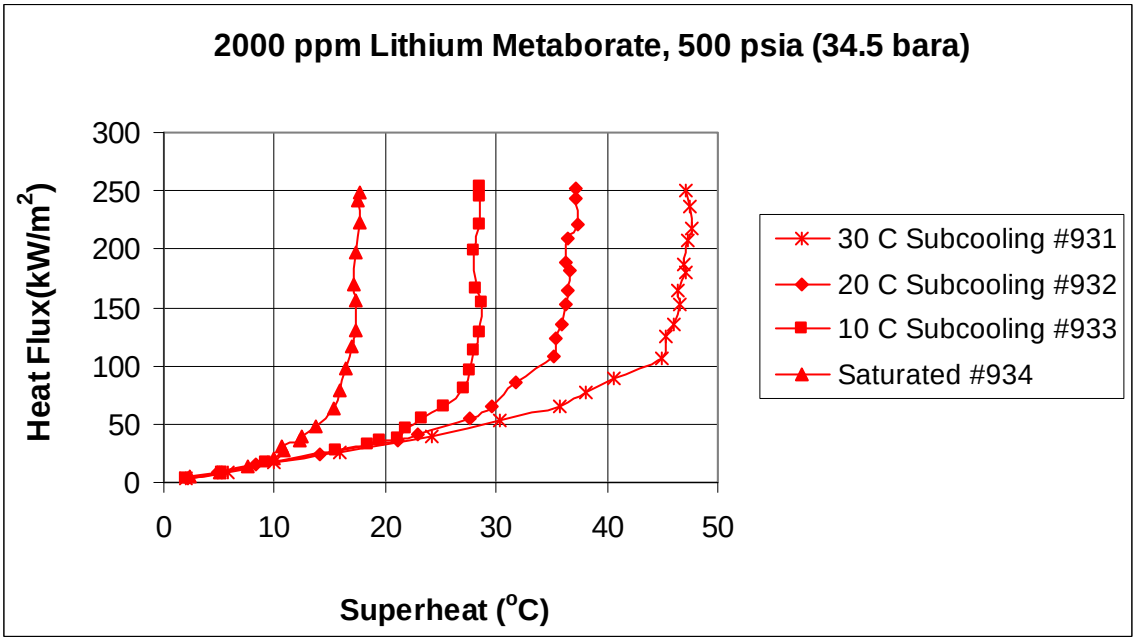

Figure 5-55 Boiling curves for tests with 2000 ppm lithium metaborate solution at pressure of 500 psia

Figure 5-56 shows the variation in boiling curves for saturated temperature and Figure 5-57 indicates the degradation of heat transfer coefficient due to the addition of lithium metaborate at 2000 ppm concentration. It can be observed that heat transfer coefficient is reduced by 22.4% (for heat flux of 170 kW/m^2) for 2000 ppm lithium metaborate solution. It is also interesting to note that the at 5000 ppm concentration the degradation of heat transfer is not significantly different from that at 2000 ppm when compared with boiling heat transfer coefficients of water.

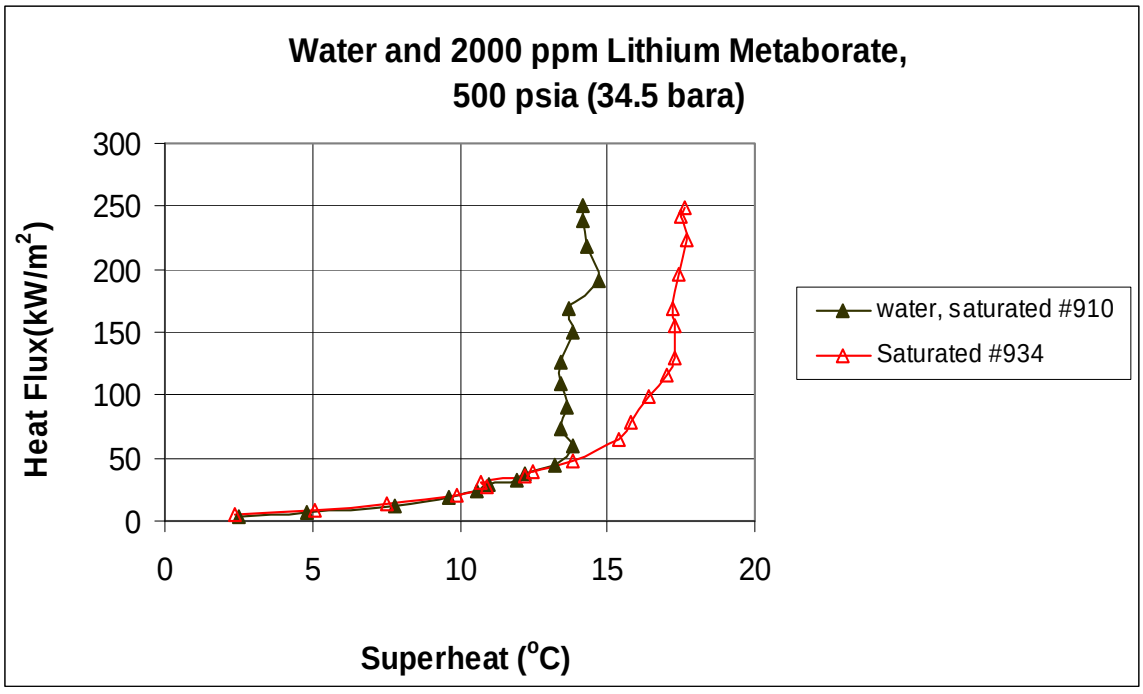

Figure 5-56 Effect of 2000 ppm lithium metaborate concentration on heat transfer at saturated condition and 500 psia pressure

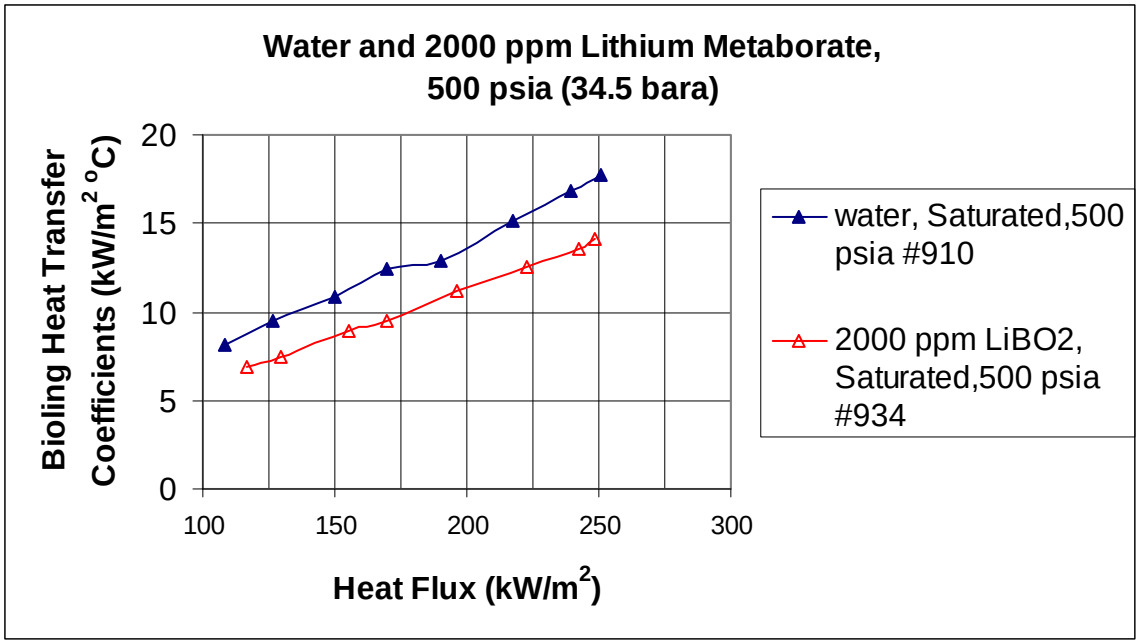

Figure 5-57 Degradation of boiling heat transfer coefficients in presence of lithium metaborate (2000 ppm) at 500 psia

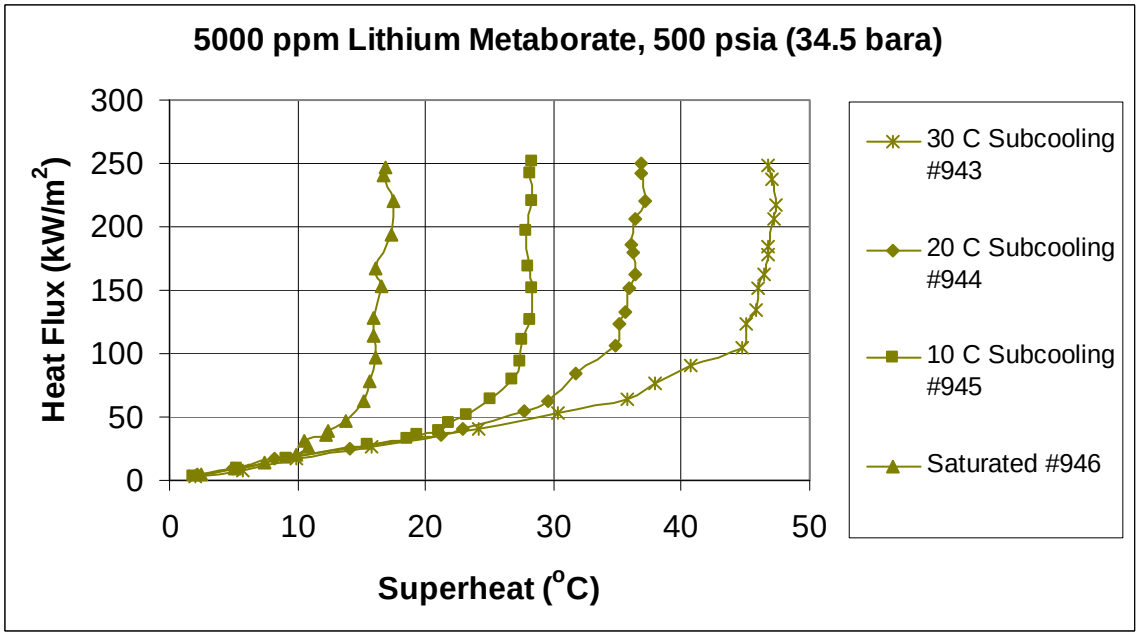

Figure 5-58 Boiling curves for tests with 5000 ppm lithium metaborate solution at pressure of 500 psia

Figure 5-59 shows the degradation in heat transfer coefficients for 5000 ppm concentrated lithium metaborate solution at saturated conditions. For instance, the heat

transfer coefficient was decreased by 23% for 5000 ppm concentration of lithium metaborate for test numbered 946 (at heat flux of 169 kW/m^2). This trend indicates that increase in the presence of lithium in the coolant beyond a certain concentration does not have a significant effect on the heat transfer coefficients. It was observed that for coolant concentrations more than 2000 ppm, the change in nucleation pattern due to additive ($libo_2$) to solution is very minimal.

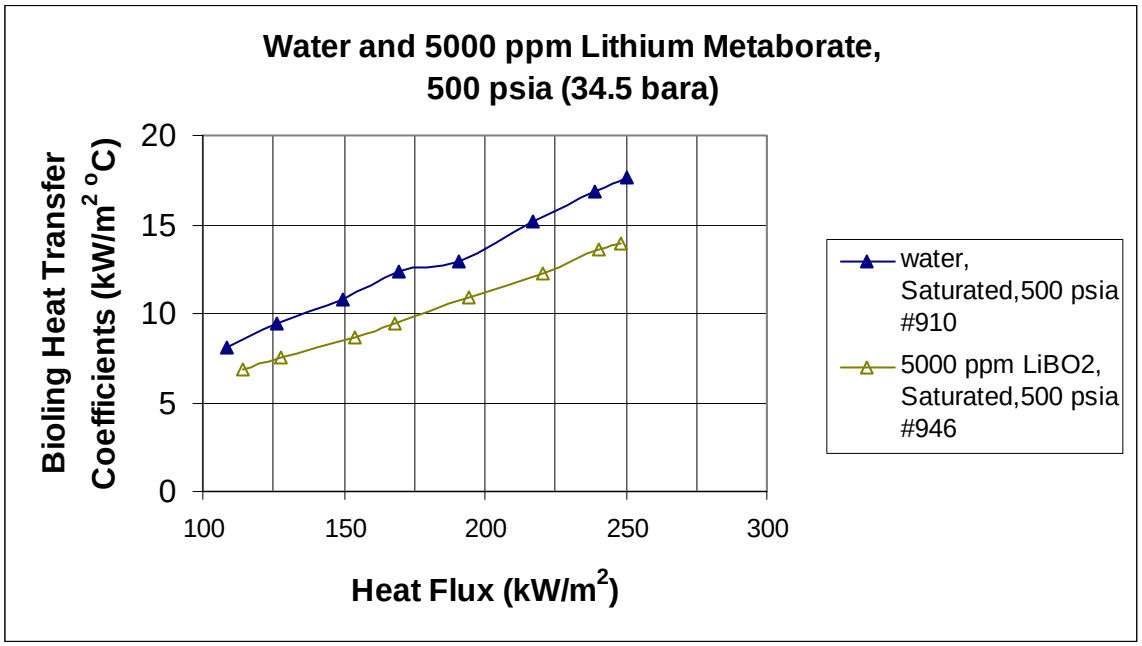

Figure 5-59 Degradation of boiling heat transfer coefficients in presence of lithium metaborate (5000 ppm) at 500 psia

5.6 Tests at Pressure of 1000 psia

Boiling tests done at 1000 psia are very significant as it is done at pressures approaching those typical of PWR conditions. Figure 5-60 shows the boiling curves for deionized water at 1000 psia for tests through 951 through 954. Boiling curves show a similar trend for all the subcooled conditions and saturated conditions as that of lower

pressures. The boiling curves coincide well for lower heat flux indicating that increase of pressure does not have any effect on heat transfer by natural convection.

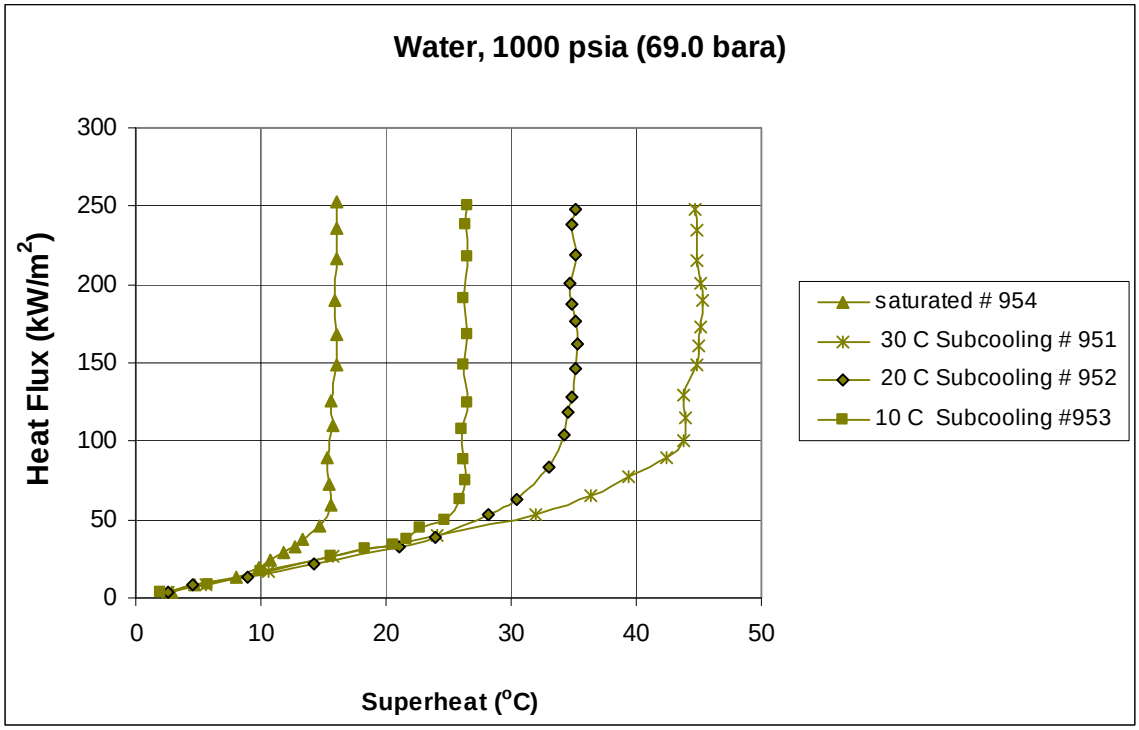

Figure 5-60 Boiling curves for deionized water at 1000 psia

The saturation temperature of water at 1000 psia is 284.6 °C. It was observed that the heat transfer coefficients decreased slightly when compared to tests done with deionized water at lower pressures. Marginal degradation of heat transfer coefficients could be explained by the nucleation pattern. It was observed that at higher pressures, the nucleation was restricted by fluid pressure. Due to higher pressures the cavities, which act as nucleation sites are completely filled with liquid, therefore causing resistance for formation of new bubbles. It may be recalled that cavities, which are partially wetted, have more chance of being nucleation sites than cavities that are completely wetted [Collier and Thome, 1994].

Repeatability is an important concern during boiling tests. The reproducibility of results depends on the following the same defined procedure for conducting the boiling tests. Boiling tests were performed in regular intervals for same conditions to check the repeatability of results. Repeated pool boiling tests were performed with deionized water at 10^{o} C subcooling. The results of test 953, 983, 985 and 986 had a boiling heat transfer coefficient of 9.05 kW/m^{2o}C, 9.5 kW/m^{2o}C, 8.75 kW/m^{2o}C and 9.1 kW/m^{2o}C for a heat flux of 238 kW/m^2 at a pressure of 1000 psia and saturated temperature. The maximum boiling heat transfer coefficient was found to be 4.3% more than average heat transfer coefficient, while the minimum was 3.8% less than average boiling heat transfer coefficient. The deviation in results is likely due to the uncertainty in measurement of temperatures, voltage and current. The deviations obtained in the heat transfer coefficients were within the uncertainty as detailed in section 4.7.

5.6.1 Tests with Boric Acid Solution

Figure 5-61 shows the boiling curves for tests through 958 and 961 for 500 ppm boric acid solution. It can be observed from Figure 5-62 that the influence of the boric acid solution at 500 ppm concentration is not significant. The change in heat transfer coefficients was found to be less than 5% and could be considered as not significant since it is less than reduction in heat transfer coefficients at higher concentration of boric acid. The test results for 500 ppm boric acid solution at 1000 psia pressure also indicate that the bulk fluid pressure has little effect on heat transfer coefficients. When compared with boiling curves for 500 ppm concentrated boric acid in Figure 5-40, it can be noticed that there is no significant different in superheat values for a constant heat flux. This indicates

that the effect of bulk fluid pressure on heat transfer coefficients is less than 5% even in the presence of boric acid.

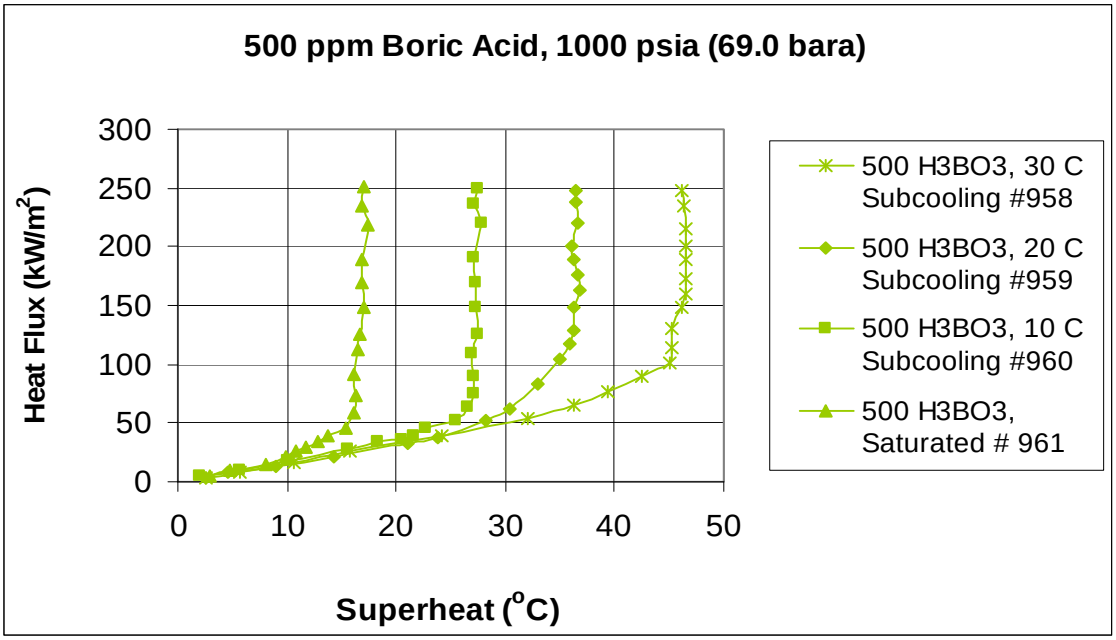

Figure 5-61 Boiling curves for tests with 500 ppm boric acid solution at pressure of 1000 psia

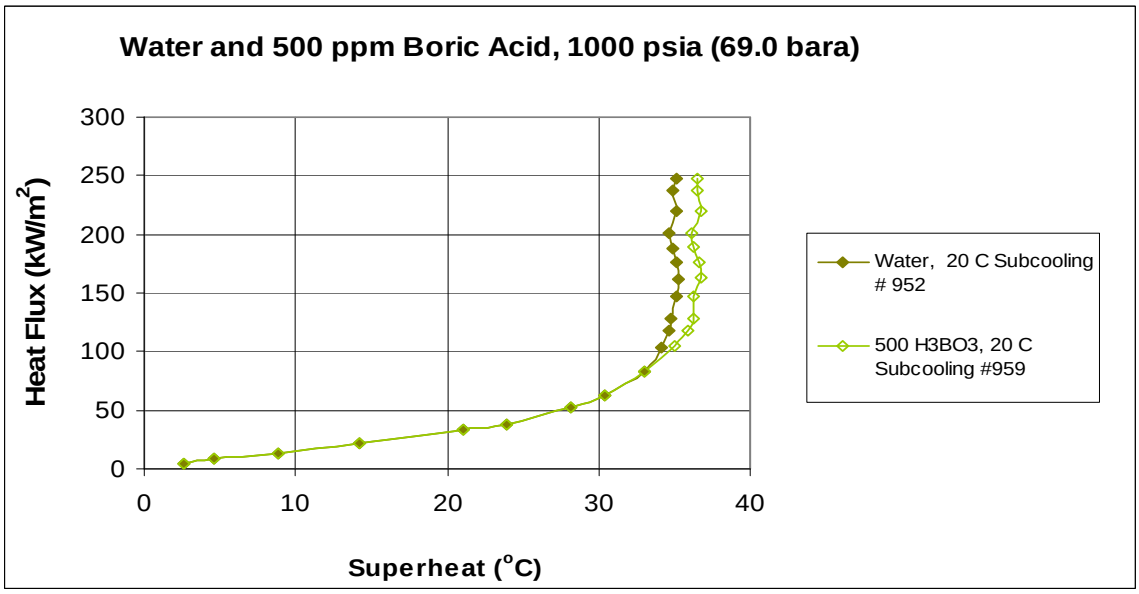

Figure 5-62 Effect of boric acid concentration on heat transfer at 20° C subcooling and 1000 psia pressure

Figure 5-63 shows the boiling test results for all subcooled and saturated conditions with 1000 ppm boric acid solution. It can be observed that the temperature difference between the wall and bulk fluid is higher than that of deionized water indicating that the nucleation affects the heat transfer coefficients. Figure 5-65 shows boiling curves obtained from tests 975 through 978.

Figure 5-66 and Figure 5-67 show the change in boiling curves of the above mentioned test with that of deionized water and variation in heat transfer coefficients respectively. It can be observed that the addition of boric acid to water has a degrading effect on the heat transfer coefficient. Figure 5-68 displays the results of tests done with 5000 ppm concentrated boric acid. The consistent decrease in the heat transfer coefficients with the increase in coolant concentration of boric acid indicates a relation between the concentration level and heat transfer coefficients.

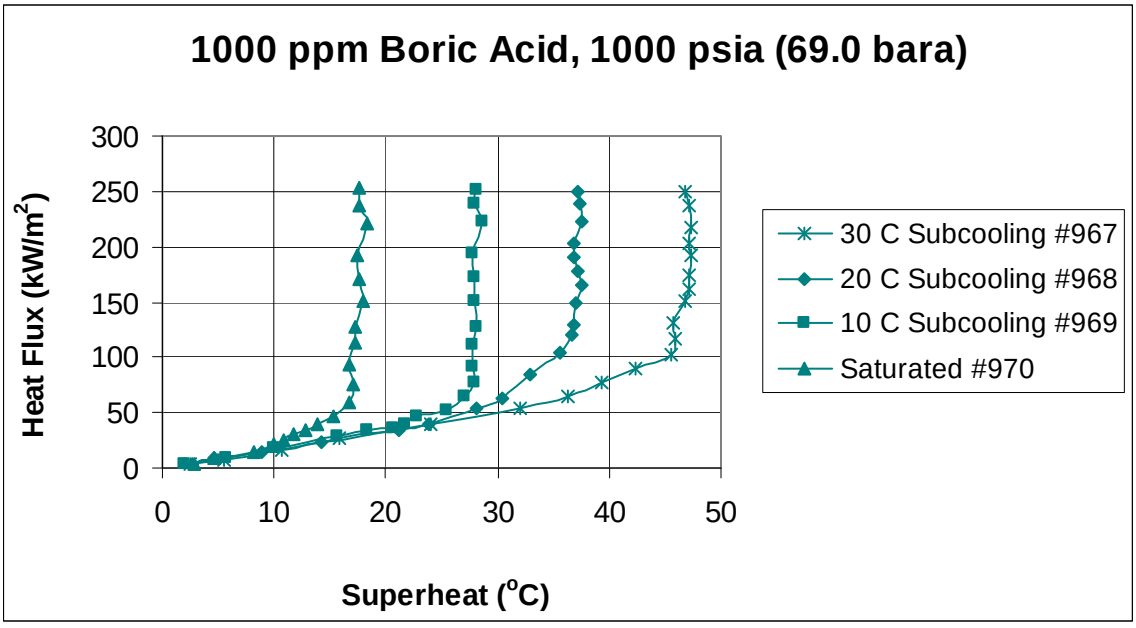

Figure 5-63 Boiling curves for tests with 1000 ppm boric acid solution at pressure of 1000 psia

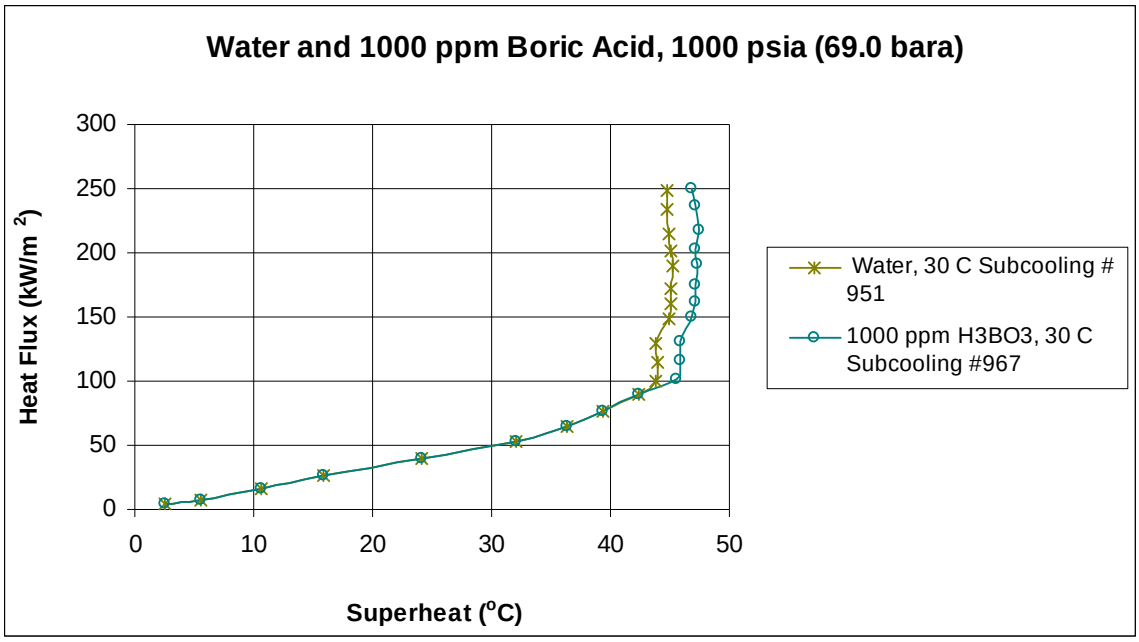

Figure 5-64 Effect of boric acid concentration on heat transfer at 30° C subcooling and 1000 psia pressure

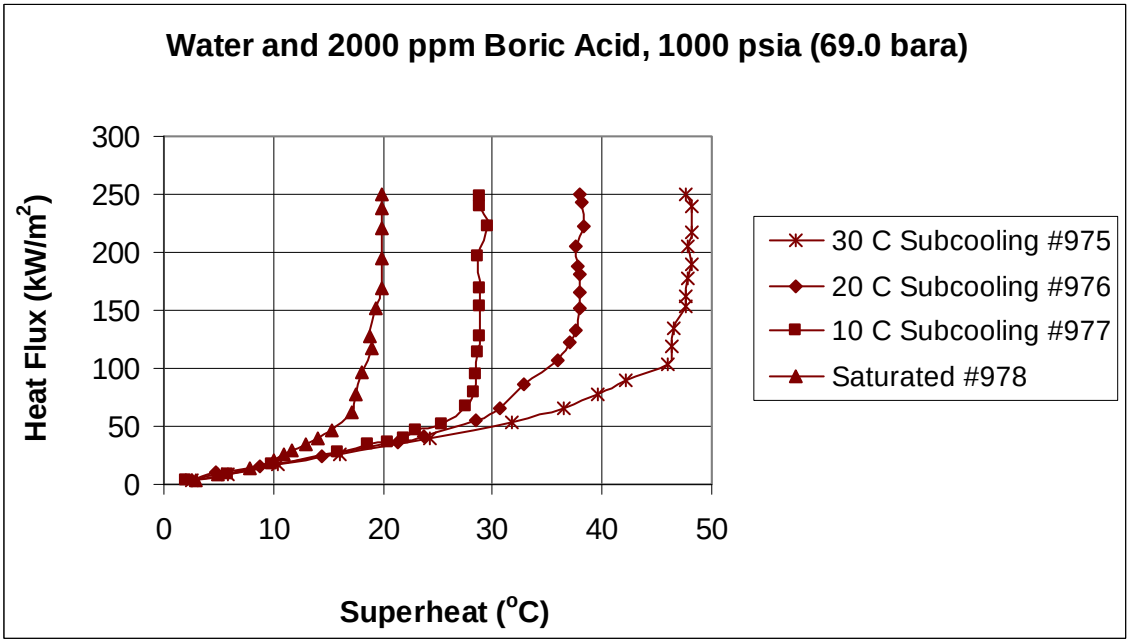

Figure 5-65 Boiling curves for tests with 2000 ppm boric acid solution at pressure of 1000 psia

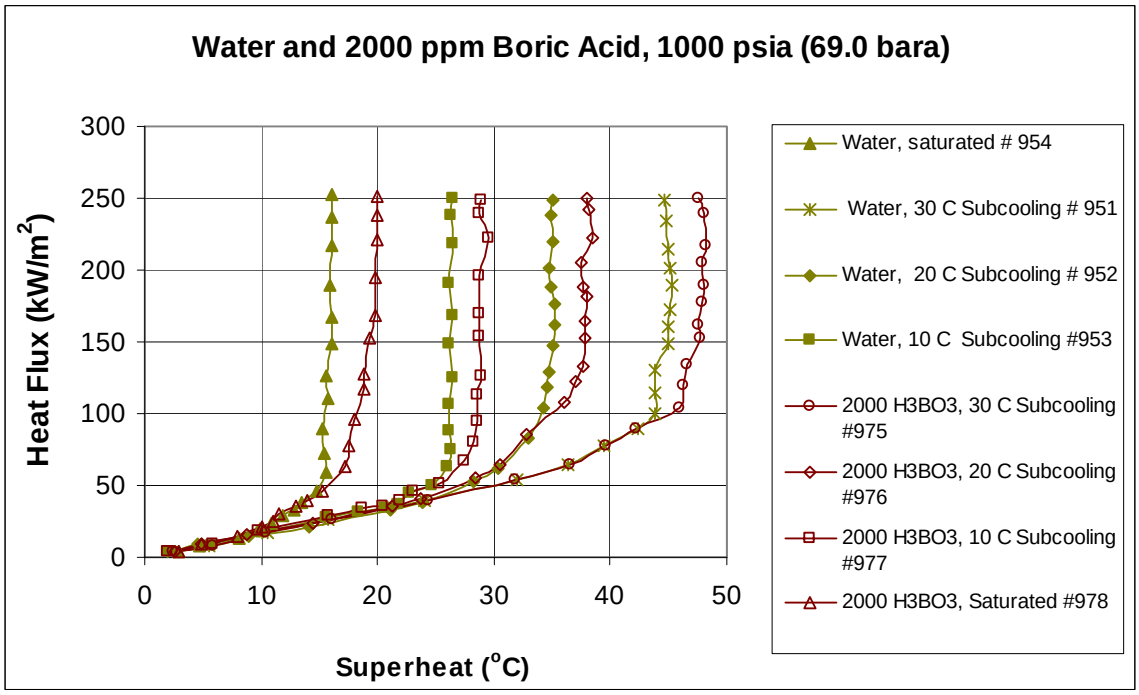

Figure 5-66 Boiling curves for deionized water and 2000 ppm concentration boric acid solution at 1000 psia

Figure 5-69 shows the degradation in heat transfer coefficients for test 992. The pool boiling heat transfer coefficient decreased by 23% (for q= 236 kW/m^2) for 5000 ppm concentrated boric acid solution at saturated temperature, when compared to heat transfer coefficient for water. The test results have thus indicated that boiling heat transfer coefficients are considerably affected by the presence of boron at higher concentrations. The likely reason for decrease of heat transfer coefficients is due to a decrease in nucleation sites. The boron particles in the solution seem to reduce the formation of new nucleation sites because of coagulation of bubbles. This results in reduction of heat transfer coefficients as the scope of formation of new isolated bubbles is decreased.

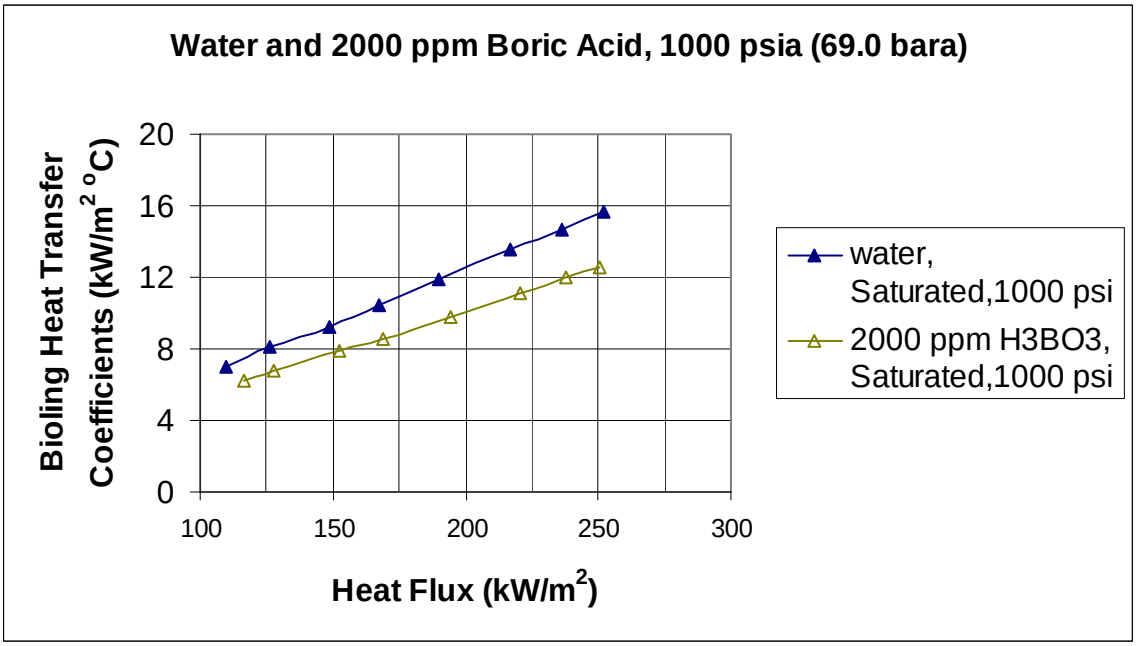

Figure 5-67 Effect of boric acid concentration (2000 ppm) on heat transfer coefficients at pressure of 1000 psia and at saturation

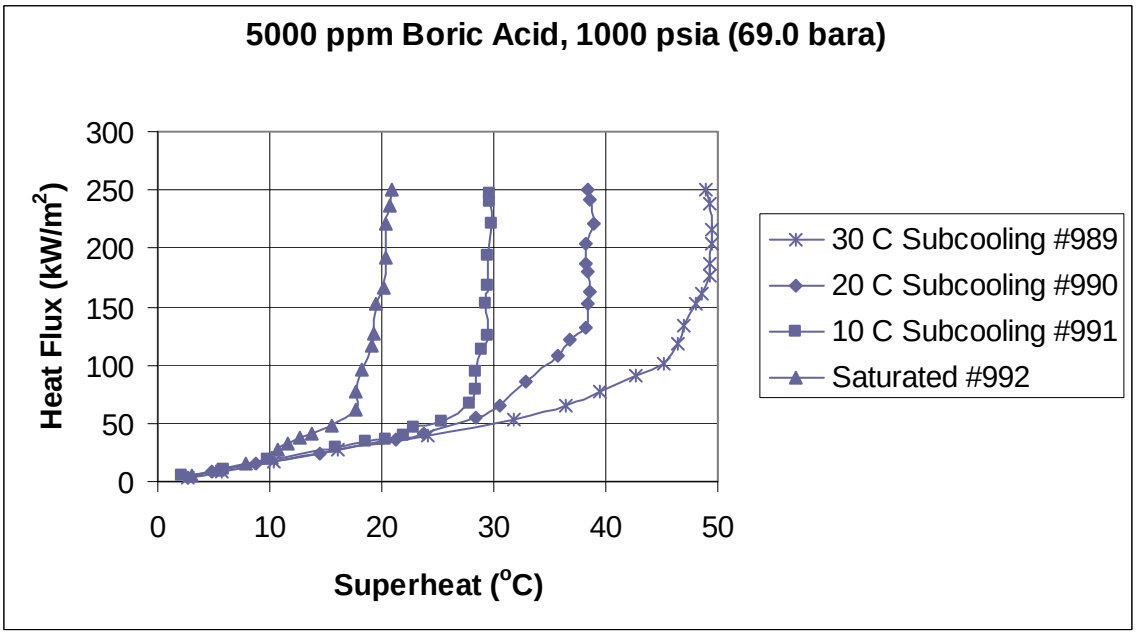

Figure 5-68 Boiling curves for tests with 5000 ppm boric acid solution at pressure of 1000 psia

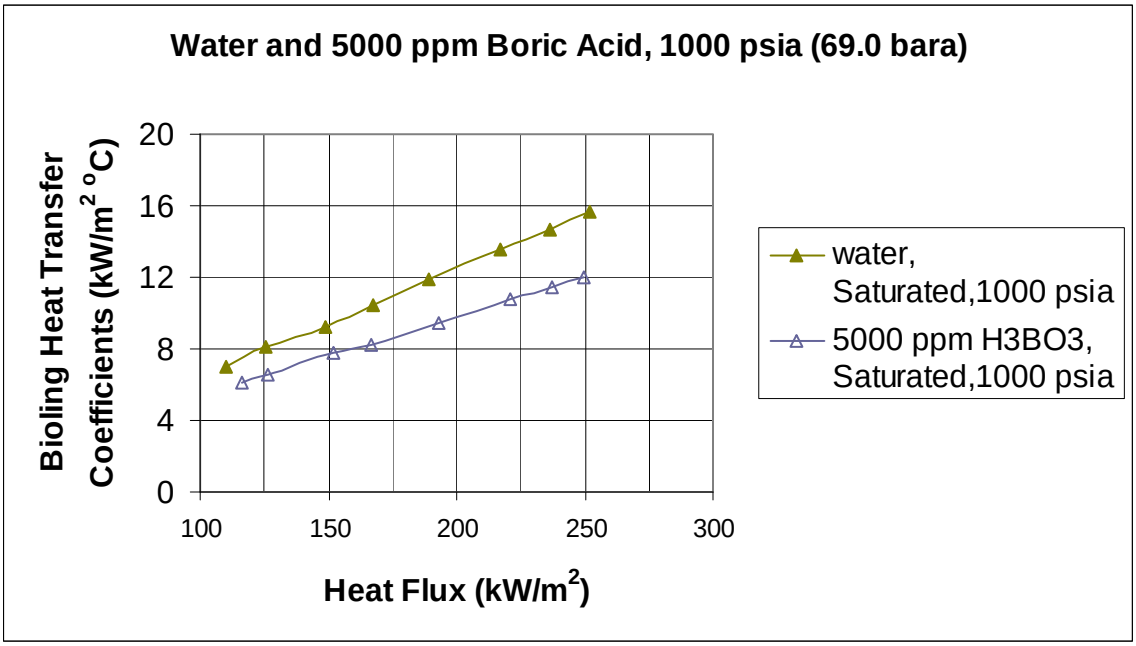

Figure 5-69 Degradation of boiling heat transfer coefficients for 5000 ppm concentrated boric acid solution at 1000 psia pressure and saturated condition

5.6.2 Tests with Lithium Metaborate

Pool boiling test results for 500 ppm concentrated lithium metaborate solution are presented in Figure 5-70. Figure 5-71 indicates the variation in superheat values for 500 ppm lithium metaborate solution relative to deionized water. The heat transfer coefficients for the 500 ppm lithium metaborate boiling test decreased by 4.5% for a heat flux of 176 kW/m^2 at bulk fluid saturation temperature. Figure 5-72 shows the results of boiling tests with 1000 ppm lithium metaborate solution (971 through 974). It can be observed that superheat values for boiling curves are higher for tests with 1000 ppm $LiBO_2$ compared to that of 500 ppm $LiBO_2$ solution. This denotes a decline in boiling heat transfer coefficient for 1000 ppm lithium metaborate over 500 ppm lithium metaborate solutions.

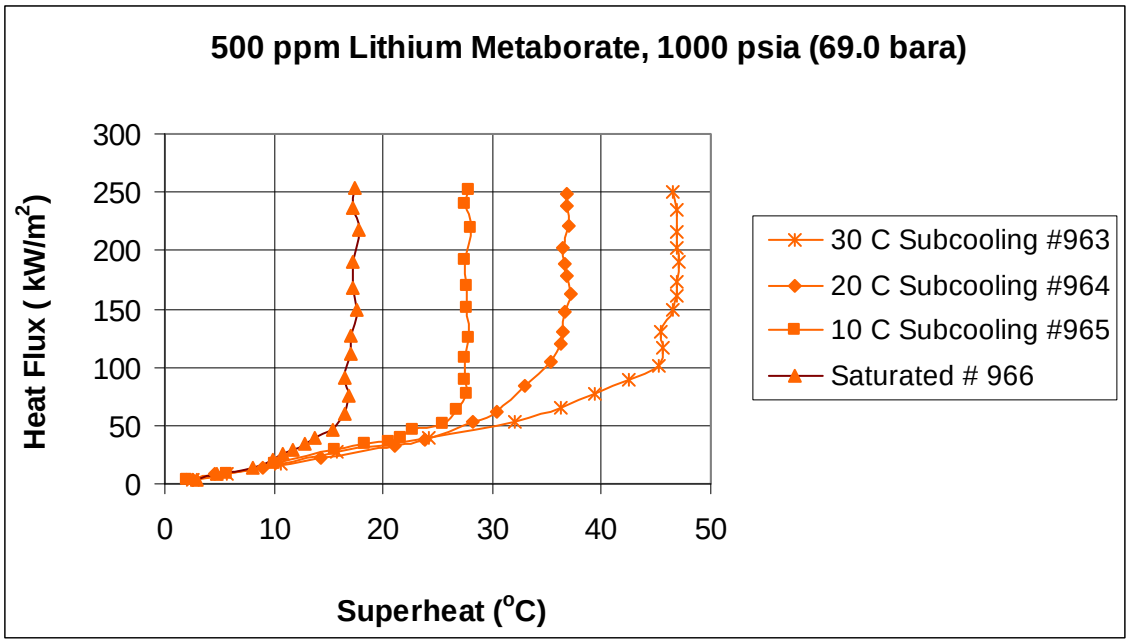

Figure 5-70 Boiling curves for tests with 500 ppm lithium metaborate solution at pressure of 1000 psia

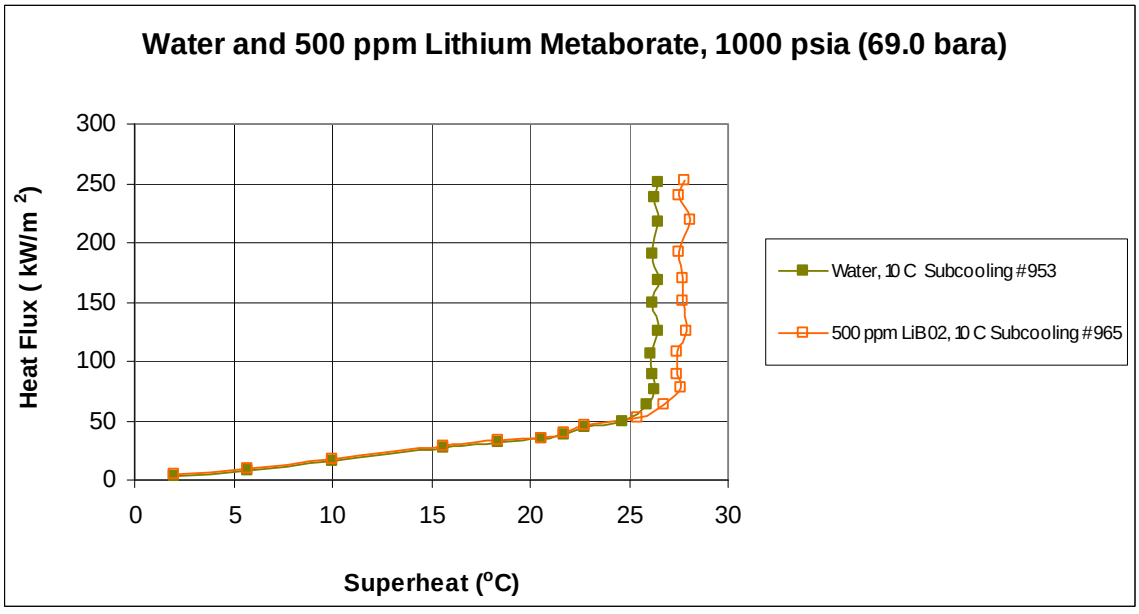

Figure 5-71 Effect of 500 ppm lithium metaborate concentration on heat transfer coefficients at 10 ^{o}C subcooling and 1000 psia

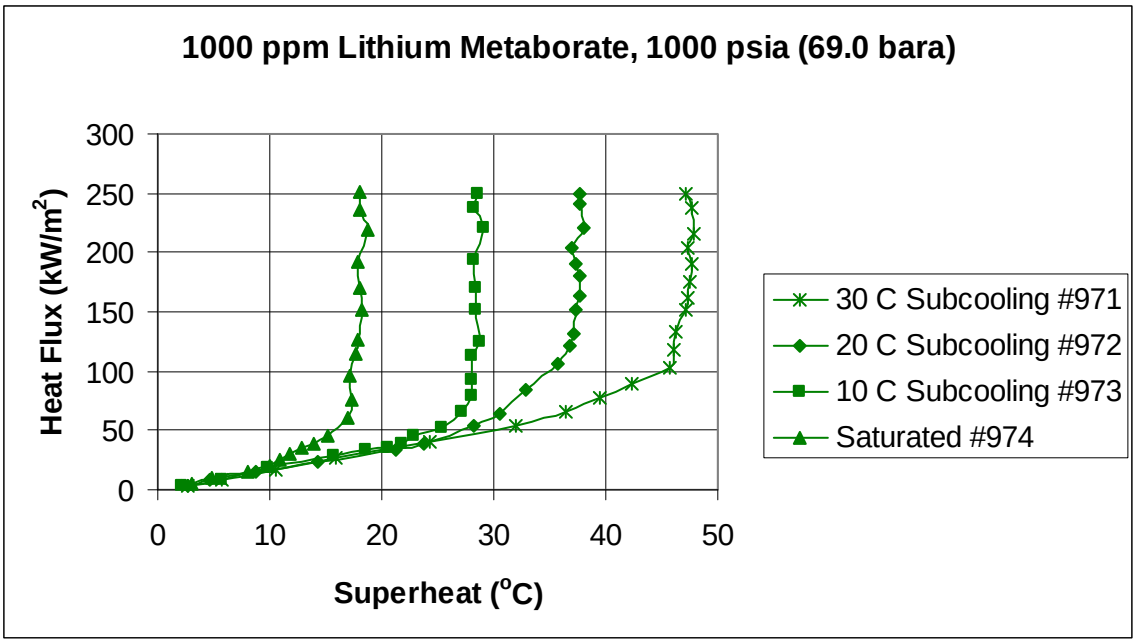

Figure 5-72 Boiling curves for tests with 1000 ppm lithium metaborate solution at pressure of 1000 psia

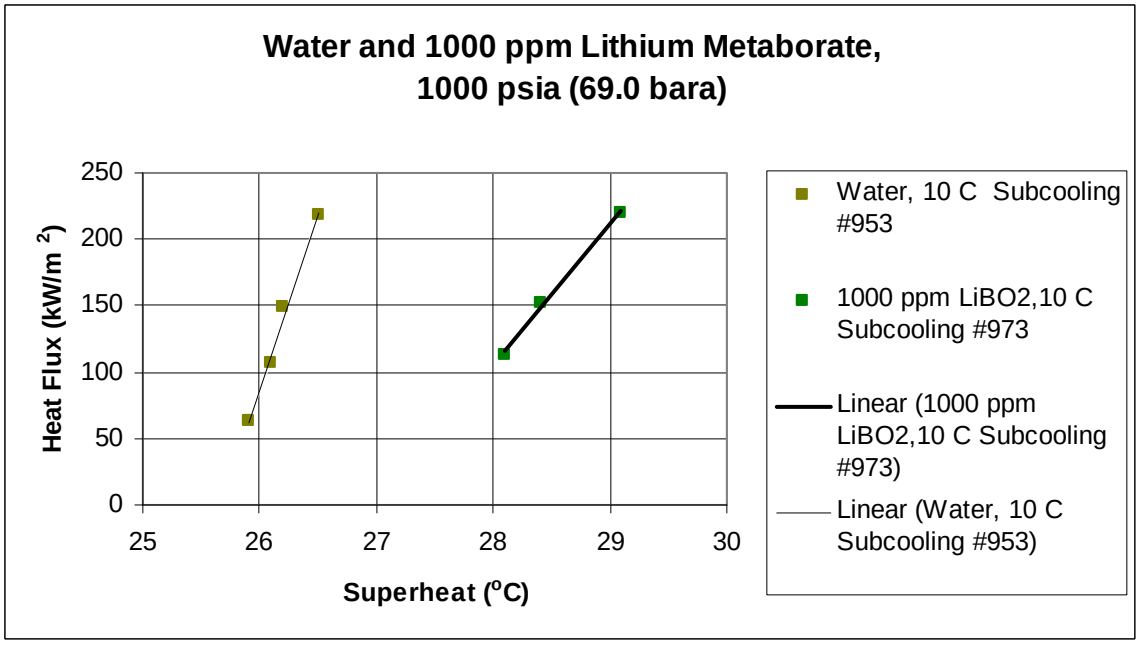

Figure 5-73 Degradation in heat transfer coefficient due to 1000 ppm lithium metaborate at 10°C subcooling

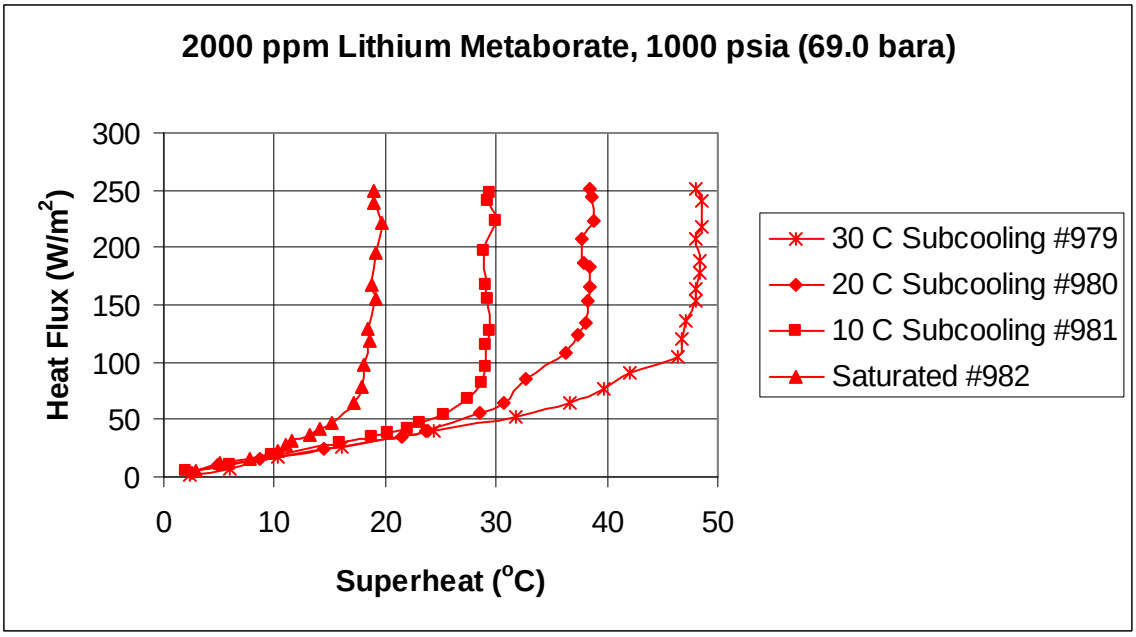

Figure 5-74 Boiling curves for tests with 2000 ppm lithium metaborate solution at pressure of 1000 psia

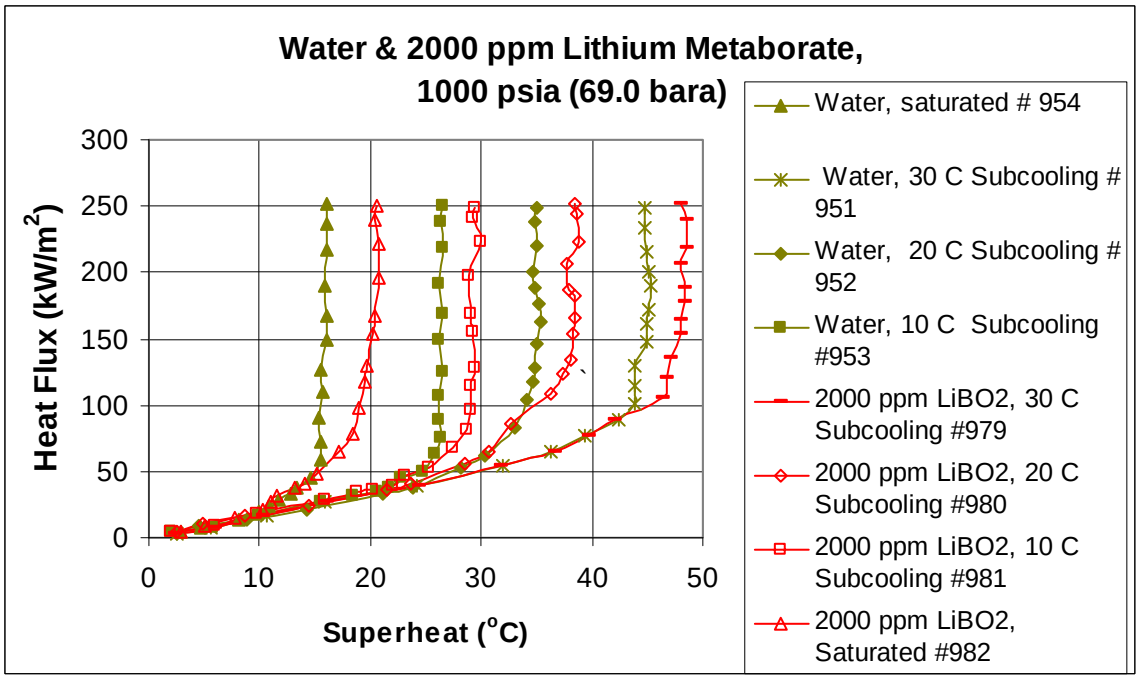

Figure 5-75 Boiling curves for deionized water and 2000 ppm concentration lithium metaborate solution at 1000 psia

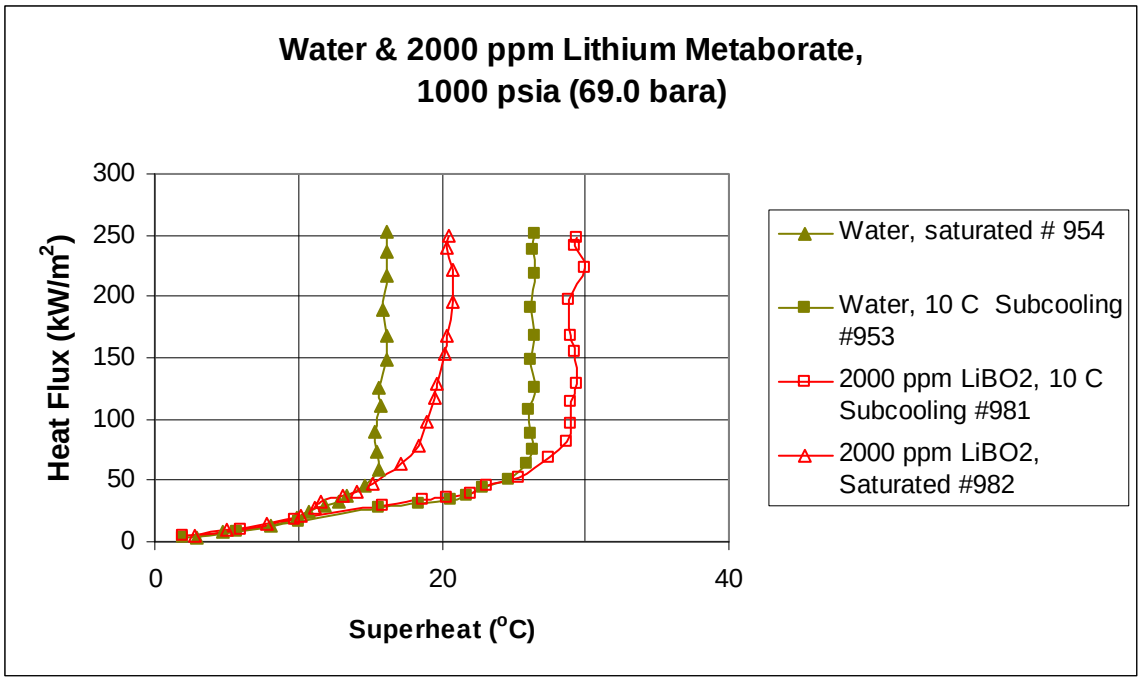

Figure 5-76 Effect of lithium metaborate concentration (2000 ppm) on heat transfer at 1000 psia pressure

Figure 5-73 indicates the variation in the slopes of boiling curves for water and 1000 ppm lithium metaborate solution. For a heat flux value of 149 kW/m2, the heat transfer coefficient decreased from 5.7 kW/m2°C to 5.3 kW/m2°C indicating a decrease of about 6 % in heat transfer coefficient for 1000 ppm lithium metaborate when compared with deionized water at 10°C Subcooled condition.

The boiling test results with 2000 ppm concentrated lithium metaborate solution are presented in Figure 5-74 . Figure 5-75 shows the boiling test results for the 2000 ppm lithium metaborate solution. Figure 5-76 show the variation in boiling curves in the presence of 2000 ppm lithium metaborate relative to water. Figure 5-77 shows the decrease in pool boiling heat transfer coefficients for 2000 ppm concentration of lithium metaborate solution in comparison to pool boiling heat transfer coefficients of deionized

water at a saturated condition. The increase in the superheat values for 2000 ppm lithium metaborate relative to water for a constant heat flux is a direct indication of a decline in the heat transfer coefficient. The boiling transfer coefficient for deionized water is 9.39 $kW/m^{2o}C$ (for heat flux =195.4 kW/m^2). The boiling heat transfer coefficient was reduced by a value of 2.7 $kW/m^{2o}C$ for 2000 ppm lithium metaborate solution when compared with pool boiling heat transfer coefficient of deionized water at 167 $kW/m^{2.}$ The reduction in heat transfer coefficients was found to be 22 % (for heat flux =167 kW/m^2.) for bulk coolant being at saturated conditions.

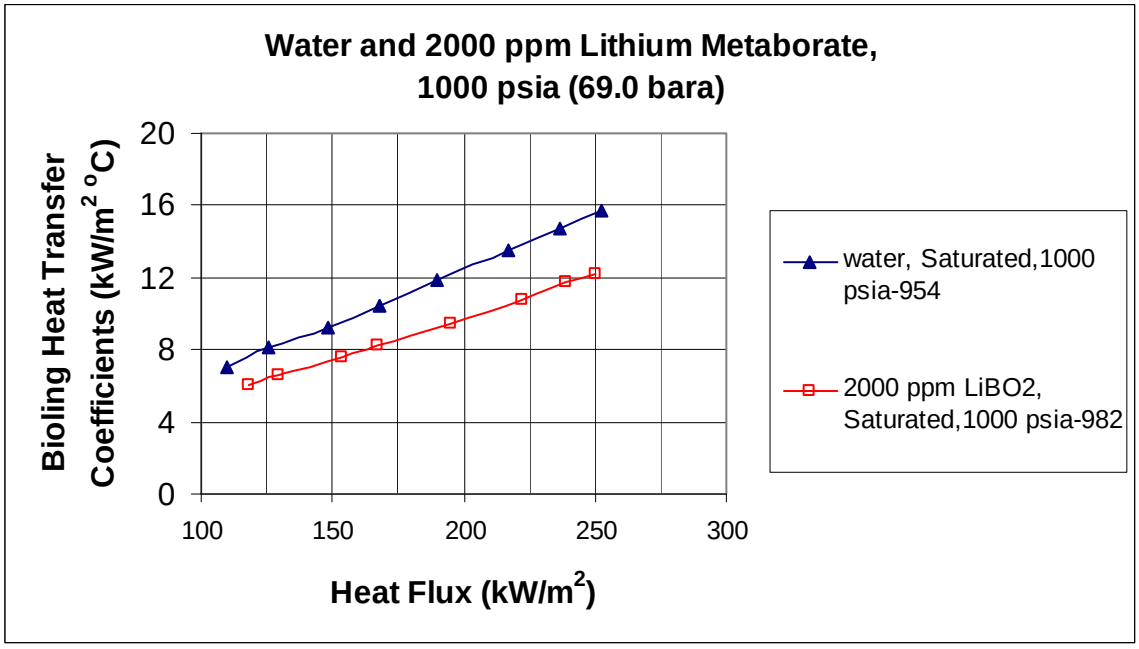

Figure 5-77 Degradation in heat transfer coefficients with influence of 2000 ppm lithium metaborate solution at saturated temperature and 1000 psia pressure

Figure 5-78 shows the boiling curves for tests from 993 through 997 for all subcooled condition and saturated condition. Figure 5-78 shows the boiling curves with 5000 ppm lithium metaborate solution.

Figure 5-79 shows the deviation in boiling curves with 5000 ppm concentration level in comparison to the boiling tests done with deionized water. Figure 5-80 shows the degradation of boiling heat transfer coefficients for 5000 ppm lithium metaborate at the saturated condition. It can be observed from Figure 5-80 that boiling heat transfer coefficient decreased to value of 10.6 $kW/m^{2o}C$ for a heat flux of 225 kW/m^2. The corresponding heat transfer coefficient for deionized water is 14 $kW/m^{2o}C$ at a heat flux of 225 kW/m^2, indicating a reduction of 24% in heat transfer coefficients for 5000 ppm lithium metaborate solution over deionized water at 1000 psia fluid pressure.

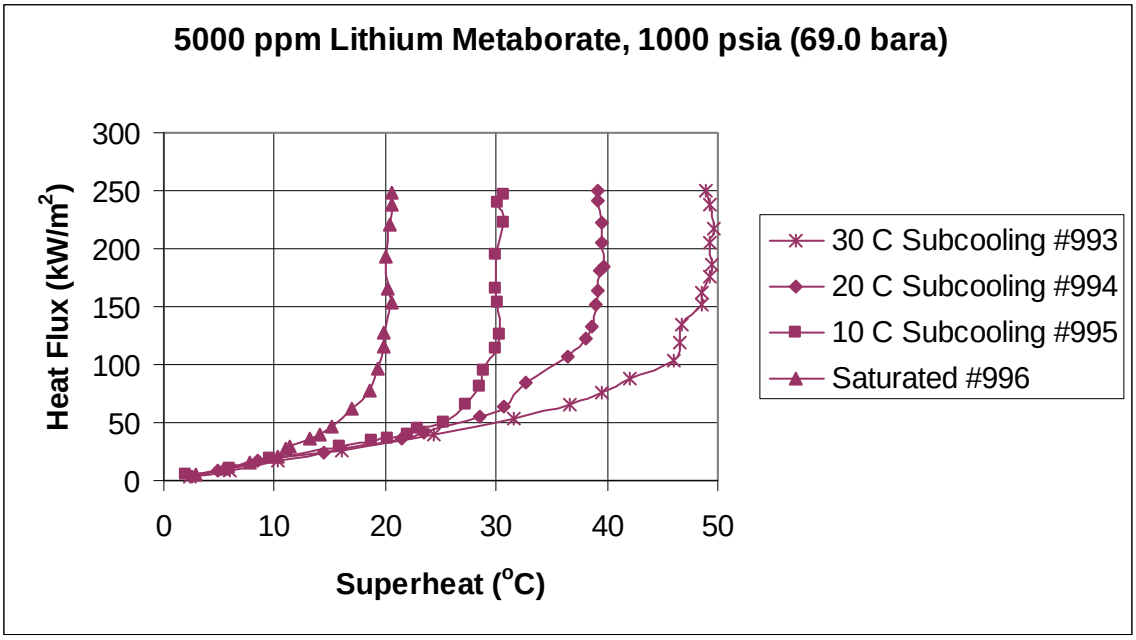

Figure 5-78 Boiling curves for tests with 5000 ppm lithium metaborate solution at pressure of 1000 psia

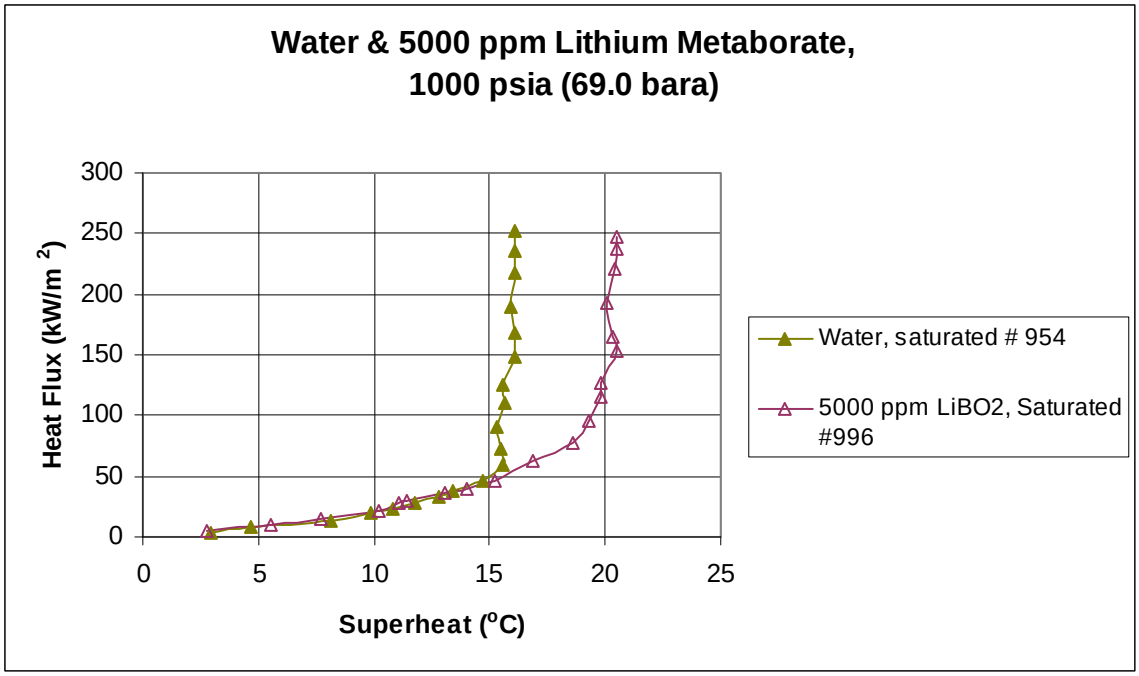

Figure 5-79 Effect of 5000 ppm lithium metaborate concentration on heat transfer coefficients at saturation temperature and 1000 psia pressure

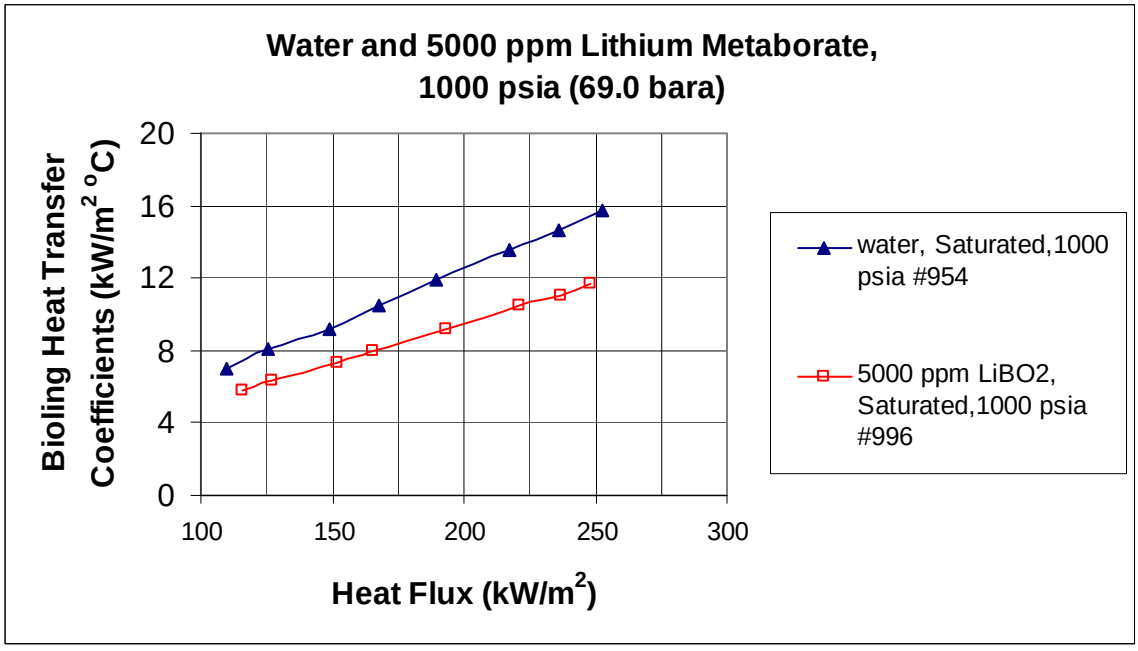

Figure 5-80 Degradation in heat transfer coefficients with influence of 5000 ppm lithium metaborate solution at saturated temperature and 1000 psia pressure

5.7 Formation of Deposits

It can be clearly concluded from the pool boiling test results, that the presence of boric acid and lithium metaborate affects the heat transfer characteristics in subcooled nucleate boiling. As discussed earlier, the main reason for occurrence of Axial Offset Anomaly is subcooled nucleate boiling at the core in PWR. The axial offset anomaly can be observed only after years of continuous running of a PWR. As it is not pragmatic to run the boiling tests for such a long period of time, boiling tests were run continuously with higher concentration of coolant for five days to simulate the conditions favorable for deposition of boron and lithium. These tests help in understanding the transient characteristics of heat transfer coefficient. The detailed test procedure is explained in the next section.

5.7.1 Test Procedure

The boiling test for deposits was conducted with 5000 ppm boric acid solution at 1000 psia pressure. The test was conducted at 10^{o}C subcooling. The procedure employed for each test is described below

1. Power was supplied to the bulk heater using a rheostat control. The coolant was heated and maintained at a steady state temperature of 274.2^{o}C, which is 10^{o}C below the saturation temperature at 1000 psia.

2. The heat flux through the test heater was increased very slowly in steps in order to reach the steady state condition. “DC electrical power supply” was used to power the test heater.

3. The current through the test heater was measured using a clamp type ammeter that can measure AC/DC current.

4. The temperature of the test heater was measured using four k-type thermocouples

5. The power supplied to the test heater was increased until a heat flux of 250 kW/m^2 is reached.

6. A constant heat flux of 250 kW/m^2 was maintained by controlling the power supplied to the test heater.

7. The temperature readings from the four K-type thermocouples of the test heater are recorded for every 20 minute time period.

8. The temperature of coolant was also recorded for 20 minute time period from T-type bulk thermocouple.

9. The entire experimental set up was keenly monitored for any sudden changes in temperature, pressure and for mechanical and failures.

10. After the test was run for 5 days, the heat flux to the deionized water was slowly decreased to zero by decreasing the power input to test heater.

11. Similarly the power supplied to bulk heater was decreased to zero in a steady process.

12. It was very essential to not disturb the test chamber as it might affect the deposits settled on the test heater.

13. The pressure in the test chamber was very gradually decreased to ambient conditions. This was done after temperature of the coolant equals ambient temperatures. Decreasing the pressure of coolant was done gradually to avoid sudden movement of coolant within test chamber.

14. After the coolant reached ambient conditions, it was discharged through bleed valve.

15. The test heater flange was unfastened from the test chamber for observation of the deposits.

16. The test heater was then carefully observed using a microscope. The deposited particles were carefully viewed and photographed.

17. Care was to be taken while transporting the test heater as to not disturb the particles deposited on the test heater.

18. After the visualization process, the deposits were then scraped into a tiny crucible for weighing. Care was to be taken to not damage the surface of the test heater. The net weight of deposits was measured. The difference in weight of the crucible before after collection yielded the net weight of deposits. Because of the surface irregularities of test heater, some particles settle in the cavities of the surface.

19. The remaining deposits were then washed thoroughly with a measured quantity of acetone. The washed liquid was carefully collected in a small beaker. The advantage of using acetone for weight measurement was its unique volatile property. After the washed liquid was collected, it was kept open to atmosphere.

Due to its extreme volatile nature, acetone evaporates leaving behind the deposits. The beaker was then weighed. The difference in weights gives the weight of the deposits.

20. The above step was repeated until the net weight of deposits for an attempt was zero. This method was very effective as acetone has good cleaning characteristics.

21. The total weight of the deposits was obtained by summations of all the net weights obtained by direct measurement and by the acetone cleaning method.

5.7.2 Boric Acid Deposits

The variation of the heat transfer coefficient during the boiling test indicates that boron deposits have considerable effect on heat transfer characteristics. The boiling curve for 'boron deposition test' is shown in Figure 5-81. The change in heat transfer coefficient with time is plotted in Figure 5-82. The trend of increase in superheat with increasing heat flux is similar to the boiling curve obtained for regular boiling test 991 as seen in Figure 5-68 until boiling curve flattens. As explained in the test procedure (5.7.1) above, the heat flux is maintained constant at about 250 kW/m^2 for very long duration. The heat flux of 250 kW/m^2 is lower than the critical heat flux for water (Incropera, 2001). As it can be seen from Figure 5-81 boiling curve appears flat because with duration of time, for a constant heat flux, the super heat increases with time. This can be explained only by increased resistance for heat transfer between the test heater and test solution with increase in duration of boiling test. The increased resistance to heat transfer

can be explained by formation of deposits on test surface reducing the heat transfer as all other parameters remain unchanged.

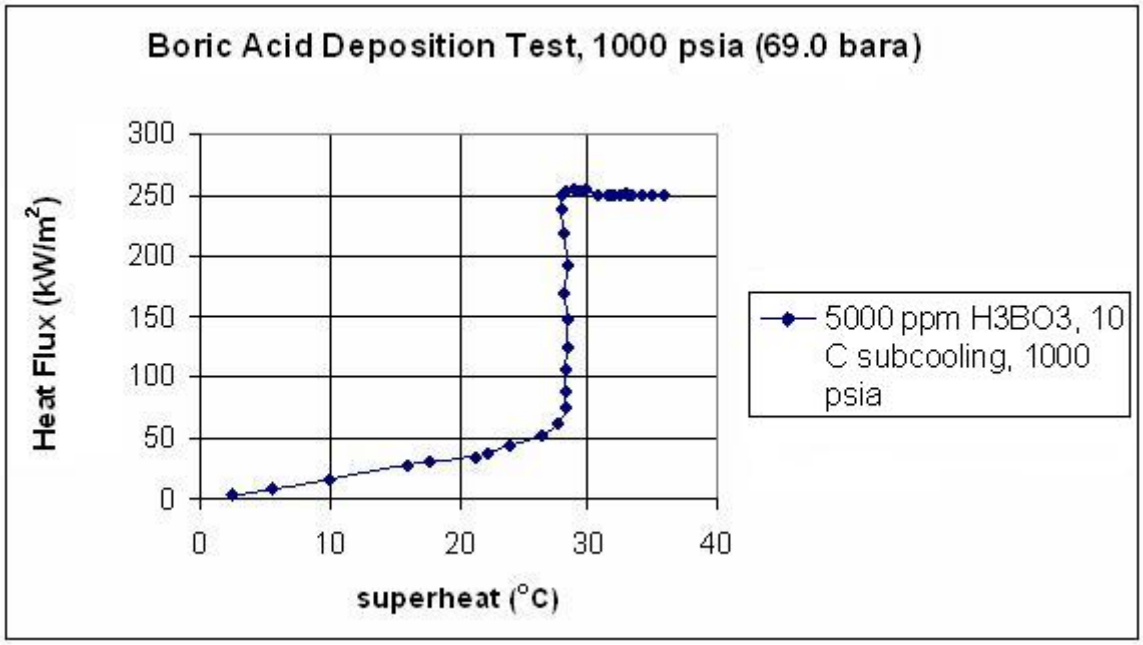

Figure 5-81 Boiling curve for 5000 ppm boric acid solution at 1000 psia

The 'deposition boiling test' was conducted with a constant heat flux of 250 kW/m^2. It can be observed from Figure 5-82 that the boiling heat transfer coefficient declined with increase of time. Initially the heat transfer coefficient increased slightly until it reached a steady state. The heat transfer coefficient seemed to be constant for the first four hours of test and declined gradually thereafter. This indicates that decline in heat transfer coefficients is most possibly due to deposition of boron precipitates. The boiling heat transfer coefficient decreased from 8.9 $kW/m^{2o}C$ to 7.0 $kW/m^{2o}C$ showing a reduction of 22% over a period of 136 hours. It can also be observed that after a running time of 80 hours there is an increase in heat transfer coefficient. The increased boiling heat transfer coefficient seems to be an anomaly in the measurements. The upward

change in heat transfer coefficients appears to a result of start of fluid motion near the surface of the test heater due to the buoyancy effect. The precipitation of boron on the heater indicates because of the subcooled boiling confirms that subcooled boiling is main cause for AOA phenomenon.

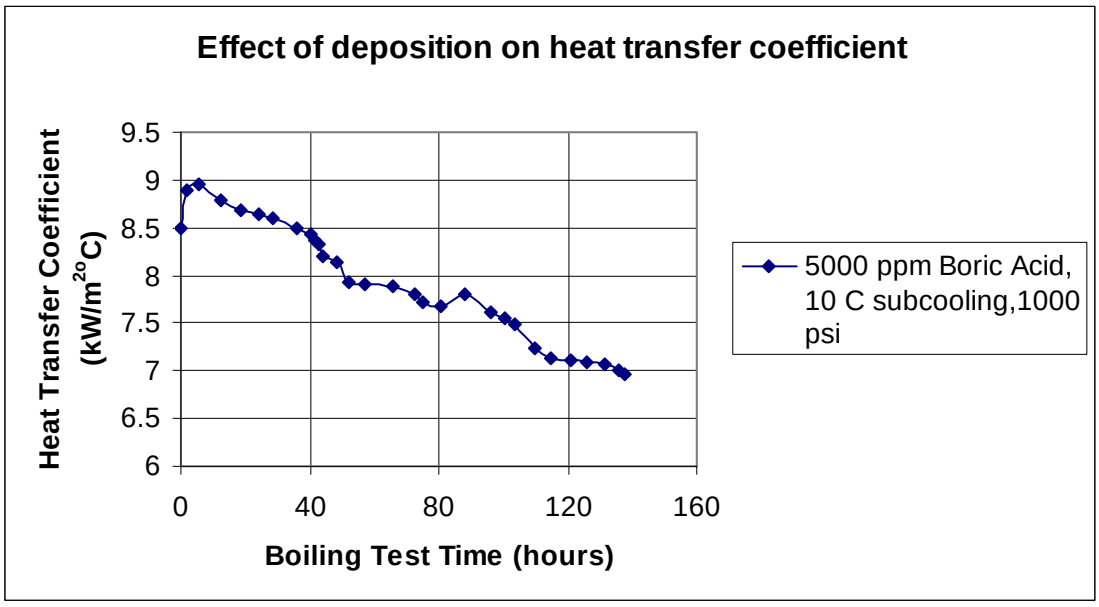

Figure 5-82 Effect of boron deposits on heat transfer coefficient at 5000ppm concentration and 1000 psia pressure

The test heater was observed using a canon high resolution camera with 400X magnification. The camera has an optical lens fitted to it and was mounted on a stand. As the surface of the test heater is cylindrical, only a portion of surface can be clearly viewed through the microscope. Images were taken at the center of the boiling region and at the beginning and end of the boiling region to get information concerning the deposit particle density. Figure 5-83 shows a microscopic image of the test heater at the end of the boiling region on the test heater. It may be recalled that the actual length of the heater filament is only one inch and away from the flange end. The boron deposits (white in

color) can be observed in Figure 5-83. The deposited particles seem to be scattered along the surface of the heater in the valleys on the surface. The surface of the test heater can also be observed at 400X magnification in Figure 5-83. The imperfections of the surface are clearly visible.

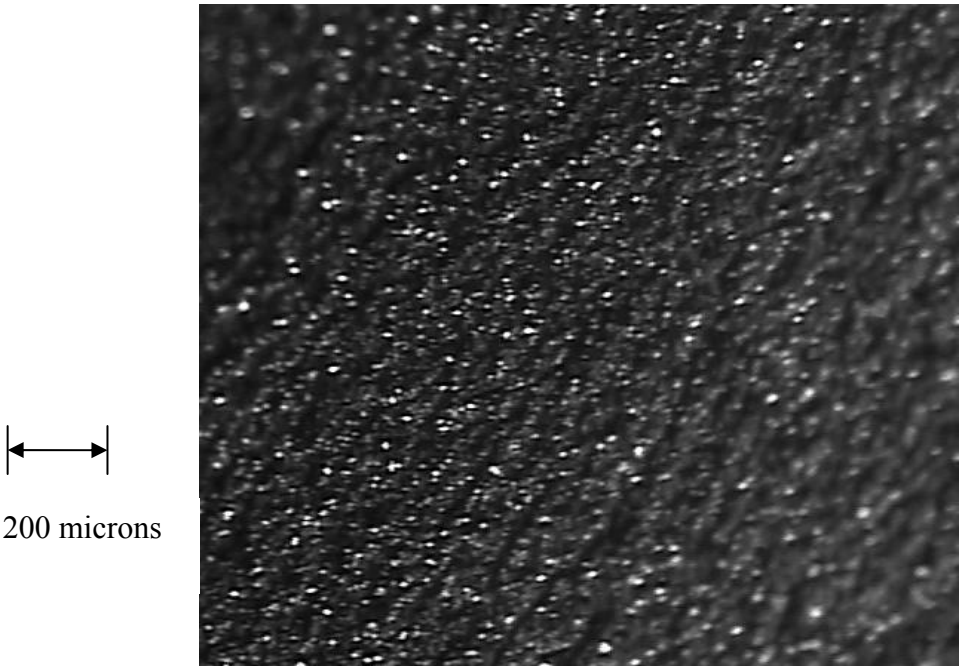

Figure 5-83 Photomicrograph of test heater adjacent to boiling region at 400X magnification after boiling test at 1000 psia with 5000 ppm boric acid

The particle size of the deposits was calculated using sigmascan. Sigmascan pro (sigma scan is a registered image analysis tool of Systat software) an image analysis software tool. Using the threshold intensity feature sigmascan, number of particles can be counted. This feature works on the principle of difference in intensity of pixels in a image. The images obtained from the Canon high resolution camera setup have been calibrated and each pixel on the image corresponds to 2.98±1.94 square microns. Using this pixel conversion factor the size of the particles and statistical data has been obtained. For instance, a particulate which covers two pixels in a image would correspond to 5.96

square microns. Figure 5-84 shows deposited particle size distribution for Figure 5-83. The average size of the particle for 136 hour duration of the test was found to be 2.98±1.94 microns (1micron =10-^{6}m), which was determined from the image analysis software sigmascan.

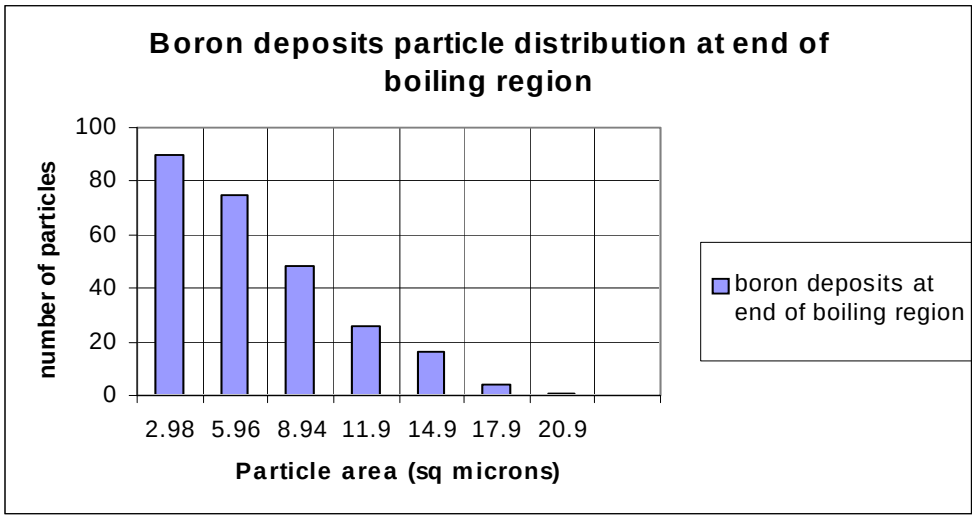

Figure 5-84 Particle size distribution of the deposited particles at end of boiling region, where the total particle count is 260 (1000 psia and 10^{o} C subcooling)

Figure 5-85 and Figure 5-87 show the photomicrographs of the test heater at the boiling region. It is clearly evident that deposits are higher in concentration, which confirms the reason for degradation in heat transfer coefficients. Figure 5-86 and Figure 5-88 show the particle size distribution characteristics for Figure 5-85 and Figure 5-87 respectively. It can be observed that maximum number of particles lie in a size range of 5.96 sq microns. The particle size is represented by the average area covered by the particle as it affects the deposits by covering the nucleation sites. It appears that most of the particulates are separate and scattered over heater surface. However some of the particulates seem to be form clusters. The average area of the particulate is 8.2 square microns at the boiling region.

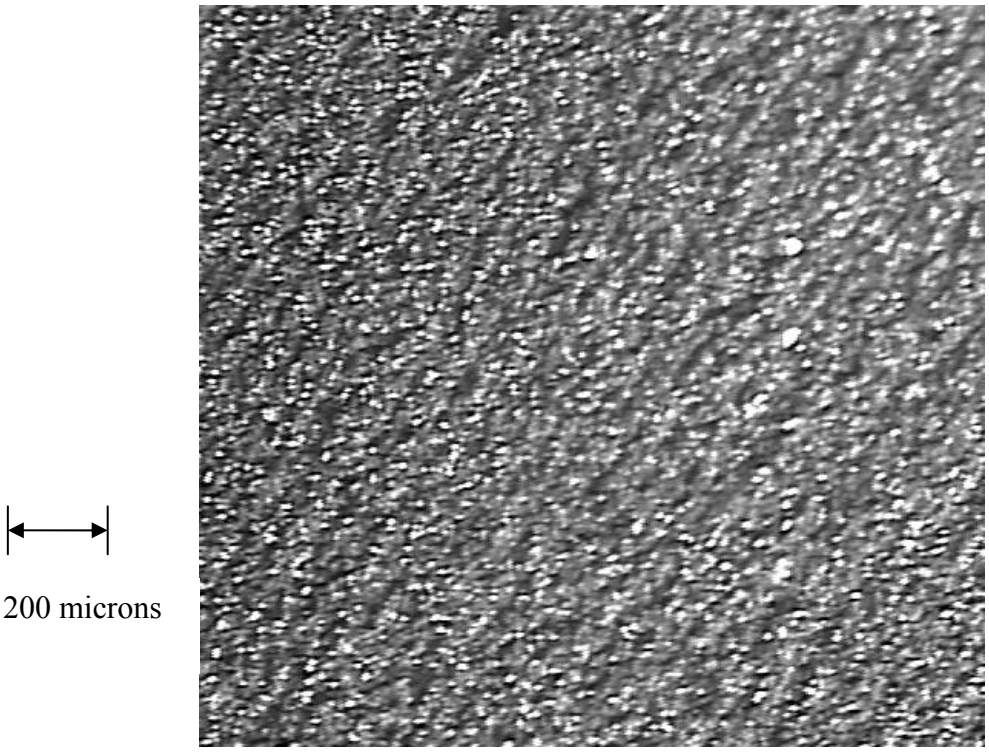

Figure 5-85 Photomicrograph of boron deposits at boiling region on test heater after boiling test at 1000 psia with 5000 ppm boric acid

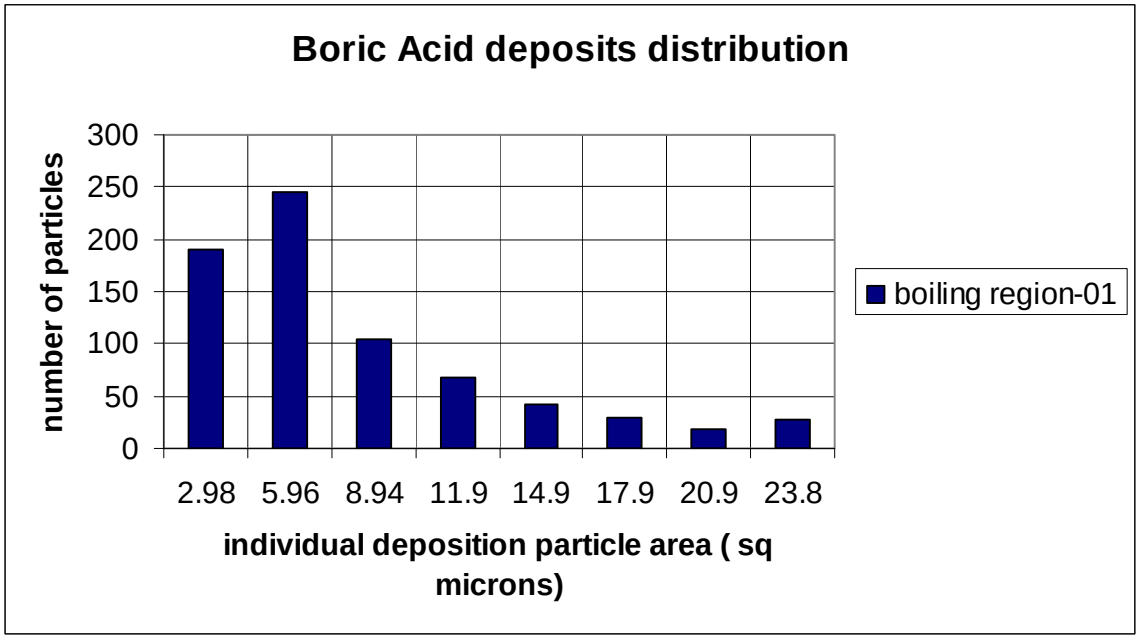

Figure 5-86 Particle size distribution for boric acid deposits for Figure 5-85

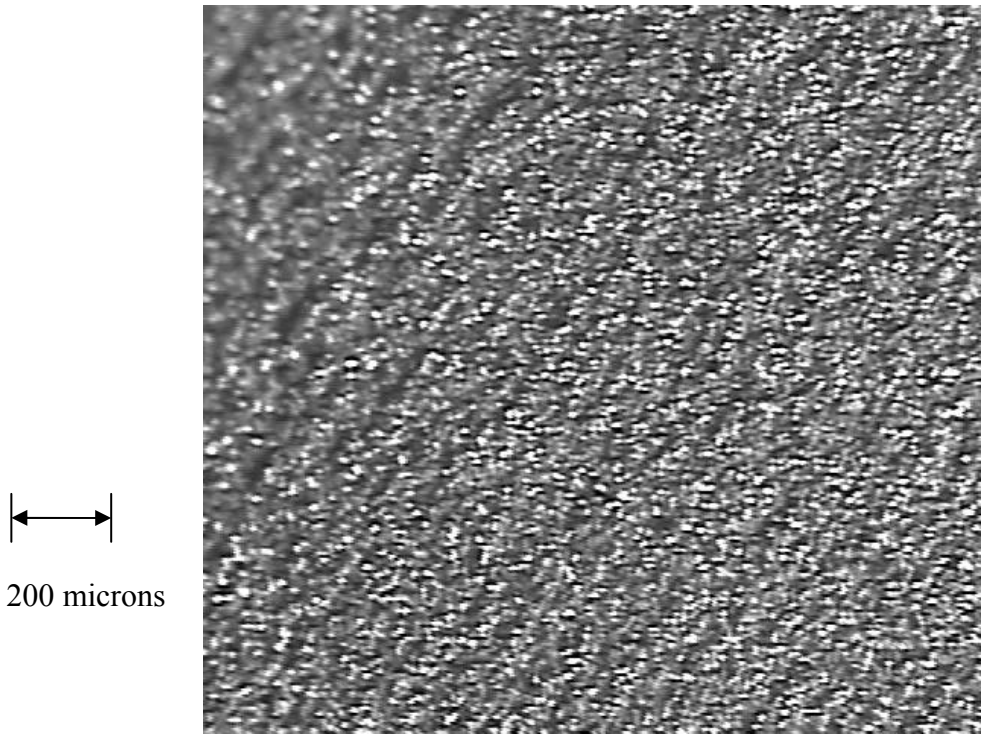

Figure 5-87 Photomicrograph of boron deposits on test heater at 400X magnification after boiling test at 1000 psia with 5000 ppm boric acid

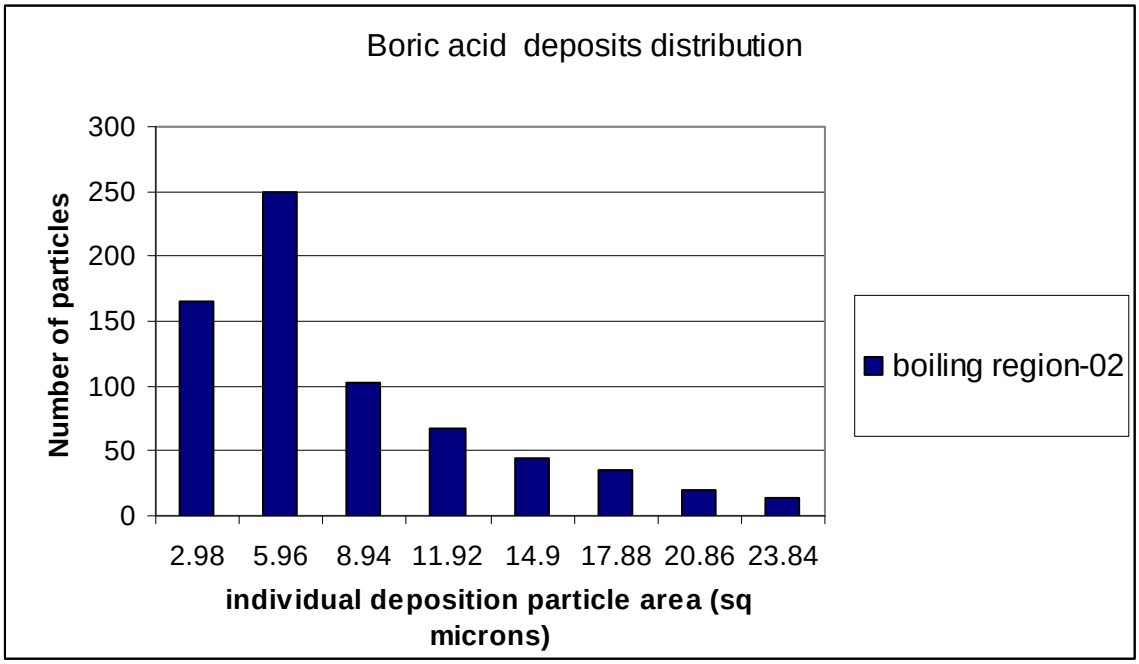

Figure 5-88 Particle size distribution for boric acid deposits for Figure 5-87 for a total particle count of 723.

It was found that boron particles settled on the surface of the test heater. Figure 5-85 shows the boron particles spread around the surface of the test heater at the boiling region. The boiling region constitutes the surface area over the heater filament. The length of boiling region is 1 inch. This indicates that the deposition occurs due to subcooled nucleate boiling. It is also to be noted that the surface roughness plays a significant role in deposition of boron particles. Figure 5-87 indicates that density of deposited particulates is higher in the valleys of the surfaces. The possible reason for higher deposition in the valleys is due to higher nucleation at valleys in the surface. Previous studies have indicated that nucleation is higher in the cavities and troughs of the hot surface. For instance, a particulate which covers two pixels in an image would correspond to 5.96 square microns.

Figure 5-89 shows a photomicrograph of test heater surface outside the one –inch long boiling region. The numbers of deposit particulates are remarkably less than deposit rates at the boiling region. The lesser density of deposits suggests that the deposition rates are directly dependent on nucleation rates. Figure 5-90 shows the particulate distribution for Figure 5-89. “Particulate area” in Figure 5-90 indicates the surface area covered by each particulate. The number of particles with area of 2.98 sq microns is eighteen, whereas in Figure 5-88, there are 162 in number for the boiling region. The uncertainty of the particle area measurement is 1.94 sq microns. It may be noticed that for 5000 ppm boric acid solution for total deposit weight of 12.2 mg, the heat transfer coefficient degraded by 22% at 10^{o}C subcooling over 136 hours of duration of the test.

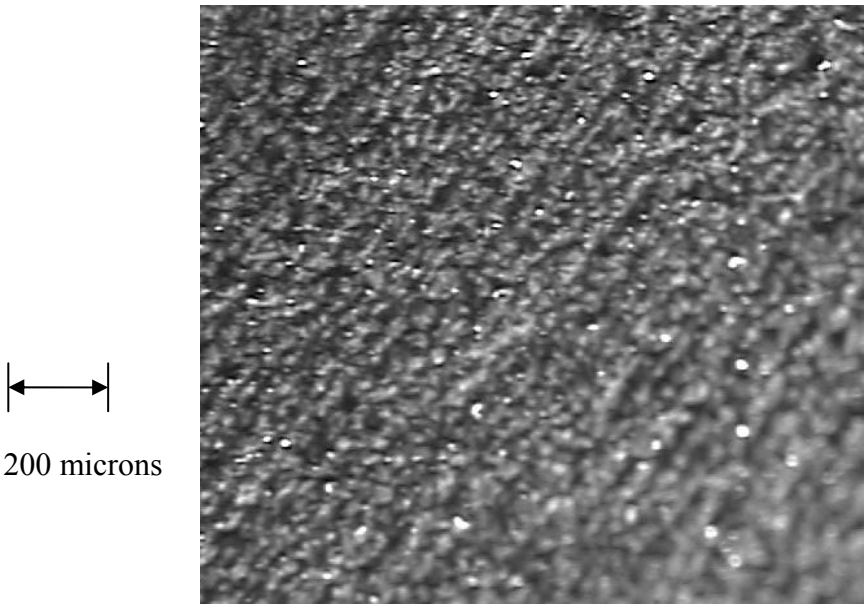

Figure 5-89 Photomicrograph of test heater outside the boiling region (400X magnification and 1000 psia pressure)

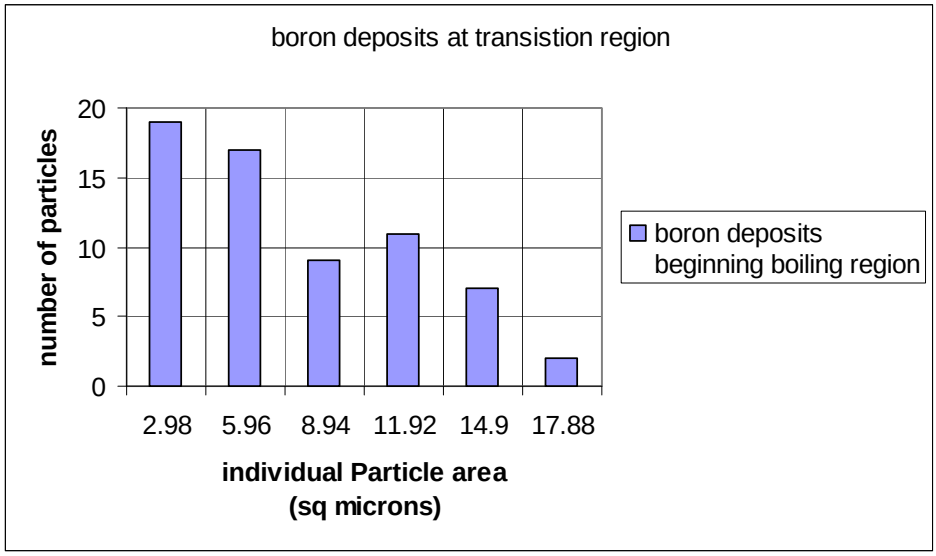

Figure 5-90 Particle size distribution for boric acid deposits for Figure 5-89 for a total particle count of 65

5.7.3 Lithium Metaborate

Boiling test for lithium Metaborate deposition was conducted with 5000 ppm concentration solution. The procedure employed is similar to that of boiling test

conducted with boric acid for deposition. A “deposition test” conducted with 5000 ppm lithium metaborate solution resulted in failure of the test heater due to high surface temperature and low heat transfer coefficient. Figure 5-91 shows the image of the failed test heater in which the Zr-4 cladding of the test heater was damaged. High precipitation of lithium was observed on the test heater. The damage of the test heater was likely due to the sudden change in the test conditions. The failure of the test heater was likely due to the increase of the surface temperature of the test heater because of excessive deposition.

Figure 5-91 Photograph of the failed test heater for lithium metaborate deposition test at 1000 psia fluid pressure

The boiling test for deposition of lithium Metaborate was conducted for a time duration of 5 days, similar to that of boric acid deposition test. Figure 5-92 shows the degradation of boiling heat transfer coefficient with time. It can be observed from Figure 5-92 that boiling heat transfer coefficient is not affected significantly for the first 300 minutes of time but thereafter decreases constantly to a value of 5.5 $kW/m^{2o}C$ from 7.8 $kW/m^{2o}C$ over a period of 140 hours. The degradation in heat transfer coefficient is due to the deposition of lithium metaborate deposits.

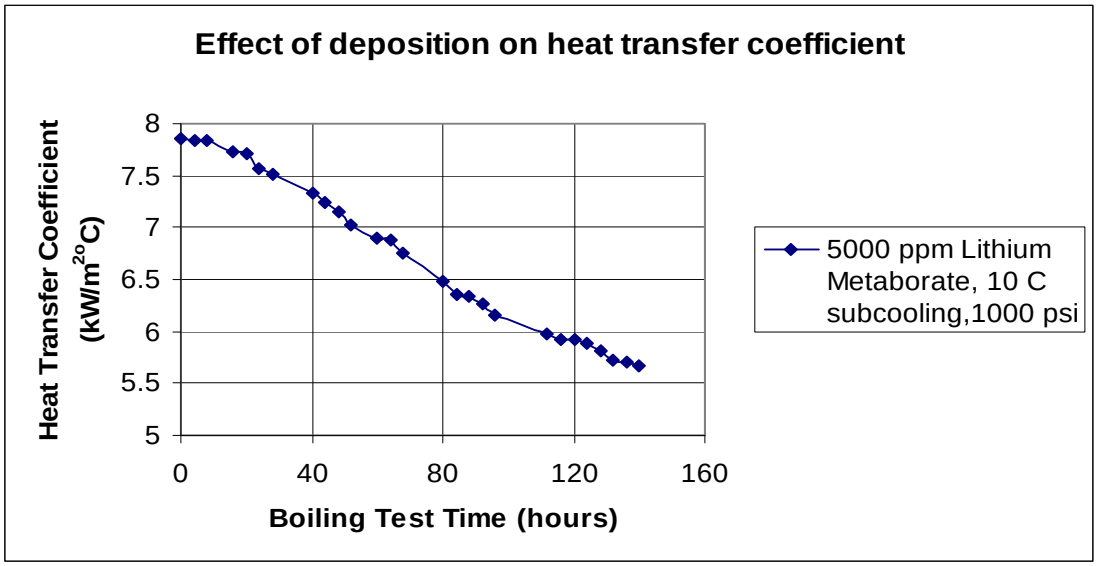

Figure 5-92 Degradation of heat transfer coefficient with boiling test time for 5000 ppm concentrated lithium metaborate solution

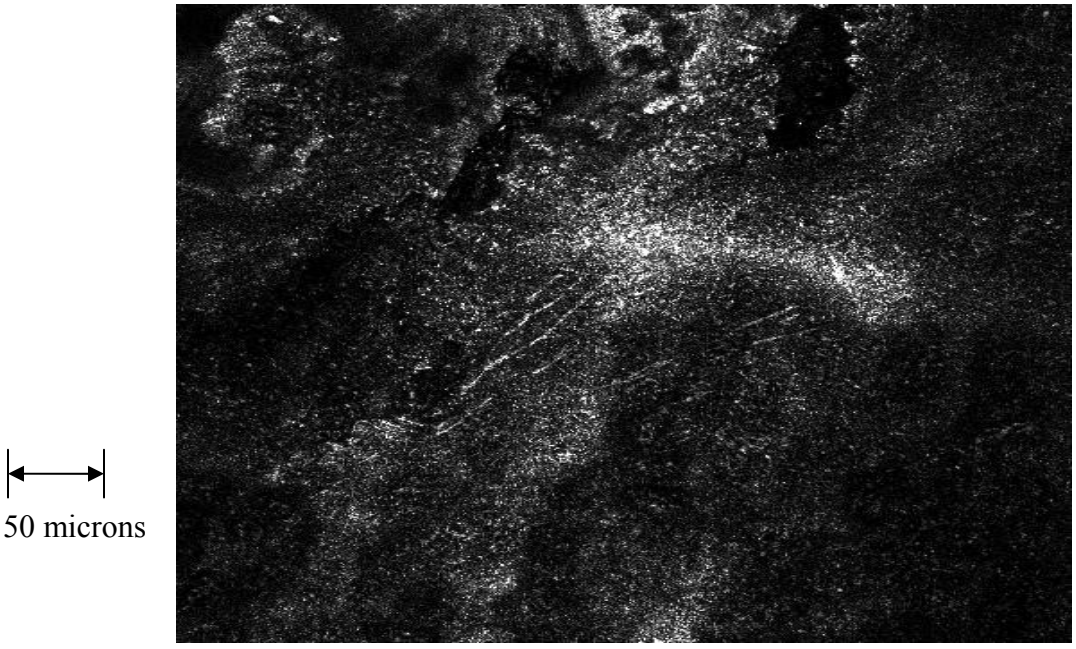

Figure 5-93 Photomicrograph of test heater with deposits of precipitate of lithium metaborate at 600X magnification after boiling test at 1000 psia

The test heater was observed using a Zeiss LSM5 Pascal microscope located in department of biology in Kansas State University. LSM 5 is a laser scanning confocal microscope capable of exciting fluorescent markers with laser lines of

458/488/514/543/633 nm. Figure 5-93 shows the photomicrograph of test heater after the boiling test with 5000 ppm concentrated lithium metaborate solution. The Figure 5-93 shows the lithium metaborate deposits on the test heater surface. It can be observed that the concentration of deposits is high at the center of the boiling region.

Figure 5-94 shows a part of image captured by the microscope at the boiling region at a magnification of 600X. The microscope scans the specimen line by line to complete an entire picture of the specimen. Figure 5-94 shows the image of the test heater surface captured in one scan. The deposits appear to be clusters of tiny particulates. Unlike boron deposits, the lithium metaborate deposits are smaller in size but higher in density. Lithium metaborate particulates seem to deposit in random clumps as in Figure 5-96...

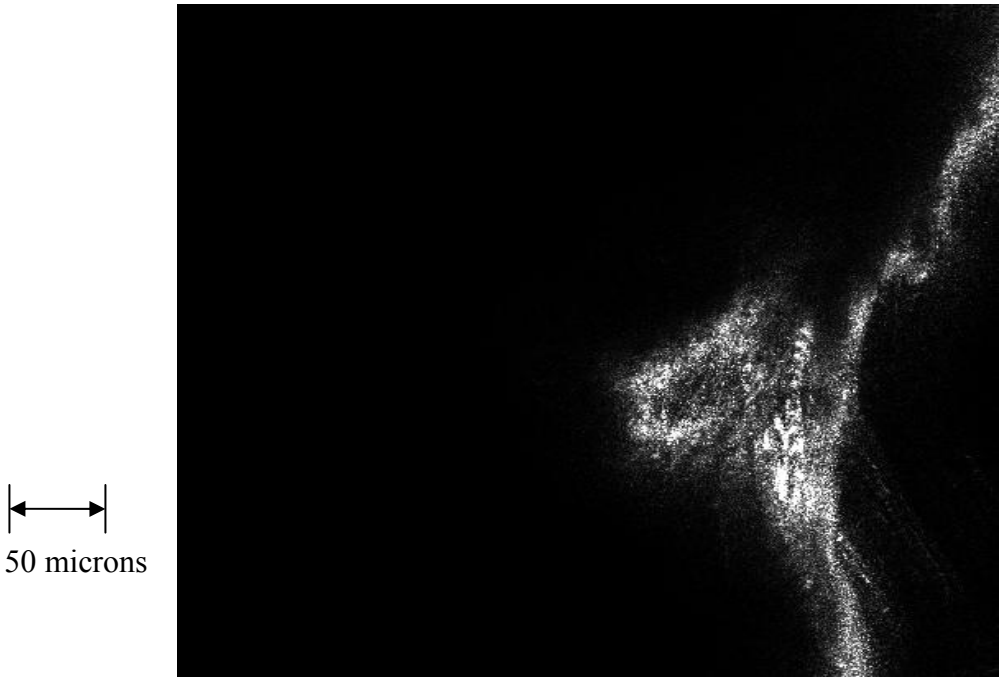

Figure 5-94 Photomicrograph of test heater with lithium metaborate deposits at magnification of 600X at 1000 psia and 5000 ppm lithium metaborate solution

Figure 5-95 shows the particulate size distribution for lithium metaborate deposits. The size of the particulates was calculated by analyzing the photomicrographs in a similar method to that of boric acid micrographs. The results reveal that most of the particulates lie in the size range of 0-3 sq microns. It can also be observed that the size of particles is relatively smaller than that of boric acid deposits. The average size of particulate over 140 hour duration of the test was found to be 5.8±0.45 sq microns. However particulates with area greater than 15 microns are higher when compared to boric acid deposits indicating that some of the particulates combine to form a cluster.

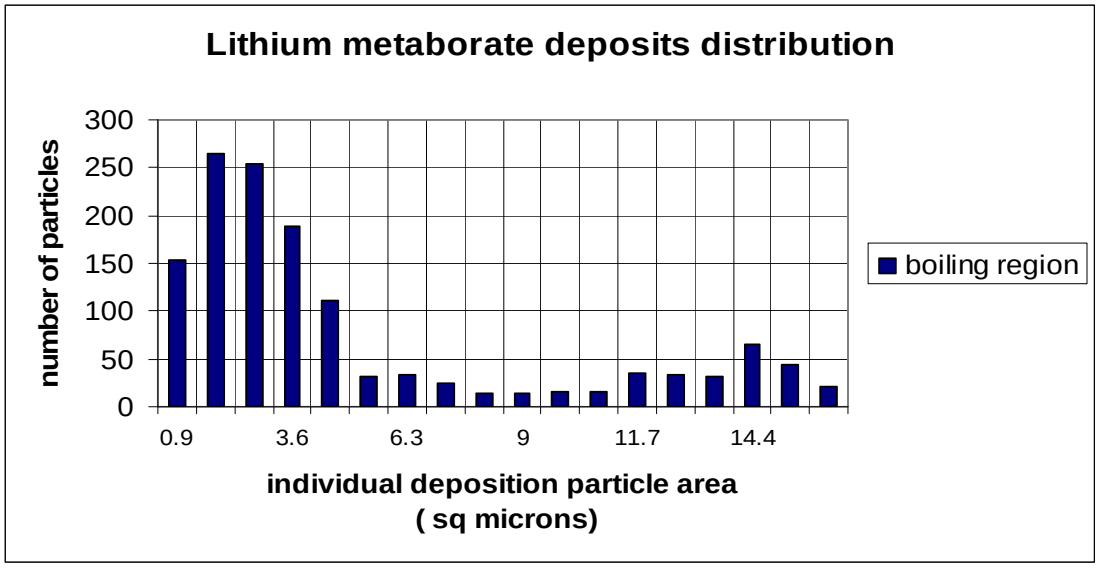

Figure 5-95 Particulate size distribution of lithium metaborate deposits on test heater for total particle count of 1326.

Figure 5-96 shows another image taken from Zeiss LSM5 pascal microscope at the boiling region with lesser magnification of 100X. The Figure 5-96 shows deposits of lithium metaborate precipitate settled on the surface of test heater. This image shows the deposits are formed in clusters of small individual particles. It may be recalled that the bubble formation occurred in odd clumps for 5000 ppm lithium metaborate solution. The

change in nucleation for 5000 ppm lithium metaborate solution, relative to water could be explained by the clusters of deposits formed on the heater surface for 5000 ppm lithium metaborate test. It appears that these deposits on the heater surface caused a restriction to the bubble formation on the heater surface leading to irregular nucleation pattern.

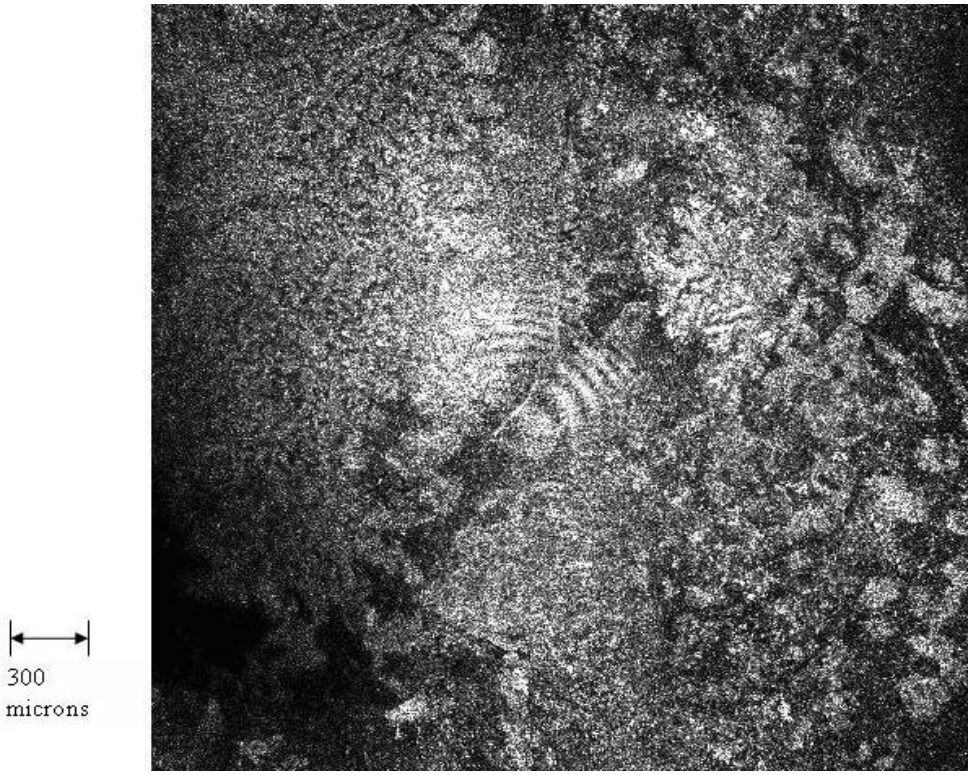

Figure 5-96 Photomicrograph of test heater after lithium Metaborate boiling test at magnification of 100X at 1000 psia pressure

Figure 5-97 shows a photomicrograph of the test heater taken outside the boiling region. The density of deposits is less compared to density of deposits at the boiling region. However there is minimal nucleation occurring at the transition region between boiling and non boiling region due to heat transfer along the test heater by conduction. The reduction in heat transfer in presence of lithium metaborate can be explained by decrease in nucleation rates due to the particulate deposition.

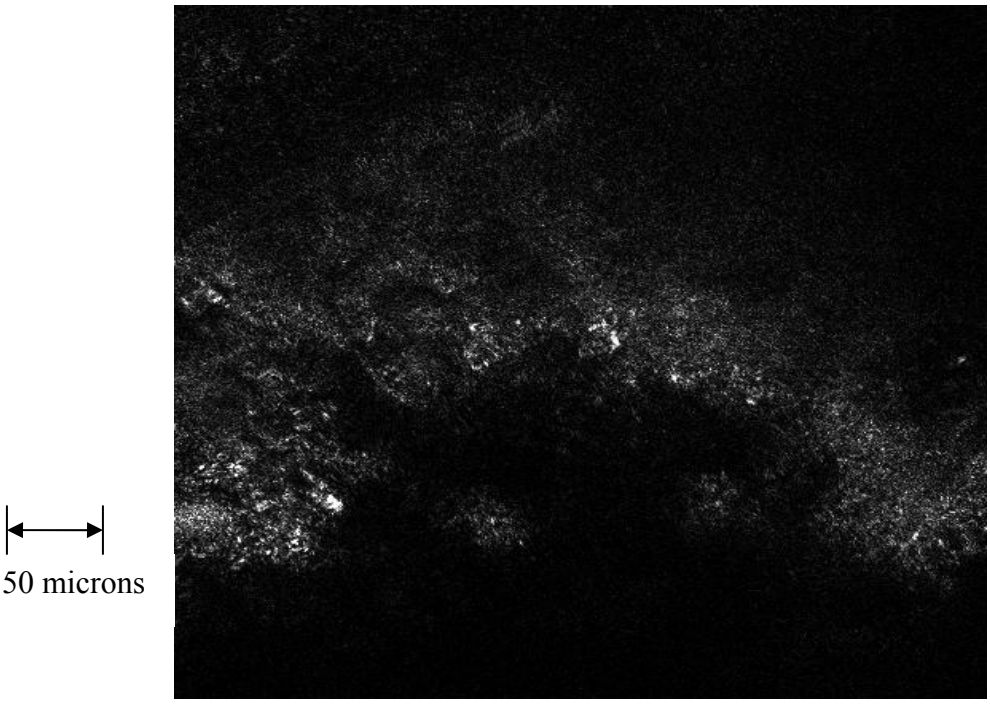

Figure 5-97 Photomicrograph of test heater after lithium Metaborate boiling test at beginning of boiling region at magnification of 600X at 1000 psia pressure

5.7.4 Nucleation

A high speed camera was used to capture the nucleation at the test heater surface. The videos were taken using 16mm Kodak Hawk Eye Surveillance film. The films were processed at Yale film studio in California [Yale Film and Video, 2006]. The boiling images were captured for tests with deionized water and different concentrations of boric acid and lithium metaborate. The processed films were later viewed using a Howell 16mm film projector Model 2580[Howell, 1985]. Observations from viewing the nucleation revealed variation in bubble behavior. It was found that nucleation was smooth for deionized water with a larger number of bubbles. Figure 5-98 shows the image captured from a film video taken for boiling test with deionized water at the 10^{o} C

subcooled condition, at 1000 psia bulk fluid pressure, and at a heat flux of 150 kW/m^2. The bubble outline has been "manually traced" to enhance the appearance of the bubbles present. Figure 5-99 shows the enhanced bubble formation pattern for a high heat flux of 240 kW/m^2 with deionized water. It has been observed that with increase of heat flux, bubble density seems to have increased and bubbles have left the heating surface by combining with new bubbles formed. The bubbles seem to be collapsing in a lesser time when compared with bubble collapsing time for 100 psia.

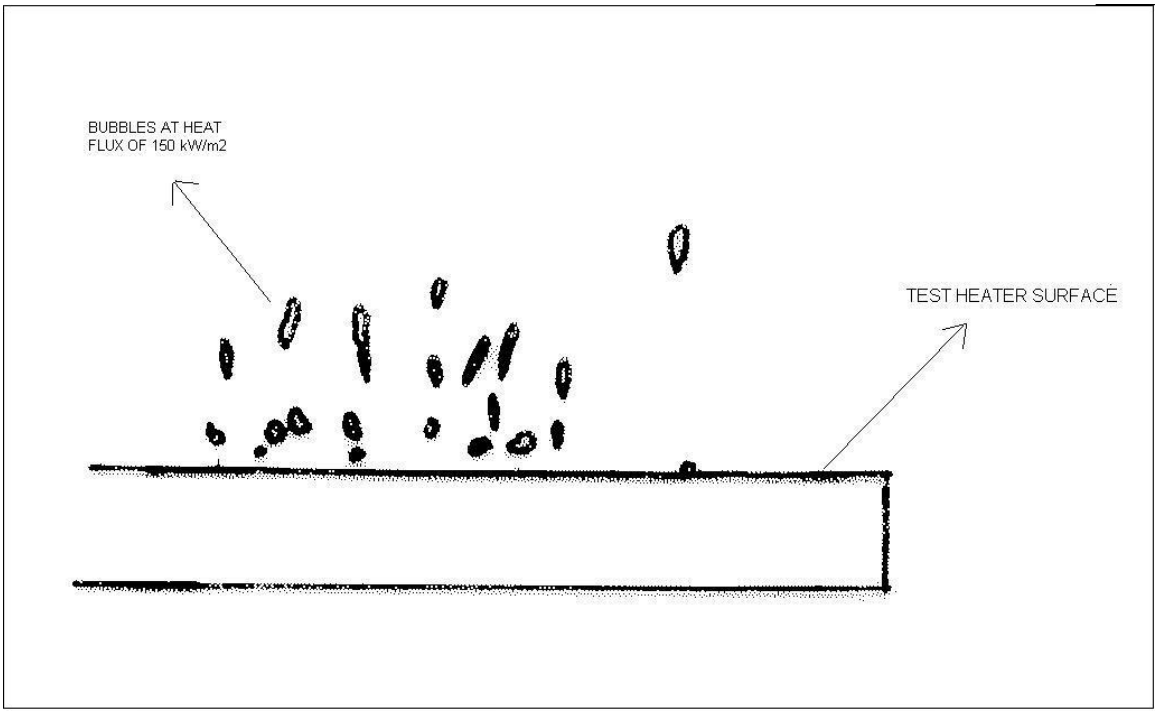

Figure 5-98 Enhanced visual image of nucleation for deionized water at 1000 psia and 20X magnification

The Figure 5-98 and Figure 5-99 were captured at speed of 500 frames per second. The Figure 5-99 shows columns of bubbles indicating that the nucleation is very

high and coalescence of bubbles leads to formation of columns of bubbles. The columns of bubbles appear to be leaving the heater surface uniformly in all directions.

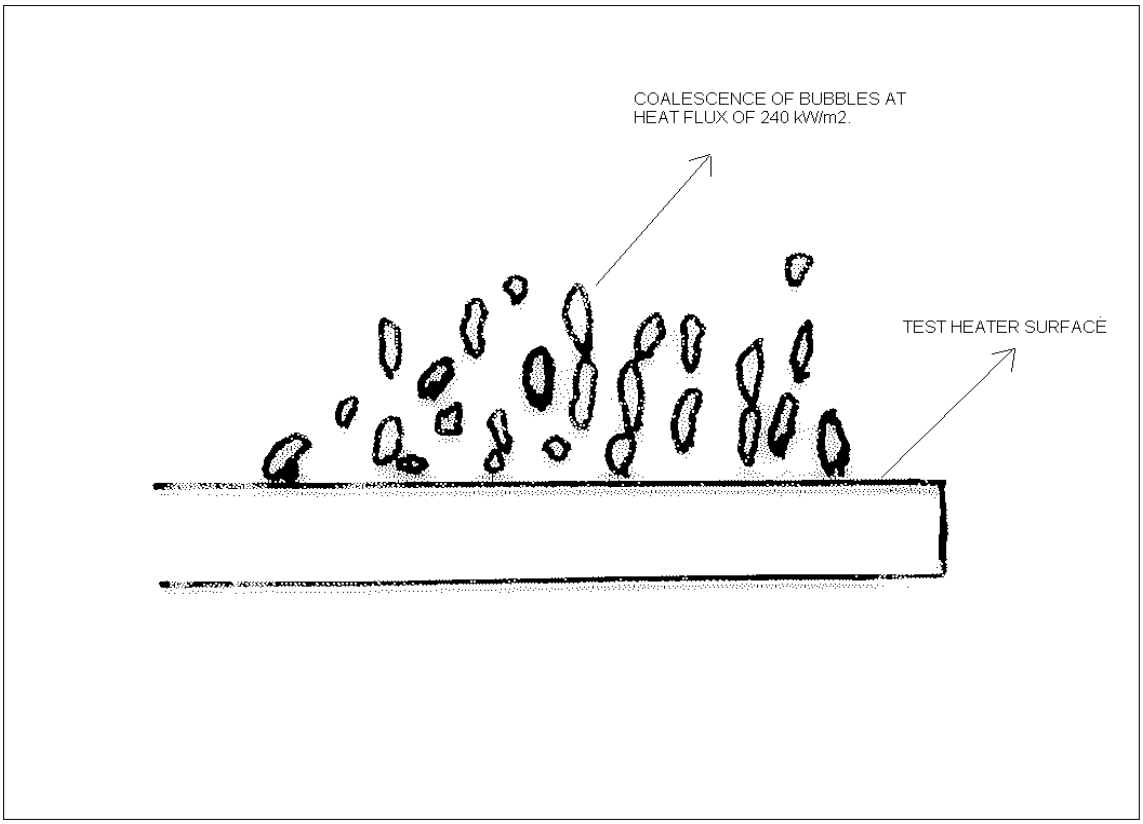

Figure 5-99 Enhanced image of bubbles on test heater surface at higher heat flux of 240kW/m^2 for deionized water at 20X magnification at 1000 psia

Images were captured at higher speed (frame rate) using HYCAM high speed camera. Figure 5-100 shows an image taken at 6000 half frames/ sec speed for boiling test with deionized water. “Half frame” indicates the shutter position in the HYCAM high speed camera. Only half of the lens view can be captured with a half frame shutter. With half frame shutter position, the number of images captured was twice that of a full frame position at constant film speed. Only the top half of the lens view is captured. The images were captured with the heat flux value being 240 kW/m^2. Figure 5-99 and Figure 5-100 show the images of nucleation of water for same conditions at 1000 psia and at a heat

flux of 240 kW/m^2 but captured at a different frame rate. It is observed that at higher flux the nucleation rate is so high that at normal frame rate, the bubbles seem to leave the surface in clusters but they are actually individual bubbles leaving heater surface. The average bubble size was found to be 1/16th inch in diameter. Observation from the enhanced image in Figure 5-100 reveals that bubbles are mostly spherical in shape and seem to be nucleating uniformly all along the boiling surface of the test heater. It was observed that the bubbles nucleated continuously from the surface of the heater without breaking intermittently.

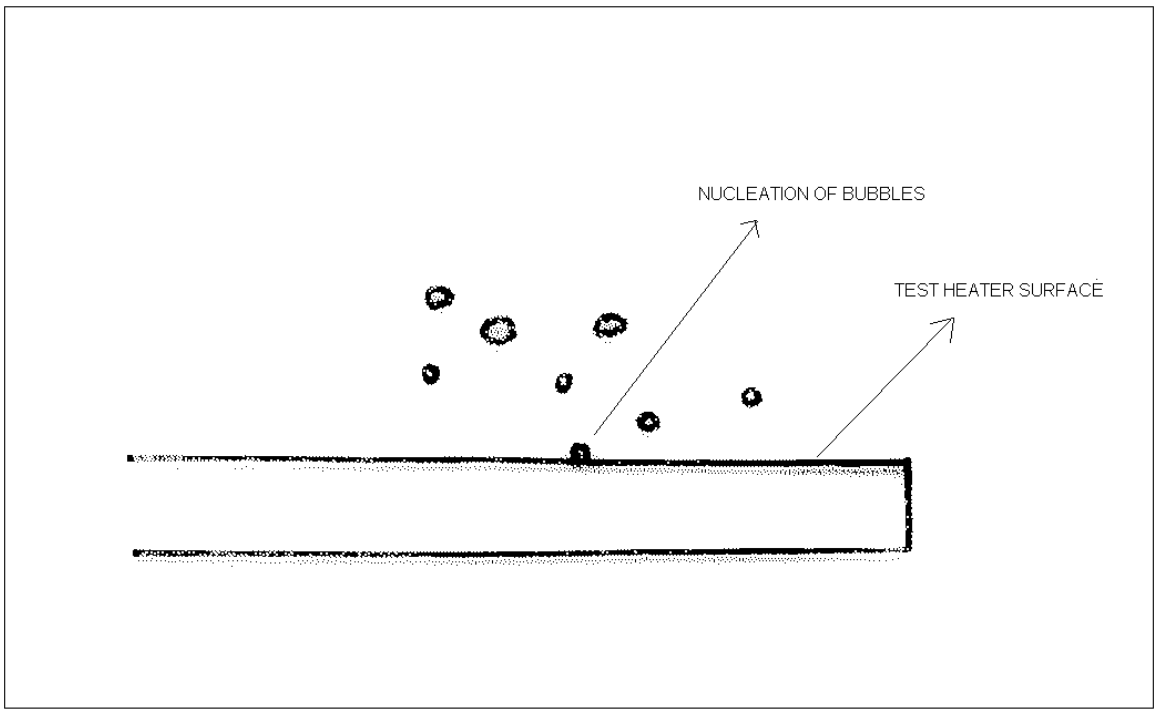

Figure 5-100 Enhanced image of bubbles captured at speed of 3000 fps, 10^{o}C subcooled and 1000 psia for at 20X magnification

Similar to images taken with deionized water, the nucleation videos were captured for a boiling test with boric acid solution at 1000 psia. The observations from the videos revealed that bubble density is lower than deionized water. The delay time between

collapsing of an old bubble and growth of a new bubble was found to 0.042 seconds whereas the value for deionized water was found to be 0.036 seconds. The delay time for 5000 ppm lithium metaborate was 0.045 seconds. Figure 5-101 shows the nucleation enhanced image captured at 3000 fps for 5000 ppm concentrated boric acid. It can be observed that the number of bubbles is relatively lower than that of deionized water at the same conditions, indicating, the effect of boric acid deposition on the surface of the test heater.

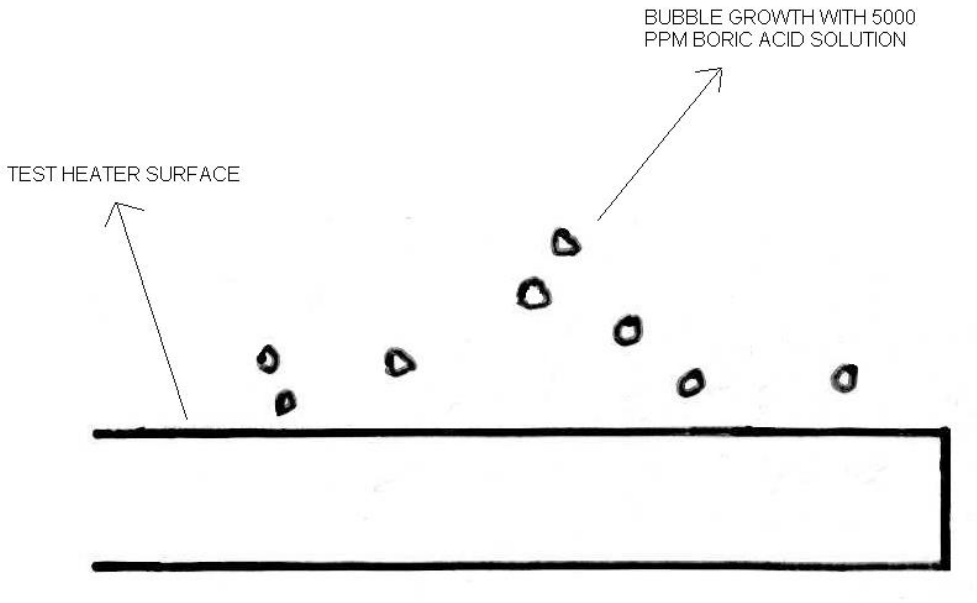

Figure 5-101 Enhanced image picture of nucleation for 5000 ppm boric acid solution with 10oC subcooling taken at 3000 fps and at 20X magnification at 1000 psia pressure

Figure 5-102 shows the nucleation image captured at 3000 fps for the boiling test with 5000 ppm concentrated lithium metaborate solution. It is clearly evident from figure

that the density of bubbles is lower than for deionized water.. The bubble density for lithium metaborate can be extrapolated based on images taken at the higher speed. The bubble density for lithium metaborate solution was found to be approximately 1406 bubbles per sq cm based on the data collected from the nucleation images. The values can be considered for comparison. Similar approximations have revealed the bubble density was 1968 per sqcm for 5000 ppm boric acid and 1406 per sq cm for deionized water. These approximations are based on a heat flux value of 200 kW/m^2. The analysis of images obtained from the high speed camera indicate that the nucleation is more uniform for deionized water and therefore leads to better boiling heat transfer coefficients. In comparison, the bubble behavior of boric acid seems to indicate bubbles of a smaller and less uniform size suggesting that boric acid deposits affect the nucleation by reducing the nucleation sites and thereby leading to a reduction in heat transfer coefficient.

Results for lithium metaborate boiling tests revealed a much smaller number of bubbles but the relative size of the bubbles was bigger compared to that of deionized water. The generation of bubbles was random in nature and seems to be occurring in clumps. This could be possibly explained by behavior of lithium metaborate deposits to form clusters thereby completely covering the nucleation sites. The deposition images of lithium metaborate revealed that the deposition occurred in patches on the heater surface.

Figure 5-102 shows an enhanced image of bubbles leaving the surface of the heater for boiling test with 5000 ppm lithium metaborate acid solution. Figure 5-102 was taken at 6000 half frames per minute speed which implies that the picture was captured in a time frame of little less than $1/100^{th}$ of a second. It can be observed in Figure 5-102 that

there are a smaller number of bubbles indicating that nucleation rate has degraded in presence of lithium metaborate.

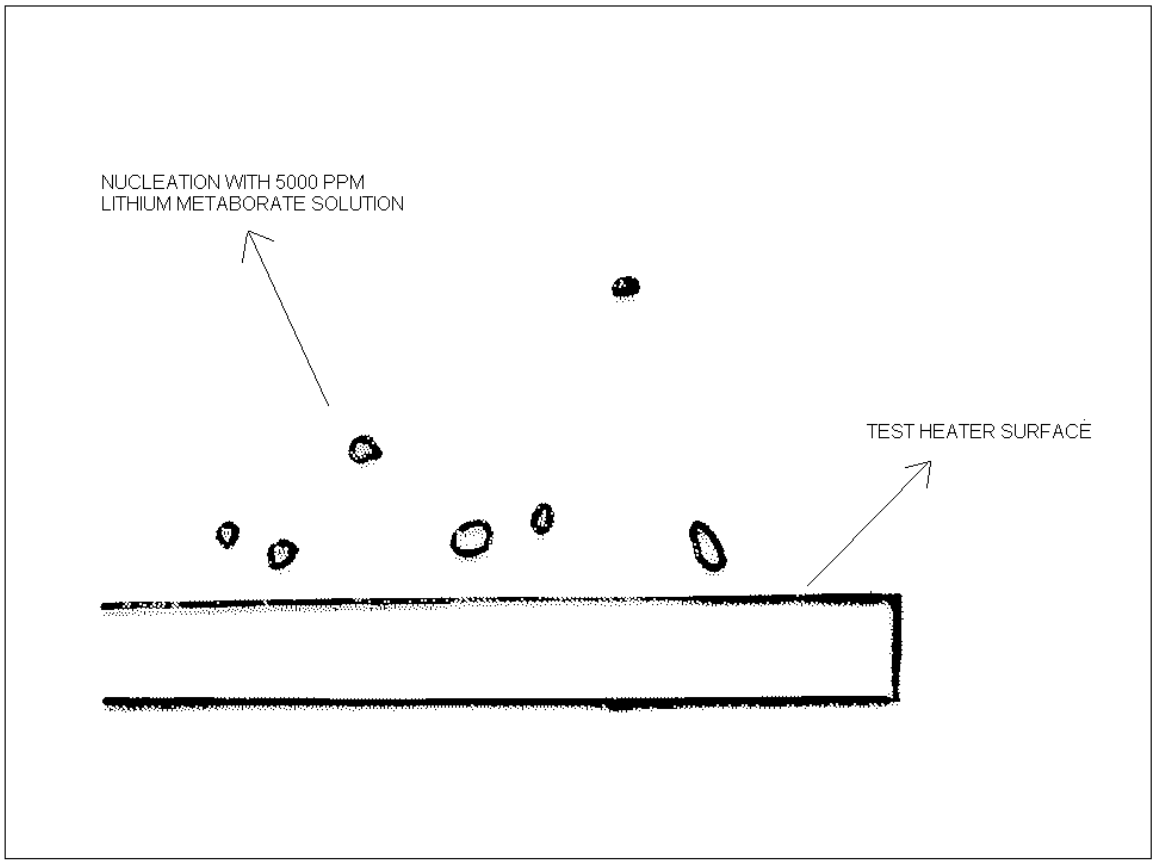

Figure 5-102 Enhanced image of nucleation for 5000 ppm lithium metaborate solution with 10^{o}C subcooling taken at 3000 fps and at 20X magnification at 1000 psia pressure

6 ANALYSIS OF RESULTS

The factors affecting the heat transfer coefficient under the experimental nucleate pool boiling conditions are discussed in this chapter. The boiling test results obtained are evaluated and the effect of various parameters affecting the boiling heat transfer coefficient is discussed.

6.1 Effect of Coolant Concentration

Evaluation of the boiling test results have revealed that the presence of boric acid and lithium metaborate in deionized water affect the boiling heat transfer coefficient by causing a resistance to the heat transfer between the heater and the bulk liquid. The details are discussed below.

6.1.1 Effect of Boric Acid

The evaluation of boiling tests performed at bulk fluid pressures of 100 psia, 200 psia, 500 psia and 1000 psia reveal that the boiling heat transfer coefficient decreases with increasing boric acid concentration in the bulk fluid (coolant). Increased resistance to uniform nucleation caused by the boric acid solution likely explains the decrease in heat transfer coefficient. The nucleation that occurs during the boiling process leads to the formation of boric acid deposits on the heater surface thereby creating a layer of resistance between the heater and bulk fluid. The photomicrographs taken after the boiling test with 5000 ppm concentration boric acid confirm the presence of boron particulates on the test heater. The effect of varying the boric acid concentration in deionized water on the heat transfer coefficient is shown in Figure 6-1 where the bulk

fluid pressure is 1000 psi in conjunction with a saturation temperature of 284.4^{o}C. Even though there is a decrease in pool boiling heat transfer coefficient for 500 ppm concentration boric acid over that of deionized water, the decrease is not significant. The heat transfer coefficient was reduced by 4.9% at a heat flux of 236 kW/m^2 when compared to the pool boiling heat transfer coefficient of 14.7 kW/m^{2o}C for deionized water. However, for 1000 ppm concentration of boric acid, the decrease in heat transfer coefficient is considerable. For a heat flux of 236 kW/m^2, the heat transfer coefficient decreased by 9% to a value of 13.4 kW/m^2.

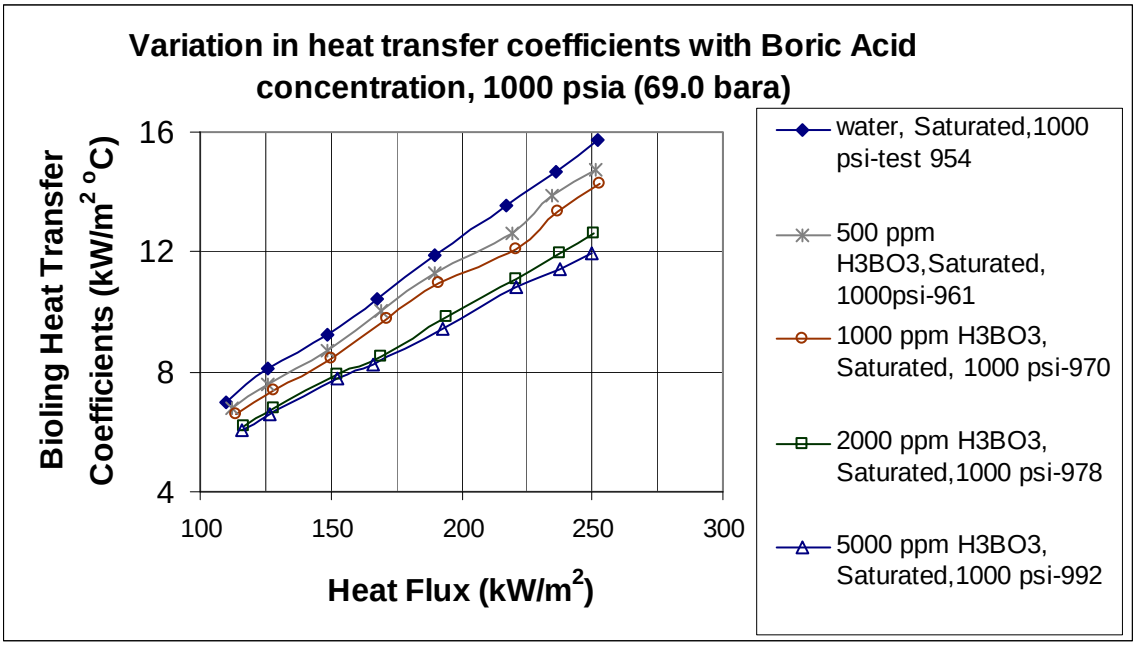

Figure 6-1 Degradation of pool boiling heat transfer coefficients with variation of coolant concentration (boric acid as additive).

The pool boiling heat transfer coefficients for 2000 ppm and 5000 ppm concentration solutions of boric acid at a heat flux of 236 kW/m^2 are 11.9 kW/m^2 and 11.4 kW/m^2, respectively. It can be observed that the pool boiling heat transfer coefficient is lowest for the coolant with a 5000 ppm concentration of boric acid. Figure 6-2 shows

the degradation of the pool boiling heat transfer coefficient with increasing boric acid concentration. Also note from Figure 6-2 that the boiling heat transfer coefficient decreases steadily up to a concentration of about 2000 ppm. The rate of decrease in the heat transfer coefficient reduces with concentrations of boric acid greater than 2000 ppm indicating that further addition of boric acid to the solution does not significantly affect the heat transfer coefficient.

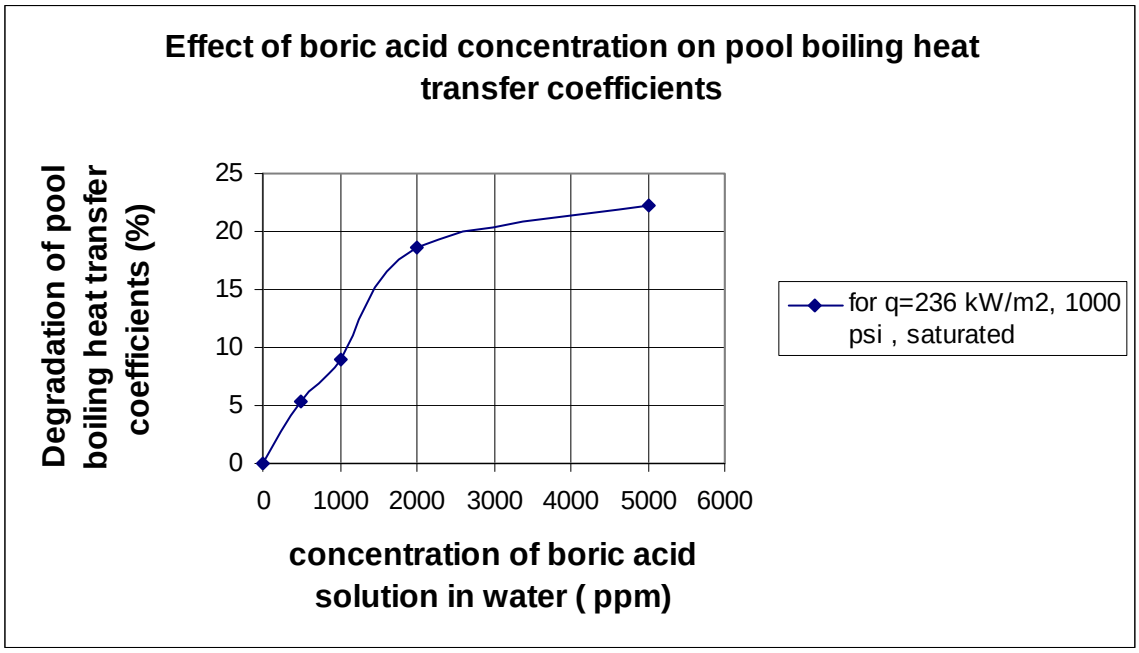

Figure 6-2 Degradation of pool boiling heat transfer coefficients of boric acid solution relative to deionized water.

6.1.2 Effect of Lithium Metaborate

The evaluation of the boiling curves obtained from tests with different concentrations of lithium metaborate indicates a similar trend as with boric acid. The pool boiling heat transfer coefficients decrease with increasing concentration of lithium metaborate in deionized water. However, the reduction rate of the pool boiling heat

transfer coefficient for lithium metaborate is slightly different from that of boric acid. Changing the bulk fluid pressure does not have a significant effect on the heat transfer coefficient which is shown in Figure 6-3 under different concentrations of lithium metaborate solution.

It can be observed from Figure 6-3 that the pool boiling heat transfer coefficient decreases with increasing concentration of the lithium metaborate solution. It is also interesting to note that the change in heat transfer coefficient is not significant for those boiling tests with 2000 ppm and 5000 ppm concentrations. This indicates that upon further addition of lithium to deionized water, the variation in boiling heat transfer coefficient will not be significant.

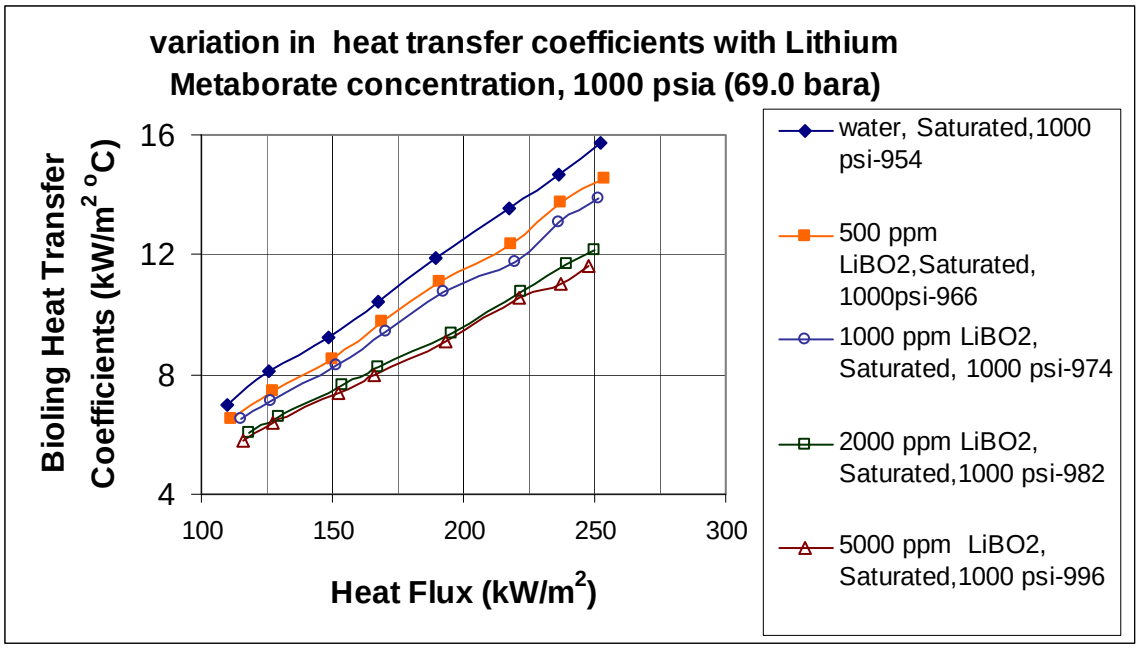

Figure 6-3 Degradation of pool boiling heat transfer coefficients with variation of coolant concentration (lithium metaborate as additive).

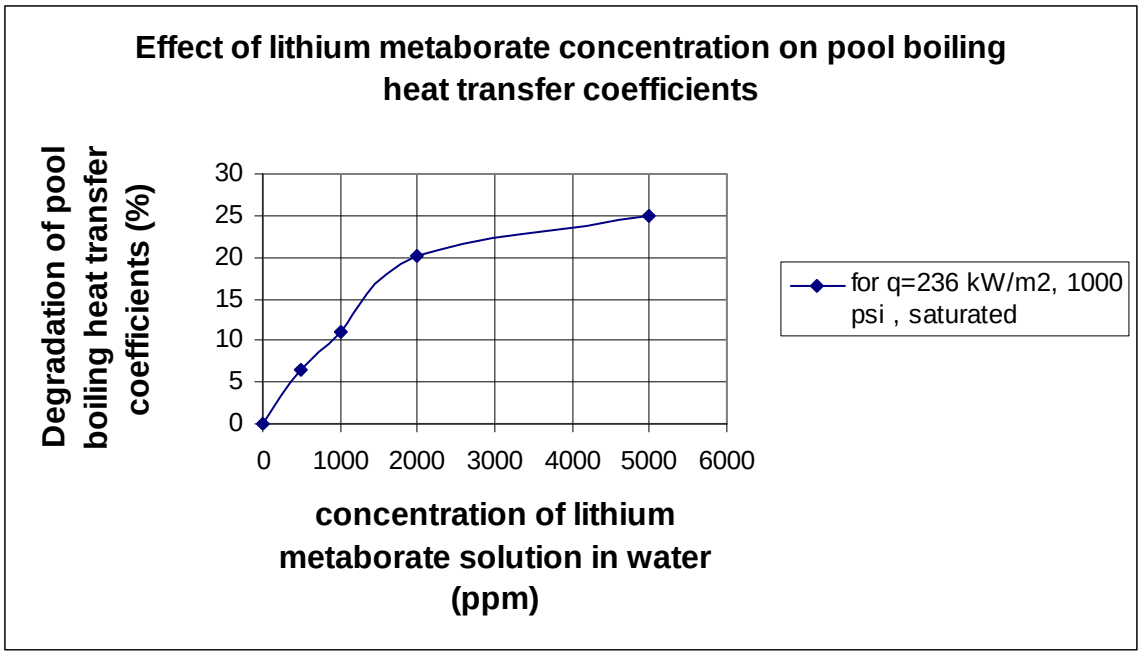

Figure 6-4 Degradation of pool boiling heat transfer coefficients of lithium metaborate solution relative to deionized water.

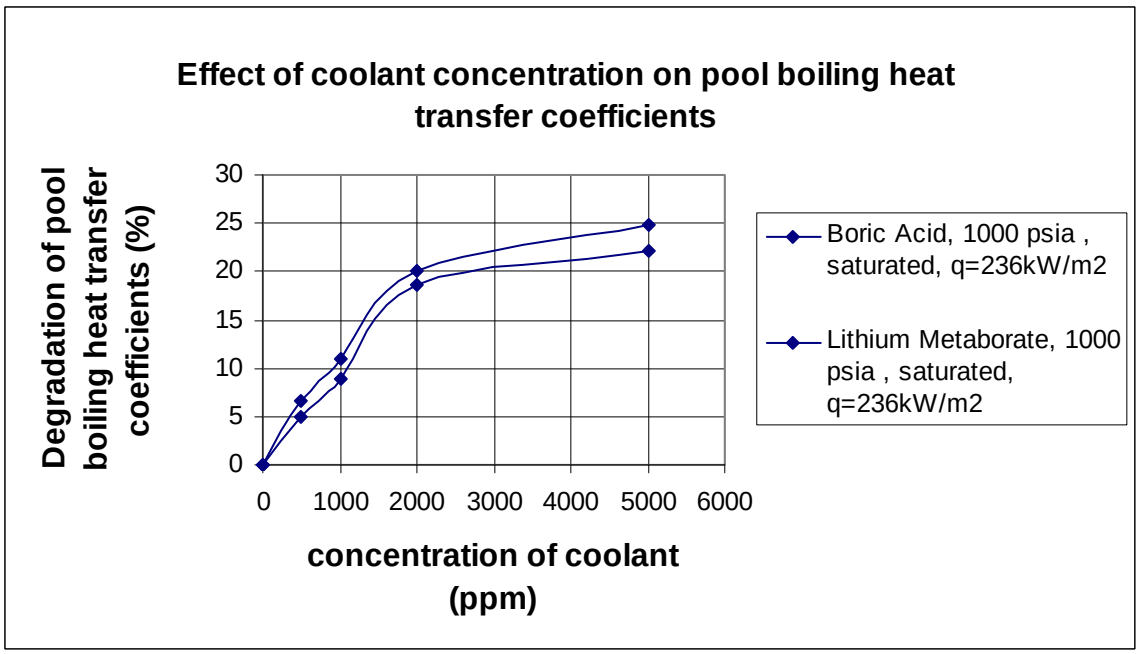

Figure 6-5 Comparison of the effect of boron and lithium concentration on pool boiling heat transfer coefficients.

Figure 6-4 shows the percentage change in the pool boiling heat transfer coefficient for varying concentration of lithium metaborate for the boiling tests done at a coolant pressure of 1000 psia and at saturation temperature of 284.4 C. The boiling heat transfer coefficient for deionized water at a heat flux of 236 kW/m^2 is 14.6 $kW/m^{2o}C$ at the saturation temperature of the bulk fluid. The pool boiling heat transfer coefficient shows a reduction of 6.6%, 12%, 20.2% and 24.9% for 500 ppm, 1000 ppm, 2000 ppm and 5000 ppm concentration of lithium metaborate solution, respectively where the bulk fluid is saturated temperature. In comparison with boric acid, it was found that lithium metaborate has a greater influence on the pool boiling heat transfer coefficient than boric acid as seen from Figure 6-4 and Figure 6-2. This is consistent with the observed nucleation and deposition patterns for associated with the boric acid and lithium metaborate solutions. Recall that the lithium metaborate deposits occurred in clusters and had a higher deposition rate than the boric acid deposits which explains the higher degradation of pool boiling heat transfer.

Figure 6-5 shows a comparison of the effects of boron and lithium on the pool boiling heat transfer coefficient where it can be observed that the addition of lithium metaborate has resulted in a higher degradation of heat transfer coefficient relative to the addition of boric acid.

6.2 Effect of Subcooling

With increasing subcooling of bulk fluid, it was found that the pool boiling heat transfer coefficient decreased. As seen in boiling curves in Figure 5-1, Figure 5-15, Figure 5-39, and Figure 5-60, the degree of superheat increased with an increase of

subcooling at all pressures. The boiling heat transfer coefficient was higher for tests conducted at saturated temperature because the onset of nucleate boiling (ONB) occurs at a lower heat flux for those boiling tests conducted at saturation pressure. The evaluation of boiling tests reveals that the pool boiling heat transfer coefficient is highest when the temperature difference between hot surface and coolant is a minimum. Figure 6-6 shows the degradation in the pool boiling heat transfer coefficient with increasing the bulk fluid subcooling. The ordinate in the Figure 6-6 indicates the heat transfer coefficient ratio ($\frac{\alpha}{\alpha_{saturation}}$), which is the ratio of the boiling heat transfer coefficient at any subcooling to the boiling heat transfer coefficient at saturation temperature. Observe that with increasing degree of subcooling, the heat transfer coefficient decreases.

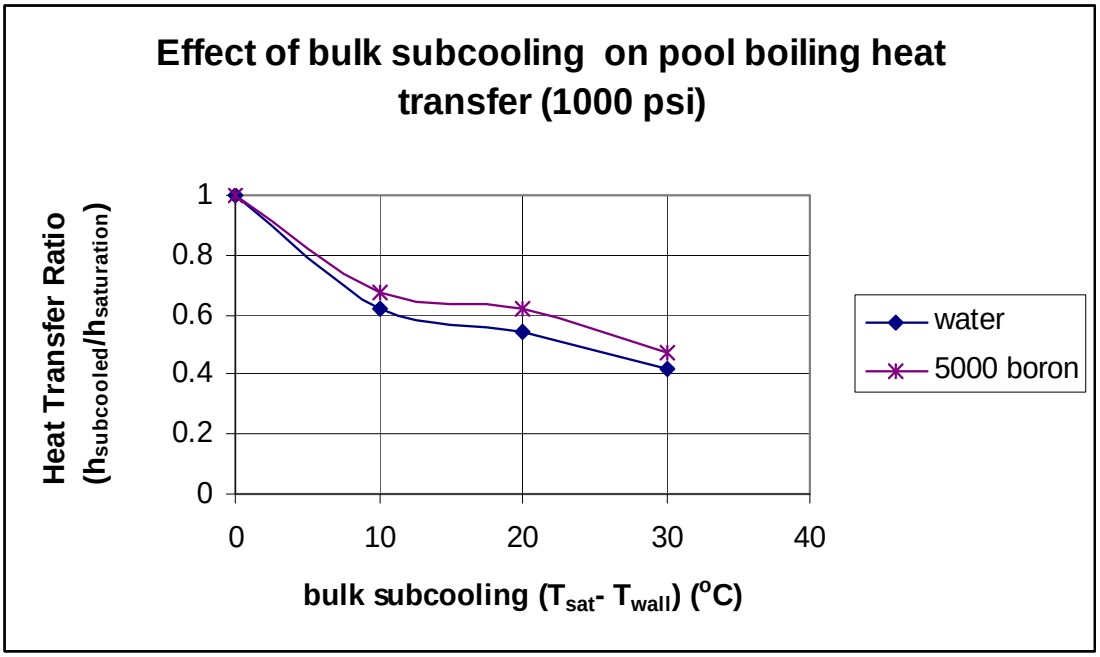

Figure 6-6 Effect of bulk subcooling on pool boiling heat transfer.

6.3 Effect of Pressure

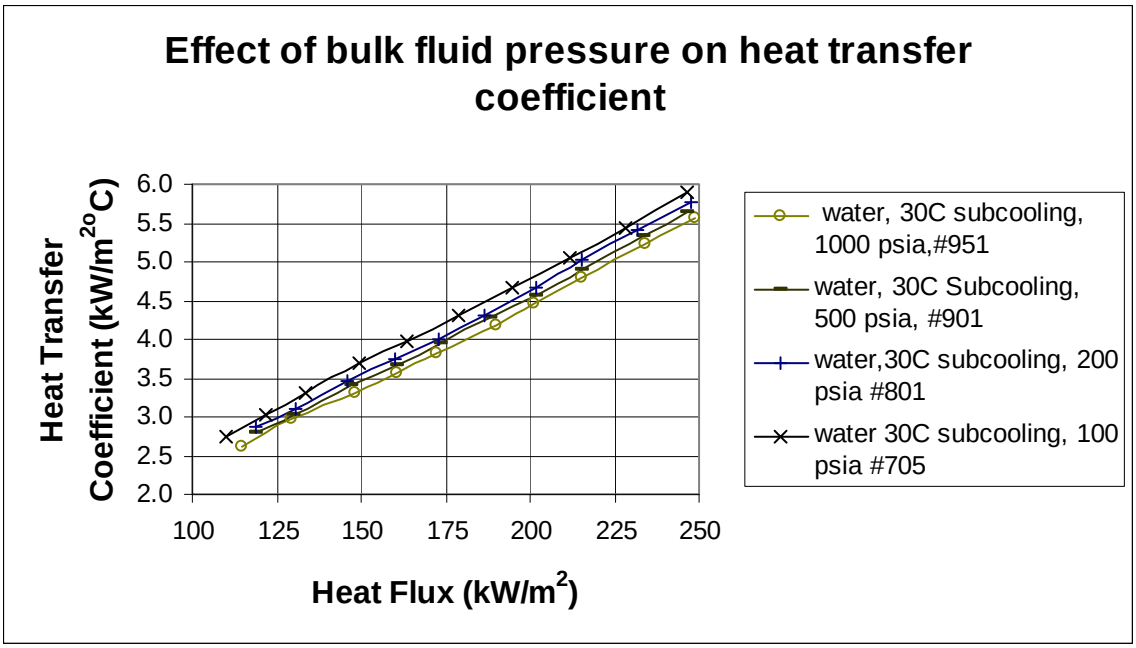

Figure 6-7 Effect of pressure on pool boiling heat transfer coefficient.

The increase of pressure does not have a significant effect on the heat transfer coefficient. However, note from Figure 6-7 that increasing bulk fluid pressure, while maintaining a fixed heat flux, reduces the nucleation rate consequently decreasing the pool boiling heat transfer coefficient. This is due to the greater external fluid pressure on the bubbles rising from the heater surface. In other words, the heat flux required for nucleation to occur increases with increasing pressure. The reduction in heat transfer coefficient can be also be explained by the possibility of active nucleation cavities being completely filled with coolant thereby limiting bubble formation in the cavity. The likelihood of a new bubble nucleating is high in semi–wet cavities and low in fully–wet cavities. Tests with varying concentrations of boric acid and lithium metaborate solutions show slight degradation of the heat transfer coefficient with increasing pressure. For a

change in system pressure from 200 psia to 1000 psia, the boiling heat transfer coefficient decreases slightly from 4.7 kW/m^{2}C to 4.3 kW/m^{2}C for a 5000 ppm concentration boric acid solution. For boiling tests with a 5000 ppm concentration of lithium metaborate, the heat transfer coefficient showed a slight degradation from 4.6 kW/m^{2}C to 4.1 kW/m^{2}C for a change of coolant fluid pressure from 200 psia to 1000 psia, respectively.

6.4 Analysis of Particulate Deposits

The photomicrographs of the boric acid deposits reveal that the particulate deposits were scattered over the entire surface above the heating element (nucleation region of the test heater). The total weight of the boric acid deposits was found to be 12mg for a boiling test with 5000 ppm boric acid solution at 1000 psia pressure and 10^{o}C bulk subcooling. The analysis of this boric acid deposition test indicates that significant deposits are formed on the test heater, which leads to a decrease in heat transfer coefficient over time. The average number of deposition particles was found to be 742 per sq mm for the 5000 ppm boric acid solution test. The increase in pool boiling heat transfer coefficient during the first few hours of the test (Figure 5-77) result from the deposits serving as heat transfer "fins" augmenting the heat transfer. Afterwards, the heat transfer coefficient decreases uniformly with the exception of 80 hours where a fraction of the boron deposits have been apparently dislodged from the heater surface. The deposition rate, however, may have reached saturation or steady state condition after 100 hours as the change in the pool boiling heat transfer coefficient appears insignificant after a time of 110 hours.

Deposits of lithium metaborate reveal that deposits of this material are denser in particle number than for lithium metaborate, where the deposits seem to form clusters of cohesive particles. The total weight of the deposits from the lithium metaborate test was found to be 22mg for 5000 ppm lithium metaborate concentration at 1000 psia and 10^{o}C subcooling. As seen in Figure 5-96, the lithium metaborate deposits occur in patches which lead to irregular nucleation patterns. The average number of deposition particles was found to be 1021 particles per sq. mm. From the test results, it appears that the lithium metaborate enhances the deposition rate of boron onto the Zr-4 clad test heater, although the deposit's chemical composition was not verified. The degradation of heat transfer coefficient in the presence of lithium metaborate is significantly higher than that of boric acid. It can be concluded that the higher deposition rate in the presence of lithium metaborate is cause for greater reduction of heat transfer coefficients.

6.5 Analysis of Bubble Growth Behavior

Observations from the visual recordings reveal that nucleation occurs in a uniform manner for deionized water. The bubble size obtained from nucleation images varied from 0.8mm to 2.5mm in diameter for a heat flux of 150 kW/m^2. The visual recordings of the nucleation obtained for boric acid solution reveal that nucleation is less uniform. The bubble size for boiling tests with 5000 ppm boric acid solution obtained from the nucleation images varied from 0.6mm to 2mm in diameter for a heat flux of 150 kW/m^2. The analysis of nucleation recordings for tests with lithium metaborate revealed that the nucleation occurred in a non-uniform and sporadic manner. The bubbles occurred in odd clumps indicating a strong presence of lithium metaborate deposits on the test heater

surface. The bubble size varied from 0.6mm to 3mm for a heat flux of 150 kW/m^2. The larger size of bubbles in the case of lithium metaborate is due to the bubbles combining with each other. However, as explained in nucleation results section of this report, the nucleation density is lower with both the boric acid and lithium metaborate coolant solutions than with deionized water, accounting for the degradation of boiling heat transfer coefficients. It is the variation in nucleation patterns that explains the change in heat transfer coefficient for the boric acid and lithium metaborate solutions. As explained in nucleation results, the coolant concentration affects the nucleation process by decreasing the nucleation densities. For 5000 ppm boric acid, the nucleation densities decreased by 20% when compared with deionized water and in presence of 5000 ppm lithium metaborate solution, the number of bubbles decreased by 38%.

7 CONCLUSIONS

This experimental investigation generated a database for subcooled pool boiling heat transfer coefficients on Zr-4 clad heater rods for coolants with varying concentration of boron and lithium. The generated empirical data includes the effect of bulk subcooling, bulk fluid pressure, heat flux and coolant concentration and is useful for better understanding of the Axial Offset Anomaly phenomenon.

Analysis of the results obtained from the investigation reveal that the increase of concentration of boric acid and lithium metaborate in water results in the degradation of boiling heat transfer coefficients. The boiling heat transfer coefficients were found to be slightly lower in presence of lithium than boron. The degradation in the heat transfer coefficients, relative to that of water was of order of 24% for boron and of order of 26% for lithium at coolant concentration of 5000 ppm respectively. For pool boiling tests at 10^{o}C subcooling, it was observed that the nucleation was relatively less affected by addition of boric acid and lithium metaborate when compared to boiling tests at saturated temperatures. However, the degradation of heat transfer coefficients was substantial for boiling tests conducted for about 100 hour test duration times with higher concentrations of boric acid and lithium metaborate. The degradation indicates that the precipitates formed on the test heater due to the subcooled boiling influence the heat transfer coefficients significantly. Results showed the decrease in heat transfer coefficients by 22% and about 29% at 10^{o}C subcooling for boron and lithium precipitates respectively. The pool boiling tests showed a consistent trend of decline of boiling heat transfer coefficients with increase of subcooling. The experimental investigation revealed that the

system fluid pressure does not have a significant effect on the pool boiling heat transfer coefficients.

The inspection of the electrical test heater clad with Zr-4, revealed formation of deposits on the surface after undergoing subcooled nucleate boiling. The formation of deposits on the heater surface confirms that the precipitation of lithiated compounds like lithium metaborate on test heater occurs during subcooled nucleate boiling. A visual recording of the nucleation was obtained at subcooled boiling conditions with varying concentrations of boric acid, and lithium metaborate. The image analysis of the deposits revealed that the boron deposits are scattered and less dense than the deposits of lithium. Higher deposition rate of lithium also explains the reason for higher effect on boiling heat transfer coefficients. The empirical data generated is useful for better understanding of AOA. The experimental results revealed that the deposition of boron and lithium is factor is determining the heat transfer coefficients. The variation of heat transfer coefficients between the fuel rod and the coolant will be very helpful in prediction of AOA in a nuclear power plant.

8 RECOMMENDATIONS FOR FURTHER WORK

The Recommendations for future work would include generating additional quantitative data that helps in further understanding of AOA. The data collected through the boiling tests in this project includes includes understanding the effect of bulk subcooling, bulk fluid pressure, heat flux and coolant concentration on pool boiling heat transfer coefficients. Similar data could be generated at higher bulk fluid pressures of above 2000 psia (typical PWR operating conditions). This data will be useful to verify the observations made for boiling tests with bulk fluid pressure of 1000 psia or lower. All the empirical data generated during the boiling tests in this project is a database of pool boiling heat transfer coefficients for varying operating conditions. Further work could be done to generate forced convective boiling heat transfer coefficients by varying a set of operating parameters similar to that of subcooled pool boiling tests. This will result in understanding the impact of bulk fluid velocity on heat transfer coefficients and the deposition on the fuel rod in a PWR.

The effect of the concentration of boric acid and lithium metaborate in the coolant on the deposits on a sample test heater were analyzed respectively in this project. The coolant used for all the boiling tests was pure deionized water without any impurities. However, in a actual operating PWR, the coolant may contain impurities like oxides due to corrosion of the plant piping. A study can be conducted to estimate the impact of the impurities in the coolant on the boiling heat transfer coefficients and the deposition rates by adding measured quantities of impurities in the coolant.

References

1. Collier, John G; Thome, John R;1994,'Convective Boiling and Condensation', Oxford University Press, ISBN-0-19-856282-9

2. Fenton, Donald, 2003, Annual Project Report submitted to DOE

3. Kamoshida, Junji; Isshiki, Naotsugu, 1994, 'Heat transfer to deionized water and deionized water/lithium halide salt solutions in nucleate pool boiling', Proceedings of the International Absorption Heat Pump Conference: p 501-507.

4. Muller-Steinhagen, H; Jamialahmadi, M, 1990, 'Scale formation during boiling. The effects of heat flux and CaSO4 concentration', Proceedings of ASME winter annual Meeting, paper 90-WA/HT-3

5. Zhao,Yaohua; Tsuruta, Takaharu,2002,'Prediction of bubble behavior in subcooled pool boiling based on microlayer model', JSME international journal, series B, vol 45, 2002.

6. Schnelle, Jay, 2002; 'Experimental investigation of aqueous glycol mixtures in pool boiling on smooth and enhanced surfaces', MS Thesis, KSU.

7. Vleet, R J Van, 1985, "A Study of the initiation of subcooled boiling during power transients", PHD Dissertation, KSU.

8. Sachdeva, R.C, 2001, 'Fundamentals of Engineering Heat and Mass Transfer', New Age international Publishers, ISBN:81-224-0076-0.

9. Loftness, Robert L., 1964, 'Nuclear power plants', D Van Nostrand company publications:p 127-128.

10. Konya, Mark J; Bryant, Kenneth R;Kock, Keith P;Hopkins, David L; Hughes, Garry A; Irwin, Randall J;1993 ' Power distribution changes brought by subcooled nucleate pool boiling at Callaway power plant', Proceedings of ASME/JSME nuclear engineering joint conference p 281-287

11. Frattini, P.L; Blok, J.;Chauffriat,S.; Sawicki,J. and Riddle,J.; 2001, 'Axial offset anomaly: coupling PWR primary chemistry with core design', Journal of Nuclear Energy, Volume 40, p 123-135

12. Nero, Anthony.V,1979, 'A Guidebook to Nuclear Reactors', University of California press, ISBN 0-520-03482-1

13. Visual Instrumentation Corporation, 2003, 'Hycam Instruction Manual for 16mm high speed motion picture camera model 41-0005'

14. Incropera, Frank P.; Dewitt, David P, 2001 'Fundamentals of Heat and Mass Transfer', John Wiley Publications, ISBN-9814-12-666-7

15. Jamialahmadi, M.; Mueller –Steinhagen, H.;1991, "Reduction of calcium sulfate scale formation during nucleate boiling addition of EDTA", Journal of Heat Transfer Engineering, volume 12, issue 4 , p 19-26

16. Hamilton, R.C, Stern laboratories, 2000, "Operation and Maintenance Manual 23 kW DC Power Supply", Stern Laboratories Inc

17. Tong, L.S.; Weisman, J; 1970, "Thermal Analysis of Pressurized Water Reactors", Published by American Nuclear Society.

18. Omega, “User’s guide to DP25-S Strain Gage Panel Meter”, Omega Technology Company.

19. Systat, (www.systat.com), A image analysis tool from Sigmascan for determining the particle size, 2006.

APPENDIX A

A.1 Program for Data Reduction in FORTRAN

Code for calculation of heat flux and heat transfer coefficient. The reference surface number for test heater is 10 (isurf =10). The parameter "alpha" in code is the heat transfer coefficient.

```
      PROGRAM PBDATA
       PARAMETER (pi=3.141593)
       PARAMETER (twopi=2*pi)
       COMMON/XDATA/idnum,idate,isurf,icomp(5),frac(5),npts,iunits,
      &            volts(40),amps(40),P(40),Tb(2,40),Tc(4,40),Te(4,40)
       COMMON/XOUTP/delt(40),Qloss(40),alpha(40),Twall(40),flux(40),
      &             TCvar1(40),TCvar2(40)
       CHARACTER*20 inpfil, datfil, sdffil
       DATA jin/1/,jinp/2/,jdat/3/,jsdf/4/,jban/5/
       OPEN(jin,FILE='test.inp',STATUS='OLD')
       OPEN(jban,FILE='pbdata.txt',STATUS='UNKNOWN')
C--- Read number of data files to be processed
       READ(jin,10)
10     FORMAT( )
       READ(jin,10)
       READ(jin,15) nfiles
15     FORMAT(3X,I3)
       READ(jin,10)
C*************** Begin BIG loop to process each data file
       DO 900 IFILE=1,nfiles
         READ(jin,20) inpfil, datfil, sdffil
20       FORMAT(3A20)
            WRITE(*,25) inpfil
```

```
25      FORMAT(/,10X,'Begin data reduction for file ',A20)
C--- open output files
        OPEN(jinp,FILE=inpfil,STATUS='OLD')
        OPEN(jdat,FILE=datfil,STATUS='UNKNOWN')
        OPEN(jsdf,FILE=sdffil,STATUS='UNKNOWN')

C--- read in the data from one file
        CALL INPUT(jinp)
C
C----------------process the data -- many possible cases
        IF (idnum.GE.1000) THEN
C***********************************************
C          FLAT DISK TEST SECTIONS
C***********************************************
          condcu = 391.0
          ri = 0.0127
          ro = 0.0159
          AI = 0.507E-03
          AO = 0.792E-03
          thick = 0.8E-03
          perim = 2. * twopi * ri + 2. * thick
          AX = twopi * ri * thick
          zlb  = ro - ri
          zlnc = 5.
          zl = zlnc * perim / condcu / AX
          D1 = 0.001
          D2 = 0.005
          D3 = 0.009
          DO 1050 I = 1, npts
            STC = Tc(1,I) + Tc(2,I) + Tc(3,I)
            SX2 = D1*D1 + D2*D2 + D3*D3
```

```
            SX  = D1 + D2 + D3
            STCX= Tc(1,I)*D1 + Tc(2,I)*D2 + Tc(3,I)*D3
            S2X = SX * SX
            Twall(I) = (STC*SX2 - SX*STCX) / (3.*SX2 - S2X)
            TBave = (Tb(1,I) + Tb(2,I))/2.
            delt(I) = Twall(I) - TBave
            watts = volts(I) * amps(I)
            Qloss(I) = SQrt(zlnc*perim*condcu*AX)*delt(I)*TANH(zl)
            flux(I) = (watts - Qloss(I)) / AI
            alpha(I)= flux(I)/delt(I)
            Qloss(I)= 100.*Qloss(I)/watts
            TCvar1(I) = 0.
            TCvar2(I) = 0.
1050        CONTINUE
         ELSEIF ((isurf.EQ.1).OR.(isurf.EQ.7).OR.(isurf.EQ.8)) THEN
C*************************************************************
C           isurf = 1,7,8
C           Smooth Tube - See section B.2, pg. 101 Shakir
C*************************************************************
           ri=  0.00630
           rt=  0.00870
           ro=  0.01110
C--          This heater had a 3 inch boiling length
           zlb= 0.07620
           zlnc=0.01270
           zl = zlb + zlnc
           condcu= 391.0
C
           DO 135 I=1,npts
             watts = volts(I)*amps(I)
             Q = watts
```

```
            TCave=(Tc(1,I)+Tc(2,I)+Tc(3,I)+Tc(4,I))/4.
            TBave=(Tb(1,I)+Tb(2,I))/2.
            TLave=(Te(1,I)+Te(2,I))/2.
            Tvar = 0.
            DO 133 J=1,4
              Tvar = Tvar + (TCave - Tc(J,I))**2
 133        CONTINUE
            TCvar1(I)= SQrt(Tvar)
            TCvar2(I)= 100.*TCvar1(I)/(TCave-TBave)
            Twall(I)= TCave - Q*(1./(twopi*condcu*zlb))*ALOG(ro/rt)
            delt(I)= Twall(I) - TBave
            flux(I)= Q/(twopi*ro*zl)
            alpha(I)= flux(I)/delt(I)
            deltL= TCave - TLave
            deltM= TLave - TBave
            Qloss(I)= condcu*pi*(ro*ro-ri*ri)*deltL/(0.5*zl) +
     &              alpha(I)*twopi*ro*zlnc*deltM
            Q = Q - Qloss(I)
            Qloss(I)= 100.*Qloss(I)/watts
            Twall(I)= TCave - Q*(1./(twopi*condcu*zlb))*ALOG(ro/rt)
            delt(I)= Twall(I) - TBave
            flux(I)= Q/(twopi*ro*zlb)
            alpha(I)= flux(I)/delt(I)
 135        CONTINUE
          ELSEIF (isurf.EQ.2) THEN
C*************************************************
C           isurf = 2, High Flux  (Bajorek)
C*************************************************
            ro= 0.009335
            RC= 0.008382
            rt= 0.007798
```

```
      ri= 0.004763
      zlb= 0.0508
      zlnc= 0.041625
      zl= zlb + zlnc
      CONDHF= 242.0
C
      DO 145 I=1,npts
        watts = volts(I)*amps(I)
        Q = watts
        TCave=(Tc(1,I)+Tc(2,I)+Tc(3,I)+Tc(4,I)+2.*(Te(2,I)+
     &          Te(4,I)))/8.
        TBave=(Tb(1,I)+Tb(2,I))/2.
        TLave=(Te(1,I)+Te(3,I))/2.
        Tvar = 0.
        DO 143 J=1,4
          Tvar = Tvar + (TCave - Tc(J,I))**2
143       CONTINUE
        TCvar1(I)= SQrt(Tvar)
        TCvar2(I)= 100.*TCvar1(I)/(TCave-TBave)
        Twall(I)= TCave - Q*(1./(twopi*CONDHF*zlb))*ALOG(ro/rt)
        delt(I)= Twall(I) - TBave
        flux(I)= Q/(twopi*ro*zl)
        alpha(I)= flux(I)/delt(I)
        deltL= (Te(2,I)+Te(4,I))/2. - TLave
        deltM= TLave - TBave
        Qloss(I)= CONDHF*pi*(ro*ro-ri*ri)*deltL/(0.5*zlnc) +
     &            alpha(I)*twopi*ro*zlnc*deltM
        Q = Q - Qloss(I)
        Qloss(I)= 100.*Qloss(I)/watts
        Twall(I)= TCave - Q*(1./(twopi*CONDHF*zlb))*ALOG(ro/rt)
        delt(I)= Twall(I) - TBave
```

```
          flux(I)= Q/(twopi*ro*zlb)
          alpha(I)= flux(I)/delt(I)
 145      CONTINUE
      ELSEIF (isurf.EQ.3) THEN
C*************************************************************
C       isurf = 3, Finned Tube, 19 Fins per Inch (Bajorek)
C*************************************************************
          ri   = 0.00470
          rt   = 0.00591
          ro   = 0.00800
          RFIN = 0.009535
          zlb  = 0.0508
          zlnc = 0.03175
          zl   = zlb + zlnc
          condcu = 391.0
          DO 155 I=1,npts
            watts = volts(I)*amps(I)
            Q = watts
            TCave=(Tc(1,I)+Tc(2,I)+Tc(3,I)+Tc(4,I))/4.
            TBave=(Tb(1,I)+Tb(2,I))/2.
            Tvar = 0.
            DO 153 J=1,4
              Tvar = Tvar + (TCave - Tc(J,I))**2
 153        CONTINUE
            TCvar1(I)= SQrt(Tvar)
            TCvar2(I)= 100.*TCvar1(I)/(TCave-TBave)
            Twall(I)= TCave - Q*(1./(twopi*condcu*zlb))*ALOG(ro/rt)
            delt(I)= Twall(I) - TBave
            flux(I)= Q/(twopi*RFIN*zl)
            alpha(I)= flux(I)/delt(I)
            deltM= 0.5 * delt(I)
```

```
            Qloss(I)=  alpha(I)*twopi*ro*zlnc*deltM
            Q = Q - Qloss(I)
            Qloss(I)=  100.*Qloss(I)/watts
            Twall(I)= TCave - Q*(1./(twopi*condcu*zlb))*ALOG(ro/rt)
            delt(I)= Twall(I) - TBave
            flux(I)= Q/(twopi*RFIN*zlb)
            alpha(I)= flux(I)/delt(I)
 155        CONTINUE
       ELSEIF (isurf.EQ.4) THEN
C*****************************************************************
C         isurf = 4    (Schnelle)
C         Smooth surface, 0.75 inch diameter, 2.5 inch boiling length
C         Four thermocouples at midpoint of heated length.
C*****************************************************************
          ri=  0.47625E-02
          rt=  0.71438E-02
          ro=  0.95250E-02
          zlb= 0.0635
C--         The length for natural convection is 1/2 + 7/8 in.
          zlnc=0.0349
          zl = zlnc + zlb
C--         zlOSS = 0.675 in. = 0.017145 m
          zlOSS = 0.017145
C          condcu= 391.0
          condcu = 339.
C
          DO 165 I=1,npts
            watts = volts(I)*amps(I)
            Q = watts
            TCave=(Tc(1,I)+Tc(2,I)+Tc(3,I)+Tc(4,I))/4.
            TBave=(Tb(1,I)+Tb(2,I))/2.
```

```
C--          TLave=(Te(1,I)+Te(2,I)+Te(3,I)+Te(4,I))/4.
             Tvar = 0.
             DO 163 J=1,4
               Tvar = Tvar + (TCave - Tc(J,I))**2
 163           CONTINUE
             TCvar1(I)= SQrt(Tvar)
             TCvar2(I)= 100.*TCvar1(I)/(TCave-TBave)
             Twall(I)= TCave - Q*(1./(twopi*condcu*zlb))*ALOG(ro/rt)
             delt(I)= Twall(I) - TBave
             flux(I)= Q/(twopi*ro*zl)
             alpha(I)= flux(I)/delt(I)
             deltL= (Te(3,I)+Te(4,I))/2. - (Te(1,I)+Te(2,I))/2.
             deltM= ((Te(1,I)+Te(2,I))/2. + TLave)/2. - TBave
             Qloss(I)= condcu*pi*(rt*rt-ri*ri)*deltL/zlOSS
             Q = Q - Qloss(I)
             Qloss(I)= 100.*Qloss(I)/watts
             Twall(I)= TCave - Q*(1./(twopi*condcu*zlb))*ALOG(ro/rt)
             delt(I)= Twall(I) - TBave
             flux(I)= Q/(twopi*ro*zlb)
             alpha(I)= flux(I)/delt(I)
 165         CONTINUE
          ELSEIF (isurf.EQ.5) THEN
C*************************************************************
*
C         isurf = 5   Smooth Tube - 0.75 in. OD  (Bajorek)
C         Three valid thermocouples at center of tube.
C*************************************************************
*
             ri=  0.47625E-02
             rt=  0.71438E-02
             ro=  0.95250E-02
             zlb= 0.05080
```

```
      zlnc=0.01905
      zl = 0.03810 + 0.05080
      condcu= 391.0
      DO 575 I=1,npts
        watts = volts(I)*amps(I)
        Q = watts
        TCave=(Tc(1,I)+Tc(2,I)+Tc(3,I))/3.
        TBave=(Tb(1,I)+Tb(2,I))/2.
        TLave=(Te(1,I)+Te(2,I)+Te(3,I)+Te(4,I))/4.
        Tvar = 0.
        DO 573 J=1,4
          Tvar = Tvar + (TCave - Tc(J,I))**2
573       CONTINUE
        TCvar1(I)= SQrt(Tvar)
        TCvar2(I)= 100.*TCvar1(I)/(TCave-TBave)
        Twall(I)= TCave - Q*(1./(twopi*condcu*zlb))*ALOG(ro/rt)
        delt(I)= Twall(I) - TBave
        flux(I)= Q/(twopi*ro*zl)
        alpha(I)= flux(I)/delt(I)
        deltL= TCave - (Te(1,I)+Te(2,I))/2.
        deltM= ((Te(1,I)+Te(2,I))/2. + TLave)/2. - TBave
        Qloss(I)= condcu*pi*(ro*ro-ri*ri)*deltL/(0.00635) +
     &            alpha(I)*twopi*ro*zlnc*deltM
        Qloss1 = condcu*pi*(ro*ro-ri*ri)*deltL/(0.00635)
        Qloss2 = alpha(I)*twopi*ro*zlnc*deltM
        Qloss(I) = Qloss2
        Q = Q - Qloss(I)
        Qloss(I)= 100.*Qloss(I)/watts
        Twall(I)= TCave - Q*(1./(twopi*condcu*zlb))*ALOG(ro/rt)
        delt(I)= Twall(I) - TBave
        flux(I)= Q/(twopi*ro*zlb)
```

```
          alpha(I)= flux(I)/delt(I)
575       CONTINUE
      ELSEIF (isurf.EQ.6) THEN
C*****************************************************************
C       isurf = 6   Smooth Tube - 0.75 in. OD  (Bajorek)
C       Four valid thermocouples at center of tube.
C*****************************************************************
          ri=  0.47625E-02
          rt=  0.71438E-02
          ro=  0.95250E-02
          zlb= 0.05080
          zlnc=0.01905
          zl = 0.03810 + 0.05080
          condcu= 391.0
C
          DO 175 I=1,npts
            watts = volts(I)*amps(I)
            Q = watts
            TCave=(Tc(1,I)+Tc(2,I)+Tc(3,I)+Tc(4,I))/4.
            TBave=(Tb(1,I)+Tb(2,I))/2.
            TLave=(Te(3,I)+Te(4,I))/2.
            Tvar = 0.
            DO 173 J=1,4
              Tvar = Tvar + (TCave - Tc(J,I))**2
173         CONTINUE
            TCvar1(I)= SQrt(Tvar)
            TCvar2(I)= 100.*TCvar1(I)/(TCave-TBave)
            Twall(I)= TCave - Q*(1./(twopi*condcu*zlb))*ALOG(ro/rt)
            delt(I)= Twall(I) - TBave
            flux(I)= Q/(twopi*ro*zl)
            alpha(I)= flux(I)/delt(I)
```

```
            deltL= TCave - (Te(1,I)+Te(2,I))/2.
            deltM= ((Te(1,I)+Te(2,I))/2. + TLave)/2. - TBave
            Qloss(I)= condcu*pi*(ro*ro-ri*ri)*deltL/(0.00635) +
     &              alpha(I)*twopi*ro*zlnc*deltM
            Q = Q - Qloss(I)
            Qloss(I)= 100.*Qloss(I)/watts
            Twall(I)= TCave - Q*(1./(twopi*condcu*zlb))*ALOG(ro/rt)
            delt(I)= Twall(I) - TBave
            flux(I)= Q/(twopi*ro*zlb)
            alpha(I)= flux(I)/delt(I)
 175        CONTINUE
        ELSEIF (isurf.EQ.9) THEN

C*****************************************************************
C       isurf = 9
C       Nuclear clad heater - 17x17 Vantage 5A clad with
C                       2-inch long cartridge heater.
C       The heater diameter after press fit is 0.245 in.
C*****************************************************************
            ri=  0.003111
C--         The thermocouples are on a 0.329 in diameter circle.
            rt=  0.004178
C--         The outside diameter is 0.374 in
            ro=  0.00475
C--         The length of the boiling region is 2.0 in.
            zlb= 0.0508
C--         Assume the length of tube in natural convection is 2 in
            zlnc=0.0508
            zl = zlb + zlnc
C--         Thermal conductivities for copper and zircalloy
            condcu= 391.0
```

```
      CONDZR= 7.51

      DO 185 I=1,npts
        watts = volts(I)*amps(I)
        Q = watts
        TCave=(Tc(1,I)+Tc(2,I)+Tc(3,I))/3.
        TBave=(Tb(1,I)+Tb(2,I))/2.
C         Since this heater lacks error TCs, assume that TLave
C         is equal to TBave.
        TLave=(Te(1,I)+Te(2,I))/2.
        Tvar = 0.
          DO 183 J=1,3
        Tvar = Tvar + (TCave - Tc(J,I))**2
183       CONTINUE
        TCvar1(I)= SQrt(Tvar)
        TCvar2(I)= 100.*TCvar1(I)/(TCave-TBave)
C         Twall(I)= TCave - Q*(1./(twopi*condcu*zlb))*ALOG(ro/rt)
        RC = 0.0002/(twopi*rt*zlb)
        Twall(I) = TCave - Q*(ALOG(ro/rt)/(twopi*CONDZR*zlb)+RC)
        delt(I)= Twall(I) - TBave
        flux(I)= Q/(twopi*ro*zl)
        alpha(I)= flux(I)/delt(I)
        deltL= TCave - TLave
        deltM= TLave - TBave
        Qloss(I)= CONDZR*pi*(ro*ro-ri*ri)*deltL/(0.5*zl) +
     &            alpha(I)*twopi*ro*zlnc*deltM
        Q = Q - Qloss(I)
        Qloss(I)= 100.*Qloss(I)/watts
        Twall(I)= TCave - Q*(1./(twopi*CONDZR*zlb))*ALOG(ro/rt)
        delt(I)= Twall(I) - TBave
        flux(I)= Q/(twopi*ro*zlb)
```

```
            alpha(I)= flux(I)/delt(I)
 185        CONTINUE
        ELSEIF (isurf.EQ.10) THEN
          C*************************************************************
C       isurf = 10
C       Nuclear clad heater - 17x17 Vantage 5A clad with
C                         1-inch long cartridge heater.
C       The heater diameter after press fit is 0.245 in.
C*************************************************************
          ri=  0.003111
C     The copper sleeve has radius:
          RCI= 0.004178
C       The thermocouples are on a 0.329 in diameter circle.
C      rt=  0.004178
C     Assume the TCs are centrally located between the sleeve
C      and the heating element.
          rt= 0.003645
C       The outside diameter is 0.374 in
          ro=  0.00475
C       The length of the boiling region is 1.0 in.
          zlb= 0.0254
C       Assume the length of tube in natural convection is 1 in
          zlnc=0.0254
          zl = zlb + zlnc
C       Thermal conductivities for copper and zircalloy
         condcu= 391.0
C              RES =0.07
C        RES is the electrical resistance of test heater
C
          DO 195 I=1,npts
            watts = amps(I)*volts(I)
```

```
      Q = watts
      TCave=(Tc(1,I)+Tc(2,I)+Tc(3,I)+Tc(4,I))/4.
      TKAVE= TCave + 273.15
      CONDZR = 7.51 + 0.0209*TKAVE - 1.45E-5*TKAVE**2 +
     &         7.67E-9*TKAVE**3
C      CONDZR = 10.0
C
      TBave=Tb(1,I)
      TLave= TBave
      Tvar = 0.
      DO 193 J=1,4
        Tvar = Tvar + (TCave - Tc(J,I))**2
193     CONTINUE
      TCvar1(I)= SQrt(Tvar)
      TCvar2(I)= 100.*TCvar1(I)/(TCave-TBave)
C      Twall(I)= TCave - Q*(1./(twopi*condcu*zlb))*ALOG(ro/rt)
C      RC is the contact resistance between the copper sleeve and
C      the Zr clad.  Based on natural conv. cooling tests.
      RC = 0.0002/(twopi*rt*zlb)
C        RC = 1.4516E-4/(twopi*rt*zlb)
      RC = 0.00069/(twopi*rt*zlb)
       Twall(I) = TCave-Q*(ALOG(ro/rt)/(twopi*CONDZR*zlb)+RC)
      delt(I)= Twall(I) - TBave
      flux(I)= Q/(twopi*ro*zl)
      alpha(I)= flux(I)/delt(I)
      deltL= TCave - TLave
      deltM= TLave - TBave
C
      FMIN = 0.1
      FMAX = 1.0
```

```
      TSAT = 100.0
C       RC = max((1.0+(FMIN-FMAX)*(TCave-TSAT)/100.),FMIN)*RC
      FRC = (TSAT-TCave)/50.
C       TCHF = TSAT+75.
C       FRC = ((TCHF-TCave)/(TCHF-70.))**3
      FRC = min(FMAX,max(FRC,FMIN))
      RC =  FRC*RC
C       FRC = max((1.0+(FMIN-FMAX)*(TCave-TSAT)/100.),FMIN)
C       Heat loss in the nuclear clad heater is assumed to be due to
C       conduction through the copper sleeve.
      DTC = 0.0015875
      ACU = pi*(RCI*RCI-ri*ri) - pi*DTC**2
C       The low TC is assumed to be pulled out 2.54 cm based on
C       conditions at nucleation.
      ZERR = 2.00*0.0254
      Qloss(I) = condcu*ACU*deltL/ZERR
C       Qloss(I) = 0.
C       Qloss(I)= CONDZR*pi*(ro*ro-ri*ri)*deltL/(0.5*zl) +
C     &           alpha(I)*twopi*ro*zlnc*deltM
      Q = Q - Qloss(I)
C       PriNT *,' I=',I,' TCave=',TCave,' TLave=',TLave
C       PriNT *,' POWER=',watts,' Q=',Q,' Qloss=',Qloss(I)
C       PriNT *,' DTGAP =',Q*RC,' RC=',RC
      RCLAD = ALOG(ro/RCI)/(twopi*CONDZR*zlb)
C       PriNT *,' DTCLAD=',Q*RCLAD,' RCLAD=',RCLAD
      WRITE(jdat,800) I, TCave,TLave,TBave
  800   FORMAT(1X,'I =',I3,' TC=',F8.2,' TL=',F8.2,' TB=',F8.2)
      WRITE(jdat,801) Q, watts, Qloss(I)
  801   FORMAT(1X,'Q=',F8.3,' POWER=',F8.3,' Qloss=',F8.3)
      WRITE(jdat,802) Q*RC, RC
  802   FORMAT(1X,'DTgap =',F8.2,' RC=',F10.5)
```

```
            WRITE(jdat,803) Q*RCLAD, RCLAD, CONDZR
 803          FORMAT(1X,'DTclad=',F8.2,' RCLAD=',F9.5,' CONDZR=',F8.3)
            Qloss(I)= 100.*Qloss(I)/watts
C             Twall(I)= TCave - Q*(1./(twopi*CONDZR*zlb))*ALOG(ro/rt)
            Twall(I) = TCave - Q*(ALOG(ro/RCI)/(twopi*CONDZR*zlb)+RC)
            delt(I)= Twall(I) - TBave
            flux(I)= Q/(twopi*ro*zlb)
            alpha(I)= flux(I)/delt(I)
            RCONV = 1./((alpha(I)*twopi*ro*zlb))
            PriNT *,' Twall=',Twall(I),' alpha=',alpha(I),' flux=',
     &              flux(I)
            WRITE(jdat,804) Q*RCONV, RCONV, Twall(I)
 804          FORMAT(1X,'DTwall=',F8.3,' RCONV=',F10.5,' Twall=',F8.3)
            WRITE(jdat,805) FRC
 805          FORMAT(1X,' FRC=',F10.5)
 195        CONTINUE




          ELSEIF (isurf.EQ.11) THEN
C
C*************************************************************
C *** isurf = 11 ****** Turbo-BIII Enhanced Tube
C     isurf = 11   Turbo-III Tube - 0.740 in. OD  (Schnelle)
C     Four valid thermocouples at center of tube.
C     Two thermocouples are assumed for estimating heat loss.
C     The loss TCs are located at the heater edge, and
C          0.675 inch (0.017145 m) inside the heated region.
C
C*************************************************************
C *** The heater diameter is 0.372 in (0.0094488 m)
```

```
      ri=  0.47244E-02
C--   The thermocouple dia. is (0.372+0.630)/2 = 0.501in = 0.0127254m
      rt=  0.63627E-02
C--   The copper sleeve OD is 0.630 in. (0.016002 m)
      RSDO = 0.008001
C--   The outside diameter of the tube is 0.740 in. = 0.018796 m
      ro=  0.93980E-02
C--   The heater has a heated length of 2.5 in = 0.0635 m
      zlb= 0.06350
      zlnc=0.02530
      zl = zlb + zlnc
C--   The error TCs are located 0.25 in off of the heater
      zlOSS = 0.039065
C--   The thermal conductivity of Alloy C12200 (ASTM B359)
C--   is k = 196 Btu/ft2-hr-F = 339.2 W/m2-K
      condcu= 339.2
      RC = 0.03

      DO 585 I=1,npts
        watts = volts(I)*amps(I)
        Q = watts
        TCave=(Tc(1,I)+Tc(2,I)+Tc(3,I)+Tc(4,I))/4.
        TBave=(Tb(1,I)+Tb(2,I))/2.
        TLave=(Te(1,I)+Te(2,I))/2.
        Tvar = 0.
        DO 583 J=1,4
          Tvar = Tvar + (TCave - Tc(J,I))**2
583       CONTINUE
        TCvar1(I)= SQrt(Tvar)
        TCvar2(I)= 100.*TCvar1(I)/(TCave-TBave)
C         Twall(I)= TCave - Q*(1./(twopi*condcu*zlb))*ALOG(ro/rt)
```

```
            Twall(I)= TCave - Q*(ALOG(ro/rt)/(twopi*condcu*zlb) + RC)
            delt(I)= Twall(I) - TBave
            flux(I)= Q/(twopi*ro*zl)
            alpha(I)= flux(I)/delt(I)
            deltL= TCave - TLave
C             deltM= ((Te(1,I)+Te(2,I))/2. + TLave)/2. - TBave
            Qloss(I)= condcu*pi*(RSDO*RSDO-ri*ri)*deltL/zlOSS
            Q = Q - Qloss(I)
            Qloss(I)= 100.*Qloss(I)/watts
C             Twall(I)= TCave - Q*(1./(twopi*condcu*zlb))*ALOG(ro/rt)
            Twall(I)= TCave-Q*(ALOG(ro/rt)/(twopi*condcu*zlb)+RC)
            delt(I)= Twall(I) - TBave
            flux(I)= Q/(twopi*ro*zlb)
            alpha(I)= flux(I)/delt(I)
 585        CONTINUE
          ELSEIF (isurf.EQ.12) THEN
C
**********************************************************************
C *** isurf = 12 ****** Turbo-BIII Enhanced Tube
C    isurf = 12   Turbo-III Tube - 0.740 in. OD  (Schnelle)
C    Four valid thermocouples at center of tube inserted thru
C    sleeve to obtain contact with Turbo-III inner surface.
C    Two thermocouples are assumed for estimating heat loss.
C    The loss TCs are located at the heater edge, and
C       0.675 inch (0.017145 m) inside the heated region.
C
**********************************************************************
C *** The heater diameter is 0.372 in (0.0094488 m)
            ri=  0.47244E-02
C--   The thermocouple dia. is (0.559+0.035)=0.594in = 0.0150876m
            rt=  0.75438E-02
C--   The copper sleeve OD is 0.630 in. (0.016002 m)
```

```
      RSDO = 0.8001E-02
C--   The outside diameter of the tube is 0.740 in. = 0.018796 m
      ro=  0.93980E-02
C--   The heater has a heated length of 2.0 in = 0.0508 m
      zlb= 0.05080
      zlnc=0.02530
      zl = zlb + zlnc
C--   The error TCs are located 0.25 in off of the heater
      zlOSS = 0.00635
C--   The thermal conductivity of Alloy C12200 (ASTM B359)
C--   is k = 196 Btu/ft2-hr-F = 339.2 W/m2-K
      condcu= 339.2

      DO 595 I=1,npts
        watts = volts(I)*amps(I)
        Q = watts
        TCave=(Tc(1,I)+Tc(2,I)+Tc(3,I)+Tc(4,I))/4.
        TBave=(Tb(1,I)+Tb(2,I))/2.
        TLave=(Te(1,I)+Te(2,I))/2.
        deltL= TCave - TLave
        Tvar = 0.
        DO 593 J=1,4
          Tvar = Tvar + (TCave - Tc(J,I))**2
593       CONTINUE
        TCvar1(I)= SQrt(Tvar)
        TCvar2(I)= 100.*TCvar1(I)/(TCave-TBave)
        Qloss(I)= condcu*pi*(RSDO*RSDO-ri*ri)*deltL/zlOSS
        Q = Q - Qloss(I)
        Qloss(I)= 100.*Qloss(I)/watts
C         Twall(I)= TCave - Q*(1./(twopi*condcu*zlb))*ALOG(ro/rt)
        Twall(I)= TCave - Q*(ALOG(ro/rt)/(twopi*condcu*zlb))
```

```
            delt(I)= Twall(I) - TBave
            flux(I)= Q/(twopi*ro*zlb)
            alpha(I)= flux(I)/delt(I)
 595        CONTINUE
       ELSE
C*************************************************
C   ERROR: not valid surface
C*************************************************
        WRITE(*,*) '****ERROR: invalid surface number', isurf
        STOP
       ENDIF
C*****************  Print out results
       CALL OUTPUT(jdat)
       CALL SDFOUT(jsdf)
       WRITE(*,225) datfil
225     FORMAT(10X,'OUTPUT FILE IS ',A20)
       WRITE(*,226) sdffil
226     FORMAT(10X,'PLOT FILE IS   ',A20)
       IF(IFILE.EQ.nfiles) CALL BANNER(jban)
       CLOSE(jinp)
       CLOSE(jdat)
       CLOSE(jsdf)
900   CONTINUE
     CLOSE(jban)
     WRITE(*,950)
950   FORMAT(/,1X,'Normal termination of Program PBDATA')
     STOP
     END

     SUBROUTINE BANNER(N)
C
**************************************************************
```

```
      C  Prints out a banner and ids of surfaces and substances
      C
*****************************************************************
         WRITE(N,10)
       10  FORMAT(/15X,

&'PPPPPP',3X,'BBBBBB',3X,'DDDDDD',4X,'AAA',4X,'TTTTTTTT',5X,'AAA',/
         &15X,'PP   PP',2X,'BB   BB',2X,'DD   DD',3X,'AA AA',3X,'T  TT  T',
         &    3X,'AA AA',/
         &15X,'PP   PP',2X,'BB   BB',2X,'DD   DD',2X,'AA   AA',2X,
         &     'T  TT  T',2X,'AA   AA',/
         &15X,'PPPPPP',3X,'BBBBBB',3X,'DD   DD',2X,'AAAAAAA',5X,'TT',
         &     5X,'AAAAAAA',/
         &15X,'PP',7X,'BB   BB',2X,'DD   DD',2X,'AA   AA',5X,'TT',
         &     5X,'AA   AA',/
         &15X,'PP',7X,'BBBBBB',3X,'DDDDDD',3X,'AA   AA',4X,'TTTT',
         &     4X,'AA   AA',//
         &15X,'ProGRAM PBDATA Version 06-Revised: February 20, 2001',/
         &30X,' --- Written by S. M. Bajorek',//)
         WRITE(N,200)
       200  FORMAT(15X,'COMPONENT INDEX:',/15X,' 1 = acetone',/
         &     15X,' 2 = 2-butanone',/15X,' 3 = Methanol',/
         &     15X,' 4 = ethanol',/15X,' 5 = benzene',/15X,' 6 = water',/
         &     15X,' 7 = 1-propanol',/15X,' 8 = 2-Propanol',/
         &     15X,' 9 = ethylene glycol',/15X,'10 = cyclohexane',/
         &     15X,'11 = Propylene glycol',/15X,'12 = methyl acetate',/
         &     15X,'13 = ethyl acetate',/15X,'14 = diethylene glycol',/
         &     15X,'15 = AMMONIA')
         WRITE(N,500)
       500  FORMAT(/15X,'SURFACE INDEX:',/
         &     15X,' 1 = smooth tube      Shakir',/
         &     15X,' 2 = high flux tube   Bajorek',/
```

```
     &      15X,' 3 = finned tube      Bajorek',/
     &      15X,' 4 = smooth tube      Schnelle',/
     &      15X,' 5 = smooth tube      Bajorek',/
     &      15X,' 6 = smooth tube      Bajorek',/
     &      15X,' 7 = smooth tube      Shakir',/
     &      15X,' 8 = smooth tube      Shakir',/
     &      15X,' 9 = nuclear clad     Schnelle',/
     &      15X,'10 = nuclear clad     Schnelle',/
     &      15X,'11 = TURBO-IIIB       Schnelle',/
     &      15X,'12 = TURBO-IIIB       Schnelle',//
     &      14X,'101 = smooth Cu flat disk',/
     &      14X,'102 = smooth Cu flat disk',/
     &      14X,'103 = 1.25 in Si wafer')

      RETURN
      END
      SUBROUTINE INPUT(jin)
C
**********************************************************************
C  Reads in an input file
C
**********************************************************************
      COMMON/XDATA/idnum,idate,isurf,icomp(5),frac(5),npts,iunits,
     &          volts(40),amps(40),P(40),Tb(2,40),Tc(4,40),Te(4,40)
      COMMON/SOLUTE/ ppmB, ppmLi

C-- Function to convert degF to degC
      FtoC(x)= (x-32.)*(5./9.)
C
C--- READ(jin,1) is a header line that is ignored
      WRITE(*,*) 'TEST input subroutine start'
      READ(jin,1)
```

```
      READ(jin,10) idnum,idate,isurf,iunits
C     READ(jin,*) idnum,idate,isurf,iunits
      READ(jin,1)
      READ(jin,20) (icomp(i),i=1,5)
      READ(jin,1)
      READ(jin,30) (frac(i),i=1,5)
      READ(jin,1)
      READ(jin,40) npts,ppmB,ppmLi
      READ(jin,1)
           C-- readin temperatures
      READ(jin,60) (volts(n),amps(n),(Tc(i,n),i=1,4),Tb(1,n),Tb(2,n),
     &           (Te(i,n),i=1,4),P(n),n=1,npts)

C-- change temps in degF (iunits=1) to degC(iunits=2) (if necessary)
      IF (iunits.EQ.1) THEN
        DO 55 n=1,npts
          DO 56 i=1,4
            Tc(i,n) = FtoC(Tc(i,n))
            Te(i,n) = FtoC(Te(i,n))
56        CONTINUE
            Tc(1,n) = FtoC(Tb(1,n))
            Tc(2,n) = FtoC(Tb(2,n))
55      CONTINUE
      ENDIF
  1   FORMAT( )
 10   FORMAT(10X,I5,9X,I6,10X,I5,10X,I5)
 20   FORMAT(5I15)
 30   FORMAT(5E15.5)
      WRITE(*,*) 'TEST 09'
 40   FORMAT(10X,I5,5X,F10.1,5X,F10.1)
 60   FORMAT(F5.1,1X,F5.2,10F6.1,1X,F6.1)
```

```
      RETURN
      END
      SUBROUTINE OUTPUT(J)
C
*****************************************************************
C  Produces output data files
C
*****************************************************************
      COMMON/XDATA/idnum,idate,isurf,icomp(5),frac(5),npts,iunits,
     &      volts(40),amps(40),P(40),Tb(2,40),Tc(4,40),Te(4,40)
      COMMON/XOUTP/delt(40),Qloss(40),alpha(40),Twall(40),flux(40),
     &      TCvar1(40),TCvar2(40)
      COMMON/SOLUTE/ ppmB, ppmLi

      WRITE(J,5)
    5 FORMAT(10X,'idnum',11X,'date',8X,'surface')
      WRITE(J,10) idnum,idate,isurf
   10 FORMAT(10X,I5,9X,I6,10X,I5)
      WRITE(J,20)
   20 FORMAT(5(6X,'Component'))
      WRITE(J,30) (icomp(i),i=1,5)
   30 FORMAT(5I15)
      WRITE(J,40)
   40 FORMAT(5(7X,'Fraction'))
      WRITE(J,50) (frac(i),i=1,5)
   50 FORMAT(5E15.5)
      WRITE(J,60)
   60 FORMAT(11X,'npts')
      WRITE(J,70) npts
   70 FORMAT(10X,I5)
```

```
      WRITE(J,80)
   80 FORMAT(/,9X,'V',4X,'I',2X,'TC-1',2X,'TC-2',2X,'TC-3',2X,'TC-4',
     &       2X,'TB-1',2X,'TB-2',2X,'TE-1',2X,'TE-2',2X,'TE-3',
     &       2X,'TE-4',4X,'P')
      WRITE(J,110) (volts(N),amps(N),(Tc(i,N),i=1,4),Tb(1,N),Tb(2,N),
     &            (Te(i,N),i=1,4),P(N),N=1,npts)
  110 FORMAT(4X,F6.2,F5.2,10F6.1,F7.1)
      WRITE(J,120)
  120 FORMAT(/,2X,'NO',1X,' SUPERHEAT',2X,'HEAT flux',5X,'alpha',
     &        5X,'Qloss',5X,'Twall',4X,'TCvar1',4X,'TCvar2')

      WRITE(J,140) (N,delt(N),flux(N),alpha(N),Qloss(N),Twall(N),
     &            TCvar1(N),TCvar2(N),N=1,npts)
  140 FORMAT(2X,I2,1X,F10.1,1X,4F10.1,F10.2,F10.1)

      IF((ppmB+ppmLi).GT.0.) THEN
        WRITE(J,150) ppmB
  150   FORMAT(/,' Boron concentration   =',F8.1,' ppm')
        WRITE(J,160) ppmLi
  160   FORMAT(/,' Lithium concentration =',F8.1,' ppm')
      ENDIF

      RETURN
      END
      SUBROUTINE SDFOUT(J)
C
C*****************************************************************
C  Creates plot data files
C
C*****************************************************************
      COMMON/XDATA/idnum,idate,isurf,icomp(5),frac(5),npts,iunits,
     &            volts(40),amps(40),P(40),Tb(2,40),Tc(4,40),Te(4,40)
```

```
      COMMON/XOUTP/ delt(40),Qloss(40),alpha(40),Twall(40),flux(40),
     &             TCvar1(40),TCvar2(40)
C
      WRITE(*,15)

      ZKW = 1000.
      WRITE(J,20) (delt(N),flux(N)/ZKW,alpha(N)/ZKW,Twall(N),
     &             Tb(1,N),P(N),N=1,npts)
      WRITE(*,20) (delt(N),flux(N)/ZKW,alpha(N)/ZKW,Twall(N),
     &             Tb(1,N),P(N),N=1,npts)

   15 FORMAT('        Delt(n)      flux/1000     alpha/1000',
     & '    Twall      Tb        P')
   20 FORMAT(5X,F10.4,5X,F10.2,5X,F10.1,3F10.1)
C
      RETURN
      END
```

A.2 Sample Data File.

Input file with data for pool boiling test at 1000 psia pressure for ionized water at 30 subcooling.

```
        IDNUM          DATE        SURFACE
         953           041406          10
COMPONENT COMPONENT COMPONENT COMPONENT COMPONENT
          6            0            0            0            0
     FRACTION   FRACTION      FRACTION      FRACTION      FRACTION
  0.10000E+01   0.00000E+00   0.00000E+00   0.00000E+00   0.00000E+00
        NPTS         PPMBN         PPMLI
          20           0.0           0.0
   V    I  TC-1  TC-2  TC-3  TC-4  TB-1  TB-2  TE-1  TE-2  TE-3  TE-4    P
0.47  6.30 258.6 257.5 256.9 257.5 254.6   0.0   0.0   0.0   0.0   0.0 1000.0
0.73  9.60 263.1 262.5 261.0 262.1 255.6   0.0   0.0   0.0   0.0   0.0 1001.0
1.05 13.60 269.4 267.9 267.6 267.8 255.4   0.0   0.0   0.0   0.0   0.0 1001.0
1.27 18.00 276.0 275.4 273.7 275.7 255.6   0.0   0.0   0.0   0.0   0.0 1000.0
1.55 21.90 287.7 284.0 282.9 284.5 255.6   0.0   0.0   0.0   0.0   0.0 1000.0
1.80 25.40 297.2 294.6 293.6 293.9 255.6   0.0   0.0   0.0   0.0   0.0 1001.0
1.97 27.80 301.2 300.4 300.7 300.6 255.8   0.0   0.0   0.0   0.0   0.0 1000.0
2.14 30.10 305.7 305.1 304.5 304.6 255.6   0.0   0.0   0.0   0.0   0.0 1000.0
2.30 32.50 309.2 310.0 309.4 310.2 255.6   0.0   0.0   0.0   0.0   0.0 1001.0
2.43 34.40 312.3 312.8 312.4 312.8 255.8   0.0   0.0   0.0   0.0   0.0 1002.0
2.60 36.40 314.8 315.0 314.7 315.0 256.0   0.0   0.0   0.0   0.0   0.0 1000.0
```

2.72 38.90 316.1 317.1 316.1 317.1 255.8 0.0 0.0 0.0 0.0 0.0 1000.0
2.91 41.40 318.5 319.7 318.9 319.4 255.4 0.0 0.0 0.0 0.0 0.0 1000.0
3.02 43.10 320.3 322.2 320.6 321.1 255.8 0.0 0.0 0.0 0.0 0.0 1001.0
3.13 44.60 322.6 324.0 322.4 322.8 255.8 0.0 0.0 0.0 0.0 0.0 1003.0
3.27 46.70 324.5 325.9 325.0 325.1 255.8 0.0 0.0 0.0 0.0 0.0 1002.0
3.37 48.00 326.6 327.5 326.2 327.1 255.8 0.0 0.0 0.0 0.0 0.0 1000.0
3.47 49.70 328.0 328.8 328.0 328.5 256.0 0.0 0.0 0.0 0.0 0.0 1001.0
3.61 51.70 330.2 330.5 330.0 331.6 256.0 0.0 0.0 0.0 0.0 0.0 1000.0
3.75 52.90 332.3 331.6 332.2 332.8 255.8 0.0 0.0 0.0 0.0 0.0 1000.0

Output file from the program ‘pbdata’

V	I	TC-1	TC-2	TC-3	TC-4	TB-1	TB-2	TE-1	TE-2	TE-3	TE-4	P
.47	6.30	258.6	257.5	256.9	257.5	254.6	.0	.0	.0	.0	.0	1000.0
.73	9.60	263.1	262.5	261.0	262.1	255.6	.0	.0	.0	.0	.0	1001.0
1.05	13.60	269.4	267.9	267.6	267.8	255.4	.0	.0	.0	.0	.0	1001.0
1.27	18.00	276.0	275.4	273.7	275.7	255.6	.0	.0	.0	.0	.0	1000.0
1.55	21.90	287.7	284.0	282.9	284.5	255.6	.0	.0	.0	.0	.0	1000.0
1.80	25.40	297.2	294.6	293.6	293.9	255.6	.0	.0	.0	.0	.0	1001.0
1.97	27.80	301.2	300.4	300.7	300.6	255.8	.0	.0	.0	.0	.0	1000.0
2.14	30.10	305.7	305.1	304.5	304.6	255.6	.0	.0	.0	.0	.0	1000.0
2.30	32.50	309.2	310.0	309.4	310.2	255.6	.0	.0	.0	.0	.0	1001.0
2.43	34.40	312.3	312.8	312.4	312.8	255.8	.0	.0	.0	.0	.0	1002.0
2.60	36.40	314.8	315.0	314.7	315.0	256.0	.0	.0	.0	.0	.0	1000.0
2.72	38.90	316.1	317.1	316.1	317.1	255.8	.0	.0	.0	.0	.0	1000.0
2.91	41.40	318.5	319.7	318.9	319.4	255.4	.0	.0	.0	.0	.0	1000.0
3.02	43.10	320.3	322.2	320.6	321.1	255.8	.0	.0	.0	.0	.0	1001.0
3.13	44.60	322.6	324.0	322.4	322.8	255.8	.0	.0	.0	.0	.0	1003.0
3.27	46.70	324.5	325.9	325.0	325.1	255.8	.0	.0	.0	.0	.0	1002.0
3.37	48.00	326.6	327.5	326.2	327.1	255.8	.0	.0	.0	.0	.0	1000.0
3.47	49.70	328.0	328.8	328.0	328.5	256.0	.0	.0	.0	.0	.0	1001.0

3.61	51.70	330.2	330.5	330.0	331.6	256.0	.0	.0	.0	.0	.0	1000.0
3.75	52.90	332.3	331.6	332.2	332.8	255.8	.0	.0	.0	.0	.0	1000.0

NO	SUPERHEAT	HEAT flux	alpha	Qloss	Twall	TCvar1	TCvar2
1	2.6	3398.7	1314.1	13.0	257.2	1.23	40.6
2	5.5	8142.0	1473.7	11.9	261.1	1.53	23.3
3	10.6	16695.1	1571.3	11.4	266.0	1.43	11.2
4	16.1	26868.9	1664.2	10.9	271.7	1.78	9.1
5	24.1	39886.0	1657.9	10.9	279.7	3.57	12.2
6	32.3	53733.6	1661.2	10.9	287.9	2.84	7.2
7	36.7	64710.8	1765.6	10.4	292.5	.59	1.3
8	39.6	76691.7	1937.7	9.7	295.2	.95	1.9
9	42.7	89534.0	2098.0	9.2	298.3	.82	1.5
10	43.9	100749.4	2293.6	8.6	299.7	.46	.8
11	44.2	114971.1	2600.0	7.9	300.2	.26	.4
12	44.3	129380.5	2919.6	7.3	300.1	1.00	1.6
13	44.8	148236.6	3305.4	6.7	300.2	.92	1.4
14	44.8	160760.8	3589.6	6.4	300.6	1.45	2.2
15	45.1	172889.6	3829.2	6.1	300.9	1.24	1.9
16	45.2	189820.2	4201.3	5.8	301.0	1.00	1.4
17	45.4	201470.5	4434.4	5.6	301.2	.98	1.4
18	44.9	215370.3	4791.3	5.3	300.9	.68	.9
19	44.9	233695.8	5206.6	5.1	300.9	1.24	1.7
20	44.8	248869.7	5553.0	4.9	300.6	.85	1.1

APPENDIX B

B.1 Sample Heat Exchanger Calculations

Sample calculations for Heat exchanger calculations, section 3.4.1.1

ΔP is the combined pressure drop in inconel tubing and supply hose.

Assuming ΔP = 40 psi.

Assuming internal diameter of inconel tube is0.5", D_i= 0.01021m

Do = Outer diameter of inconel tubing = 0.127 m

ΔP = 28122.6 N/m^2.

Head loss $h_L = \left(\frac{\Delta P}{\rho g}\right)$ =2.87m

Where ρ = density of the fluid =996 kg/m^3

g = acceleration due to gravity =9.81 m/sec^2

using equation (3.3). Initial guess f=.02

Assuming the length of the tube =8.5 m

Solid cross section of the inconel tubing = $\frac{\Pi * (D_o^{\,2} - D_i^{\,2})}{4}$ =0.0000158 sq m.

Resistance of the inconel tubes is $R = \frac{\rho l}{A}$ equation 3.1

Total Electrical resistance of the inconel tubing = $\frac{1.03 * 8.5}{0.0000158}$ =0.553 Ω.

$$V = \sqrt{\frac{2gD_i h_l}{fL}}$$

From equation (3.3) V = 1.9865 m/sec.

Viscosity of the fluid = μ =0.000855 N/m^2

Reynolds number = $\mathrm{Re} = \left(\frac{VD_i\rho}{\mu}\right)$ =27492.09

Reynolds number is greater than 2300, indicating that the flow is turbulent.

Surface area of the inconel tubes = (pi)*D_i*L = 0.317238 sqm

Corrected friction factor f (from moody chart) =.027

Prandtl number =5.846 and n=4.

From equation (3.5) Nusselt number is known

$$Nu = 0.023\,\mathrm{Re}^{\left(\frac{4}{5}\right)}\, pr^{n}$$

Nu = 165.89

Required flow rate of water to remove the heat generated in the inconel tubes

Q (flow rate) =A*V where A is the area of tube cross section and V is the velocity of the fluid.

$$A = \frac{\Pi . D_i^2}{4} = \frac{\Pi * 01021^2}{4} = 0.000111\mathrm{m}$$

Q= flow rate = A*V = 0.000111*1.9865 =0.00022 m^3/sec

Heat transfer coefficient between inconel tubes and cold water is given by following equation

$$h = \left(\frac{NuK_{water}}{D_i} \right)$$

K_{water} = Conductivity of water = .613W/mk

Substituting the values of nusselt number, thermal conductivity of water and internal diameter we have

Heat Transfer Coefficient= 8560.14 W/m^2C

Total heat transfer from Inconel tubes to water = h* A_{surf} *(ΔT)

Where A_{surf} is the interface area through which heat transfer occurs

ΔT = temperature difference.

Assuming a temperature difference to be 15^{o}C

Total heat transfer = 8.56 kW/m^2C X 0.000111 X 15 = 40.73 KW. The maximum heat generated is about 20 kW. This iteration is reputed with new friction and factor and smallest possible dimensions was chosen for inconel tubes.

B.2 Product Reference

1 Duniway Stockroom Corporation

Product: Copper –O rings, 2006, Code: SG-600

Details:

Duniway Stockroom Corporation

1305 Space Park Way

Mountain View, CA 94043

Ph :800-446-8811

2 Richard Greene Company

Product: electrical bulk heater, Code: SN6N-3206

Manufacturer Details:

Watlow

12001 Lackland Road

St Louis, MO 63146-41001

Ph: 314-878-4600, fax: 314-878-6814

3 McMaster Carr

Product : Ptfe O-rings

Manufacturer details

McMaster Carr Supply Company

Ph: 630-833-0300 fax: 530-834-9427

4 Omega Engineering Inc

Product: Pressure Transducer, Model: PX35k1-3kGV

Omega Engineering Inc

One omega drive, box 4047 Stamford, CT06907-0047

Ph: 203-359-1660 fax- 203-359-7700

5 Omega Engineering Inc

Product: Pressure Transmitter, Model: DP-25S;

T-type thermocouple, Model : HTQIN 316G-12;

Omega Engineering Inc

One omega drive, box 4047 Stamford, CT06907-0047

Ph: 203-359-1660 fax- 203-359-7700

6 Microgroup

Product : Inconel Tubes, Grade : 600

Microgroup Inc

7 Industrial Park Road

Medway, MA 02053-1732

Ph 508-533-4925 fax 508-533-5691

7 Linweld

Product: Nitrogen cylinder, Type: Industrial

Linweld Inc

P.O. Box 682 Manhattan, KS 66505

Ph: 785-537-0395

8 Yale Film and Video

Product: 16mm film processing, Model: Hawkeye Surveillance Film Details

Yale Film and Video

10555 victory blvd,

No Hollywood, CA 91606

Ph 818-508-9253 fax 818-762-0688

9 Machined Glass Specialists Inc

Product: Fused Quartz Window, Model: custom order.

Dimensions : 1.75” Dia x 0.75”thick

Machined Glass Specialist
245 Hiawatha Trail
Springboro, Ohio 45066
Ph: 937-743-6166, fax 937-743-6168

10 John C Ernest Co Inc
Product: gaskets for fused quartz, Model: 583 1.75-1.00-0.0625
John C Ernest Co. Inc
21 Gail Ct. Sparta, NJ 07871
Ph: 973-940-1600. www.sightglass.com

11 Visual Instrumentation Corporation
Product: high speed camera, 1984, Model: Hycam: 41-0005
Visual Instrumentation Corporation
1110 West Avenue L-12, Unit 2, Lancaster,
CA, USA 93534-7039
Ph: 661-945-7999 fax 661-723-5667

12 Stern Laboratories Inc
Product: electrical test heater, DC power Supply
1590 Burlington Street East, Hamilton, Ontario
Canada L8H 3L3
Ph 905-548-5300 fax 905-545-5399

13 Alfa Aesar
Product : Lithium metaborate puratonic , Boric Acid
www.alfaaesar.com

14 Swagelok
Product: union joints,
Kansas City Valve & Fitting Co

4707 Roe Parkway

Roeland Park, Kansas 66205

15 Fluke

Product : Clamp ammeter, Model : i-410

Description : Used to measure AC/DC current.

www.fluke.com

16 Systat Inc

Product : Sigmascan- Image analysis software.

Description: http://www.systat.com/products/SigmaScan/